

**INCREASING ADSORPTION EFFICIENCY OF
ACTIVATED CARBON FOR H₂S REMOVAL BY
SURFACE OXIDATION AND METAL ADDITION**

Somkiat Kruaysawat

**A Thesis Submitted in Partial Fulfillment of the Requirements for
the Degree of Doctor of Philosophy in Environmental Engineering**

Suranaree University of Technology

Academic Year 2006

ISBN 974-533-500-2

การเพิ่มประสิทธิภาพการดูดซับของถ่านกัมมันต์เพื่อกำจัด
ไฮโดรเจนซัลไฟด์ โดยวิธีออกซิเดชันพื้นผิวและเติมโลหะ

นายสมเกียรติ กรวยสวัสดิ์

วิทยานิพนธ์นี้เป็นส่วนหนึ่งของการศึกษาตามหลักสูตรปริญญาวิศวกรรมศาสตรดุษฎีบัณฑิต

สาขาวิชาวิศวกรรมสิ่งแวดล้อม

มหาวิทยาลัยเทคโนโลยีสุรนารี

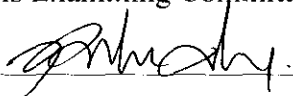
ปีการศึกษา 2549

ISBN 974-533-500-2

**INCREASING ADSORPTION EFFICIENCY OF ACTIVATED
CARBON FOR H₂S REMOVAL BY SURFACE OXIDATION AND
METAL ADDITION**

Suranaree University of Technology has approved this thesis submitted in partial fulfillment of the requirements for the Degree of Doctor of Philosophy.

Thesis Examining Committee



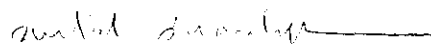
(Asst. Prof. Dr. Sudjit Karuchit)

Chairperson



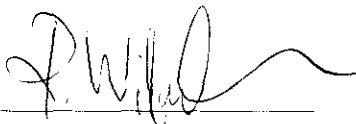
(Assoc. Prof. Dr. Chaiyot Tangsathitkulchai)

Member (Thesis Advisor)



(Assoc. Prof. Dr. Suntud Sirianuntapiboon)

Member



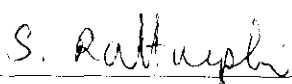
(Asst. Prof. Dr. Ratanawan Kiattikomol)

Member



(Dr. Jareeya Yimrattanabovorn)

Member



(Assoc. Prof. Dr. Saowanee Rattanaphani)

Vice Rector for Academic Affairs



(Assoc. Prof. Dr. Vorapot Khompis)

Dean of Institute of Engineering

สมเกียรติ กรวยสวัสดิ์: การเพิ่มประสิทธิภาพการดูดซับของถ่านกัมมันต์
เพื่อกำจัดไฮโดรเจนซัลไฟด์โดยวิธีออกซิเดชันพื้นผิวและเติมโลหะ (INCREASING
ADSORPTION EFFICIENCY OF ACTIVATED CARBON FOR H₂S REMOVAL
BY SURFACE OXIDATION AND METAL ADDITION.) อาจารย์ที่ปรึกษา :
รองศาสตราจารย์ ดร.ชัยยศ ตั้งสติย์กุลชัย, 207 หน้า. ISBN 974-533-500-2

งานวิจัยนี้มุ่งศึกษาวิธีการเพิ่มความจุในการดูดซับของไฮโดรเจนซัลไฟด์ด้วยถ่านกัมมันต์
โดยเทคนิคการออกซิเดชันและเติมโลหะ ถ่านกัมมันต์ตัวอย่างจากกะลามะพร้าวได้รับการปรับเคมี
พื้นผิวโดยใช้โอโซนและกรดไนตริกเป็นตัวออกซิไดส์ ซึ่งเทคนิคการออกซิเดชันทำให้เกิดหมู่
ฟังก์ชันเช่น C-O และ C=O บนพื้นผิวของถ่านกัมมันต์ ตัวอย่างหมู่ฟังก์ชันที่เกิดขึ้นได้แก่ หมู่ไฮ
ดรอกซิล คีโตน กรดคาร์บอกซิลิกและอีเทอร์ ซึ่งวิเคราะห์โดยใช้เทคนิคสเปกโทรสโกปีฟลูออริเยอร์
แทรนซ์ฟอร์มอินฟราเรด (FTIR) ซิงค์แอซีเตต [Zn(C₂H₃O₂)₂] ถูกใช้เป็นสารตัวกลางในขั้นตอนการ
เติมโลหะหลังจากออกซิไดส์ถ่านกัมมันต์ด้วย โอโซนหรือกรดไนตริกแล้ว แก๊สผสมเตรียมได้จาก
การผสมไฮโดรเจนซัลไฟด์ร้อยละ 1.01 โดยน้ำหนักกับแก๊สไนโตรเจนเพื่อใช้ในการทดลองการดูด
ซับ ไฮโดรเจนซัลไฟด์ที่ออกจากกระบวนการดูดซับแบบเบดนิ่ง ณ เวลาใดๆซึ่งตรวจวัดโดยเครื่องมืออิ
เล็กโทรเคมีคอลเซนเซอร์เพื่อสร้างกราฟเบรคทลู เวลาที่จุดเบรคทลูและความจุของการดูดซับ
(มิลลิกรัม-ไฮโดรเจนซัลไฟด์/กรัม-ตัวดูดซับ)ถึงเวลาที่จุดเบรคทลูถูกใช้ในการประเมิน
ประสิทธิภาพการกำจัดไฮโดรเจนซัลไฟด์ ถ่านกัมมันต์ตัวอย่างที่เติมโลหะสังกะสีให้ค่าความจุใน
การดูดซับสูงกว่าตัวอย่างที่ถูกออกซิไดส์เพียงอย่างเดียวและตัวอย่างที่ยังไม่ได้ปรับปรุงที่อุณหภูมิ
10, 30 และ 45 องศาเซลเซียส ถ่านตัวอย่างที่เตรียมจากกรดไนตริก 6.0 โมลาร์ และเติมโลหะ
สังกะสี ให้ค่าความจุในการดูดซับไฮโดรเจนซัลไฟด์สูงสุดโดยประสิทธิภาพการดูดซับเพิ่มขึ้นร้อยละ
230 (24.72 มิลลิกรัม-ไฮโดรเจนซัลไฟด์/กรัม-ตัวดูดซับ) ซึ่งมากกว่าประสิทธิภาพการดูดซับของ
ถ่านตัวอย่างที่ยังไม่ได้ปรับปรุงที่อุณหภูมิ 45 องศาเซลเซียส ในถ่านตัวอย่างที่ออกซิไดส์ด้วย
โอโซนและเติมโลหะสังกะสีพบว่าการเพิ่มประสิทธิภาพในการดูดซับสูงสุดถึงร้อยละ 180 (19.24
มิลลิกรัม-ไฮโดรเจนซัลไฟด์/กรัม-ตัวดูดซับ) การดูดซับของไฮโดรเจนซัลไฟด์มีแนวโน้มเพิ่มขึ้น
ตามปริมาณของโลหะสังกะสีที่อยู่บนพื้นผิวถ่านกัมมันต์ตัวอย่างที่อุณหภูมิของการดูดซับสูงกว่า 45
องศาเซลเซียส แสดงถึงการดูดซับทางเคมีมีบทบาทอย่างมีนัยสำคัญต่อการกำจัดไฮโดรเจนซัลไฟด์

สาขาวิชาวิศวกรรมสิ่งแวดล้อม

ปีการศึกษา 2549

ลายมือชื่อนักศึกษา Sankiet Kruay Sawat

ลายมือชื่ออาจารย์ที่ปรึกษา Chaiyot

SOMKIAT KRUAYSAWAT : INCREASING ADSORPTION
EFFICIENCY OF ACTIVATED CARBON FOR H₂S REMOVAL
BY SURFACE OXIDATION AND METAL ADDITION. THESIS
ADVISOR : ASSOC. PROF. CHAIYOT TANGSATHITKULCHAI,
Ph.D., 207 PP. ISBN 974-533-500-2

ACTIVATED CARBON/ ADSORPTION/ H₂S REMOVAL/ SURFACE
OXIDATION

This research was undertaken to study the method of improving the adsorption capacity of activated carbon for H₂S by surface oxidation and metal addition techniques. The coconut shell-based activated carbon samples were pretreated with O₃ and HNO₃ oxidants. The oxidation techniques were used to introduce the functional groups such as C-O and/or C=O on the surface of activated carbon samples. These include, for example, hydroxyl, ketone, carboxylic acid, and ether structures and their existence were ascertained by FT-IR spectroscopy. Zinc acetate [Zn(C₂H₃O₂)₂] was used as an impregnant for the metal addition step after the carbon samples were oxidized with O₃ or HNO₃. A synthetic gas mixture of 1.01 wt % H₂S plus balance N₂ was used for the fixed-bed adsorption experiments. The outlet concentration of H₂S from the fixed-bed adsorber was followed as a function of time by an electrochemical sensor to be used for constructing the breakthrough curve. The breakthrough time and the adsorption capacity (mg H₂S adsorbed/g adsorbent) up to the breakthrough time was used to assess the efficiency of H₂S removal. Zn-impregnated samples gave higher adsorption capacity than the single-step oxidized samples and the untreated

samples at temperatures of 10, 30 and 45° C. The carbon sample treated with 6.0 M HNO₃ and Zn impregnation gave the highest adsorption capacity for H₂S, with increased adsorption efficiency of 230% (24.72 mg H₂S/g adsorbent) over that of the untreated sample at 45°C. The maximum increase of 180% (19.24 mg H₂S/g adsorbent) adsorption efficiency over that of untreated sample was observed for the O₃ oxidized sample impregnated with Zn. There was a tendency that the adsorption of H₂S increased with the amount of Zn impregnated on the surface sample at temperatures of adsorption higher than 45°C, indicating the significant role of chemisorption in H₂S removal.

School of Environmental Engineering

Academic Year 2006

Student's Signature Somkiat Kruaysawat

Advisor's Signature 

ACKNOWLEDGEMENTS

The author wishes to express his gratitude to Assoc. Prof. Dr. Chaiyot Tangsathitkulchai (thesis advisor) who has extended guidance and assistance to carry out this study and research work. He also express his thanks towards Assoc. Prof. Dr. Suntud Sirianuntapiboon, Asst. Prof. Dr. Sudjit Karuchit, Asst. Prof. Dr. Ratanawan Kiattikomol, and Dr. Jareeya Yimrattanabovorn for serving as dissertation examination committee members.

Likewise, special thanks are due to Asst. Prof. Dr. Ranjna Jindal and Assoc. Prof. Dr. Nurak Krissadanurak for giving valuable suggestions to prepare thesis proposal. Also, the author would like to express thanks to staff members of the school of environmental engineering, chemical engineering laboratory, and including laboratory supervisors of Suranaree University of Technology for their assistance.

In addition, he would like to acknowledge the valuable contributions from Sripatum University and Shell 100 Years Education Fund for the financial support of this work. He would also like to thank the C. Gigantic Carbon Co. Ltd., for the activated carbons used in this study.

Somkiat Kruaysawat

TABLE OF CONTENTS

	Page
ABSTRACT (THAI)	I
ABSTRACT (English).....	II
AcknowledgmentS	IV
Table of Contents	V
LIST OF TABLES	VIII
List of Figures	X
List of SYMBOLS Abbreviations	XXVI
 CHAPTER	
I INTRODUCTION	1
1.1 Statement of the Problem.....	1
1.2 Objectives of the Study	3
1.3 Hypothesis of the Study	4
1.4 Scope of the Study	4
1.5 Expected Results	5
II LITERATURE REVIEW	6
2.1 Adsorption.....	6
2.2 Surface Area and Capacity of the Adsorbent	8
2.3 Classification of Adsorption Isotherms	31

TABLE OF CONTENTS (Cont.)

	Page
2.4 Activated Carbon	29
2.5 Carbon Surface Modification by Oxidation.....	29
2.6 Ozone	31
2.7 Past Studies on Carbon Surface Oxidation	34
2.8 Chemisorption on Activated Carbon	41
III RESEARCH METHODOLOGY.....	46
3.1 Experimental Location.....	46
3.2 Materials and Methods.....	46
IV RESULTS AND DISSCUSSION	68
4.1 Properties of Activated Carbon Samples	68
4.2 FT-IR Spectroscopy	69
4.3 Boehm's Titration.....	87
4.4 Determination of Oxygen	89
4.5 Atomic Absorption Spectrometry Analysis.....	94
4.6 Nitrogen Isotherms	98
4.7 Surface Area and Porosity Analysis	101
4.8 H ₂ S Adsorption by Fixed Bed Activated Carbon	103

TABLE OF CONTENTS (Cont.)

	Page
V CONCLUSIONS AND RECOMENDATIONS	156
5.1 Conclusions.....	156
5.2 Recommendations.....	159
REFERENCES	161
APPENDICES	166
Appendix A FT-IR Spectra.....	166
Appendix B BET Isotherms.....	188
Appendix C Estimation of Flow Rate for Gas Fluidization.....	194
Appendix D Increasing Efficiency for H ₂ S Removal Calculation	197
Appendix E Specific Surface Areas and Porosity.....	200
Appendix F Selected Functional Groups	203
Appendix G Group Assignments in Infrared Spectra.....	205
BIOGRAPHY	207

LIST OF TABLES

Table	Page
2.1 Properties of some raw materials used in the manufacture of activated carbon.....	26
4.1 Properties of the original activated carbon sample used in the present study.....	69
4.2 Possible FT-IR peak assignments by FT-IR spectroscopy for the samples.....	71
4.2 Possible FT-IR peak assignments by FT-IR spectroscopy for the samples (continued).....	72
4.3 Total peak areas of some untreated and treated activated carbon samples examined by FT-IR spectroscopy.....	87
4.4 Results of Boehm's Titration.....	89
4.5 Oxygen content in the O ₃ oxidized carbon samples.....	92
4.6 Oxygen content in HNO ₃ oxidized carbon samples.....	93
4.7 Oxygen content in HNO ₃ oxidation followed by O ₃ oxidation.....	93
4.8 Effects of zinc acetate concentration and time on the uptake of zinc by the untreated activated carbon as analyzed by AA _s	95
4.9 The amount of zinc metal added to the oxidized activated carbon samples.....	97

LIST OF TABLES (Cont.)

Table	Page
4.10 Specific surface areas and porosities in activated carbon samples by N ₂ adsorption.....	102
4.11 Breakthrough times of HNO ₃ oxidation and Zn addition for exposure limits (TWA value).....	104
4.12 Breakthrough times of O ₃ oxidation and Zn addition for exposure limits (TWA Value).....	105
4.13 Increasing H ₂ S removal efficiency of treated carbon samples over that of original untreated sample.....	152
E.1 Specific surface areas in activated carbon samples by nitrogen adsorption.....	201
E.2 Porosity in activated carbon samples by nitrogen adsorption.....	202

LIST OF FIGURES

Figure	Page
2.1 The plot for the Langmuir adsorption isotherm.....	9
2.2 The plot for the Freundlich isotherm.....	10
2.3 The plot for the BET isotherm.....	12
2.4 The plot of the Dubinin-Radushkevich (DR) isotherm.....	13
2.5 The adsorption wave and breakthrough curve.....	16
2.6 Typical activated carbon adsorption isotherm.....	17
2.7 Types of isotherms for gaseous adsorption.....	19
2.8 Molecular screening in pores of activated carbons.....	24
2.9 Schematic representation of a constituent region of an activated carbon particle.....	24
2.10 Physical activation manufacture process.....	28
2.11 Resonance structures of ozone.....	31
2.12 Diagram of a generic corona cell	32
2.13 Lowther – type air – cooled plate ozone generator.....	34
3.1 Research methodology for the original sample.....	47
3.2 Research methodology for HNO ₃ oxidized sample.....	48
3.3 Research methodology for O ₃ oxidized sample.....	48
3.4 Diagram of HNO ₃ oxidation in a reflux column.....	50

LIST OF FIGURES (Cont.)

Figure	Page
3.5 Schematric diagram of ozone oxidation in a fluidized-bed reactor.....	51
3.6 An ozone generator (Model OZ-7500), type corona discharge.....	52
3.7 Ozone oxidation in a reflux column.....	52
3.8 A Fourier transform infrared spectroscopy.....	57
3.9 A special die for preparing KBr pellet.....	57
3.10 An elements analyzer CHNS/O	58
3.11 An atomic absorption spectrophotometer.....	61
3.12 An automatic surface analyzer.....	62
3.13 A scanning electron microscope (SEM).....	62
3.14 Schematic diagram of H ₂ S removal by activated carbon adsorption.....	64
3.15 Typical electrochemical sensor setup.....	65
3.16 Q-RAE PLUS monitor.....	65
3.17 Valve connection and regulator.....	67
4.1 Typical SEM images obtained from the original sample.....	69
4.2 The FT-IR spectrum of the original sample.....	74
4.3 Effect of preparation temperature for FT-IR spectra of the air oxidized samples at air flow rate 1.2 L/s for 90 min(oxidation temperature(°C): A=150, B=205, C=225, D=275).....	76

LIST OF FIGURES (Cont.)

Figure	Page
4.4 Effect of air flowrate FT-IR spectra of air oxidized samples at 275°C for 90 min(air flow rate (L/s): A=1.1, B=1.2, C=1.3).....	77
4.5 FT-IR spectra of ozone oxidized samples in fluidized-bed (oxidation flow rate 5.5 L/min at various temperatures and times of: A= 180°C, 30 min, B= 240°C, 30 min, C= 180°C, 90 min, D= 190°C, 60 min).....	79
4.6 Comparison of FT-IR spectra for the original sample (A) with ozone oxidized samples in a reflux column (O ₃ gas flow rate 1.5 L/min at various times of: B=60 min, C=120 min, D=180 min).....	80
4.7 Comparison of FT-IR spectra for the original sample (A) with ozone oxidized samples in a reflux column and metal (Zn) addition (O ₃ gas flow rate 1.5 L/min at various times of: B=60 min, C=120 min, D=180 min).....	81
4.8 Comparison of FT-IR spectra for the original sample (A) with HNO ₃ oxidized samples at 105°C for 120 min. (HNO ₃ concentration : B=2.0 M, C=6.0 M, D=10.0 M).....	83
4.9 FT-IR spectra for ozone oxidized samples (A=210°C, 90 min, in fluidized- bed, B=90°C, 60 min, in a reflux column) and HNO ₃ oxidized samples in a reflux column (C=6.0 M HNO ₃ , D=10.0 M HNO ₃).....	84
4.10 FT-IR spectrum for pure KBr (Merck, for spectroscopy).....	86

LIST OF FIGURES (Cont.)

Figure	Page
4.11 Initial zinc acetate concentrations in a solution of ion-exchange process for metal addition of the original samples effect to zinc uptake into activated carbon. Time = 90 min, T = 30°C.....	96
4.12 The times during ion-exchange process on metal addition of the original samples effect to zinc uptake into activated carbon. T= 30°C.....	96
4.13 Adsorption isotherms of N ₂ of activated carbons treated with HNO ₃ oxidation and Zn addition at 77 K.....	99
4.14 Adsorption isotherms of N ₂ on activated carbons treated with O ₃ oxidation and Zn addition at 77 K.....	100
4.15 Adsorption isotherms of N ₂ on the different treatments of activated carbons at 77 K.....	101
4.16 H ₂ S breakthrough curve for the original activated carbon sample. Gas composition: 1.01% H ₂ S, balance N ₂ . T = 10 °C, P = 1.0 bar.....	107
4.17 H ₂ S breakthrough curve for the original activated carbon sample. Gas composition: 1.01% H ₂ S, balance N ₂ . T = 30°C, P = 1.0 bar.....	108
4.18 H ₂ S breakthrough curve for the original sample. Gas composition: 1.01% H ₂ S + balance N ₂ (T = 45 °C, P = 1.0 bar).....	108

LIST OF FIGURES (Cont.)

Figure	Page
4.19 Comparison of H ₂ S breakthrough curves for the original activated carbon samples at various temperatures. Gas composition: 1.01% H ₂ S + balance N ₂ . P=1.0 bar.....	109
4.20 H ₂ S breakthrough curve for the original activated carbon sample after impregnated with Zn. Gas composition: 1.01% H ₂ S, T = 10°C.....	110
4.21 H ₂ S breakthrough curve for the original activated carbon sample after impregnated with Zn. Gas composition: 1.01% H ₂ S, T =45°C.....	110
4.22 Comparison of H ₂ S breakthrough times for the original activated carbon and the original impregnated with Zn samples at various temperatures, P=1.0 bar. Gas composition: 1.01% H ₂ S in balance N ₂	111
4.23 H ₂ S breakthrough curve for activated carbon sample after oxidized with 6.0 M HNO ₃ . Gas composition: 1.01% H ₂ S, balance N ₂ . T = 10°C, P = 1.0 bar.....	113
4.24 H ₂ S breakthrough curve for activated carbon sample after oxidized with 2.0 M HNO ₃ . Gas composition:1.01% H ₂ S, balance N ₂ . T = 30°C, P = 1.0 bar.....	114
4.25 H ₂ S breakthrough curve for activated carbon sample after oxidized with 6.0 M HNO ₃ . Gas composition: 1.01% H ₂ S, balance N ₂ . T = 30°C, P = 1.0 bar.....	115

LIST OF FIGURES (Cont.)

Figure	Page
4.26 H ₂ S breakthrough curve for activated carbon sample after oxidized with 10.0 M HNO ₃ . Gas composition: 1.01% H ₂ S, balance N ₂ . T = 30°C, P = 1.0 bar.....	116
4.27 H ₂ S breakthrough curve for activated carbon sample after oxidized with 6.0 M HNO ₃ . Gas composition: 1.01% H ₂ S, balance N ₂ . T = 45°C, P = 1.0 bar.....	117
4.28 Comparison of H ₂ S breakthrough curves for 6.0 M HNO ₃ oxidized samples with different temperatures, P=1.0 bar. Gas composition: 1.01% H ₂ S, balance N ₂	118
4.29 Comparison of H ₂ S breakthrough curves for 6.0 M HNO ₃ oxidized samples at 30°C with different concentration, P=1.0 bar. Gas composition: 1.01% H ₂ S, balance N ₂	119
4.30 H ₂ S breakthrough curve for activated carbon sample after 6.0 M HNO ₃ oxidized and impregnated with Zn Gas composition: 1.01% H ₂ S, balance N ₂ (T = 10°C, P = 1.0 bar).....	123
4.31 H ₂ S breakthrough curve for activated carbon sample after 6.0 M HNO ₃ oxidized and impregnated with Zn. Gas composition: 1.01% H ₂ S, balance N ₂ . T = 30°C, P = 1.0 bar.....	124

LIST OF FIGURES (Cont.)

Figure	Page
4.32 H ₂ S breakthrough curve for activated carbon sample after 10.0 M HNO ₃ oxidized and impregnated with Zn. Gas composition: 1.01% balance N ₂ . T = 30°C, P = 1.0 bar.....	125
4.33 H ₂ S breakthrough curve for activated carbon sample after 6.0 M HNO ₃ oxidized and impregnated with Zn. Gas composition: 1.01% H ₂ S, balance N ₂ . T = 45°C, P = 1.0 bar.....	126
4.34 H ₂ S breakthrough curve for activated carbon sample after 10.0 M HNO ₃ oxidized and impregnated with Zn Gas composition: 1.01% H ₂ S, balance N ₂ . T = 45°C, P = 1.0 bar.....	127
4.35 Comparison of H ₂ S breakthrough curves for 6.0 M HNO ₃ oxidized and Zn impregnated samples at various temperatures. Gas composition: 1.01% H ₂ S, balance N ₂ . P=1.0 bar.....	128
4.36 Comparison of H ₂ S breakthrough times for 6.0 M HNO ₃ oxidized only and impregnated with Zn samples at various temperatures, P=1.0 bar. Gas composition: 1.01% H ₂ S in balance N ₂	129
4.37 Comparison of H ₂ S breakthrough times for the original activated carbon and 6.0 M HNO ₃ oxidized and impregnated with Zn samples at various temperatures, P=1.0 bar. Gas composition: 1.01% H ₂ S in balance N ₂	130

LIST OF FIGURES (Cont.)

Figure	Page
4.38 Comparison of H ₂ S breakthrough times for 6.0 and 10.0 M HNO ₃ oxidized and impregnated with Zn samples at various temperatures, P=1.0 bar. Gas composition: 1.01% H ₂ S in balance N ₂	130
4.39 H ₂ S breakthrough curve for activated carbon sample after O ₃ oxidized (in fluidized-bed, 210°C, 90 min) and impregnated with Zn Gas composition: 1.01% H ₂ S, balance N ₂ . T=10°C, P=1.0 bar.....	132
4.40 H ₂ S breakthrough curve for activated carbon sample after O ₃ oxidized (in a reflux column, 90°C, 60 min) and impregnated with Zn. Gas composition: 1.01 % H ₂ S, balance N ₂ . T=10°C, P=1.0 bar.....	133
4.41 H ₂ S breakthrough curve for activated carbon sample after O ₃ oxidized (in a reflux column, 90°C, 120 min) and impregnated with Zn. Gas composition: 1.01% H ₂ S, balance N ₂ . T=10°C, P=1.0 bar.....	134
4.42 H ₂ S breakthrough curve for activated carbon sample after O ₃ oxidized (in a reflux column, 90°C, 180 min) and impregnated with Zn. Gas composition: 1.01 % H ₂ S, balance N ₂ . T=10°C, P=1.0 bar.....	135
4.43 H ₂ S breakthrough curve for activated carbon sample after O ₃ oxidized (in fluidized-bed, 210°C, 90 min) and impregnated with Zn. Gas composition: 1.01 % H ₂ S, balance N ₂ . T= 30°C, P=1.0 bar.....	136

LIST OF FIGURES (Cont.)

Figure	Page
4.44 H ₂ S breakthrough curve for activated carbon sample after O ₃ oxidized (in fluidized-bed, 210°C, 90 min) and impregnated with Zn. Gas composition: 1.01% H ₂ S, balance N ₂ . T= 30°C, P=1.0 bar.....	137
4.45 H ₂ S breakthrough curve for activated carbon sample after O ₃ oxidized (in a reflux column, 90°C, 60 min) and impregnated with Zn. Gas composition: 1.01% H ₂ S, balance N ₂ . T= 30°C, P=1.0 bar.....	138
4.46 H ₂ S breakthrough curve for activated carbon sample after O ₃ oxidized (in a reflux column, 90°C, 120 min) and impregnated with Zn. Gas composition: 1.01% H ₂ S, balance N ₂ . T= 30°C, P=1.0 bar.....	139
4.47 H ₂ S breakthrough curve for activated carbon sample after O ₃ oxidized (in a reflux column, 90°C, 180 min) and impregnated with Zn. Gas composition: 1.01% H ₂ S, balance N ₂ . T= 30°C, P=1.0 bar.....	140
4.48 H ₂ S breakthrough curve for activated carbon sample after O ₃ oxidized (in fluidized-bed, 210°C, 90 min) and impregnated with Zn. Gas composition: 1.01% H ₂ S, balance N ₂ . T= 45°C, P=1.0 bar.....	141
4.49 H ₂ S breakthrough curve for activated carbon sample after O ₃ oxidized (in a reflux column, 90°C, 60 min) and impregnated with Zn. Gas composition: 1.01% H ₂ S, balance N ₂ . T= 45°C, P=1.0 bar.....	142

LIST OF FIGURES (Cont.)

Figure	Page
4.50 H ₂ S breakthrough curve for activated carbon sample after O ₃ oxidized (in a reflux column, 90°C, 120 min) and impregnated with Zn. Gas composition: 1.01% H ₂ S, balance N ₂ . T= 45°C, P=1.0 bar.....	143
4.51 Comparison of H ₂ S breakthrough curves for O ₃ oxidized and Zn impregnated samples at 10°C, P=1.0 bar, with different conditions. Gas composition: 1.01% H ₂ S, balance N ₂	144
4.52 Comparison of H ₂ S breakthrough curves for O ₃ oxidized and Zn impregnated samples at 30°C, P=1.0 bar, with different conditions. Gas composition: 1.01% H ₂ S, balance N ₂	145
4.53 Comparison of H ₂ S breakthrough curves for O ₃ oxidized and Zn impregnated samples at 45°C, P=1.0 bar, with different conditions. Gas composition: 1.01% H ₂ S, balance N ₂	146
4.54 The H ₂ S outlet concentration values (ceiling limit = 20 ppm) of O ₃ oxidized and impregnated with Zn samples at 10°C, P=1.0 bar with various conditions. Gas composition: 1.01% H ₂ S in balance N ₂	147
4.55 The H ₂ S outlet concentration values (ceiling limit = 20 ppm) of O ₃ oxidized and impregnated with Zn samples at 30°C, P=1.0 bar with various conditions. Gas composition: 1.01% H ₂ S in balance N ₂	147

LIST OF FIGURES (Cont.)

Figure	Page
4.56 The H ₂ S outlet concentration values (ceiling limit = 20 ppm) of O ₃ oxidized and impregnated with Zn samples at 45°C, P=1.0 bar with various conditions. Gas composition: 1.01% H ₂ S in balance N ₂	148
4.57 The geometry of [Zn (H ₂ S) ₄] ²⁺ complex ion.....	149
4.58 The orbitals of Zn ²⁺ ion.....	149
4.59 The orbitals of Zn ²⁺ and sp ³ hybrid orbitals.....	149
4.60 The orbitals of [Zn (H ₂ S) ₄] ²⁺ complex ion.....	150
4.61 Comparison of increasing %H ₂ S removal at 20 ppm for different treated samples at 10°C (adsorption temperature), P=1.0 bar. Gas composition: 1.01% H ₂ S in balance N ₂	153
4.62 Comparison of increasing %H ₂ S removal at 20 ppm for different treated samples at 30°C (adsorption temperature), P=1.0 bar. Gas composition: 1.01% H ₂ S in balance N ₂	154
4.63 Comparison of increasing %H ₂ S removal at 20 ppm for different treated samples at 45°C (adsorption temperature), P=1.0 bar. Gas composition: 1.01% H ₂ S in balance N ₂	155
A.1 The original sample from the company.....	167
A.2 An air oxidized sample in fluidized-bed at 150°C, flow rate 1.2 L/s, 90 min.....	167

LIST OF FIGURES (Cont.)

Figure	Page
A.3 An air oxidized sample in fluidized-bed at 205°C, flow rate 1.2 L/s, 100 min.....	168
A.4 An air oxidized sample in fluidized-bed at 225°C, flow rate 1.2 L/s, 90 min.....	168
A.5 An air oxidized sample in fluidized-bed at 275°C, flow rate 1.2 L/s, 90 min.....	169
A.6 An air oxidized sample in fluidized-bed at 275°C, flow rate 1.1 L/s, 90 min.....	169
A.7 An air oxidized sample in fluidized-bed at 275°C, flow rate 1.3 L/s, 90 min.....	170
A.8 An air oxidized sample in fluidized-bed at 245°C, flow rate 1.3 L/s, 90 min.....	170
A.9 An air oxidized sample in fluidized-bed at 265°C, flow rate 1.1 L/s, 90 min.....	171
A.10 An air oxidized sample in fluidized-bed at 225°C, flow rate 1.1 L/s, 90 min.....	171
A.11 An air oxidized sample in fluidized-bed at 225°C, flow rate 1.1 L/s, 30 min.....	172

LIST OF FIGURES (Cont.)

Figure	Page
A.12 An air oxidized sample in fluidized-bed at 180° flow rate 5.5 L/min, 90 min.....	172
A.13 An oxygen oxidized sample in fluidized-bed at 180°C, flow rate 5.5 L/min, 90min.....	173
A.14 An ozone oxidized sample in fluidized-bed at 150°C flow rate 5.5 L/min, 30min.....	173
A.15 An ozone oxidized sample in fluidized-bed at 150°C, flow rate 5.5 L/min, 60min.....	174
A.16 An ozone oxidized sample in fluidized-bed at 90°C, flow rate 5.5 L/min, 30min.....	174
A.17 An ozone oxidized sample in fluidized-bed at 180°C, flow rate 5.5 L/min, 30min.....	175
A.18 An ozone oxidized sample in fluidized-bed at 240°C, flow rate 5.5 L/min, 30min.....	175
A.19 An ozone oxidized sample in fluidized-bed at 190°C, flow rate 5.5 L/min, 60min.....	176
A.20 An ozone oxidized sample in fluidized-bed at 180°C, flow rate 5.5 L/min, 90min.....	176

LIST OF FIGURES (Cont.)

Figure	Page
A.21 A 2.0 M nitric acid oxidized sample in a reflux column at 100°C, 30 min.....	177
A.22 A 2.0 M nitric acid oxidized sample in a reflux column at 100°C, 60min.....	177
A.23 A 2.0 M nitric acid oxidized sample in a reflux column at 100°C, 120 min.....	178
A.24 A 4.0 M nitric acid oxidized sample in a reflux column at 105°C, 120 min.....	178
A.25 A 6.0 M nitric acid oxidized sample in a reflux column at 105°C, 120 min.....	179
A.26 A 8.0 M nitric acid oxidized sample in a reflux column at 105°C,120 min.....	179
A.27 A 10.0 M nitric acid oxidized sample in a reflux column at 120 min.....	180
A.28 A 2.0 M nitric acid oxidation sample in a reflux column at 100°C, 120 min, and repeated that with ozone oxidation for 30 min.....	181
A.29 A 6.0 M nitric acid oxidation sample in a reflux column at 105°C, 120 min, and repeated that with ozone oxidation for 30 min.....	182

LIST OF FIGURES (Cont.)

Figure	Page
A.30 A 10.0 M nitric acid oxidation sample in a reflux column at 105°C, 120 min, and repeated that with ozone oxidation for 30 min.....	183
A.31 An ozone oxidized sample in a reflux column (hot water 90°C), 60 min.....	183
A.32 An ozone oxidized sample in a reflux column (hot water 90°C), 60 min and Zn addition.....	184
A.33 An ozone oxidized sample in a reflux column (hot water 90°C), 120 min.....	184
A.34 An ozone oxidized sample in a reflux column (hot water 90°C), 120 min and Zn addition.....	185
A.35 An ozone oxidized sample in a reflux column (hot water 90°C), 180 min.....	186
A.36 An ozone oxidized sample in a reflux column (hot water 90°C), 180 min and Zn addition.....	187
B.1 Nitrogen adsorption isotherm at 77 K for the original activated carbon sample from the C-Gigantic company.....	189
B.2 Nitrogen adsorption isotherm at 77 K for the original activated carbon sample from the C-Gantic company after metal (Zn) addition.....	189
B.3 Nitrogen adsorption isotherm at 77 K for activated carbon sample after nitric acid (6 M) oxidation.....	190

LIST OF FIGURES (Cont.)

Figure	Page
B.4 Nitrogen adsorption isotherm at 77 K for activated carbon sample after nitric acid (6 M) oxidation and metal (Zn) addition.....	190
B.5 Nitrogen adsorption isotherm at 77 K for activated carbon sample after nitric acid (10 M) oxidation and metal (Zn) addition.....	191
B.6 Nitrogen adsorption isotherm at 77 K for activated carbon sample after ozone oxidation (in fluidized-bed, 90 min) and metal (Zn) addition.....	191
B.7 Nitrogen adsorption isotherm at 77 K for activated carbon sample after ozone oxidation(in hot water, 60 min) and metal (Zn) addition.....	192
B.8 Nitrogen adsorption isotherm at 77 K for activated carbon sample after ozone oxidation(in hot water, 120 min) and metal (Zn) addition.....	192
B.9 Nitrogen adsorption isotherm at 77 K for activated carbon sample after ozone oxidation(in hot water, 180 min) and metal (Zn) addition.....	193
F.1 Select functional group.....	204
G.1 Group Assignments in Infrared Spectra.....	206

LIST OF SYMBOLS AND ABBREVIATION

A	=	Surface area (m^2g^{-1})
AA _s	=	Atomic Absorption Spectroscopy
B	=	Affinity constant or Langmuir constant being a function of temperature.
C _e	=	Equilibrium concentration of adsorbate after adsorption
C	=	Constant
cm^{-1}	=	Wavenumber
°C	=	Degree Celcius
BET	=	Brunauer-Emmett-Teller
DR	=	Dubinin-Radushkevich
E _o	=	Characteristic adsorption energies (kJ mol^{-1})
FT-IR	=	Fourier transform infrared
g	=	Gram
K	=	Kelvin
K _f , n	=	Empirical constants
L	=	Liter
M	=	Molar, concentration of solution (mol/dm^3)
min	=	Minute
mg	=	Milligram
nm	=	Nanometer
N _{AV}	=	Avogadro number ($6.02 \times 10^{23} \text{ mol}^{-1}$)
P	=	Pressure

LIST OF SYMBOLS AND ABBREVIATION (Cont.)

P/P^0	=	Relative pressure
P	=	The equilibrium pressure of adsorption
P^0	=	Vapor pressure of adsorbate
s	=	Second
SEM	=	Scanning Electron Microscope
T	=	Temperature
wt	=	Weight
V	=	Volume of adsorbed gas at equilibrium
V_m	=	Volume of adsorbed gas required to cover the surface of adsorbent with a single layer of molecules (a monolayer)
w_0	=	The total volume of the micropore system ($\text{cm}^3 \text{g}^{-1}$) or the adsorption potential $\{A = -RT(P/P^0), \text{kJ mol}^{-1}\}$
x	=	Relative pressure (P/P^0)
x/m	=	Amount adsorbate adsorbed per unit weight of adsorbent (carbon)
β	=	Affinity coefficient ($\text{NH}_3 = 0.315$, $\text{H}_2\text{S} = 0.484$)
σ_{N_2}	=	The projected area covered by a nitrogen molecule (0.162 nm^2)
μm	=	Micrometer
u_{mf}	=	Minimum fluidization velocity
v_s	=	Symmetric vibration
v_{as}	=	Asymmetric vibration

CHAPTER I

INTRODUCTION

1.1 Statement of the problem

Hydrogen sulfide is a colorless, highly flammable gas, which in low concentrations has an offensive odor similar to that of rotten eggs. Hydrogen sulfide is a toxic gas that is extremely poisonous even present in very small quantities. Although the odor of hydrogen sulfide can be detected at a very low concentration (less than 10 ppm), the sense of smell is lost in just a few minutes after exposure, due to olfactory fatigue. This makes it impossible to sense the level of dangerous concentrations. Inhaling hydrogen sulfide at a few hundred ppm may result in acute poisoning (Chou, 2000).

Hydrogen sulfide is a by-product of oil and gas production operations. It is contained within gas or crude oil underground. Alternatively, hydrogen sulfide can be produced by microbial decay of sulfur compounds and microbial reduction of sulfate, from geothermal steam, wood pulping, and a number of miscellaneous natural sources (Manahan, 1993). In addition, hydrogen sulfide is also released during the decaying of organic materials such as in sewage treatment plants. However, it finds many applications in various industries, for example, in the preparation of metallic sulfides, phosphorus, and oil additives (Chou, 2000).

Adsorption is a simple and inexpensive operation for removing process gases and vapors from the air, for example, by passing them through an adsorption bed

packed with a porous adsorbent. Air purification by adsorption can be effective where the pollutants are emitted even at very low concentrations (below 100 ppm) but needs to be controlled because of their highly malodorous or toxic nature (Theodore and Buonicore, 1994). Among various available adsorbents, activated carbon is most commonly used in odor control applications. It can be produced from a variety of carbonaceous feedstocks such as wood, coal, coconut shell, nutshells, and petroleum-based products (Mycock, McKenna, and Theodore, 1995). Although adsorption by activated carbon can be effectively used for air purification but this can not solve the problem entirely. In general, any organic compounds having molecular weight greater than 45 is likely to be effectively adsorbed on activated carbon (Noll, Gounaris, and Hou, 1992). However the efficiency of activated carbon is poor for low molecular weight gas, in particular H_2S (Spengler, Samet, and McCathy, 2000). These problems have motivated and created interest to study the use of adsorption by increasing the adsorptive efficiency of activated carbon for H_2S elimination from wastewater treatment plants. This is because large quantities of wastewater generated from chemical and refinery operations must be treated. These effluents are also a source for malodorous elements. H_2S can produce objectionable odor through open tanks, channels, and leaks in sewer systems (Cheremisinoff, 1993). Efficiency of adsorption can be enhanced by increasing the functional groups such as C-O and / or C=O on the surface of activated carbon by oxidation, resulting in more active polar adsorption sites. The main aim of oxidation of a carbon surface is obtaining a more hydrophilic surface structure with a relatively large number of oxygen-containing surface groups. Because the oxygen-containing groups behave as acids or bases, which possess ion-exchange properties (Jae-Woon, et al., 2001). This can be used in

the preparation of carbon-supported transition metal catalysts by exchange with cationic metal complexes. One of the process for increasing the concentration of functional groups is by oxidation. For example, hot air, oxygen gas, potassium hydroxide (KOH), phosphoric acid (H_3PO_4) or nitric acid (HNO_3) may be used as oxidizing agents. HNO_3 is a strong oxidizing agent and is popularly used for increasing the functional groups on activated carbon surface. However, this is a complicated procedure, since it has a high operating cost and requires considerable electrical energy (Cal, Strickler, and Lizzio, 2000). Alternatively, an ozone (O_3) oxidation process may be a good choice because it is a stronger oxidizing agent compound than HNO_3 . In this study attempt was made to improve the adsorption of H_2S by introducing acid surface functional groups on the activated carbon using O_3 and HNO_3 as oxidants and also by the addition of zinc via an ion-exchange (IE) process to further enhance the capture efficiency for H_2S . The transition metal, such as Zn has unfilled low-energy d orbitals that can accept electron pairs from the Lewis base (H_2S) to form coordination compound $[\text{Zn}(\text{H}_2\text{S})_4]^{2+}$ (Birk, 1994).

1.2 Objectives of the Study

- 1.2.1 To introduce and identify the functional groups on activated carbon surfaces after pretreating them by ozone and nitric acid oxidation, respectively.
- 1.2.2 To investigate the efficiency of hydrogen sulfide adsorption by activated carbon samples after pretreating them with nitric acid oxidation and metal addition, and ozone oxidation and metal addition.

1.3 Hypothesis of the Study

Increasing efficiency of hydrogen sulfide adsorption by activated carbon samples pretreated with ozone, nitric acid and metal-zinc addition are the better adsorbents in comparison with the original activated carbon sample for malodorous elimination and control.

1.4 Scope of the Study

- 1.4.1 To study surface treatments of activated carbons by ozone oxidation, nitric acid oxidation and metal(Zn) addition.
- 1.4.2 To study the adsorption of low molecular weight gases by activated carbon with hydrogen sulfide gas being used as a representative gas.
- 1.4.3 A synthetic mixture of hydrogen sulfide and nitrogen gases would be prepared for the adsorption experiments. Nitrogen gas is the carrier gas.
- 1.4.4 H₂S adsorption in a fixed-bed adsorber would be carried out for various types of pretreated activated carbon samples at constant temperatures. The efficiency of adsorbent would be evaluated by following the outlet concentrations of hydrogen sulfide as a function of time to obtain the breakthrough curves.
- 1.4.5 The effect of temperature on H₂S adsorption in the fixed-bed mode would be investigated.

1.5 Expected Results

- 1.5.1 We can apply the techniques developed from this work for treating other gases having low molecular weights e.g. ammonia gas and formaldehyde from chemical and petroleum industries.
- 1.5.2 We can increase adsorption efficiency of activated carbon for H₂S removal by surface oxidation and metal addition at the various temperatures of 10, 30, and 45°C.

CHAPTER II

LITERATURE REVIEW

2.1 Adsorption

Adsorption is a process where molecules from the gas phase or liquid (solution) are concentrated in a condensed layer on a solid or liquid surface. The molecules that bind to the surface are called the adsorbate or sorbate while the substance that holds the adsorbate is called adsorbent. The reverse process of removal of the adsorbed molecules from the adsorbent surface is called desorption. In any solid or liquid, atoms at the surface are subject to unbalanced forces of attraction normal to the surface plane. In order to understand the fundamentals of adsorption, it is useful to distinguish between physical adsorption, involving only relatively weak intermolecular forces, and chemical adsorption, which involves essentially the formation of a chemical bond between the sorbate molecules and the adsorbent surface.

2.1.1 Physical Adsorption

Physical adsorption on the non-polar solids surface is attributed to the forces of interactions between the solid surface and adsorbate molecules that are similar to the van der Waals forces between molecules. Nearly all vapors tend to adsorb onto inorganic solids at temperatures not too much above their boiling point. The intermolecular attractive forces which cause vapors to adsorb (or condense) are generally dominated by the London dispersion (instantaneous dipole) forces, an

attraction caused by the perturbation of electron cloud by adjacent atoms. These forces, generally proportional to the product of the polarizability per unit volume, are much stronger for most inorganic solids than for water or organic materials, and that is why inorganic solids are the stronger adsorbents.

Physical adsorption is not site specific and no covalent bonds occur between the adsorbent and the adsorbate. The adsorbed molecules are free to cover the entire surface. This enables surface area measurements of a solid adsorbent. Some amount of heat is released during the adsorption process. The heat of physical adsorption (15-20 kcal/mol) is low compared to that of chemical adsorption (20-30 kcal/mol). The upper limit for physical adsorption may be higher than 20 kcal/mol for adsorbents with very narrow pores (Noll et al., 1992).

2.1.2 Chemical Adsorption

Chemical adsorption involves the force of attraction related to the chemical bonding between adsorbate molecules and solid atoms by electron exchange or through two electrons sharing by two atoms. Such force of attraction is stronger than in physical adsorption. Chemisorbed molecules are linked to reactive parts of the surface and the adsorption is necessarily confined to a monolayer. In contrast, chemical adsorption is site specific, chemisorbed molecules are fixed at specific sites. An activation energy is often involved in chemical adsorption and at low temperature the system may be not have sufficient thermal energy to attain thermodynamic equilibrium.

2.2 Surface Area and Capacity of the Adsorbent

An adsorption isotherm gives the relationship between the concentration of adsorbate and the amount of the adsorbate at a given temperature that will be adsorbed at equilibrium on the adsorbent surface. Some isotherms, like the Langmuir isotherm and Freundlich isotherm are appropriate for some uses. The other two isotherms that a user of activated carbon should be aware of are the BET and the Dubinin-Radushkevich isotherms (Spengler et al., 2000).

2.2.1 Langmuir Isotherm

Due to the nature of Langmuir's derivation of the adsorption isotherm, it is valid only for unimolecular layer adsorption (Karl and Charles, 2002). The derivation of the Langmuir adsorption isotherm for a single gas component involves five implicit assumptions :

1. The adsorbed gas behaves ideally in the vapor phase.
2. The adsorption gas is confined to a monomolecular layer.
3. The surface is homogeneous, that is, the affinity of each binding site for gas molecules is the same.
4. There is no lateral interaction between adsorbate molecules.
5. The adsorbed gas molecules are localized, that is, they do not move around on the surface.

The Langmuir adsorption isotherm is shown as Equation (2.1).

$$(V/V_m) = [bP/(1+bP)] \quad (2.1)$$

Equation (2.1) can be linearized as:

$$(P/V) = (1/bV_m) + (P/V_m) \quad (2.2)$$

Where, V = amount of gas adsorbed

V_m = amount of monolayer coverage

b = affinity constant or Langmuir constant being a function of temperature

P = the equilibrium pressure of adsorption

By measuring P and V and plot P/V versus P , the slope of the straight line obtained is $1/V_m$, and the intercept is $1/(bV_m)$ as demonstrated in Figure 2.1.

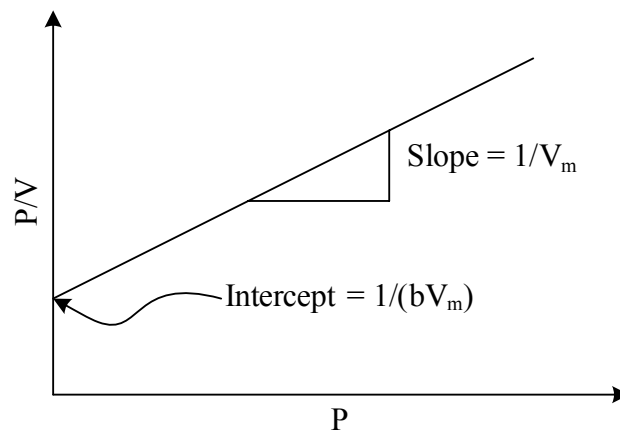


Figure 2.1 The plot for the Langmuir adsorption isotherm

2.2.2 Freundlich Isotherm

The Freundlich isotherm is used most commonly to describe the adsorption characteristics of the activated carbon used in water and water treatment (Tchobanoglous et al., 2003). It is also applicable in gas phase systems having heterogeneous surface, providing the range of pressure is not too wide as this isotherm equation does not have a proper Henry law behavior at low pressure, and it does not have a finite limit when pressure is sufficiently high (Do, 1998). Therefore,

it is generally valid in the narrow range of adsorption data. This equation is defined as the following form:

$$x/m = K_f C_e^{(1/n)} \quad (2.3)$$

where, x/m = amount adsorbate adsorbed per unit weight of adsorbent (carbon)

K_f, n = empirical constants

C_e = equilibrium concentration of adsorbate after adsorption

Equation (2.3) can be linearized as:

$$\log \left(\frac{x}{m} \right) = \log K_f + \frac{1}{n} \log C_e \quad (2.4)$$

The constants in the Freundlich isotherm can be determined by plotting (x/m) versus C_e as shown in Figure 2.2. The Freundlich isotherm equation may be derived by assuming a heterogeneous surface with adsorption on each class of sites that obey the Langmuir equation. According to the Freundlich equation, the amount adsorbed increases infinitely with increasing concentration or pressure. At low concentration, this equation does not reduce to the linear isotherm.

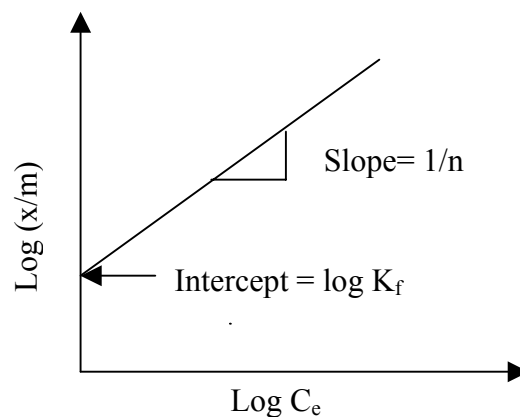


Figure 2.2 The plot for the Freundlich isotherm.

2.2.3 The Brunauer-Emmett-Teller (BET) Isotherm

The BET isotherm is very useful in describing the adsorption of light gases, especially at low temperatures, such as at the temperature of liquid nitrogen. This isotherm is represented by Equation (2.5) and shown plotted in Figure 2.3 (Spengler et al., 2000).

$$\frac{X}{V(1-X)} = \frac{(C-1)X}{V_m C} + \frac{1}{V_m C} \quad (2.5)$$

where, X = relative pressure (P/P^0)

P^0 = vapor pressure of adsorbate

V = volume of adsorbed gas at equilibrium

V_m = volume of adsorbed gas required to cover the surface of adsorbent
with a single layer of molecules (a monolayer)

C = constant

The BET isotherm is also important because it allows the determination of the surface area of an adsorbent. If the left hand side of Equation (2.5) is plotted against x , a straight line would be obtained as shown in Figure 2.3 with a slope of $(C-1)/V_m C$ and the intercept of $1/(V_m C)$. Thus, from the slope and y intercept of this line, V_m can be determined, and if the surface covered by an individual molecule is known, the surface area of the adsorbent can be calculated by using Equation (2.6).

$$A = V_m N_{AV} \sigma_{N_2} \quad (2.6)$$

where, A = Surface area ($m^2 g^{-1}$)

V_m = Volume of adsorbed gas required to cover the surface of adsorbent
with a single layer of molecules (a monolayer) ($mol g^{-1}$)

N_{AV} = Avogadro number ($6.02 \times 10^{23} mol^{-1}$)

σ_{N_2} = The projected area covered by a nitrogen molecule (0.162 nm²)

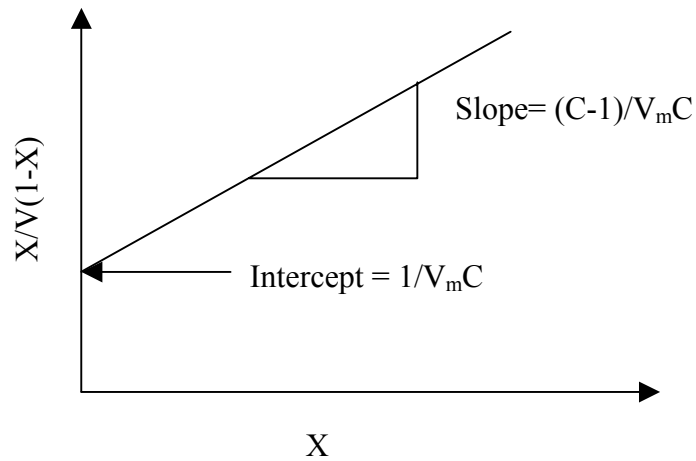


Figure 2.3 The plot for the BET isotherm

2.2.2 The Dubinin-Radushkevich Isotherm (DR)

The Dubinin-Radushkevich isotherm, as shown in Equation (2.7), has been found to give better result in the adsorption of large molecules, such as volatile organic compounds (Spengler et al., 2000). The basis of this equation is the assumption that the activated carbon contains micropores in which the adsorbed organic vapors can condense out in the form of a liquid. (Spengler et al., 2000).

$$\ln(w) = \ln(w_0) - \left(\frac{A}{\beta E_0} \right)^2 \quad (2.7)$$

Equation (2.7) can be rewritten as:

$$\ln(w) = \ln(w_0) - \left[\left(\frac{1}{E_0} \right)^2 \left(\frac{A}{\beta} \right)^2 \right] \quad (2.8)$$

where , w_0 = the total volume of the micropore system ($\text{cm}^3 \text{g}^{-1}$)

A = the differential molar work or the change of Gibbs free energy (ΔG , kJ mol^{-1}) or the adsorption potential $\{A = -RT (P/P^0), \text{kJ mol}^{-1}\}$

E_0 = characteristic adsorption energies (kJ mol^{-1})

β = affinity coefficient ($\text{NH}_3 = 0.315$, $\text{H}_2\text{S} = 0.484$)

w = the volume of gas adsorbed

If the function of $(A/\beta)^2$ and $\ln(w)$ of Equation (2.8) is plotted, a straight line would be obtained as shown in Figure 2.4 with a slope of $(1/E_0)^2$ and intercept of $\ln(w_0)$. Average micropore size (L) would be estimated from the value $L = K/E_0$ where K would be taken to be $17.25 \text{ kJ nm mol}^{-1}$. Thus, DR isotherm can be used to determine E_0 and w_0 (Lee and Reucroft, 1999b).

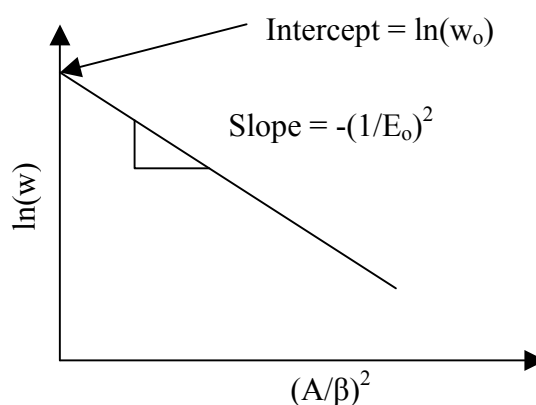


Figure 2.4 The plot of the Dubinin-Radushkevich (DR) isotherm.

2.2.5 Fixed-Bed Adsorption Systems

Adsorption applications in air pollution control generally involve the use of dynamic system. The adsorbent is generally used in a fixed-bed, and contaminated

air is passed through the adsorbent bed. Depending on the concentration, the contaminant is either recovered or discarded when the loading of the adsorbent requires regeneration. Although isotherms are indicative of the efficiency of an adsorbent for a particular adsorbate removal, they do not supply data to enable the calculation of contact time or the amount of adsorbent required to reduce the contaminant concentration below the required limits (Cheremisinoff, 1993). Dynamic adsorption results are expressed in term of dynamic capacity, or breakthrough capacity at given inlet concentrations, temperatures, and flow rate conditions of the bed, together with the bed dimensions. It is important that the adsorber bed should be least as long as the transfer zone length of the key component to be adsorbed. Therefore, it is necessary to know the depth of this mass transfer zone.

2.2.5.1 Mass Transfer Zone

As more gas is passed through and adsorption proceeds, the saturated zone moves forward until the breakthrough point is reached, at which time the exit concentration begins to rise rapidly above whatever limit has been fixed as the desirable maximum adsorbate level of the fluid. If the passage of the fluid is continued on still further, the exit concentration continues to rise until it becomes substantially the same as the inlet concentration. At this point, the bed is fully saturated. While the concentration when saturated is a function of the material used and the temperature at which it is operated, the dynamic capacity is also dependent on the operating conditions, such as inlet concentration, fluid flow rate, and bed depth. The dependence of inlet concentration and fluid flow rate arises from heat effect and mass transfer rate, but then dependence on bed depth, as can be seen from the above description depends on the relative sizes of unsaturated and saturated

zones. The zone of the bed where the concentration gradient is present or the area of the granular activated carbon bed in which sorption is occurring is often called the mass transfer zone (MTZ). The dynamics of fixed-bed adsorption are shown graphically in Figure 2.5. In the upper part of the figure, a fixed-bed is shown at three different times representing the interval from the initial admission of adsorbate to the time at which a significant concentration of adsorbate breaks through the bed. The plot in lower half of the figure depicts the effluent concentration from the bed as a function of the volume of effluent, or time of operation. This type of plot is called breakthrough curve, and provides valuable information on the adsorption rate in the bed (Cooper and Alley, 2002). During depletion of the bed, an active adsorption zone (AZ) moves through the bed. Behind the AZ, the adsorbent is saturated, whereas in front of the AZ, the bed is virtually free of adsorbate. The length (or height) of the zone is a function of the rate of transfer of adsorbate from the gas to the adsorbent. A shallow AZ indicates good adsorbent utilization and is represented by a steep breakthrough curve. Conversely, a wide or deep AZ denotes poor bed utilization and indicated by a gradual slope on the breakthrough curve. The length of the AZ determines the minimum depth of the adsorbent bed.

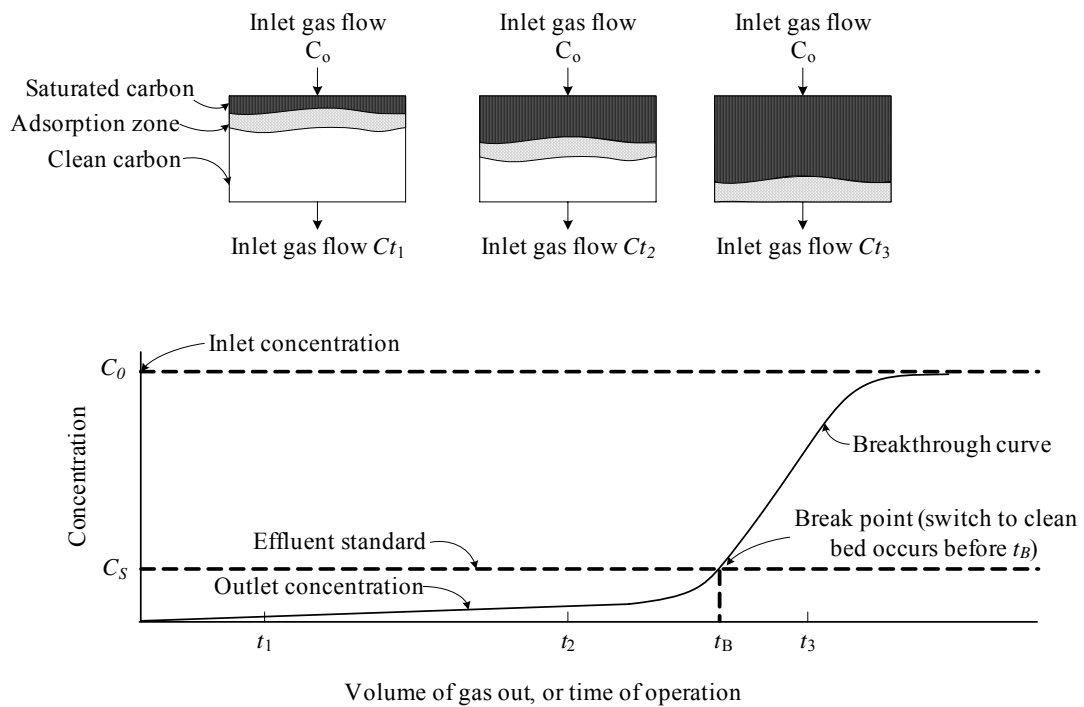


Figure 2.5 The adsorption wave and breakthrough curve (Cooper and Alley, 2002).

2.2.5.2 Carbon Adsorption Capacity

The adsorptive capacity of a given carbon estimated from isotherm data are plotted and shown in Figure 2.6. It can be estimated by extending a vertical line from the point on the horizontal axis corresponding to the initial concentration C_o , and extrapolating the isotherm to intersect this line. The $q_e = (x/m)_{C_o}$ value at the point of intersection can be read from the vertical axis. The $(q_e)_{C_o}$ value presents the amount of constituent adsorbed per unit weight of carbon when the carbon is at equilibrium with the initial concentration of constituent C_o . The equilibrium condition generally exists in the upper section of a carbon bed during column treatment, and it therefore represents the ultimate capacity of the carbon for a particular waste (Tchobanoglous et al., 2003).

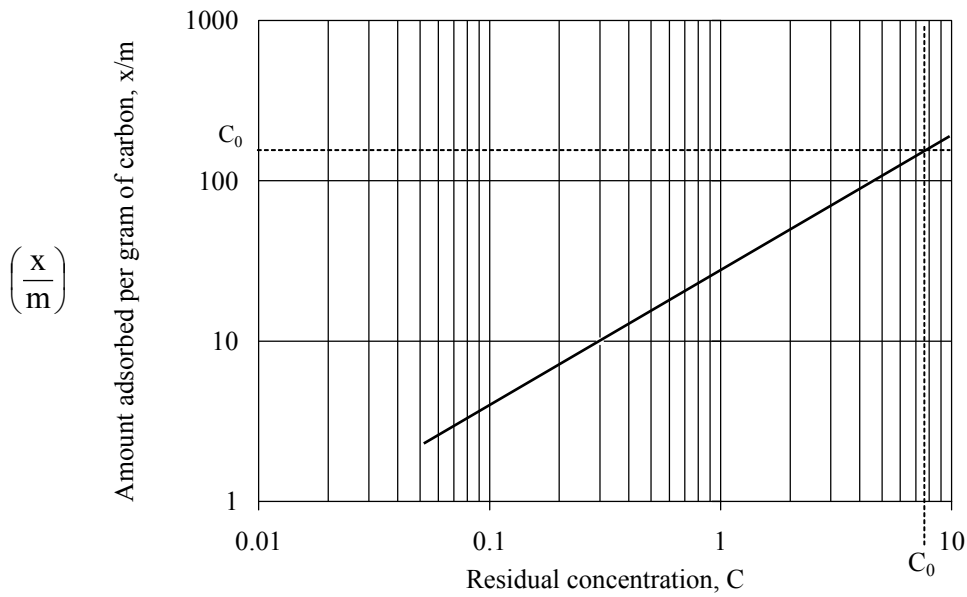


Figure 2.6 Typical activated carbon adsorption isotherm (Tchobanoglous et al., 2003).

2.2.5.3 Breakthrough Adsorption Capacity

The breakthrough adsorption capacity $(x/m)_b$ of the granular activated carbon in the full-scale column is some percentage of the theoretical adsorption capacity found from the isotherm. The $(x/m)_b$ of a single column can be assumed to be approximately 25 to 50 percent of the theoretical capacity, $(x/m)_o$. The value of $(x/m)_b$ can be determined using the small-scale column test. The time to breakthrough (t_b) can be approximated by solving the following Equation (2.9) for t_b (Tchobanoglous et al., 2003).

$$(x/m) = x_b/m_{GAC} = Q(C_o - C_b/2) t_b/m_{GAC} \quad (2.9)$$

Where, $(x/m)_b$ = field breakthrough adsorption capacity, g/g

x_b = mass of organic material adsorbed in the GAC column at
breakthrough, g

m_{GAC} = mass of carbon in the column, g

Q = flow rate, m³/d

C_o = influent concentration, g/m³

C_b = breakthrough concentration, g/m³

t_b = time to breakthrough, d

2.2.5.4 Adsorbent Bed Depth

Bed depth on adsorption mass transfer has two effects. First, it is important that the bed be deeper than the length of the transfer zone which is unsaturated. The second is that any multiplication of the minimum bed depth gives more than proportional increased capacity. Generally, it is advantageous to size the adsorbent bed to the maximum length allowed by pressure drop considerations. The determination of the depth of the mass transfer zone (MTZ) or unsaturated depth may be determined by experiment through the use of in Equation (2.10) (Cheremisinoff, 1993).

$$MTZ = D_1 / (1-X) [1 - (C_1/C_s)] \quad (2.10)$$

Where, D_1 = bed depth

C_1 = breakthrough capacity of bed D_1

C_s = saturation capacity

X = the degree of saturation in the MTZ

C_s of the above equation can be obtained by measuring the breakthrough capacities of two beds and by using in Equation (2.11).

$$C_s = (C_2 D_2 - C_1 D_1) / (D_2 - D_1) \quad (2.11)$$

Where, C_1 = breakthrough capacity for bed length of D_1

C_2 = breakthrough capacity for bed length of D_2

2.3 Classification of Adsorption Isotherms

The majority of physical adsorption isotherms may be grouped into six types as shown in Figure 2.7 (Rouquerol et al., 1999). The horizontal axis shows the relative pressure P/P^0 and the vertical axis shows specific amount adsorbed. In most cases at sufficiently low surface coverage, the isotherm reduces to a linear form, which is often referred to as the Henry's Law region.

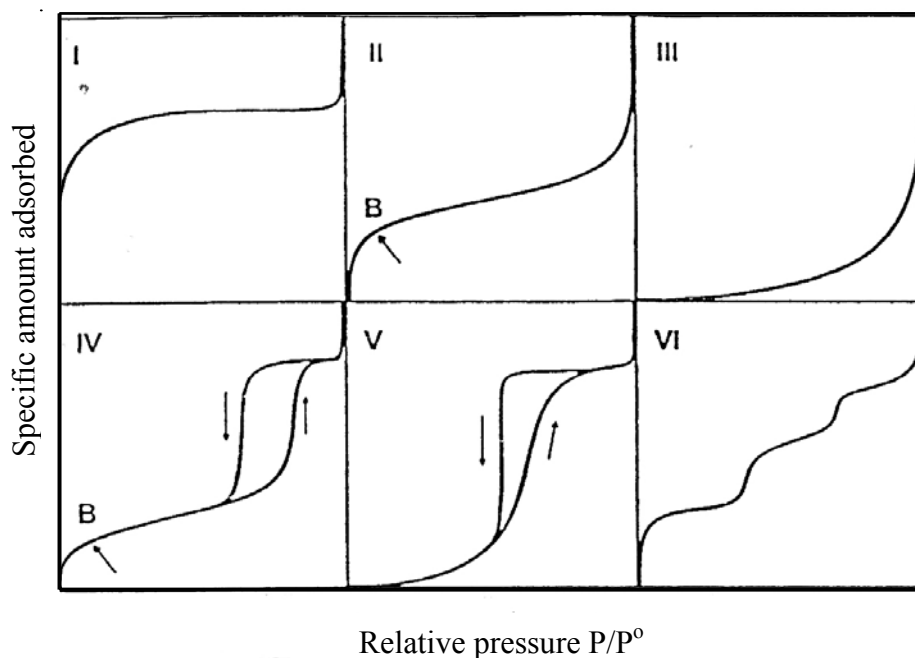


Figure 2.7 Types of isotherms for gaseous adsorption. (Rouquerol et al., 1999)

Type I : This isotherm is concave to the relative pressure (P/P^0) axis. It rises sharply at low relative pressures and reaches a plateau. The amount adsorbed by the unit mass of solid, approaches a limiting value at $P/P^0 \rightarrow 1$.

Type II : This isotherm is initially concave to the P/P^0 axis, then almost linear and finally convex. It indicates the formation of an adsorbed layer whose thickness increases progressively with increasing relative pressure until $P/P^0 \rightarrow 1$. When the equilibrium pressure is equal to the saturation vapor pressure, the adsorbed layer becomes a bulk liquid on solid. If the inflection point of the isotherm called knee of the isotherm is sharp, the uptake at point B, the beginning of the middle quasilinear section, is usually considered to represent the completion of monomolecular layer and the beginning of the formation of the multimolecular layer. The ordinate of point B gives an estimation of the amount of adsorbate required to cover the unit mass of solid surface with a complete monomolecular layer. Type II isotherms are obtained with non-porous or macroporous adsorbents, which allow unrestricted monolayer-multilayer adsorption to occur at high P/P^0 . If the adsorbent temperature is at, or below, the normal boiling point of the adsorptive (adsorbable substance in the fluid phase), it is not difficult to establish the course of the adsorption-desorption isotherm over the entire range of P/P^0 . Complete reversibility of the desorption-adsorption isotherm is the first condition to be satisfied for normal monolayer-multilayer adsorption on an open and stable surface.

Type III : This isotherm is convex to the P/P^0 axis over the complete range and therefore has no point B. This feature is indicative of weak adsorbent-adsorbate interaction. True Type III isotherms are not common.

Type IV : This isotherm, whose initial region is closely related to the Type II isotherm, tends to level off at high relative pressures. It exhibits a hysteresis loop, the lower branch of which represents measurements obtained by progressive addition of gas of the adsorbent, and the upper branch by progressive withdrawal. The hysteresis

loop is usually associated with the filling and emptying of the mesopores by capillary condensation. Type IV isotherms are common but the exact shape of the hysteresis loop varies from one system to another.

Type V : This isotherm is initially convex to the P/P^0 axis and also levels off at high relative pressures. As in the case of the Type III isotherm, this is indicative of weak adsorbent-adsorbate interactions. A Type V isotherm exhibits a hysteresis loop which is associated with the mechanism of pore filling and emptying. Such isotherms are relatively rare.

Type VI : This isotherm, or stepped isotherm, is also relatively rare and is associated with layer by layer adsorption on a highly uniform surface. The sharpness of the steps is dependent on the system and the temperature.

2.4 Activated Carbon

Activated carbons are unique and versatile adsorbents because of their large surface area, microporous structure, high adsorption capacity, and high degree of surface reactivity. Their important applications are related to their use in removal of color, odor, taste, and other undesirable organic impurities from potable waters, in the treatment of domestic and industrial wastewater, solvent recovery, air purification in inhabited spaces such as restaurants, food processing and chemical industries, in air pollution control, and in a variety of gas phase applications. There are two types of systems for application in air pollution control. One is purification of air for immediate use in inhabited spaces. The other system prevents air pollution of the atmosphere from exhaust airstreams emitted from various industrial operations. In addition, the characterization of the carbon surface and its porous structure with

respect to the chemical composition of the surface, pore size distribution, and surface area are of vital importance whenever quantitative data for processes are occurring or starting at the surface of the carbon. The following sections briefly describe the basic steps involved in the manufacture of activated carbons, the selectivity and suitability of different raw materials.

2.4.1 Classification of Activated Carbons

Activated carbons are complex products which are difficult to classify on the basis of their behavior, surface characteristics, and properties. Activated carbons are therefore classified on the basis of their particle size and particle shapes into powdered, granulated, spherical, or pelleted activated carbons.

2.4.1.1 Powdered Activated Carbons

Powdered activated carbons have a fine granulometry of less than 100 μm with average diameter between 15 and 25 μm . Thus they present a large external surface and a small diffusion distance. The rate of adsorption is very high and the problems related to mass transfer are very low. They are thus preferably used for adsorption from solution phase because of their low diffusion rates. These carbons are generally prepared by chemical activation methods from sawdust.

2.4.1.2 Granulated Activated Carbons

Granulated activated carbons have a relatively larger size of carbon particles in the granules compared to carbon powders and consequently present smaller external surface. Typically a coarse activated carbon may have a mesh size of 4 \times 8, and a fine-activated carbon may have a mesh distribution of 16 \times 30. Carbons used in gas phase systems are manufactured in granular form, usually between 4 \times 6 to 4 \times 20 mesh in size. Diffusion of the adsorbate thus is an important

factor. These carbons are therefore preferred for the adsorption of gases and vapors as their rates of diffusion are faster. In fact, the size of the grains is chosen depending upon the height of the bed to be used. Granulated activated carbons can also be prepared by the physical activation methods using a variety of carbonaceous materials such as bituminous, and lignite coals (Bansal et al., 1988).

2.4.2 Micropores and Surface Area

The structure of activated carbon is like a natural sponge, having a network of pores extending throughout the bulk of the material. As in a natural sponge, there are a wide variety of pore diameters, with the pore smaller than 2 nm termed micropores, the pores between 2 and 50 nm termed mesopores, and those greater than 50 nm termed macropores. Virtually all pores are invisible without a microscope. Pores with diameters less than 5 nm account for most of the adsorptive capacity. Internal surface areas of good quality activated carbons are in the range of 1100 to 1200 m²/g. With this degree of activation, approximately half the carbon atoms in the adsorbent are on the internal surface of the pores and available to adsorb contaminants (Spengler et al., 2000). Figure 2.8 illustrates molecule movement in the pores. In addition, the larger pore sizes (macro and transitional) contribute little to molecule capture. The vapor pressure of the adsorbates in these larger areas is too low to be effectively removed (Mycock, McKenna, and Theodore). Figure 2.9 is a schematic presentation of a constituent region of an activated carbon particle where the macropores have diameters of greater than 50 to 1000 nm and the micropores diameters are in the 1 to 2 nm range.

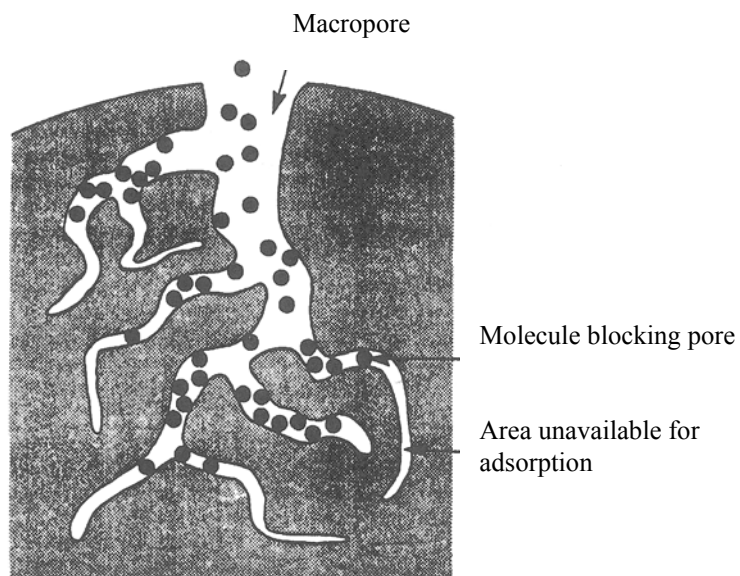


Figure 2.8 Molecular screening in pores of activated carbons (Mycock et al., 1995)

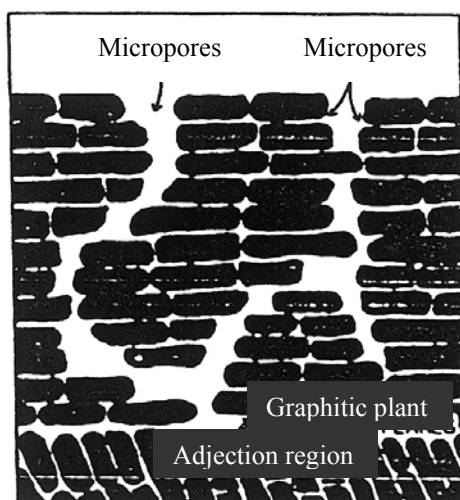


Figure 2.9 Schematic representation of a constituent region of an activated carbon particle. (Noll et al., 1992)

2.4.3 Manufacture

Any cheap materials with a high carbon content, and low inorganic minerals can be used as a raw material for the production of activated carbon. In early production procedures, preference was given to younger fossil materials such as wood, peat, and wastes of vegetable origin, which included fruit stones, nutshells, and sawdust. The chars obtained from them could be activated easily and produced reasonably high-quality activated carbons. The properties of some of the raw materials and the most general uses of the activated carbon obtained from them are seen in Table 2.1. The adsorbent properties of activated carbons are essentially attributed to their large surface area, a high degree of surface reactivity, universal adsorption effect, and favorable pore size, which makes the internal surface accessible, enhances the adsorption rate, and enhances mechanical strength (Bansal et al., 1988). The manufacture of activated carbon can be achieved by two activation processes namely, physical activation and chemical activation processes.

Table 2.1 Properties of some raw materials used in the manufacture of activated Carbon (Bansal et al., 1988)

Raw material	Carbon (%)	Volatiles (%)	Density (kg/L)	Ash (%)	Texture of activated carbon	Application of activated carbon
Soft wood	40-45	55-60	0.4-0.5	0.3-1.1	Soft, large pore volume	Aqueous phase adsorption
Hard wood	40-42	55-60	0.55-0.80	0.3-1.2	Soft, large pore volume	Aqueous phase adsorption
Lignin	35-40	58-60	0.3-0.4	-	Soft, large pore volume	Aqueous phase adsorption
Nutshells	40-45	55-60	1.4	0.5-0.6	Hard, large micropore volume	Vapor phase adsorption
Lignite	55-70	25-40	1.00-1.35	5-6	Hard, small pore volume	Wastewater treatment
Soft coal	65-80	20-30	1.25-1.50	2-12	Medium hard, medium micropore volume	Liquid and vapor phase adsorption
Petroleum coke	70-85	15-20	1.35	0.5-0.7	Medium hard, medium pore volume	Wastewater treatment
Semihard coal	70-75	10-15	1.45	5-15	Hard, large pore volume	Gas vapor adsorption
Hard coal	85-95	5-10	1.5-1.8	2-15	Hard, large pore volume	Gas vapor adsorption

2.4.4 Physical Activation

In this process, the raw material is first subjected to the process of carbonization. Carbonization involves thermal decomposition of the carbonaceous material, eliminating non-carbon species and producing a fixed carbon mass and rudimentary pore structure. The process is usually carried out in rotary kilns or multiple hearth furnaces at temperature below 800°C in a continuous stream of an inert gas. The char produced in this manner is sometimes further calcinated at 1000°C in the absence of any gas. The important parameters that determine the quality and the yield of the carbonized product are the rate of heating, the final temperature, the

soaking time at final temperature, and the nature and physical state of the raw (Bansal et al., 1988).

The carbonized product is further activated to enhance the volume and to enlarge the diameters of the pores which were created during the carbonization process and to create some new porosity. This step is generally carries out at temperatures between 800 and 1100°C in the presence of suitable oxidizing gases such as steam, carbon dioxide, air or any mixture of these gases. The structure of the pores and their pore size distribution are largely predetermined by the nature of the raw material and the history of its carbonization. Figure 2.10 is a schematic representation of the manufacture of activated carbon by physical activation.

2.4.5 Chemical Activation

Chemical activation usually is carried out when the raw material is of wood origin. The starting material is impregnated with the activating agent in the form of concentrated solution usually by mixing and kneading.

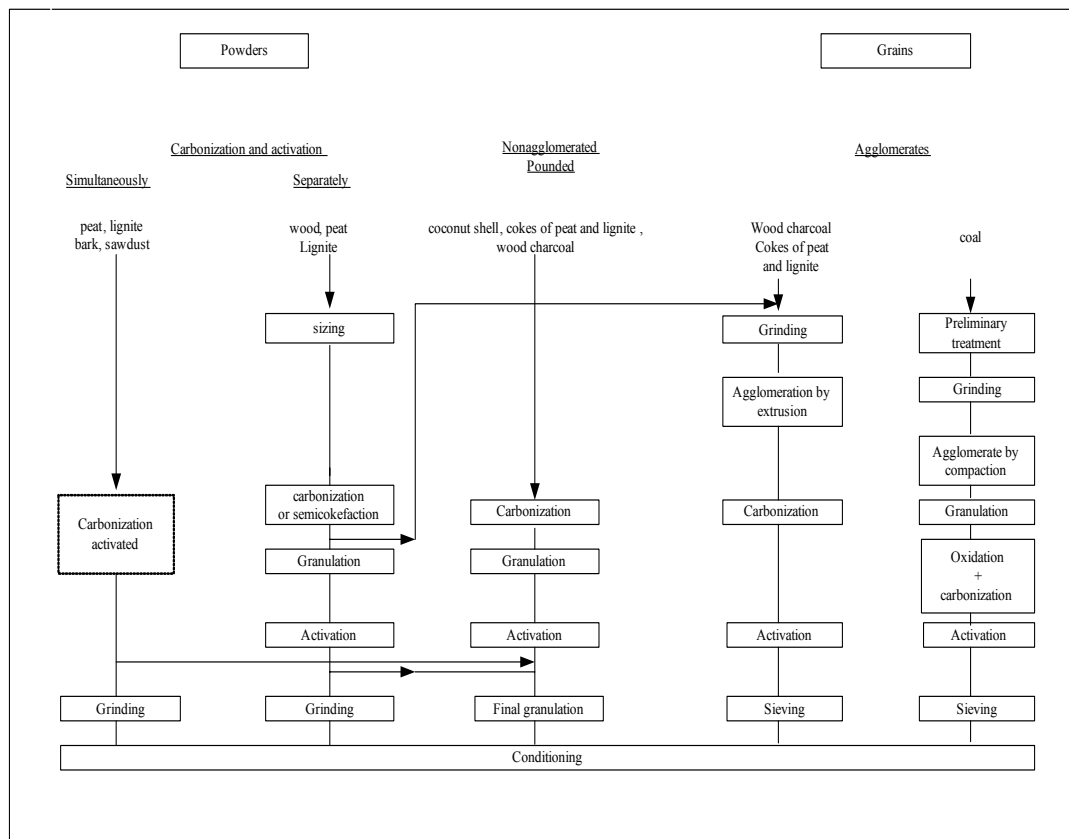
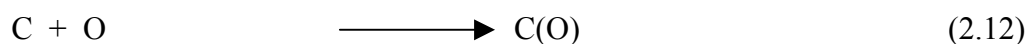


Figure 2.10 Physical activation manufacture process. (Bansal et al., 1988).

The chemical impregnated material is then extruded and pyrolyzed in a rotary kiln between 400 and 600°C in the absence of air. The pyrolyzed product is cooled and washed to remove the activating agent, which is recycled. Disadvantages of this impregnation is its short lifespan-it may lose 75 percent of its effectiveness in a year, release of the impregnating compounds which causes breathing discomfort known to be carcinogenic.

2.5 Carbon Surface Modification by Oxidation

Surface functionalities of carbons can be affected by heat treatment in air, carbon dioxide or oxygen. The nature and the amount of surface oxides formed on treatment with oxygen depends on the nature of the carbon and the history of its formation, its surface area, and the temperature of treatment. The reaction of carbons with oxygen can proceed in several ways depending on the temperature at which the reaction is carried out:



At temperatures below 400°C, the chemisorption of oxygen and formation of the carbon-oxygen surface compounds dominate as in Equation (2.12). At temperature above 400°C, the decomposition of the surface compounds and the gasification of the carbon are the domination reactions according to in Equations (2.13) and (2.14). In case of oxidative treatments in solutions, the major reaction is the formation of the surface compounds, although some gasification may also occur depending on the strength of the oxidative treatment and the severity of the experimental conditions (Bansal et al., 1988).

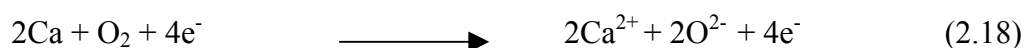
Some chemical reaction relates to an activated carbon impregnation is a redox reaction. An oxidation-reduction reaction, commonly called a redox reaction, involves an exchange of electrons, The species that loses electrons is said to be oxidized. The other species, with gains electrons, is reduced. Consider the formation of calcium oxide (CaO) from calcium and oxygen as shown in Equation (2.15).



Calcium oxide is an ionic compound made up of Ca^{2+} and O^{2-} ions. In this reaction, two Ca atoms give up or transfer four electrons to two O atoms in O_2 . For convenience, this process can be considered as two separate steps, one involving the lose of four electrons by the two Ca atoms and the other being the gain of four electrons by an O_2 molecule as shown in Equations (2.16) , and (2.17).



Each of these steps is called a half-reaction, which explicitly shows the electrons involved. The sum of the half reactions gives the overall reaction as shown in Equations (2.18)-(2.19).



If we cancel the electrons that appear on both sides of the equation.



Finally, the Ca^{2+} and O^{2-} ions combine to form CaO in equation (2.20).



By convention, we do not show the charges in the formula of an ionic compound, so that calcium oxide is normally represented as CaO rather than $2\text{Ca}^{2+} \text{O}^{2-}$. The half-reaction that involves loss of electrons is called an oxidation reaction. The half-reaction that involves gain of electrons is called a reduction reaction. In this example, calcium is oxidized. It is said to act as a reducing agent because it donates electrons to oxygen and cause oxygen to be reduced. Oxygen is reduced and act as an oxidizing agent because it accepts electrons from calcium, causing calcium to be oxidized.

2.6 Ozone

Ozone has been most widely used for cleavage of carbon-carbon double bonds to produce carbonyl compounds or alcohols, depending on work up condition (Burke and Danheiser 1999). The ozone molecule contains three atoms (O_3), while the more common oxygen molecule has two atoms (O_2). Ozone is a more powerful oxidizing agent than oxygen, and oxidation with ozone take places with evolution of more heat and usually starts at lower temperature than when oxygen is used. Ozone is utilized in the treatment of drinking water supplies. Odor and taste producing hydrocarbon are effectively eliminated by ozone oxidation.

2.6.1 General Properties of Ozone

The extreme forms of resonance structures in ozone molecules can be represented as in Figure 2.11.

Physical data:

Molecular weight	=	48.00
Melting point	=	-193°C
Boiling Point	=	-111.9°C
Density at 0°C, gas	=	2.14 g/L
Solubility	=	0.1-0.3% by weight in hydrocarbon solvents at - 80 to - 100°C

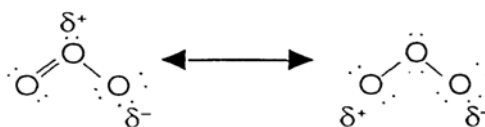


Figure 2.11 Resonance structures of ozone (Langlais et al.,1991)

2.6.2 Ozone Preparation – Ozone Generator

Ozone is a colorless to faint blue gas which is usually generated in the laboratory by passing dry air or oxygen through two electrodes connected to an alternating current source of several thousand volts. From air, ozone is typically generated at concentrations of 1-2%, from oxygen, concentrations are typically 3-4%. Several laboratory scale generators are commercially available. First, oxygen atoms are formed as in reaction (2.21). Some of these oxygen atoms then attach themselves to oxygen molecules as in reaction (2.22). The excess energy in the newly formed ozone is carried off by any available molecule (M) of gas, thus stabilizing the ozone molecule (Parker, 1993).



The corona discharge principle employed in all types of commercial ozone generators involves applying a high-voltage alternating current between two electrodes which are separated by layer of dielectric material and narrow gap through which the oxygen bearing gas is passed (Figure 2.12).

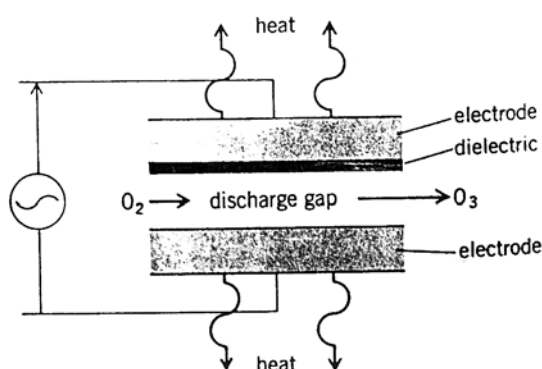


Figure 2.12 Diagram of a generic corona cell (Parker, 1993).

The Lowther-type air-cooled plate ozone generator is the most widely used for producing ozone gas. This kind of ozone generator operates on a dielectric composed of a glass or ceramic-covered steel electrode separated from a second identical electrode by silicon bracing that provides the discharge space, as illustrated in Figure 2.13. Each of the electrodes is coupled with an aluminum ventilator designed to cool the ozonated gas with ambient air. The upper effective pressure in the cell is about 1 bar. This type ozone generator runs on 9 kV electric current at a frequency of 2000 Hz.

2.6.3 Ozone Analysis

The amount of ozone generated can be determined based on the liberation of iodine from potassium iodide solution according to Equation (2.23), followed by thiosulfate titration to determine the amount of iodine produced as in Equation (2.24). On the other hand photometric detectors are available which can determine the concentration of ozone in a metered gas stream (Burke and Danheiser, 1999).



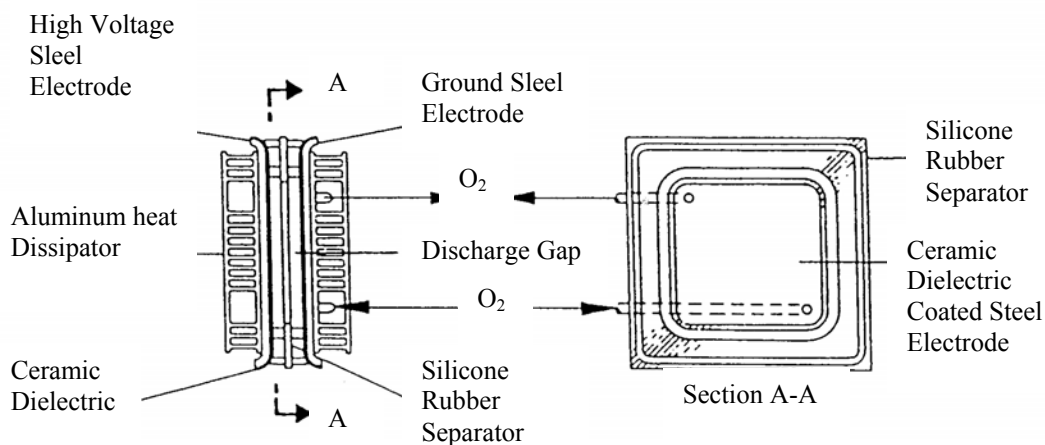


Figure 2.13 Lowther-type air-cooled plate ozone generator.(Langlais et al., 1991).

2.6.4 Handling, Storage and Precautions

Ozone is highly toxic in concentrations greater than 0.1 ppm by volume. It has a characteristic odor which can be detected at a level as low as 0.01 ppm. All operation scrubbing system employing thiosulfate solutions can be used to change excess ozone to sulfate compound, as shown in Equation (2.25).



2.7 Past Studies on Carbon Surface Oxidation

In past research, coal-and wood-based activated carbons were prepared using a chemical oxidation. An oxygen gas, potassium hydroxide, phosphoric acid or nitric acid may be used as oxidizing agents. An oxidation on activated carbons used for increasing functional groups such as C-O and/or C=O may be achieved by the following different oxidizing agents.

2.7.1 Nitric Oxidation

Cal et al. (2000a, 2000b) used nitric acid (HNO_3) as an oxidizing agent in their experimentation. After steam activation, most activated carbon samples were oxidized with aqueous nitric acid treatment. The activated carbon was added to 45% HNO_3 by mass solution and heated to 90°C for 2.5 hours. A reflux column was used to prevent excessive HNO_3 loss. The reason for oxidizing the carbon samples with HNO_3 was to create more carbon-oxygen (C-O) complexes. Then temperature programmed desorption (TPD) was used to quantify the oxygen content of HNO_3 oxidized carbon-based sorbents. TDP results showed that HNO_3 oxidized samples had a surface oxygen content between 10 and 15% by weight, while steam activated carbon had a surface oxygen content between 2 and 4% by weight. But surface areas of steam activated samples decreased from 600 to $470\text{m}^2/\text{g}$ after HNO_3 oxidation.

Jae-Woon Shim, Soo-Jin Park, and Seung-Kon Ryu (2001) modified pitch-base activated carbon fibers (ACFs) with nitric acid and sodium hydroxide. Their physicochemical properties were investigated in terms of N_2 adsorption, mass transition, FTIR and metal adsorption. The specific surface area of the ACFs decreased after oxidation with 1 M nitric acid, but the total acidity increased three times compared to the untreated ACFs, resulting in an improved ion-exchange capacity of the ACFs. The points of zero charge of the ACFs that effect the selectivity for the ionic species changed from pH 6 to pH 4 by 1 M nitric acid and to pH 10 by 1 M sodium hydroxide treatment. Upon oxidation of the ACFs with nitric acid, surface oxide groups were observed in the FTIR spectra by absorption peaks at $1750\text{-}1400\text{ cm}^{-1}$. The carbonyl groups of ACFs decreased, while the lactone groups increased after the sodium hydroxide treatment.

Bhabendra K. Pradhan and N. K. Sandle (1999) studied about two commercially available activated carbons (activated charcoal cloth [ACC] and activated granular carbon [AGC]) which were oxidized with different oxidizing agents such as HNO_3 , H_2O_2 , and $(\text{NH}_4)_2\text{S}_2\text{O}_8$, in order to introduce surface oxygen complexes. The effect of oxidizing agent treatment on the surface chemical nature and surface texture were characterized by ultimate elemental analysis, bulk chemical analysis, FTIR, XRD and nitrogen adsorption isotherms studies. FTIR showed that carboxylic groups were essentially fixed along with ketone and ether groups after being treated by the oxidizing agents. The HNO_3 treatment affects the surface area and the porosity of the samples to a greater extent than the others. The micropore volume calculated from DR and α_s methods reveals that 70% of the adsorption capacity of activated carbons is due to the contribution from micropore.

2.7.2 Potassium Hydroxide Oxidation

Lee and Reucroft (1999a) prepared the carbon samples from Illinois bituminous coals and white oaks using a chemical activation process with potassium hydroxide (KOH) at different temperatures. The x-ray photon spectroscopy (XPS) technique was used to determine surface oxygen concentrations of each carbon sample. The resulting data showed that higher oxygen concentration were found on the lower surface area carbon samples. It was also found that the lower surface area carbon samples contained a higher density of carbon surface oxygen functional groups such as C-O and C=O, resulting in more active polar adsorption sites.

2.7.3 Phosphoric Acid Oxidation

Lee and Reucroft (1999a) conducted experiments on vapor adsorption on coal-and wood-based chemically activated carbons, surface oxidation states and

adsorption of H₂O. Wood-based activated carbons prepared using phosphoric acid (H₃PO₄) activates at high heat treatment temperatures of 300, 350 and 450°C respectively, were chosen as activated carbon samples for this study. X-ray photoelectron spectroscopy (XPS) was employed to evaluate the surface element distribution, concentration and surface chemical structure of coal-and wood-based chemically activated carbons and to investigate the effect of these features on the adsorption of water vapor at low relative pressure and room temperature. It was found that high surface area carbon samples generally showed low concentrations of surface oxygen and low surface area carbon samples generally showed high concentrations of surface oxygen. The concentrations of carbon surface oxygen groups such as C-O and C=O generally decreased with increasing heat treatment temperature. Increased water vapor adsorption on the lower surface area activated carbons can be correlated with higher concentrations of surface oxygen functional groups.

2.7.4 Oxygen Gas Oxidation

Vicente Gomez-Serrano, Fernando Piriz-Almeida, Carlos Javier Duran-Valle and Jose Pastor-Villegas (1999) using cherry stone (CS) as a starting material and air as an activating agent to investigate the formation of oxygen structures in activated carbon. In the preparation of samples, CS was first heated at temperature between 450 and 900°C in N₂ atmosphere. Then, in a successive activated stage, the product carbonized at 600°C was maintained in contact with an air stream at 25-325°C for 24 h, 300-600°C for 1 h, and 250°C for 1-96 h. The starting material, carbonized products, and activated carbon were examined by FTIR spectroscopy. A number of carbon-hydrogen atomic groupings and of oxygen groups and structures,

i.e., OH, C=O, and C-O-C were identified in CS. The yield of activation and carbonization processes and also the chemical structure of the resultant product were strongly dependent on the carbonization temperature. For the products carbonized at 600-900°C, only ether type structures were detected. The activation at 250°C in air results in activated carbons that contained different oxygen structures when CS was carbonized at 450 or 600°C. At 700 or 900°C, by contrast, oxygen structures were not formed as a result of the activation treatment. This also applied when the carbonization product of CS at 900°C was activated solely in CO₂ or first in CO₂ and then in air.

Shibagaki and Motojima (2000) investigated the surface properties of carbon micro-coils oxidized by a low concentration of oxygen gas. In this study the carbon coils were treated in a mildly oxidizing atmosphere of O₂ at a low flow-rate as a clean, simple and low cost method. To utilize the carbon coils as functional materials for various composites, it is essential to introduce the oxygen containing functional groups on the surface for improving the adhesion of the carbon coils with the matrix materials. The O1s/C1s intensity ratio of the XPS spectra measured on the surface increased on using the oxidation treatment.

2.7.5 Oxygen Plasma Oxidation

Boudou, Martinez-Alonzo and Tascon (2000) studied the introduction of acidic groups at the surface of activated carbon by microwave-induced oxygen plasma at low pressure. Functional groups at the surface of a commercial granulated activated carbon were modified at low temperatures in an oxygen plasma. Changes in the chemistry of the surface were monitored by thermal desorption, titration of acidic groups, and XPS. A comparison of untreated and plasma treated carbon, both before

and after acid-washing and cursing, showed that the reactions in oxygen plasma yield a low surface acidity with minimal modification of the initial sample porosity. Carboxylic groups, which are largely responsible for the surface acidity, appeared to be unstable in the presence of the most reactive oxygen species of the plasma.

Takada, Nakahara, Kumakai, and Sanada (1996) modified the surface of carbon black with an oxygen plasma treatment. The initial increase and following reduction of carbon back weight due to the treatment were observed as the treatment time was increased. The chemical structure of carbon back surface formed by the oxidation process was characterized by X-ray photoelectron spectroscopy (XPS). The XPS O/C atomic ratio of the surfaces showed a plateau after an initial increase and saturated at about 0.42 after 120 minutes regardless of the plasma input power. The introduction rate of oxygen-containing functional groups on to the carbon back surface increased by increasing the plasma input power. The oxygen plasma was found to cause changes in surface C=O or O---C---O and O---C=O functionalities, and their concentrations were proved to increase with the treatment time up to about 120 minutes irrespective of the input power.

2.7.6 Oxygen and Ozone Oxidation

Mul, Neeft, Kapteijn, and Moulijn (1997) investigated the formation of carbon surface oxygen complexes by oxygen and ozone, the effect of transition metal oxides. In order to study the interaction of activated oxygen species with the investigated catalysts and carbon black, and to further analyze the stability of surface oxygen complexes, ozone was used as an oxidative agent at relatively low temperatures. Ozonized carbon black was prepared in a closed quartz tube, with a porcelain crucible containing the sample placed inside, and an ozonizer which

produced approximately 10% by volume of ozone in oxygen. The catalyst carbon black samples, physically mixed in a ratio of 2 : 1 in the ball mill, were allowed to react for 60 minutes in an oxygen ozone flow of approximately $10 \text{ m}^3/\text{min}$ at 313 K. Carbon black was treated under similar conditions, and also at 400 K for three hours, to induce the formation of highly oxidized sample. The amount and nature of the oxygenated species formed on the carbon black surface by oxidation in ozone is related to the time and temperature of the ozone treatment

2.7.7 Ozone Oxidation

Fu, Lu, and Chung (1998) conducted experiments on ozone treatment of carbon fiber for reinforcing cement. In this work, by oxidation with ozone at 160°C for 5 minutes, they have greatly improved the effectiveness of carbon fibers for reinforcing cement. Ozone treatment of isotropic pitch based carbon fiber was found to increase the surface oxygen concentration and change surface oxygen from C-O to C=O, thereby causing the contact angle between fiber and water to be decreased to zero.

Douglas B. Mawhinney and John T. Yates, Jr. (2001) investigated the reaction of ozone (O_3) with activated carbon by FTIR spectroscopy. A wide range of carbonyl species are observed to form with stretching mode frequencies ranging up to 1900 cm^{-1} , but individual carbonyl species cannot be resolved. A $\nu(\text{C-O})$ mode is observed near 1190 cm^{-1} , as well as a broad $\nu(\text{CO-H})$ mode at 3450 cm^{-1} , which is indicative of the O_3 -induced formation of associated COOH groups. The original surface contains both aromatic and aliphatic $\nu(\text{C-H})$ mode absorbances, which are consumed similar rates by the O_3 . A mechanism is proposed for COOH formation

through decomposition of an ozonide, where the hydrogen originates from C-H bonds initially present on the carbon surface.

2.8 Chemisorption on activated carbon

Activated carbon is not effective in removing sulfur dioxide, low molecular weight aldehyde and organic acids, especially formaldehyde and hydrogen sulfide, but it can be impregnated with chemicals that do react with these contaminants. In this case, the activated carbon serves as a carrier of the impregnants, enhancing the reaction rate by providing a large surface on which the chemical reaction can transpire. For example, activated carbon is immersed in a solution of sulfur dissolved in carbon disulfide. The carbon is then dried, leaving the elemental sulfur coating on the surface of carbon. The treated carbon is especially effective in removing mercury vapors from an air stream because the sulfur reacts with mercury vapor to form mercuric sulfide (Spengler et al., 2000). However, because a chemical reaction is involved, the contact time must be sufficiently long to allow the chemical reaction to a near a completion time that in practice can vary greatly from 0.01 to 0.4 seconds.

Ion exchange method has been applied for metal addition in activated carbon. Because ion exchange of resins include largely molecules of organic compounds and high polymers compounds, they have active group that can attract some ions from a solution for exchange on the resins. The two types of resins are the cation exchange resins, that can exchange with cation in a solution and the anion exchange resins, that can exchange with anion in the solution. So, the meaning of ion exchange process is a reversible interchange of ions in the solid phase, in this case is ion exchange resins and ions are in liquid phase that mean, ions in the solution. If we assign M^+A^- as an

ion exchange resins, thus A^+ is an active group and immerses in the solution, and B^+ is a solute in this solution the equation of reaction is shown in Equation (2.26) (Suppachai Chaithiumwong, 1996).



where M^-A^+ and M^-B^+ are in the solid phase, so M^- is fixed with the solid phase and is called fixed anion. On the other hand, A^+ and B^+ can exchange each other, are called counter-ions. Anions that are in the solution with the original B^+ is a negative charge similar to fixed anion and is called co-ions. For the resins that include negative active group, when they are immersed in to the solution, the exchange occurs between the negative group in the solution and the active group on the resins as shown by Equation (2.27).



2.8.1 Metal-Zinc or Metal-copper by Ion Exchange for H₂S Removal

Cal et al. (2000a) studied about high temperature hydrogen sulfide adsorption on activated carbon, effects of gas composition and metal addition. After HNO₃ oxidation, a portion of steam activated sorbents was impregnated with selected metal to improve H₂S adsorption performance. Metal (Zn or Cu) acetate which was used for the source of metals were added to the carbon surface by an aqueous ion-exchange (IE) process. Typically, about 20.5 grams of zinc acetate [Zn(C₂H₃O₂)₂] was added to 0.5 liters deionized H₂O and mixed. About 10 grams of the oxidized

carbon sample were added and the mixture was continuously stirred for 1.5 hours at 23° C. The sample was filtered once and rinsed with deionized H₂O and then air dried. For copper acetate, the experiment followed the same condition as the zinc acetate method. H₂S adsorption experiments were conducted in a quartz reactor system. Four types of activated carbon were tested to obtain the breakthrough times. They are HNO₃ oxidized activated carbon with Zn addition, steam activated and HNO₃ oxidized activated carbon, steam activated carbon, and a commercial activated carbon. Considering the breakthrough times at H₂S concentration of 200 ppm_v it was found that the breakthrough times were 380, 290, 260 and 40 minutes, respectively for H₂S removal.

Cal et al. (2000_b) studied effects of gas temperature and gas pressure on high temperature H₂S adsorption with activated carbon. Several types of activated carbon sorbents were evaluated for removal of H₂S at high temperatures (400-600°C) in an integrated gasification combined cycle (IGCC) power generation process. The result of an adsorption experiments with Zn impregnated activated carbon samples produced almost identical breakthrough times at varied temperature (400-600°C). High pressure (10 atm) adsorption experiments showed significantly longer breakthrough times at 10 atm compared to at 1 atm.

Lee and Reucroft (1999c) studied NH₃ and H₂S adsorption on coal- and wood-based chemically activated carbons carried out at room temperature using a gravimetric adsorption technique. E₀ values (characteristic adsorption energies) obtained from ammonia adsorption were higher than those obtained from H₂S adsorption due to the strong adsorptive attraction between surface oxygen atoms and the hydrogen atoms in ammonia molecules. The adsorption capacity of NH₃ and H₂S

in the very low relative pressure range was independent of the degree of surface area development. This can be attributed to the presence of smaller average micropore sizes and the presence of a higher density of surface oxygen on the low surface area activated carbons. The degree of surface area development and the limiting micropore volume generally control the adsorption process in the high relative pressure range through the micropore filling mechanism. The average micropore size and surface chemistry have dominant effects to the adsorption process in very low relative pressure range.

2.8.2 Effect of Surface Characteristics of Wood-Based Activated carbons on Adsorption of Hydrogen Sulfide

Adib et al. (1999) used three wood-based commercial activated carbons supplied by Westvaco as adsorbents for hydrogen sulfide. The initial materials were characterized using sorption of nitrogen, Boehm's titration, potentiometric titration, water sorption, thermal analysis, and temperature-programmed desorption. The breakthrough testes were done at low concentrations of H₂S in the input gas to simulate conditions in water pollution control plants where carbon beds are used as odor adsorbents. In spite of apparent general similarities in the origin of the materials, method of activation, surface chemistry, and porosity, significant differences in their performance as hydrogen sulfide adsorbents were observed. Results show that the combined effect of the presence of pores large enough to accommodate surface functional groups and small enough to have the film of water at relatively low pressure contributes to oxidation of hydrogen sulfide. Moreover, there are features of activated carbon surfaces such as local environment of acidic/basic groups along with the presence of alkali metals which are important to the oxidation process.

2.8.3 Influence of Surface Properties on the Mechanism of H₂S Removal

by Alkaline Activated carbons

Yan et al. (2004) studied about alkaline activated carbon for use as adsorbents for H₂S, one of the major odorous compounds arising from sewage treatment facilities. Although a number of studies have explored the effects of various parameters, mechanisms of H₂S adsorption by alkaline carbon are not yet fully understood. The major difficulty seems to lie in the fact that little is known with certainty about the predominant reactions occurring on the carbon surface. In this study, the surface properties of alkaline activated carbons were systematically investigated to further exploit and better understand the mechanisms of H₂S adsorption by alkaline activated carbons. The surface properties of both the original and the exhausted carbons were characterized using the sorption of nitrogen (BET test), surface pH, Boehm's titration, thermal and FTIR analysis. Porosity and surface area provide detailed information about the pore structure of the exhausted carbons with respect to the reaction extent facilitating the understanding of potential pore blockages. Results of Boehm's titration and FTIR both demonstrate the significant effects of functional groups, and identification of oxidation products confirmed the different mechanisms involved with the two carbons. Although both carbons are coal-based and of KOH impregnated type, performances of different carbons differ significantly. A correlation is well established to link the reaction extent with various surface properties. In summary, not only homogeneous alkali impregnation and physical porosity but also the carbon surface chemistry are significant factors influencing the performances of alkaline activated carbons as H₂S adsorbents.

CHAPTER III

RESEARCH METHODOLOGY

3.1 Experimental Location

Experimental works were carried out at the Equipment Building number1 (F1), 2(F2), 4(F4), and 5(F5) at Suranaree University of Technology, Nakhon Ratchasima Province.

3.2 Materials and Methods

All samples of activated carbon (code No.CGC-11A) used in this study were supplied by C. Gigantic Carbon Co.Ltd., in the Province of Nakhon Ratchasima, Thailand. The CGC-11A is a granulated activate carbon (commercial grade) made from coconut shell and has a particle size of 8 x 16 mesh (1800-3600 μm). The experimental methods used in this study include the following steps: the oxidation and metal addition of activated carbons characterization of modified samples and adsorption of H_2S by activated carbons. The characterization of chemical structure of carbon samples as a result of O_3 and HNO_3 oxidations were performed using FT-IR spectroscopy, an elements analyzer (CHNS/O) and Boehm's titration. The concentrations of zinc impregnated activated carbon samples from metal addition process were characterized by atomic absorption spectroscopy (AAs). Also, the specific surface area and pore volume of activated carbon samples were estimated by BET analysis. The adsorption tests for H_2S removal were carried out in a fixed-bed

adsorber with the exit gas mixture being monitored by an electrochemical sensor.

All the experimental methods are schematically outlined in Figures 3.1, 3.2 and 3.3.

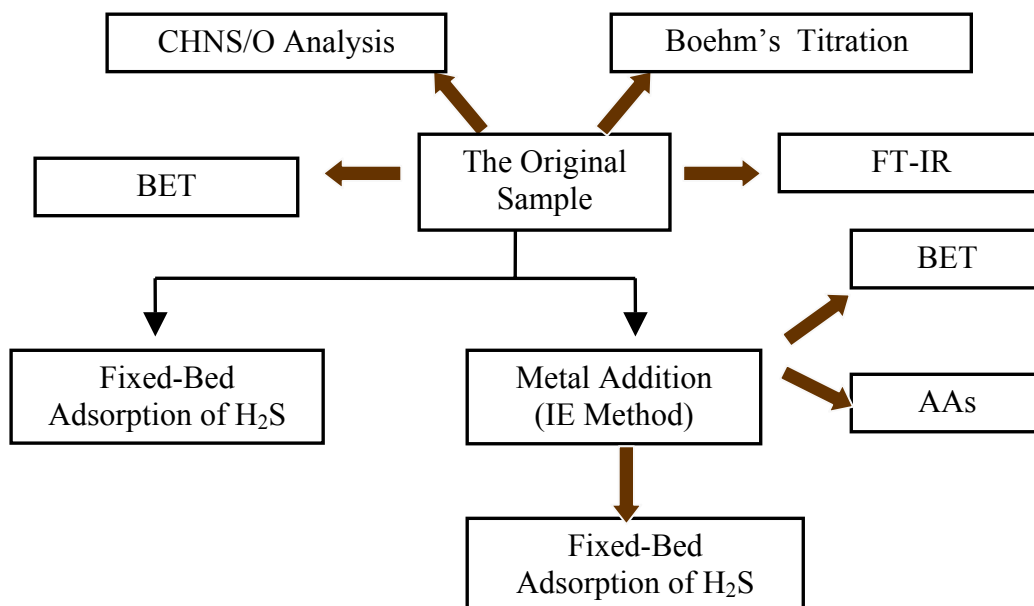


Figure 3.1 Research methodology for the original sample

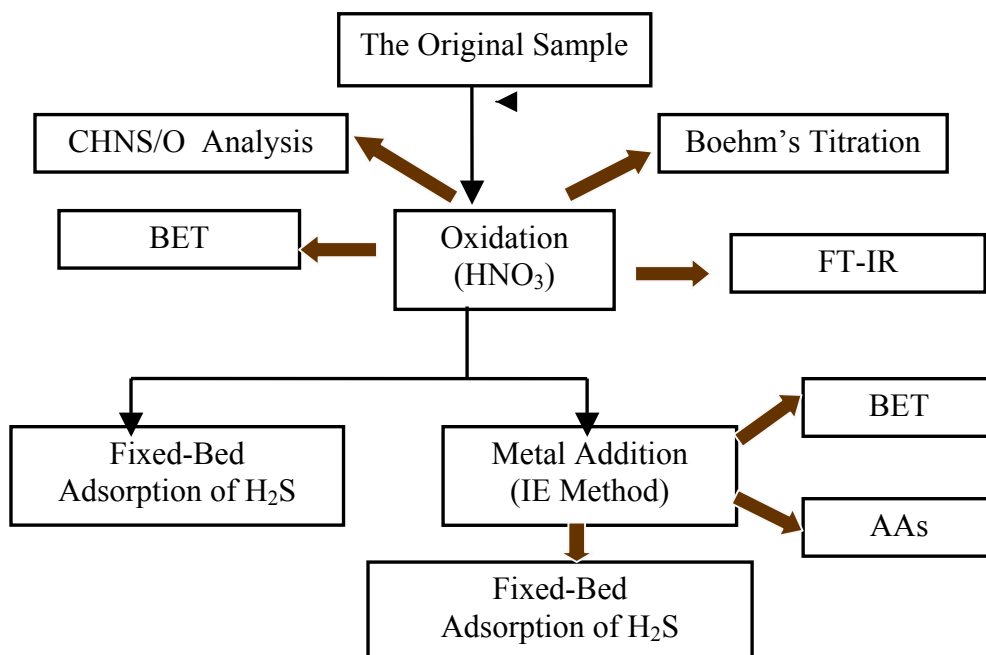


Figure 3.2 Research methodology for HNO₃ oxidized sample

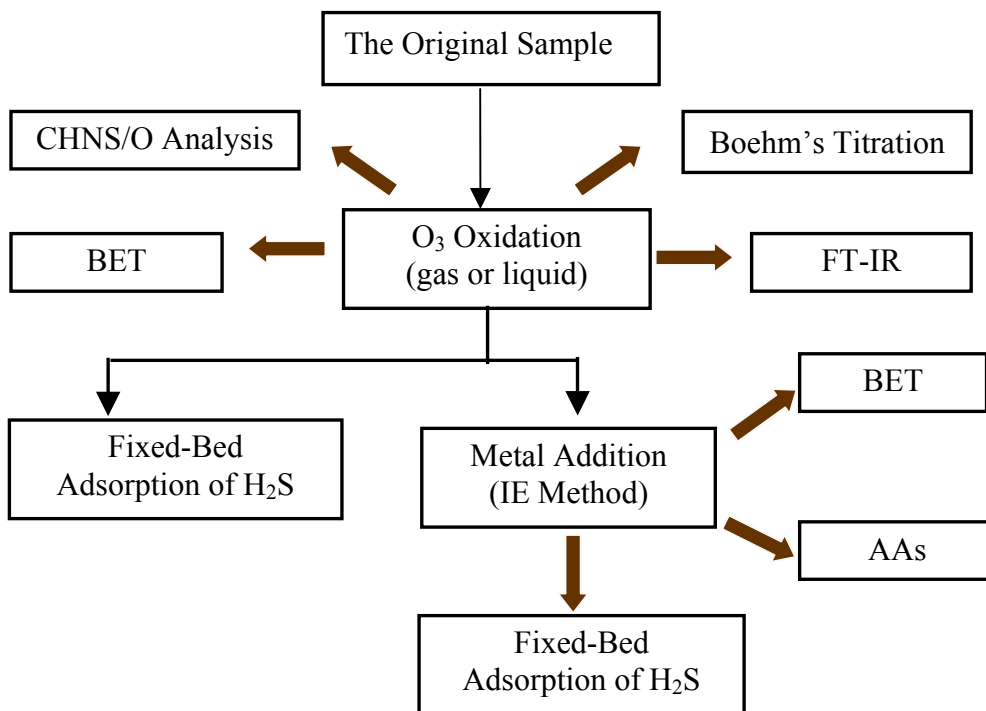


Figure 3.3 Research methodology for O₃ oxidized sample.

3.2.1 Surface Modification Methods

3.2.1.1 Air Oxidation

A batch of 90 g of activated carbon samples were oxidized with air at temperatures between 150-300°C for 120 min in a fluidized-bed reactor externally heated by inserting it in a vertical tube furnace (Carbolite, model: RKC CB 400). The fluidized-bed reactor was constructed from a stainless steel pipe of 5.0 cm inside diameter and 55 cm in length and equipped with a porous hastalloy gas distributor plate at the bottom of the reactor. The fluidizing air flow rate of 1.1-1.3 L/s ($u_{mf} \approx 0.87-1.04$ m/s) was used with the minimum fluidization velocity (u_{mf}) being 0.79 m/s. When the heating was completed, the samples inside the reactor were cooled down to room temperature under the continuous flow of air.

3.2.1.2 Nitric acid Oxidation

The concentrations of HNO₃ solution used in this study were between 2.0 and 10.0 M (2.0, 4.0, 6.0, 8.0, and 10.0 M) with 70% HNO₃ being used as a starting concentrated solution. About 20 g of the original activated carbon sample was put into the HNO₃ solution and the mixture was continuously stirred and heated for 2 hours at 90-105°C (near the boiling point of water) in a reflux column (see Figure 3.4). A reflux column was used to prevent excessive loss of HNO₃. After that, the sample was washed thoroughly with distilled water and then dried in a hot air oven at 103°C for 12 hours.

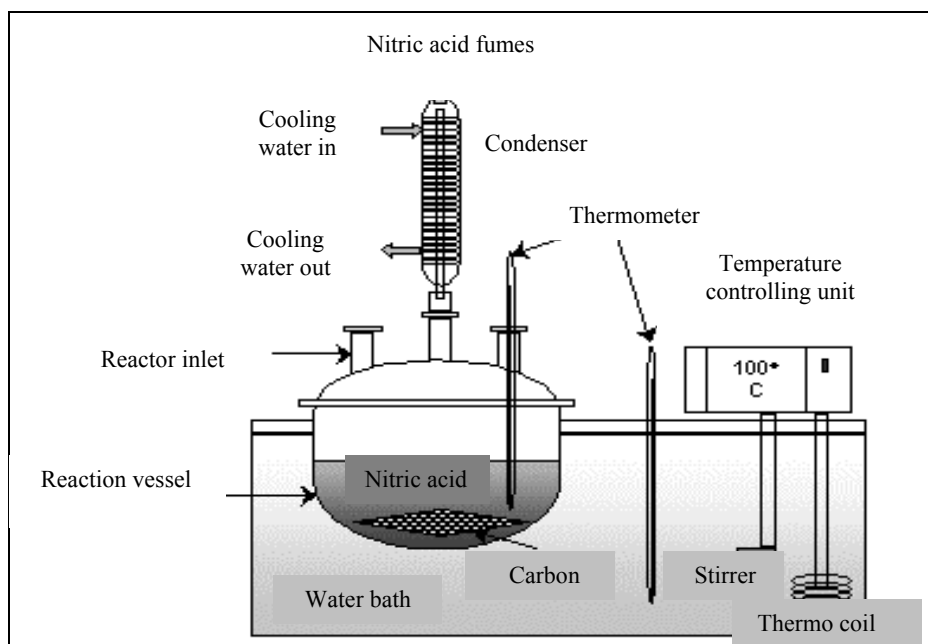


Figure 3.4 Diagram of HNO₃ oxidation in a reflux column

3.2.1.3 Ozone Oxidation

For gas phase oxidation, the original activated carbon weighing about 3.7 g was packed into a fluidized-bed column. The column was constructed from stainless steel pipe (type 304) of 1.2 cm inside diameter and 50 cm in height with a porous hastalloy gas distributor plate at 15 cm above the bottom of the column. The fluidized-bed unit was heated in a tube furnace and ozone gas from an ozone-oxygen generator was passed through the column as illustrated in Figure 3.5. The ozone generator, model OZ-7501 type corona discharge air cool with ozone capacity 1 g/h and maximum air flow rate of 6 L/min, was used in the experiment (see Figure 3.6). Ozone concentration of 1-3% by weight in air can be produced as reported by the manufacturer. The experiments were performed in gas phase at varying temperatures between 90 and 250°C, the oxidation period from 30 to 90

minutes and air (O₂) flow rate was kept constant at 5.5 L/min corresponding to gas superficial velocity of 0.79 m/s. The minimum fluidization velocity was estimated to be 0.79 m/s.

For liquid phase oxidation, about 20 g of the original activated carbon sample was mixed with 0.6 L distilled water and loaded in to a reflux column and continuously stirred at 90°C (see Figure 3.7). Then, ozone gas from the ozone generator with flow rate of 1.5 L/min was passed through the solution in the reflux column for different durations of 60, 120, and 180 minutes. The final solution was filtered and the filtered product was dried in the hot air oven at 103°C for 12 hours.

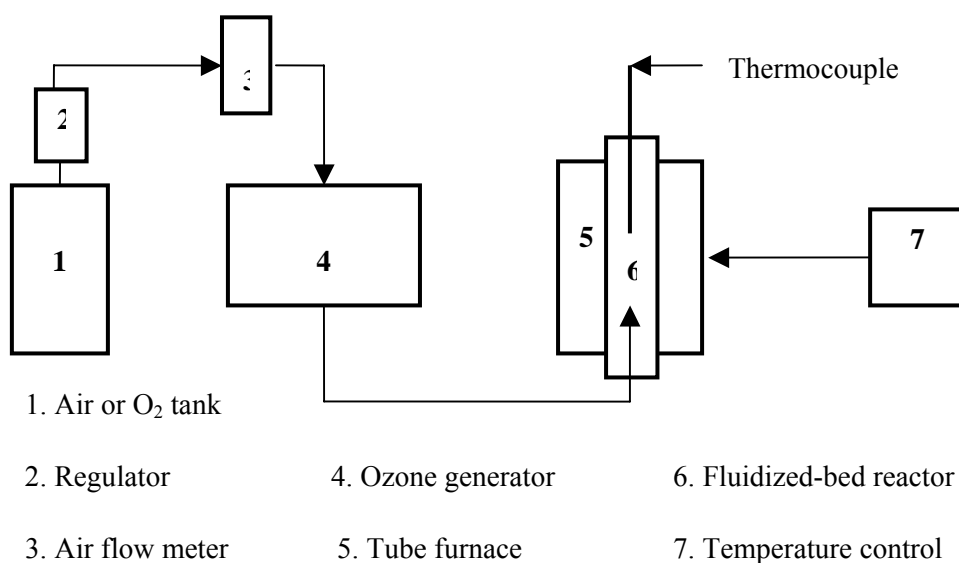


Figure 3.5 Schematic diagram of ozone oxidation in a fluidized-bed reactor.



Figure 3.6 An ozone generator (Model OZ-7501), type corona discharge.



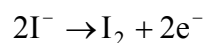
Figure 3.7 Ozone oxidation in a reflux column.

3.2.1.4 Iodometric Method

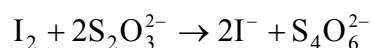
The iodometric procedure was used for determining the ozone concentration in the gas stream. This includes measurement of ozone concentration discharging from the generator and the gas leaving the aqueous solution. For the iodometric method, the ozone-containing gas is passed into an aqueous solution

containing excess potassium iodide, in which the ozone oxidizes iodide ion.

Numerous methods are based upon the reducing properties of iodide ion:



Iodine, the reaction product, is ordinarily titrated with a standard sodium thiosulfate solution, with starch serving as the indicator:



Preparation of solutions:

- a) Sodium thiosulfate ($\text{Na}_2\text{S}_2\text{O}_3 \cdot 5\text{H}_2\text{O}$): about 1 L of distilled water was for 15 min. Allow the water to cool to room temperature; then added about 25 g of $\text{Na}_2\text{S}_2\text{O}_3 \cdot 5\text{H}_2\text{O}$ and 0.1 g of Na_2CO_3 . Stir until the solid has dissolved. Transfer the solution to a clean glass bottle and store in a dark place.
- b) Potassium iodate (KIO_3): dry about 0.3579 g of primary standard KIO_3 at 110°C for at least 1 h and cool in a desiccator. Weigh about 0.3562 g into 100-cm^3 volumetric flask.
- c) Potassium iodide (KI): weigh about 10 g of KI into a 100-cm^3 volumetric flask.
- d) Starch indicator: rub 1 g of soluble starch and 15 cm^3 of water into a paste.

Dilute to about 500 cm^3 with boiling water, and heat until the mixture is clear. The cool indicator is kept in a tightly stoppered bottle. For most titration, 3 to 5 cm^3 of the indicator is used.

Standardization of sodium thiosulfate against potassium iodate: Solutions of sodium thiosulfate are conveniently standardized by titration of the iodine produced

when an unmeasured excess of potassium iodide is added to a known volume of an acidified standard potassium iodate solution. The reaction is



Each formula weight of iodate results in the production of three formula weights of then titrated with the thiosulfate solution. The overall stoichiometry of the process is



Procedure: Pipet 25 cm³ aliquots of standard iodate solution into 250 cm³ conical flasks. Pipet 10 cm³ potassium iodide (10% KI) and swirl the flask to hasten solution. Add 5 cm³ of 1.0 M H₂SO₄, and immediately titrate with thiosulfate until the solution becomes pale yellow. Introduce 2 cm³ of starch indicator, and titrate with constant stirring to the disappearance of the blue color, calculate the molarity of the iodine solution.

Calculation: A solution of sodium thiosulfate was standardized by dissolving 0.3562 g of KIO₃ (molecular weight = 214.00 g) in water, adding a large excess of KI, and acidifying with 5 cm³ of 1.0 M H₂SO₄. The liberated iodine required 24.6 cm³ of the thiosulfate solution to decolorize the blue starch / iodine complex. Calculate the molarity of the Na₂S₂O₃.

$$\begin{aligned} \text{Amount Na}_2\text{S}_2\text{O}_3 &= 0.3562 \text{ g} \\ \text{KIO}_3 \times \frac{1 \text{ m mol KIO}_3}{0.21400 \text{ g KIO}_3} \times \frac{6 \text{ m mol Na}_2\text{S}_2\text{O}_3}{\text{m mol KIO}_3} &= 9.9869 \text{ m mol Na}_2\text{S}_2\text{O}_3 \\ \text{Concentration of Na}_2\text{S}_2\text{O}_3 &= 9.9869 \times 10^{-3} \text{ mol Na}_2\text{S}_2\text{O}_3 \times \frac{1000 \text{ cm}^3}{24.6 \text{ cm}^3} \\ &= 0.4060 \text{ M} \end{aligned}$$

Measurements of ozone concentration from generator: Pipet 30 cm³ potassium iodide (10% KI) into 250-cm³ conical flask. Oxygen (commercial grade) as a feed gas passed through an ozone generator type corona discharge air cool, air flow rate (O₂) 200-cm³/ min. At the exhaust gas outlet of the Ozone generator is passed into an aqueous solution containing 10% KI, flow rate 200 cm³/ min for 1 min. Introduce approximately 5 cm³ of 2.0 M HCl, and titrate immediately with standard sodium thiosulfate until the solution becomes a faint straw yellow. Added about 2 cm³ of starch indicator, and complete the titration, taking as end point the change in color from blue to colorless.

Calculation: The liberated iodine required 4.7 cm³ of the thiosulfate solution to decolorize the blue starch/iodine complex.

$$\begin{aligned} \text{Amount Na}_2\text{S}_2\text{O}_3 &= 0.4060 \text{ mol Na}_2\text{S}_2\text{O}_3 \times \frac{4.7 \text{ cm}^3 \text{Na}_2\text{S}_2\text{O}_3}{1000 \text{ cm}^3 \text{Na}_2\text{S}_2\text{O}_3} \\ &= 1.9082 \times 10^{-3} \text{ mol Na}_2\text{S}_2\text{O}_3 \end{aligned}$$

$$\begin{aligned} \text{Amount O}_3 &= 1.0 \text{ mol O}_3 \times \frac{1.9082 \times 10^{-3} \text{ mol Na}_2\text{S}_2\text{O}_3}{6.0 \text{ mol Na}_2\text{S}_2\text{O}_3} \\ &= 3.1803 \times 10^{-3} \text{ mol O}_3 \end{aligned}$$

$$\begin{aligned} \text{mg O}_3 / \text{L}(\text{O}_2) &= 48 \times 10^3 \text{ mg O}_3 \times \frac{3.1803 \times 10^{-4} \text{ mol O}_3}{1.0 \text{ mol O}_3} \times \frac{1000 \text{ cm}^3}{200 \text{ cm}^3} \\ &= 76.3272 \text{ mg O}_3 / \text{L}(\text{O}_2) \end{aligned}$$

3.2.1.5 Metal Addition by Ion Exchange (IE)

About 10-20 g of each of the original, HNO₃ oxidation, and O₃ oxidation carbon samples was mixed with zinc acetate [Zn(C₂H₃O₂)₂] solution. Zinc ions from zinc acetate solution can attach to the carbon surface by an aqueous ion

exchange process (Cal, et al.,2000). The concentrations of the solution were varied between 0.05 and 0.40 M (0.05, 0.10, 0.20, 0.30 and 0.40 M). The mixture solution was continuously stirred for various times of 30, 60, 90, and 120 minutes at room temperature. After completion the sample was filtered and washed with deionized H₂O and then dried in the hot air oven at 103°C for 12 hours.

3.2.2 Characterization Techniques

3.2.2.1 Fourier Transform Infrared Spectroscopy (FT-IR) Analysis

The surface functional groups of carbon samples were identified from transmission infrared spectra obtained from a Fourier transform infrared spectroscopy (Perkin Elmer, model spectrum GX) as shown in Figure 3.8. The analysis was as follows, potassium bromide (KBr) pellet was first prepared by mixing about 1.0 mg of powder activated carbon with about 300 mg of KBr (Merck; for spectroscopy) in an agate mortar. The mixture was compressed under a very high pressure in a special die(see Figure 3.9) at 15,000 pounds per square inch to form a small disk about 1 cm in diameter and 1-2 mm thick. The disk is transparent to IR radiation and can be analyzed directly. The FT-IR spectra of the samples were recorded between 4000 and 800 cm⁻¹ with 40 scans obtained at 4 cm⁻¹ resolution, for the following samples:

- 1) the original activated carbon sample from the company
- 2) the HNO₃ oxidized samples
- 3) the O₃ oxidized samples
- 4) the HNO₃ oxidized samples impregnated with Zn
- 5) the O₃ oxidized samples impregnated with Zn.



Figure 3.8 A Fourier transform infrared spectroscopy.



Figure 3.9 A special die for preparing KBr pellet.

3.2.2.2 Determination of Oxygen

An elements analyzer (CHNS/O) instrument is one of the most important quantitative applications of infrared absorption to determine the percentage

composition of the elements carbon, hydrogen, nitrogen, oxygen, and sulphur in some compounds. In this study an elements analyzer instrument (LECO model, CHNS-932) was used to determine the percentage of oxygen in the activated carbon samples as shown in Figure 3.10. Weighing about 2.0 mg of the sample and kept in a closed container before measurement to avoid oxidation. The sample was put into a reactor and heated to 1300°C, quantitative conversion of oxygen to carbon dioxide.



Figure 3.10 An elements analyzer CHNS/O.

3.2.2.3 Boehm's Titration

The titration method suggested by Boehm is already described in the literature (Moreno-Castilla, et al., 1998). This method was used to calculate the concentration of acid groups on activated carbon surface under the following assumptions. Sodium hydroxide (NaOH) neutralizes carboxylic, phenolic and lactonic groups. Sodium carbonate (Na_2CO_3) neutralizes only carboxylic and phenolic groups. Sodium bicarbonate (NaHCO_3) only neutralizes carboxylic groups. About 1.0 g of activated carbon was mixed with each of 50 cm³ solution (0.1 M) of NaOH, NaHCO_3 and Na_2CO_3 respectively, for 24 hours with continuous stirring.

Then, the solid phase was separated from the aqueous solution by vacuum filtration. Ten milliliters of each filtrate was used for the excess acid titration by 0.1 M HCl (hydrochloric acid). The phenolic group content on the carbon surface was determined as the amount of 0.1 M NaHCO₃ consumed by the sample. Lactonic group content was calculated as the difference between the amounts of 0.1 M Na₂CO₃ and 0.1 M NaHCO₃ consumed by the activated carbon sample. Carboxylic group contained by subtracting the amount of 0.1 M Na₂CO₃ consumed by the activated carbon from the amount of 0.1 M NaOH consumed. NaOH is one of the basic bases commonly used in the laboratory. However, it is difficult to obtain solid NaOH in a pure form because it has a tendency to absorb water from air and its solution reacts with carbon dioxide (Chang, 2002). For these reasons, a solution of NaOH must be standardized before it can be used in accurate analytical work. In this experiment, we can standardize the NaOH solution by titrating it against an acid solution of accurately known concentration. The acid often chosen for the task is a monoprotic acid called potassium hydrogen phthalate (KHP), for which the molecular is KHC₈H₄O₄. KHP is a white, soluble solid that is commercially available in highly pure form. In addition, Na₂CO₃, NaHCO₃ and HCl must be standardized before they can be used in the analysis.

3.2.2.4 Atomic Absorption Spectroscopy (AAs) Analysis

Metal contents of zinc impregnated activated carbon samples by IE method was determined using an atomic absorption spectrophotometer (Varian model spectrAA-250 plus) as shown in Figure 3.11. Activated carbon samples were dissolved in hydrochloric acid aqua regia before the analysis. An aqua regia is a mixture of one part by volume of concentrated nitric acid and three parts of

concentrated hydrochloric acid. The zinc atoms from atomizer are absorbed at wavelength 213.9 nm. Quantitative analysis of zinc by atomic absorption spectroscopy technique was made with the following samples:

- 1) the original sample and impregnated with Zn
- 2) the HNO₃ oxidized samples and impregnated with Zn, and
- 3) the O₃ oxidized samples and impregnated with Zn.

After the step of ion exchange, the samples were analyzed by atomic absorption spectroscopy as follows:

- 1) To each test tube, adding about 0.1 g of sample (powder) into aqua regia solution 10.0 cm³. Stopper the test tube with a rubber stopper and shake gently a few times.
- 2) Using a pipet, transfer the aqueous solution amount 1.0 cm³ to a 50 cm³ volumetric flask for dilution.
- 3) Prepared the standard zinc solutions various concentrations of 0.50, 1.00, and 2.00 ppm.
- 4) Using the settings recommended by the manufacturer such as air flow 13.7 L/min, acetylene flow 2.0 L/min slit width 1.0 nm, and wave length 213.9 nm.
- 5) Calibration curves were calculated for each set of analyses using standard solutions.



Figure 3.11 An atomic absorption spectrophotometer.

3.2.2.5 BET Surface Area and Micropores Analysis

Specific surface area and pore volume of the activated carbon samples were estimated from nitrogen (N_2) adsorption isotherms at 77 K using an automatic surface analyzer instrument (Micromeritics, model : ASAP2010) as shown in Figure 3.12. BET (Brunauer-Emmett-Teller) theory and DR (Dubinin-Radushkevich) equation were used for the determination of surface area and micropore volume, respectively. The total pore volume was determined from the amount of N_2 gas adsorbed at a relative pressure of 0.98 by converting it to the volume of N_2 in liquid state. The analysis was made for the following samples

- 1) the original activated carbon sample from the company
- 2) the HNO_3 oxidized samples
- 3) the O_3 oxidized samples
- 4) the HNO_3 oxidized samples and impregnated with Zn, and
- 5) the O_3 oxidized samples and impregnated with Zn.



Figure 3.12 An automatic surface analyzer.

3.2.2.6 Scanning Electron Microscope (SEM)

The scanning electron microscope (JEOL model, JSM 6400) shown in Figure 3.13 was used for obtaining structural images of activated carbon particles. In this study, the SEM was used to scan an internal structure of the original sample particles.

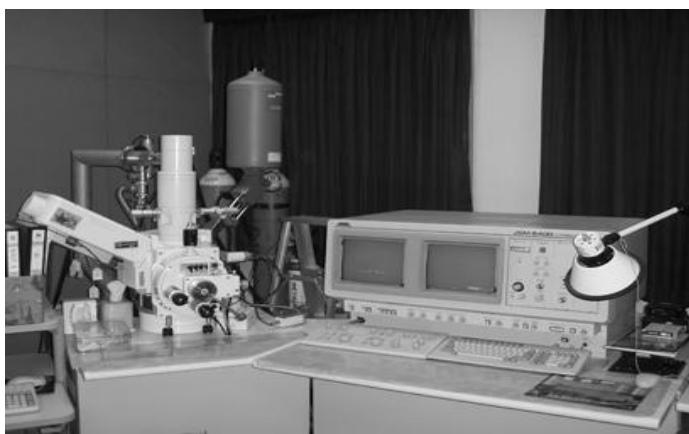


Figure 3.13 A scanning electron microscope (SEM).

3.2.3 Adsorption tests

The adsorption tests for H₂S removal were performed in a fixed-bed column made of stainless steel with 1.2 cm inside diameter. About 3 g of activated carbons (untreated or treated samples) were loaded into the adsorber to a height of approximately 5.5 cm. A mixture of 1.01wt% H₂S in balance N₂ was allowed to flow into the adsorption column at a constant flow rate of 150 cm³/min (contact time \approx 9.9 seconds). The exit concentration of H₂S was continuously monitored by an electrochemical sensor (Q-RAE PLUS, model PGM 2000) every 5 seconds. Figure 3.14 shows the experimental arrangement. The breakthrough curves so obtained can be used to estimate the breakthrough time, and the amount of H₂S removed up to the breakthrough time. The effect of temperature on the adsorption performance was studied at temperatures 10, 30, and 45°C. The following activated carbon samples were used for the adsorption tests

- 1) the original activated carbon sample from the company
- 2) the HNO₃ oxidized samples
- 3) the O₃ oxidized samples
- 4) the HNO₃ oxidized samples and impregnated with Zn, and
- 5) the O₃ oxidized samples and impregnated with Zn.

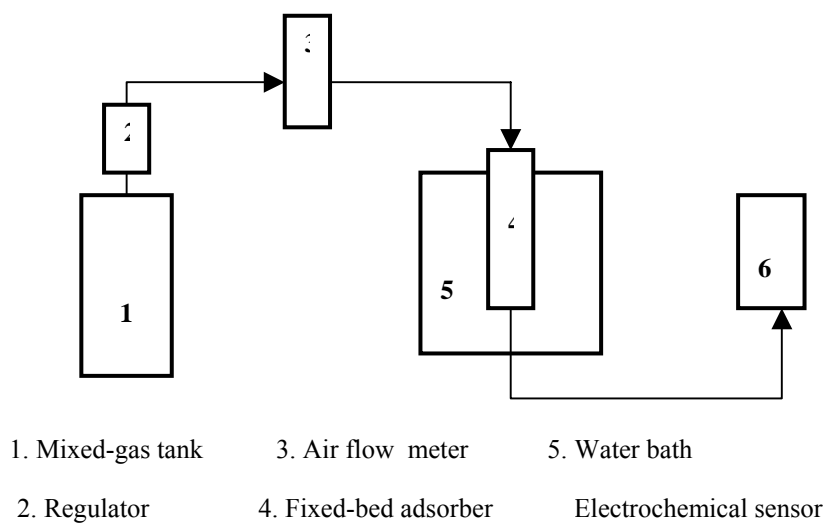


Figure 3.14 Schematic diagram of H₂S removal by activated carbon adsorption.

3.2.3.1 The electrochemical sensors

Electrochemical sensors operate by reacting with the gas of interest and producing an electrical signal proportional to the gas concentration. A typical electrochemical sensor consists of a sensing electrode and a counter electrode separated by a thin layer of electrolyte (see Figure 3.15). Gas that comes in contact with the sensor first passes through a small capillary-type opening and then diffuses through a hydrophobic barrier and eventually reaches the electrode surface. The gas that diffuses through the barrier reacts at the surface of the sensing electrode involving either an oxidation or reduction mechanism. These reactions are catalyzed by the electrode materials specifically developed for the gas of interest.

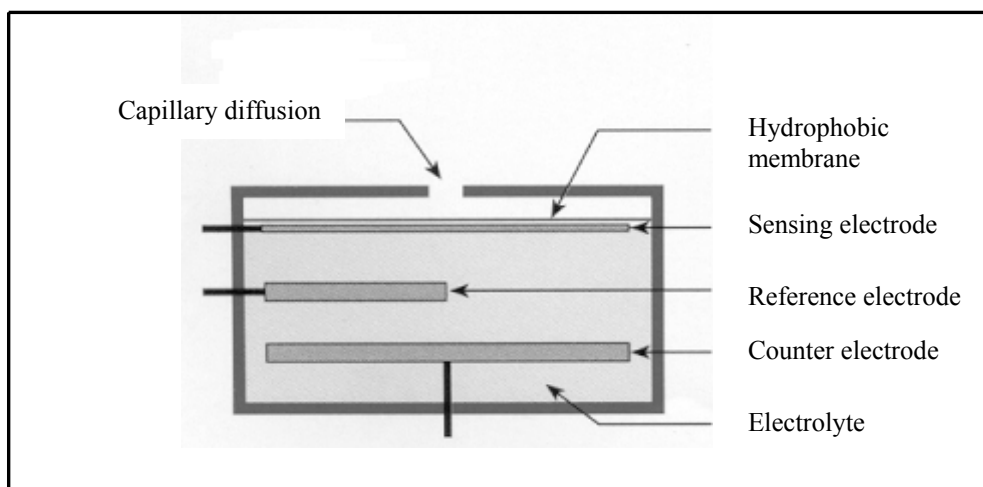


Figure 3.15 Typical electrochemical sensor setup.

The sensor used in this experiment is the Q-RAE PLUS (see Figure 3.16) which is a programmable multi-gas monitor designed to provide continuous exposure monitoring of toxic gases, oxygen and combustible gases for workers in hazardous environments.



Figure 3.16 Q-RAE PLUS monitor.

It monitors inorganic toxic gases and oxygen concentrations with electrochemical sensors but monitors combustible gases with a combination catalytic bead and thermal conductivity sensors. The Q-RAE PLUS monitor uses up to four different sensors to measure a variety of gases. A single microcomputer chip is used to control the operation of the alarm buzzer, LED, pump and light sensor. It measures the sensor readings and calculates the gas concentrations based on calibration to standard, known gases. The data is stored in nonvolatile memory so that it can be sent to a Personal Computer (PC) for record keeping.

3.2.3.2 Calibration of Q-RAE PLUS monitor

In programming mode, the user may re-calibrate the sensors in the Q-RAE PLUS monitor. Calibration of the gas sensor involves two steps. First, “fresh air” which is clean dry air with 20.9% oxygen and without any organic, toxic or combustible gases or impurities is used to set the zero point for each sensor. If such an air bottle is not available, any clean ambient air without detectable contaminants can also be used. In this experiment, a charcoal filter was used to ensure the ambient air’s purity. Then a standard reference gas, which contains a known concentration of a given gas, is used to set the second point of reference to complete the calibration. The Q-RAE PLUS monitor in this experiment is factory calibrated with standard calibration gas (10 ppm H₂S balance N₂). It was further checked with standard gas (5 ppm H₂S) from BOC company, Guildford GU2 7XY, UK.

3.2.3.3 H₂S preparation

The standard gas mixture of 1.01wt% H₂S in balance N₂ used for an experiment contained in an aluminum high pressure cylinder size 2.9 L, gas

content 2175 Psi/0.43 m³. It was supplied by the National Oxygen Pte Ltd, Singapore. Analytical accuracy (± 2 % relative) is calculated from known source and reference standards by gas chromatography, thermal conductivity detector (TCD). Valve connection and high purity pressure regulator are type CGA 330 stainless steel for H₂S mixture (see Figure 3.17).



Figure 3.17 Valve connection and regulator.

CHAPTER IV

RESULTS AND DISCUSSION

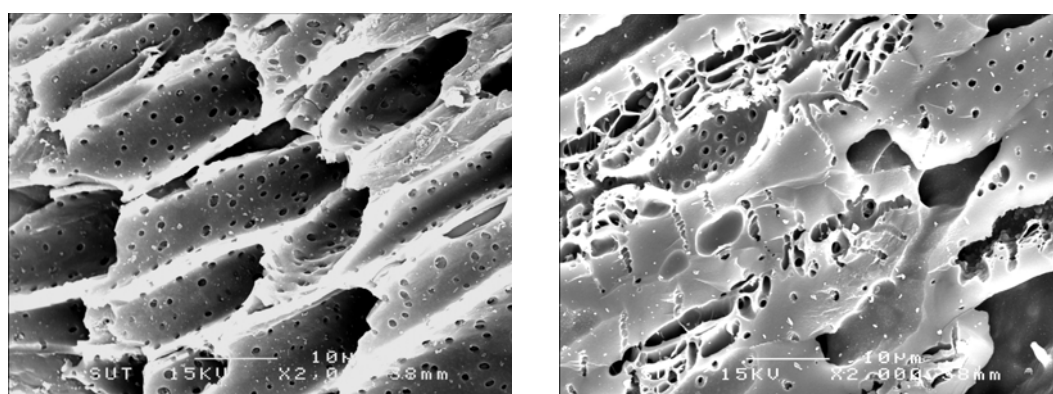
The main objective of the present work is to increase the adsorption efficiency of activated carbon for H₂S removal by surface modification techniques. The changes of surface chemistry and the texture of the activated carbons are investigated after their treatment with different oxidizing agents and addition of zinc. The changes of physicochemical properties of the modified activated carbon samples are determined in terms of BET specific surface area, total acidity and oxide functional groups with changing treatment conditions. This study also includes the adsorption experiments of H₂S removal by untreated and treated activated carbon samples as modified by the introduction of surface oxide groups and metal addition.

4.1 Properties of Activated Carbon Samples

The original activated carbon used in this study is a granulated activated carbon prepared from coconut shell and has the properties as summarized in Table 4.1. Figure 4.1 shows typical SEM image of the original activated carbon sample. Relatively large pore sizes are observed throughout the carbon surface.

Table 4.1 Propertie of the original activated carbon sample used in the present study.

Particle size: 1800-3600 μm	Micropore volume: 0.38 cm^3/g
Micropore area: 878 m^2/g	Particle density: 1516.0 kg/m^3
Average pore size: 1.85 nm	BET surface area: 1119 m^2/g

**Figure 4.1** Typical SEM images obtained from the original sample.

4.2 FT-IR Spectroscopy

The FT-IR spectroscopy provides information on the chemical structure of the material in activated carbon samples. The functional groups of all the activated carbon samples spectra are determined by a handbook of standard FT-IR spectra (Smith, 1999) and the spectrum soft ware of FT-IR spectroscopy (Perkin Elmer model spectrum GX). Wavenumber assignments for the spectra of the treated and untreated activated carbon samples (see Appendix A) are summarized in Table 4.2, which indicate that the samples contain a number of atomic groupings and structures. The position and shape of the band at about $3440\text{-}3420\text{ cm}^{-1}$ are due to the

involvement of hydroxyl groups in hydrogen bonding. Because of the electronegativity differences between the oxygen and hydrogen atoms in a water molecule (from KBr pellet), the electron in the O-H bond spend most of their time near the oxygen atom. This causes the oxygen atom to have a partial negative charge (δ^-) and the hydrogen atom to have a partial positive charge (δ^+). Otherwise, the band should be located at significantly higher wavenumbers and should be much sharper. For free OH groups the band is located at about 3625 cm^{-1} for alcohols, 3605 cm^{-1} for phenols, and 3530 cm^{-1} for carboxylic acids (Gomez-Serrano, et al., 1999).

Table 4.2 Possible FT-IR peak assignments by FT-IR spectroscopy for the samples.

Wavenumber, cm ⁻¹	Vibration mode	Atomic groupings
Original sample		
3428	$\nu(\text{O-H})$	Hydrogen bonding
2037	$\text{C}=\text{C}=\text{C}=\text{C}$	Cumulene (Triene)
1628	$\nu(\text{C}=\text{C})$	Alkene
1559	$\nu(\text{C}=\text{C})$	Haloalkene
1111	$\nu_{\text{as}}(\text{C-O-C})$	Aliphatic ethers
Air oxidized samples		
3435-3425	$\nu(\text{O-H})$	Hydrogen bonding
2920	$\nu(\text{C-H})$	Aromatic- CH_3
2845	$\nu_{\text{s}}(\text{C-H})$	Alkane
2334	$\text{O}=\text{C}=\text{O}$	CO_2 contaminate
2051-2031	$\text{C}=\text{C}=\text{C}=\text{C}$	Cumulene (Trienes)
1635-1628	$\nu(\text{C}=\text{C})$	Alkene
1384-1370	$-\text{O}-\text{CO}-\text{CH}_3$	Acetate ester
1129-1116	$\nu_{\text{as}}(\text{C-O-C})$	Aliphatic ethers
O_3 oxidized samples (in gas and liquid conditions)		
3440-3424	$\nu(\text{O-H})$	Hydrogen bonding
2922-2918	$\nu(\text{C-H})$	Aromatic – CH_3
2336-2331	$\text{O}=\text{C}=\text{O}$	CO_2 contaminate
2078-2052	$\text{C}=\text{C}=\text{C}=\text{C}$	Cumulene (Trienes)
1637-1630	$\nu(\text{C}=\text{C})$	Alkene
1868	$-\text{CO}-\text{O}-\text{CO}$	Carbonyl

Table 4.2 Possible FT-IR peak assignments by FT-IR spectroscopy for the samples
(continued).

Wavenumber, cm^{-1}	Vibration mode	Atomic groupings
1732	$\nu(\text{C}=\text{O})$	Carboxylic acid
1706	$\nu(\text{C}=\text{O})$	Ketone
1573-1551	$\nu(\text{C}=\text{C})$	Haloalkene
1384-1370	-O-CO-CH ₃	Acetate ester
1339	-CH(CH ₃) ₂	Alkane
1128-1110	$\nu_{\text{as}}(\text{C}-\text{O}-\text{C})$	Aliphatic ethers
1033	$\nu(\text{O}-\text{H})$	Aliphatic alcohol
HNO₃ oxidized samples		
3439-3436	$\nu(\text{O}-\text{H})$	Hydrogen bonding
2922	$\nu(\text{C}-\text{H})$	Aromatic – CH ₃
2343-2322	O=C=O	CO ₂ contaminate
2142-2113	C=C=C	Allenes
2086-2050	C=C=C=C	Cumulene(Trienes)
1712	$\nu(\text{C}=\text{O})$	Carboxylic acid
1705	$\nu(\text{C}=\text{O})$	Ketone
1637-1621	$\nu(\text{C}=\text{C})$	Alkene
1384	-O-CO-CH ₃	Acetate ester
1161	$\nu(\text{C}-\text{N})$	Primary amine
1135-1132	-CH(CH ₃) ₂	Alkane
1120-1110	$\nu_{\text{as}}(\text{C}-\text{O}-\text{C})$	Aliphatic ethers

A broad band in the range of frequencies below 3700 cm^{-1} was hydrogen bonds of type $(\text{H}_2\text{O}\dots\text{H}\dots\text{OH}_2)^+$, which were formed between water and protons of acidic groups. Two such bands, which are in the spectra of the samples at 2922-2918 and 2845 cm^{-1} are connected with $\nu_{\text{as}}(\text{C-H})$ and $\nu_{\text{s}}(\text{C-H})$ vibrations (s=symmetric, as=asymmetric). The bands centered near 2300 cm^{-1} can be seen in FT-IR of all oxidized samples and are assigned to carbon-oxygen groups due to ketone or CO_2 contamination (Shim, et al., 2001). The absorption band at about 1868 cm^{-1} is assigned to $-\text{CO-O-CO}$ vibration in carbonyl structure. This group may be more prevalent during ozone treatment than during air oxidation. Indeed ozone can break unsaturated $\text{C}=\text{C}$ bonds to yield unstable ozonides as intermediates, which may rearrange to produce anhydrides or lactones (Chen, et al., 2003). The $\nu(\text{C}=\text{O})$ vibration near 1712 cm^{-1} is the specific peak for the carboxylic acid group, and is observed for the activated carbon oxidized with HNO_3 (Pradhan and Sandle, 1999). For O_3 oxidation and HNO_3 oxidation, the $\nu(\text{C}=\text{O})$ vibration can be seen at 1705 cm^{-1} assigned to ketone groups (Mawhinney and Yates Jr., 2000). In the spectral region between 1700 and 1600 cm^{-1} there is overlapping of bands and that, as a result, the absorption maximum may shift toward lower wavenumbers. Band displacements from ~ 40 to 60 cm^{-1} and a substantial increase in its intensity are normally observed when the olefinic $\text{C}=\text{C}$ bond is conjugated with an aromatic nucleus, another $\text{C}=\text{C}$ bond or a $\text{C}=\text{O}$ bond (Gomez-Serrano, et al., 1999). Thus, the band in this study at 1637 to 1621 cm^{-1} are $\nu(\text{C}=\text{C})$ vibrations in alkene structures. The $\nu(\text{C}=\text{C})$ vibration mode at about 1586 to 1551 cm^{-1} are probably due to haloalkene ($\text{Br}_2\text{C}=\text{CHBr}$) structures (Dean, 1999). A band at 1384 cm^{-1} of all the oxidized samples are assigned to $-\text{O-CO-CH}_3$ group in acetate ester. The oxidized samples as well as the original

sample spectra have a broad absorption band extended between $1100\text{--}1129\text{ cm}^{-1}$. This has been assigned to $\nu_{\text{as}}(\text{C-O-C})$ mode of aliphatic ethers. The FT-IR spectra of the ozone oxidized samples present band at near 1033 cm^{-1} indicating $\nu(\text{O-H})$ vibration in aliphatic alcohols. Figure 4.2 shows the FT-IR spectrum of the original sample. The important functional groups on the original activated carbon surface before being treated with oxidizing agents were $\text{C}=\text{C}=\text{C}=\text{C}$, $\nu(\text{C}=\text{C})$ and $\nu(\text{C-O-C})$ vibrations in triene alkene and aliphatic ether, respectively.

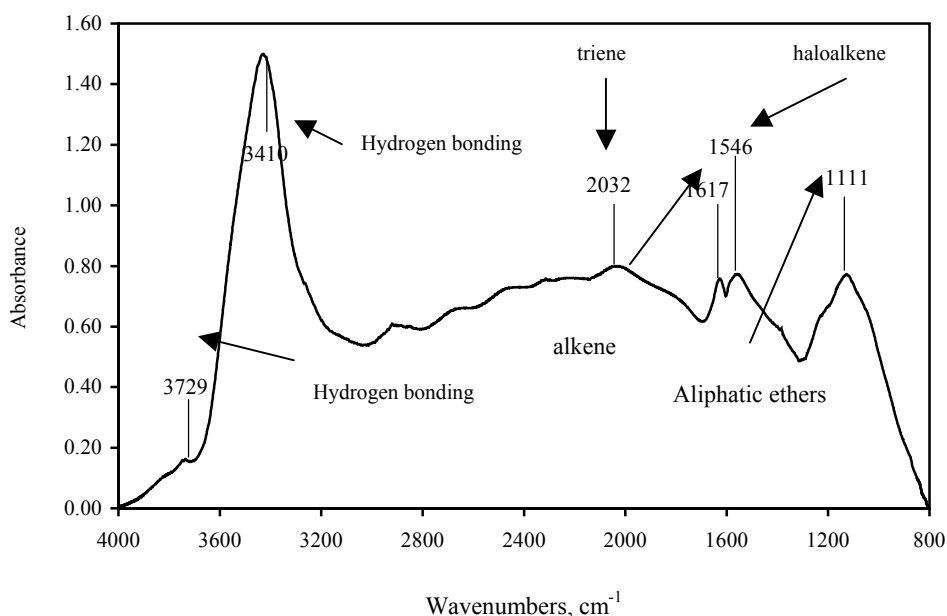


Figure 4.2 The FT-IR spectrum of the original activated carbon sample.

4.2.1 FT-IR spectra of the air oxidized samples

The FT-IR spectra for air oxidized samples at varying temperatures (Figure 4.3) show significant differences concerning the number, position, and intensity of the absorption bands. Firstly, the defined band located at about 1114 cm^{-1} ,

1540, and 1619cm^{-1} due to aliphatic ethers, haloalkene and alkene, respectively can be observed for the spectra of A, B, C and D but band located at 1372 cm^{-1} (acetate ester) is absent from the spectrum A. Secondly, the band near 2906 cm^{-1} (aromatic- CH_3) in the spectra is observed for samples B, C, and D but is absent from the spectrum A. The $-\text{O}-\text{CO}-\text{CH}_3$ grouping (about $1370\text{-}1384\text{ cm}^{-1}$) of acetate ester and methyl groups of aliphatic- CH_3 occurred when the temperature of treatment was increased. This group occurs at every treated temperature except for sample A. In addition, the functional group at 3734 cm^{-1} is hydrogen bonds of type $(\text{H}_2\text{O}\dots\text{H}\dots\text{OH}_2)^+$ which were formed between water (caused by the preparation KBr pellets) and protons of acidic groups. After the original samples were oxidized with air, the new functional groups such as aromatic alkane, alkane and acetate ester occurred on the surface activated carbon samples (see Table 4.2 for comparison).

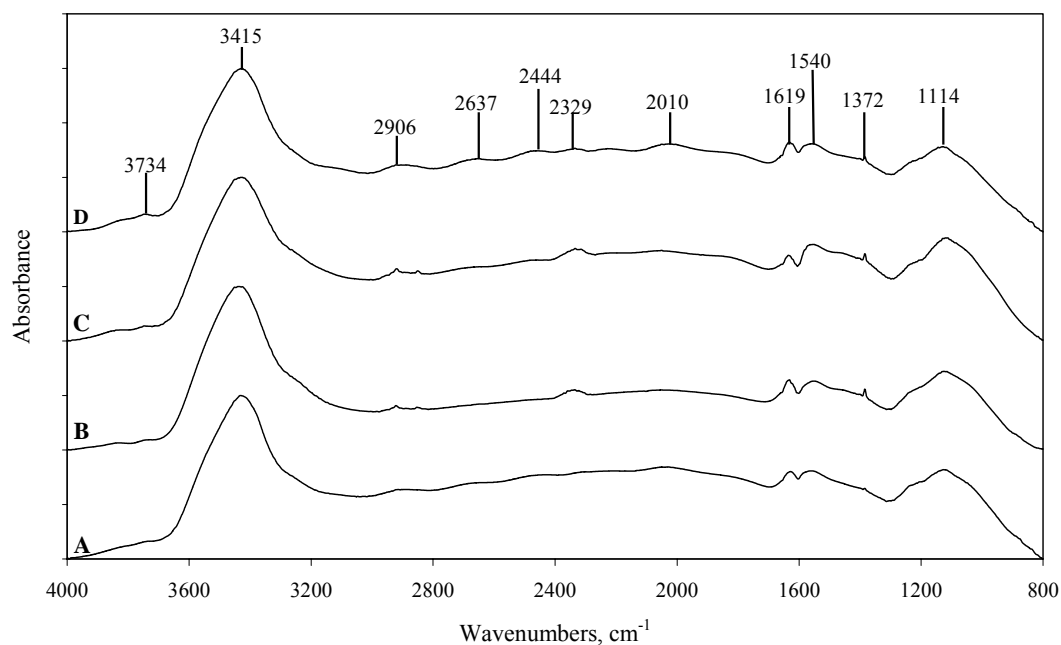


Figure 4.3 Effect of preparation temperature for FT-IR spectra of the air oxidized samples at air flow rate 1.2 L/s for 90min (oxidation temperature (°C): A=150, B=205, C=225, D=275)

The effect of air fluidizing velocity on the spectra of oxidized samples are shown in Figure 4.4, for different air fluidizing velocity (1.1-1.3 L/s or 0.87-1.04 m/s). Within the narrow range of changing air velocity the spectra of these samples show almost the same intensity and also contain similar types of chemical structures. Therefore, the narrow variation of fluidizing velocity used in this study had no effect on the type and concentration of the surface functionalities on activated carbon samples.

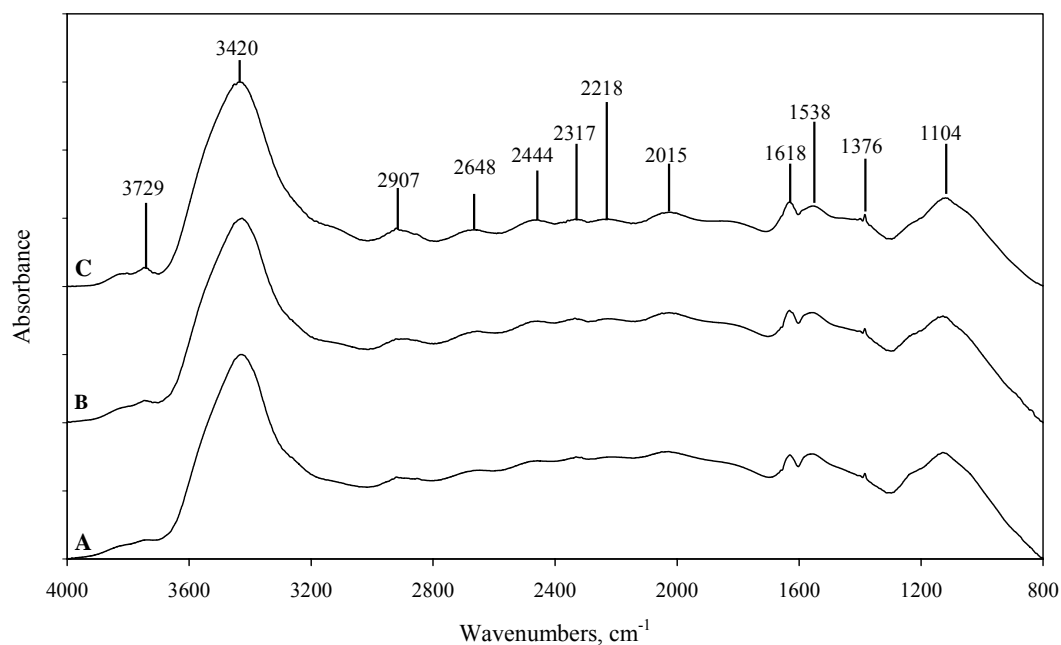


Figure 4.4 Effect of air flow rate for FT-IR spectra of air oxidized samples at 275°C for 90 min (flow rate (L/s): A=1.1, B=1.2, C=1.3).

4.2.2 FT-IR spectra of the O₃ oxidized activated carbon samples in gas phase

Because of the highly reactive nature of O₃ and of the complex surface chemistry of the activated carbon, a number of competitive reactions may occur when O₃ was brought into contact with the activated carbon samples. The reactions may involve free radicals of high oxidation potential that could initiate chain reactions, which in turn further provoke the decomposition of more O₃ on the activated carbon surface (Gomez-Serrano, et al., 2002). As a result, it is not an easy task to predict a simple mechanism for the ozonation of the activated carbon. Molecular ozone is able to act as a 1,3-dipole, an electrophile, or a nucleophile (Gomez-Serrano, et al., 2002). The electrophilic ozonolysis of carbon-carbon double bonds in olefinic structures of

carbon is expected to occur in a process involving three steps: (1) 1,3-dipolar addition of O₃ to the double bond to give an unstable primary ozonide; (2) decomposition of ozonide by a 1,3-dipolar reversion to yield a carbonyl compound and a carbonyl oxide; (3) the carbonyl oxide may give a normal ozonide, dimerizes to aldehyde or ketone diperoxides, or polymerizes to give polymeric peroxides or ozonide (Gomez-Serrano, et al., 2002). In fact, peroxides, ozonides, and carbonyl structures may be found in the ozonation products of activated carbon. Figure 4.5 shows typical FT-IR spectra for the samples oxidized with O₃ in a fluidized-bed at various treatment times and temperatures. All spectra of these samples display weak bands at 2907, and 2320 cm⁻¹ which are connected with $\nu_{\text{as}}(\text{C-H})$, O=C=O vibrations assigned to aromatic alkane and carbon-oxygen groups due to ketone or CO₂ contaminate, respectively. The spectra for C and D samples show the intensity of the bands at 1108, 1556, 1618, and 1702 cm⁻¹. The bands at 1108, 1556, and 1618 cm⁻¹ are due to $\nu(\text{C-O})$ vibrations in aliphatic ether, $\nu(\text{C=C})$ vibrations in haloalkene, and $\nu(\text{C=C})$ vibrations in alkene, respectively. The band at 1702 cm⁻¹ was attributed to $\nu(\text{C=O})$ vibrations in ketone, which is absent from the spectra of A and B samples. The time treatment of A and B samples for 30 minutes shows the similar shape but the band intensities at 2907, 2320, and 1702 cm⁻¹ are less than C and D samples. In addition, the time treatment of A and C samples for 30 and 90 minutes respectively show the band intensity at 1702 cm⁻¹ of C sample which is absent in the spectrum of A sample. The spectrum of B sample (240°C, 30 min) displays more intensity band at 1618 cm⁻¹ than the A sample (180°C, 30 min). Thus, the different band intensities (the concentration of functional groups) of each spectrum which were compared in Figure 4.5 depended on time and temperature for oxidation.

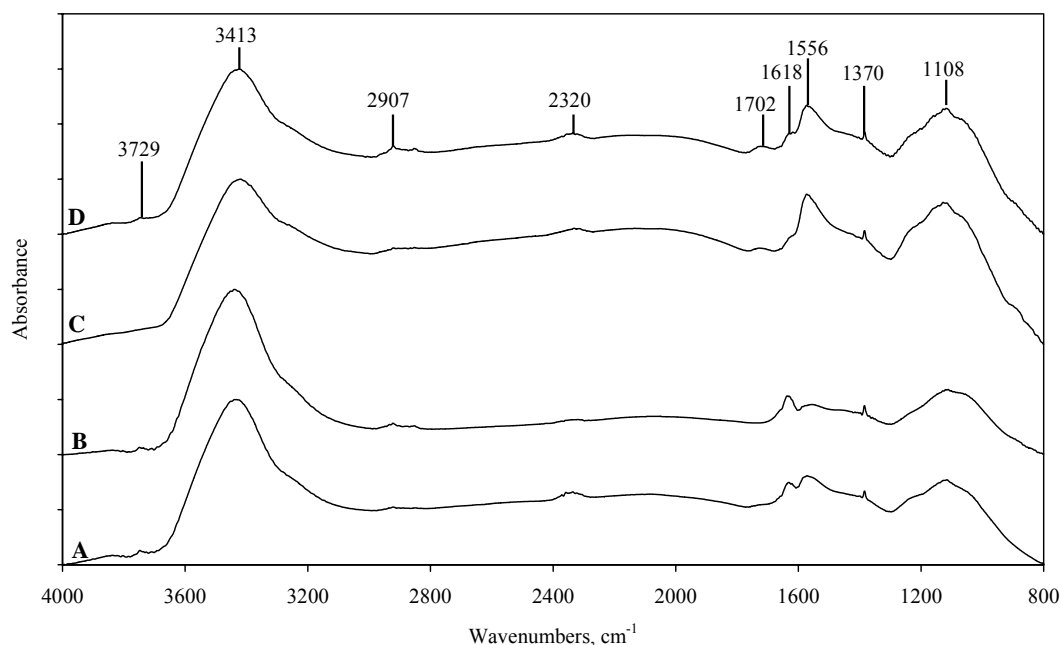


Figure 4.5 FT-IR spectra of ozone oxidized samples in fluidized-bed (oxidation flow rate 5.5 L/min at various temperatures and times of: A= 180°C, 30 min, B= 240°C, 30 min, C= 180°C, 90 min, D= 190°C, 60 min).

4.2.3 FT-IR spectra of the O₃ oxidized activated carbon samples in liquid phase

The FT-IR spectroscopy results for the ozone oxidized samples in a reflux column (hot water, 90°C) compared with that of the original sample are shown in Figure 4.6. The broad band at 1111 cm⁻¹ shows a shoulder at 1030 cm⁻¹ which is due to hydroxyl group in primary aliphatic alcohol and this occurs in the spectra of B, C, and D. The bands centered near 2300 cm⁻¹ are assigned to carbon-oxygen groups due to ketone (Jae-Woon, et al., 2001) or CO₂ contamination (Chen, et al., 2003), which is absent in the spectrum of A (original untreated carbon). The similar shape of the spectra for samples B, C, and D showing two shoulders at 3842 and

3725 cm^{-1} is due to $\nu(\text{O-H})$ vibrations in hydrogen bonding. It is noted that the bands centered near 2300 cm^{-1} obtained from the O_3 oxidized samples in liquid phase display higher intensity than the same position bands obtained from the O_3 oxidized samples in gas phase (see Figures 4.5 and 4.6 for comparison).

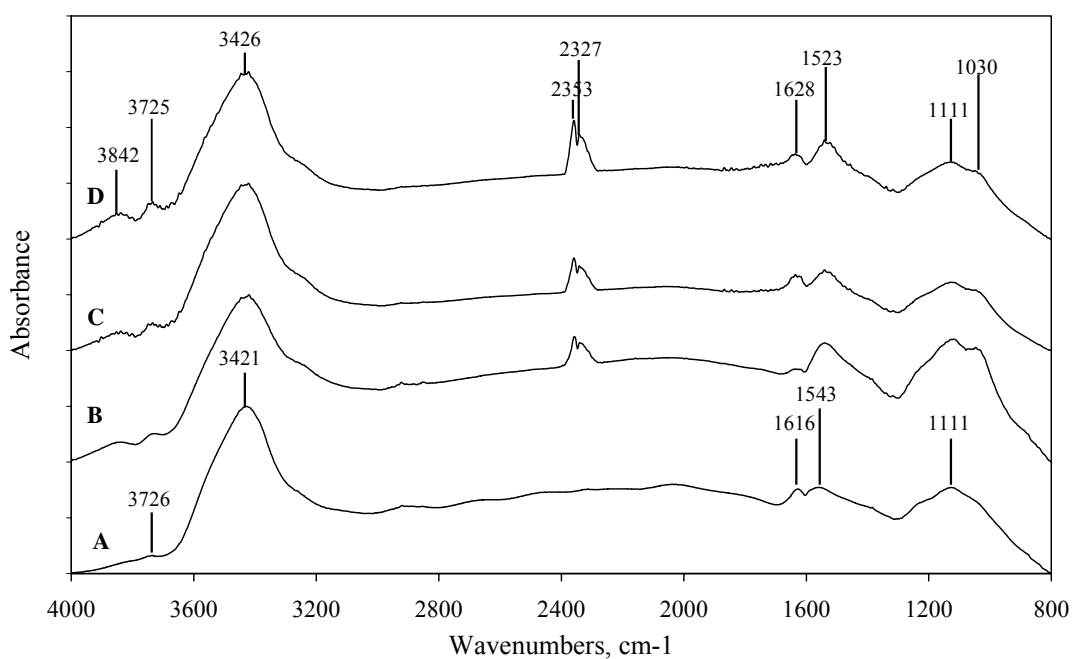


Figure 4.6 Comparison of FT-IR spectra for the original sample (A) with ozone oxidized samples in a reflux column (O_3 gas flow rate 1.5 L/min at various times of: B=60 min, C=120 min, D=180 min).

4.2.4 FT-IR spectra of the O_3 oxidized activated carbon samples with Zn impregnation

The FT-IR spectra of the ozone oxidized samples in a reflux column followed by zinc addition are shown in Figure 4.7. Most of all spectral bands greatly increase in intensity when compared with the FT-IR spectra in Figure 4.6, which

results from metal (Zn) addition by ion exchange process on surface area of these samples. The band at 2356 cm^{-1} is assigned to carbon-oxygen groups due to ketone or CO_2 contamination.

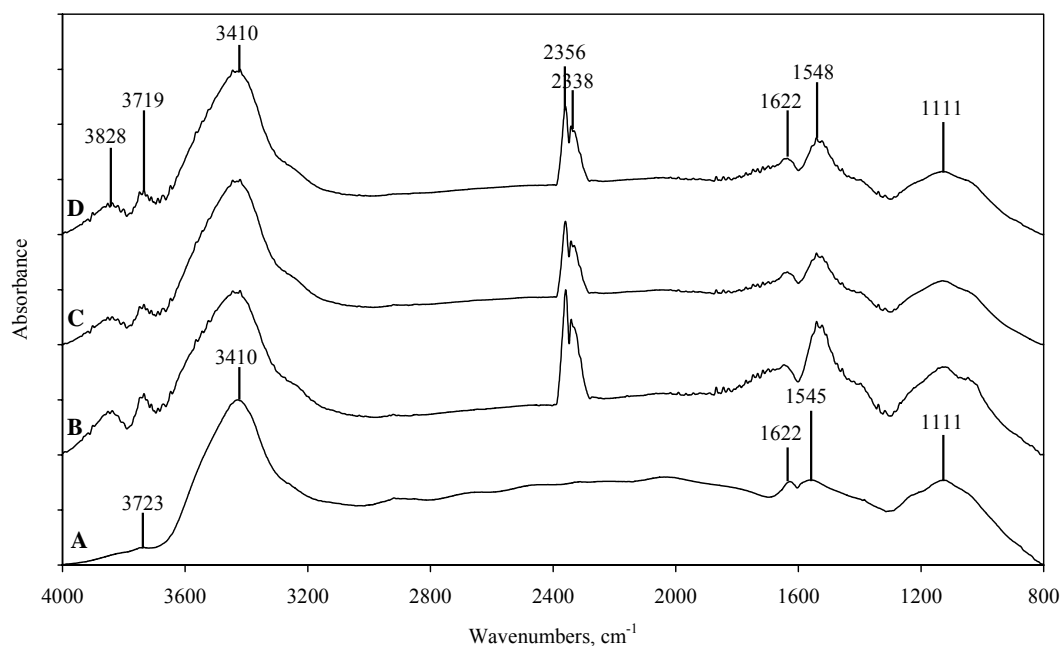


Figure 4.7 Comparison of FT-IR spectra for the original sample (A) with ozone oxidized samples in a reflux column and metal (Zn) addition (O_3 gas flow rate 1.5 L/min at various times of : B=60 min, C=120 min, D=180 min).

4.2.5 FT-IR spectra of HNO_3 oxidized activated carbon samples

Comparison of FT-IR spectra for the original sample and sample with HNO_3 oxidation is shown in Figure 4.8. The FT-IR spectra of the original sample presents the intensity of the bands at 1116 , 1572 , 1616 , and 3417 cm^{-1} due to $\nu(\text{C-O})$ vibrations in aliphatic ether, $\nu(\text{C=C})$ vibrations in haloalkene, $\nu(\text{C=C})$ vibrations in

alkene, and hydroxyl groups in hydrogen bonding, respectively. The HNO₃ oxidized samples as well as the original sample spectra have a broad absorption band extended between 1000 and 1300 cm⁻¹. This has been assigned to $\nu(\text{C-O})$, and $\delta(\text{O-H})$ vibrations of alcoholic, phenolic, and carboxylic groups. The band at 1705 cm⁻¹ can be assigned to the $\nu(\text{C=O})$ vibrations from ketones, aldehydes, or carboxylic acids. For the activated carbon oxidized with HNO₃ there is a large increase in the intensity of the band at 1705 cm⁻¹, which is absent from the original sample. In this study, the intensity of the band at 1705 cm⁻¹ depended on the concentrations of HNO₃ used for treatment of the activated carbon samples. The great intensity of this band occurred when the concentration of HNO₃ for treatment was increased. The band at 3700 cm⁻¹ is due to $\nu(\text{O-H})$ vibration in hydrogen bonding.

Figure 4.9 shows the comparison of FT-IR spectra for O₃ oxidized samples (in a fluidized-bed and a reflux column) with HNO₃ oxidized samples. The broad band at 1108 cm⁻¹ shows a shoulder at 1021 cm⁻¹ which is due to hydroxyl group in primary aliphatic alcohol and this occurs in the spectra of A and B. The bands centered near 2300 cm⁻¹ for samples A and B are assigned to carbon-oxygen groups due to ketone or CO₂ contamination, which are absent in the spectra of C and D. The bands at 1702 and 1705 cm⁻¹ for samples C and D can be assigned to the $\nu(\text{C=O})$ vibration from ketone, aldehydes, or carboxylic acids, but are absent in the spectra of A and B. Surface oxygen complexes are formed on activated carbons when they are oxidized with HNO₃ in a reflux column. Fixation of the acidic groups on the surface of activated carbons makes it more hydrophilic and it also effects the surface area and pore texture of the activated carbons (Pradhan and Sandle, 1999).

The change in the surface chemistry of activated carbon due to the formation of acidic oxygen complexes will effect the behavior of the samples when they are used as adsorbents.

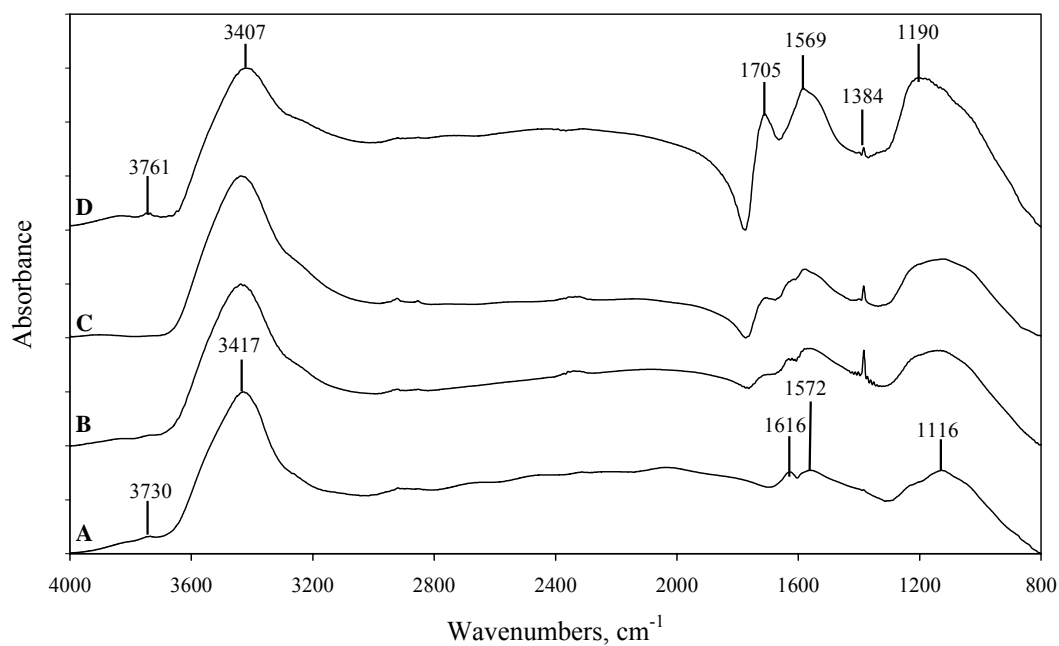


Figure 4.8 Comparison of FT-IR spectra for the original sample (A) with HNO₃ oxidized samples at 105°C for 120 min (HNO₃ concentration: B=2.0 M, C=6.0 M, D=10.0 M).

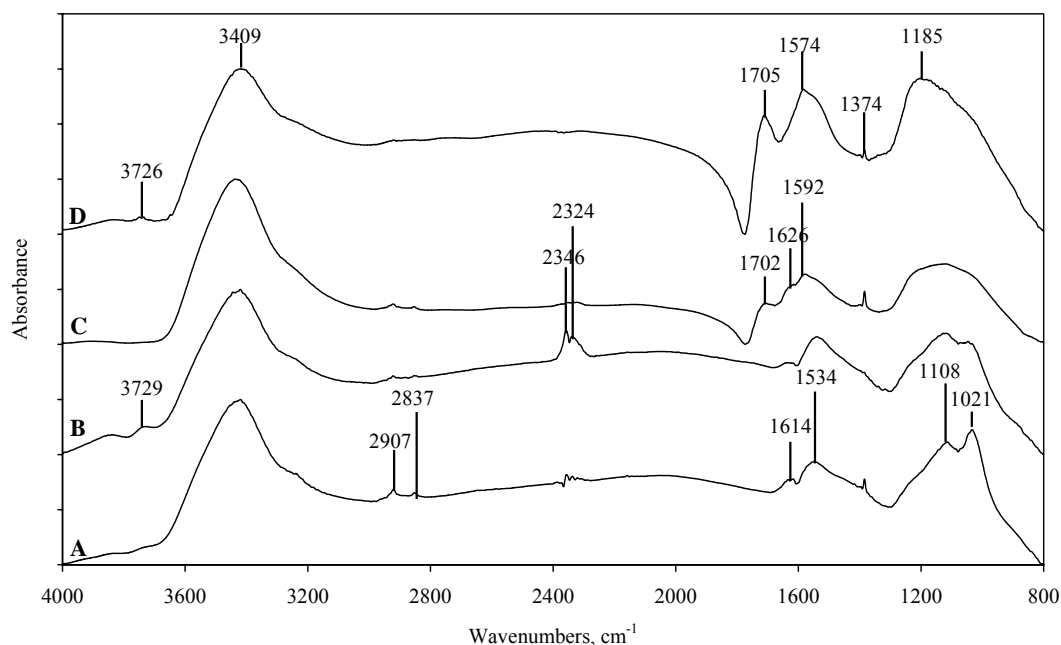


Figure 4.9 FT-IR spectra for ozone oxidized samples (A=210°C, 90 min, in fluidized-bed, B=90°C, 60 min, in a reflux column) and HNO₃ oxidized samples in a reflux column (C=6.0 M HNO₃, D=10.0 M HNO₃)

4.2.6 Measuring a total peak area of untreated and treated activated carbon

Attempt was made in this section to quantify the amounts of surface functional groups from the area under the curve of FTIR spectra. According to the Lambert-Beer law, the absorbance can be related directly to the concentration of a compound in a sample. A peak area evaluation represents a summation of all absorbance values over the wavenumber range in which the band appears. Therefore, the number of points in practical measurements depends on the wavenumber interval of the data and the upper and lower wavenumber limits of the band. Table 4.3 shows total peak areas (proportional to the functional group concentration) of untreated and

treated activated carbon samples for relative comparison of some functional groups from FT-IR spectra for the band occurring in the same spectral region. The total area is the area between the spectrum and zero absorbance or 100% transmittance that lies within the marker bar limits. Double bonds of alkene groups (C=C) of carbon are attacked by O₃ and HNO₃ oxidizing agents. The oxidation begins as addition reactions, but continues beyond to the point where alkene molecules are split apart at the double bond. The products of alkene oxidations can be ketones, carboxylic acids, carbon dioxide, or mixtures of these. The total peak areas values of carboxylic acids or ketones groups increased significantly for treated carbon samples as compared to the untreated ones, resulting from the reaction of O₃ or HNO₃ oxidation. In the case of O₃ treatments, the total peak areas values of carboxylic acids or ketones decreased (see Table 4.3) for O₃ oxidized samples impregnated with Zn by ion-exchange process. This is because an exchange between Zn²⁺ from zinc acetate solution and H⁺ of carbonyl groups of treated activated carbon samples. Other total peak areas values of ether and alkene from O₃ oxidized samples were decreased (see Table 4.3) after impregnated with Zn. The results can be explained as in the case of carboxylic acids or ketones. The position and shape of the bands at about 3440-3410 cm⁻¹ (see Appendix A) are compatible with the involvement of the hydroxyl groups in hydrogen bonding. However, the existence of these bands of hydrogen bonding are those caused by the adsorbed moisture into the KBr pellets during the sample preparation for FTIR analysis (see Figure 4.10).

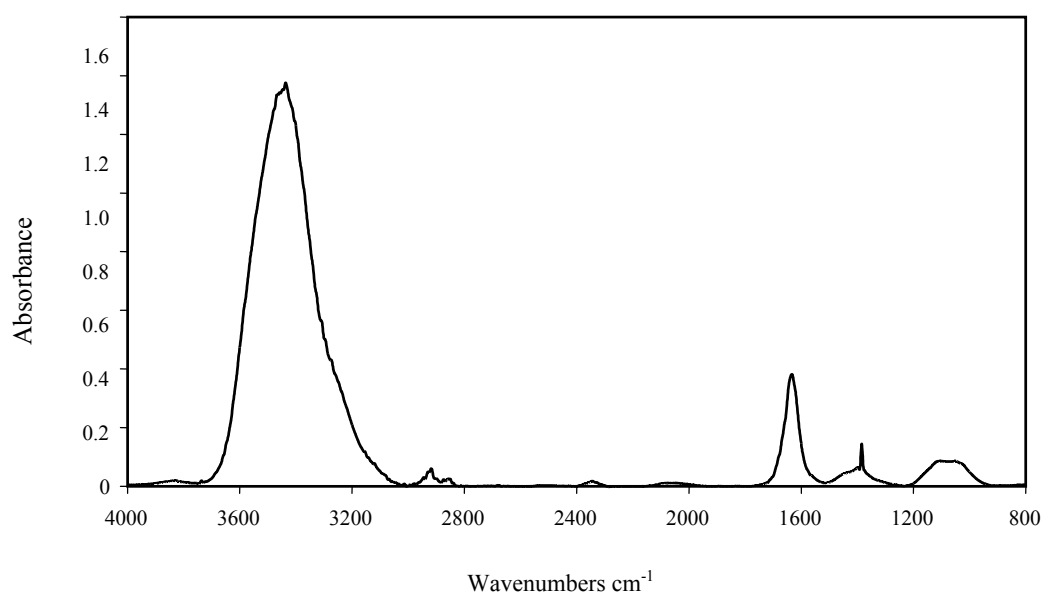


Figure 4.10 FT-IR spectrum for pure KBr (Merck, for spectroscopy).

Table 4.3 Total peak areas of some untreated and treated activated carbon samples examined by FT-IR spectroscopy.

Sample description	Total peak area : A.cm ⁻¹				
	hydrogen bonding	carboxylic or ketone	ester	ether	alkene
Original	571.27	-	-	248.87	63.89
6M HNO ₃	524.72	325.54	27.43	245.31	151.65
10M HNO ₃	644.48	1013.72	16.00	493.99	270.71
O ₃ (reflux 60 min)	670.97	498.91	-	343.28	448.53
O ₃ (reflux 60 min) + Zn	561.52	279.51	-	237.90	94.88
O ₃ (reflux 120 min)	548.44	347.69	-	216.03	438.06
O ₃ (reflux 120 min) + Zn	527.45	267.07	-	172.93	149.10
O ₃ (reflux 180 min)	548.44	347.69	-	216.03	438.06
O ₃ (reflux 180 min) + Zn	511.58	281.21	-	174.97	147.64

4.3 Boehm's Titration

The oxygen complexes identified previously by spectroscopy for the HNO₃ and O₃ oxidized samples were further determined by applying the technique of titration method. This method called the Boehm's titration technique was used for the selective quantification of carboxylic, lactonic, and phenolic. The analysis of the surface acidity resulted from HNO₃ and O₃ treatment are presented in Table 4.4. The original activated carbon sample contains some acidity (phenolic) which can originate from precursor characteristics. The acidity enhancement is evident due to oxidation of the samples. The general trend for the content of a given oxygen complex depends on increasing HNO₃ concentration for oxidation. The total acidity of the activated carbon

oxidized by 10.0M HNO₃ is maximum (3.89 mmol/g-sample). Furthermore, as inferred from FT-IR spectra of HNO₃ and O₃ oxidized sample (see Table 4.2), the most abundant oxygen complexes in these samples are ketone, ester and ether-type structures, which were not analyzed in this study. On the other hand, the HNO₃ oxidized and impregnated with Zn treatment of activated carbons showed a decrease in carboxylic surface groups. This may arise from the ability of Zn ions from Zinc acetate solution in exchanging with H ions from carboxylic acid on activated carbon surface. It should be stated that the results obtained by both FT-IR and Boehm's titration methods are in good agreement.

As an example, consider further the case of 6 M HNO₃ oxidized samples. The amount of carboxylic groups decreased from 1.68 mmol/g-sample to 0.78 mmol/g-sample. According to ion-exchange mechanism 2 mol H⁺ from carboxylic groups can exchange with 1 mol of Zn²⁺ from impregnated zinc samples. The molecular weight, atomic radius, covalent radius, and van der Waals radius of Zn are 65.38, 0.135 nm, 0.131 nm, and 0.139 nm respectively. We can convert the amount of the decreased carboxylic groups (1.68 - 0.78 = 0.9 mmol/g-sample) to the amount of Zn²⁺ being exchanged. In this case, the amount of zinc ions calculated based on the result of ion-exchange with H⁺ is equal to 30.4 mg Zn²⁺/g-sample. This result can be compared to the amount of zinc ions which was measured by atomic absorption spectroscopy (AAs) shown in Table 4.9 (31.60 mg Zn²⁺/g-sample). In the case of 10 M HNO₃ oxidized samples after impregnated with zinc treatment, the carboxylic groups decreased from 2.34 to 1.70 mmol/g-sample. The amount of zinc ions obtained by similar calculation is equal to 41.5 mg Zn²⁺/g-sample while atomic absorption analysis gives the zinc concentration as 52.77 mg Zn²⁺/g-sample. It is probable that,

in compariry with the 6 M HNO₃ sample the 10 M HNO₃ oxidized sample may contain higher amounts of acidic groups that were not detected by the Boehm's titration method used in this work, for example, the carbonyl group which can also exchange for zinc ion. This should explain in part why the amount of zinc ion estimated from ion-exchange process was lower than that determined by AA analysis. Further work is required to substantiate this hypothesis.

Table 4.4 Results of Boehm's Titration.

Sample	Concentration of acidic groups (mmol / g- sample)			
	Carboxylic	Phenolic	Lactonic	Total acidity
Original	0.00	0.20	0.00	0.20
O ₃ oxidation	0.04	0.23	0.08	0.35
6 M HNO ₃	1.68	0.52	0.76	2.96
6 M HNO ₃ +Zn	0.78	1.22	0.69	2.69
10 M HNO ₃	2.34	0.71	0.84	3.89
10 M HNO ₃ +Zn	1.07	1.50	0.84	3.41

4.4 Determination of Oxygen Content

The stage of oxygen chemisorption is of particular interest in this study because it is responsible for the formation of oxygen structure on the carbon surface. The determination of oxygen content confirms the effectiveness of the different oxidizing agents (air, O₂, O₃, and HNO₃) in oxidizing activated carbons. The results of the

laboratory analyses in determining the percentage composition of the oxygen element in the activated carbon samples are shown in Tables 4.5, 4.6, and 4.7. The oxygen elements were successfully analyzed by CHNS/O analyzer. Both air and ozone oxidation enhance an oxygen contents on the surface area of activated carbon samples compared to the original sample and the results are shown in Table 4.5. In the case of the samples oxidized with air (O₀₂ sample), the percentage composition of the oxygen complexes is slightly lower than that of using pure oxygen (O₀₃ sample) as the oxidizing gas at the same conditions. The longer contact time for air oxidation enhances the oxygen complexes on the surface of activated carbon. That is, the oxygen content of O₄₂₁ sample (contact time = 60 min), compared to O₄₂ sample (contact time = 30 min), shows a slight increase from 7.92 to 8.34%. The oxygen percentage was found to increase when the oxidation process was heat treated to a higher temperature. For example, the percentage of the O₃ oxidized sample obtained from the fluidized-bed reactor such as O₅₁ sample (T=90°C), O₅₂₂ sample (T=180°C), and the O₅₂₅ sample (T=240°C), the O₂ contents were 8.22, 9.87, and 10.12% respectively. The longer contact time for the O₃ oxidation process increase the oxygen content as in the case of the air oxidation, this is due to the formation of surface oxygen complexes by the oxidation of surface carbons. For example, the O₅₂₂ sample (T=180°C, time=30 min) and the O₅₂₃ sample (T=180°C, time=90 min), the amounts of oxygen content were 9.87 and 10.95%, respectively. Therefore, the chemical structure of the resultant products (oxygen complexes) are strongly dependent on the ozonation temperature and contact time in the fluidized-bed reactor. Table 4.6 shows typical conditions used in the HNO₃ oxidation and the results of the oxygen percentage from this process. The percentage increase for an oxygen

complexes in the HNO_3 oxidized samples depended on the contact time in a reflux column and the concentration of HNO_3 . The HNO_3 oxidation treatment of the $\text{N}_{2.02}$, $\text{N}_{2.01}$, and $\text{N}_{2.0}$ samples produced a significant increase the amounts of oxygen content of 19.73, 23.55, and 25.26% when the contact times are 30, 60, and 120 min, respectively. In this experiment, the $\text{N}_{10.0}$ sample contain 32.76% oxygen content which is the highest while the $\text{N}_{2.02}$ sample has 19.73% oxygen giving the lowest oxygen content. Table 4.7 shows the results of O_2 contents in the carbon samples which were treated with HNO_3 and followed by ozone oxidation. The oxygen percentage of the $\text{N}_{2.0}$ and $\text{N}_{6.0}$ samples is found to decrease from 25.06 to 20.87% and 28.71 to 27.95%, respectively, but the $\text{N}_{10.0}$ sample shows the increase from 32.76 to 33.12%.

Table 4.5 Oxygen content in the O₃ oxidized carbon samples.

O ₃ , O ₂ , and air oxidized samples	Sample description	Air flow rate (L/min)	Temp. in fluidized-bed (°C)	Time (min)	% oxygen by CHNS/O analyzer
O ₀₁	The original sample	-	-	-	7.10
O ₄₂	Ozonation treatment air as feed gas	5.5	150	30	7.92
O ₄₂₁	Ozonation treatment air as feed gas	5.5	150	60	8.34
O ₅₁	Ozonation treatment oxygen as feed gas	5.5	90	30	8.22
O ₅₂₂	Ozonation treatment oxygen as feed gas	5.5	180	30	9.87
O ₅₂₅	Ozonation treatment oxygen as feed gas	5.5	237-240	30	10.22
O ₅₂₄	Ozonation treatment oxygen as feed gas	5.5	180-190	60	11.24
O ₅₂₃	Ozonation treatment oxygen as feed gas	5.5	180	90	10.95
O ₀₂	Air only as feed gas from air pump	5.5	173-180	90	10.06
O ₀₃	Oxygen only as feed gas (commercial grade)	5.5	173-180	90	10.74

Table 4.6 Oxygen content in HNO₃ oxidized carbon samples.

HNO ₃ conc.(M)	Time for HNO ₃ oxidation (min)	Time for O ₃ oxidation (min)	Temperature in fluidized-bed (°C)	% oxygen by CHNS/O analyzer
2.0	120	30	200	20.87
6.0	120	30	200	27.95
10.0	120	30	200	33.12

Table 4.7 Oxygen content in HNO₃ oxidation followed by O₃ oxidation.

Sample description	HNO ₃ conc.(M)	Temperature in a reflux column (°C)	Time (min)	% oxygen by CHNS/O analyzer
HNO ₃ oxidation	2.0	100-105	30	19.73
HNO ₃ oxidation	2.0	100-105	60	23.55
HNO ₃ oxidation	2.0	100-105	120	25.06
HNO ₃ oxidation	4.0	100-105	120	23.95
HNO ₃ oxidation	6.0	100-105	120	28.71
HNO ₃ oxidation	8.0	100-105	120	29.67
HNO ₃ oxidation	10.0	100-105	120	32.76

In summary, the data of the elemental (oxygen) analysis for O_3 and HNO_3 oxidized samples can be used to support the FT-IR spectra data of these samples. For example, in the case of ketones or carboxylic acids ($C=O$), their contents which is analyzed from FT-IR spectra data increased after treatment and the oxygen content from the elemental analysis data by CHNS/O analyzer also increased (see Tables 4.3, 4.5 and 4.6 for comparison).

4.5 Atomic Absorption Spectrometry Analysis.

The presence of metal content in zinc impregnated carbon samples by ion exchange method was determined using an atomic absorption spectrometry. Table 4.8 shows the effects of zinc acetate concentration and time on the uptake of zinc into the original activated carbon. Zinc content of the original samples by ion exchange method was found to vary between 22.08 and 28.13 mg-Zn/g-sample for the range of 0.05-0.4 M zinc acetate concentration impregnated at 30°C for 90 min as shown in Figure 4.11. This figure shows the effect of initial zinc acetate concentrations in a solution of ion-exchange process on the zinc uptake into the original activated carbon. The maximum uptake of zinc (~28.31 mg-Zn/g-sample) occurs over a narrow range of feed solution of 0.1-0.2 M. Figure 4.12 shows the effect of impregnation time during ion-exchange process on zinc uptake into activated carbon (mg-Zn/g-sample). In this study, when the ion-exchange condition was controlled at 30°C and with initial zinc acetate concentration of 0.2 M, the highest zinc content of 32.81 mg-Zn/g-sample was obtained at 120 min and the lowest is 16.17 mg-Zn/g-sample at 30 min contact time. Thus, the increase in zinc content of samples depended directly on the contact time during an ion-exchange process.

Table 4.8 Effects of zinc acetate concentration and time on the uptake of zinc by the untreated activated carbon as analyzed by AA_s.

The original sample condition			Sample wt.(g)	Zinc conc. (ppm)	mg- Zn/g-sample
Zinc acetate conc.(M)	Temperature (°C)	Time (min)			
0.05	30	90	0.1359	3.0	22.08
0.1	30	90	0.1102	3.1	28.13
0.2	30	90	0.1088	3.0	27.57
0.3	30	90	0.1052	2.4	22.81
0.4	30	90	0.1048	2.5	23.85
0.2	30	30	0.1051	1.7	16.18
0.2	30	60	0.1048	2.7	25.76
0.2	30	90	0.1088	3.0	27.57
0.2	30	120	0.1158	3.8	32.82

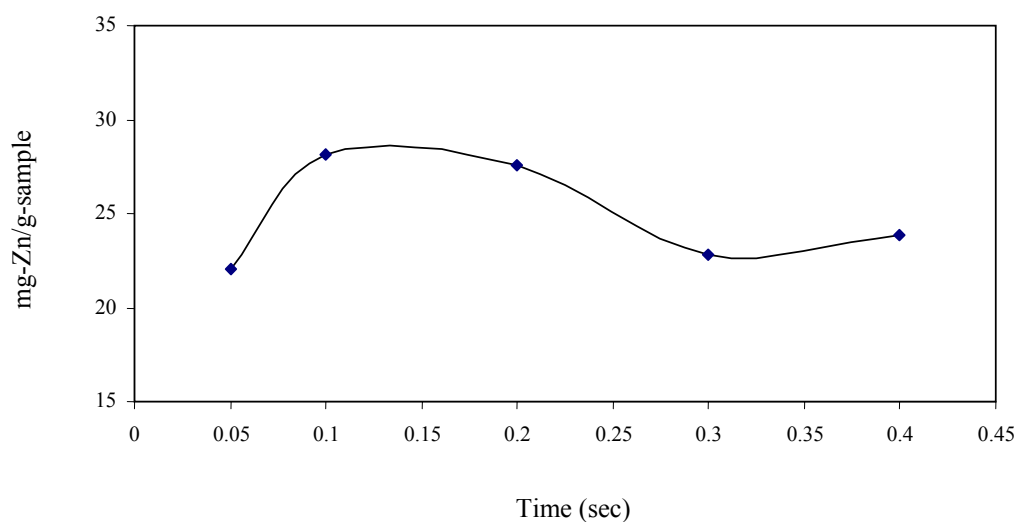


Figure 4.11 Initial zinc acetate concentrations in a solution of ion-exchange process for metal addition of the original samples affecting zinc uptake into activated carbon. Time = 90 min, T = 30°C.

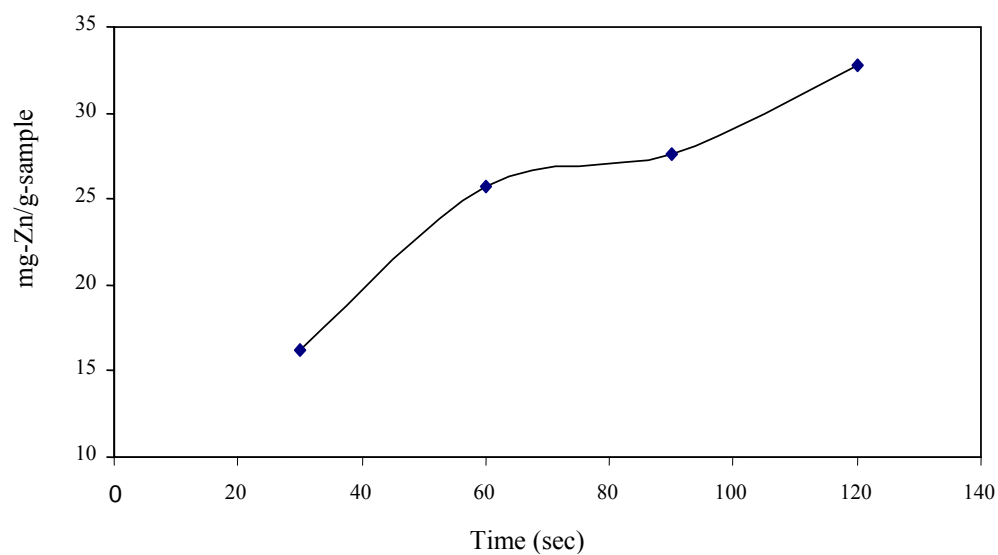


Figure 4.12 The times during ion-exchange process on metal addition of the original

samples effect to zinc uptake into activated carbon. T= 30°C.

The amount of zinc metal added to the oxidized samples (O₃ and HNO₃ oxidation) is given in Table 4.9. For the activated carbon sample oxidized with O₃ in the fluidized-bed at 210°C for 90 min, the maximum amount of added zinc metal is found to be 36.04 mg-Zn/g-sample. In the case of O₃ oxidation in a reflux column at 90°C, the amount of zinc metal in these samples decreased with increasing the contact time. For HNO₃ oxidation samples, the trend of increasing zinc metal uptake on surface area of the impregnated samples depended on the HNO₃ concentrations used for the oxidation process. In this case, sample oxidized with 10.0 M, HNO₃ gives the maximum in the zinc content, while with 2.0 M HNO₃ it gives the minimum.

Table 4.9 The amount of zinc metal added to the oxidized activated carbon samples.

Sample description			Sample wt.(g)	Zinc conc. (ppm)	mg- Zn/g-sample
Oxidation methods	Maximum temp. (°C)	Time (min)			
O ₃ oxidation in fluidized-bed reactor	150	60	0.1177	1.6	13.59
	180	30	0.1048	1.8	17.18
	190	60	0.1120	2.0	17.86
	210	90	0.1304	4.7	36.04
O ₃ oxidation in a hot water(reflux)	90	60	0.1300	4.8	36.92
	90	120	0.1308	3.4	25.99
	90	180	0.1299	3.2	24.63
2.0M HNO ₃ oxidation (reflux)	90	120	0.1084	2.2	20.30
6.0M HNO ₃ oxidation (reflux)	105	120	0.1234	3.9	31.60
10.0M HNO ₃ oxidation (reflux)	110	120	0.1175	6.2	52.77

Note Zn added to sample by ion-exchange (0.2 M zinc acetate, time = 120 min).

4.6 Nitrogen Adsorption Isotherms

Nitrogen adsorption isotherm is a standard tool for the characterization of porous materials, especially porous carbonaceous adsorbents. The adsorption isotherm can be measured to yield valuable information about surface area and pore structure of an adsorbent, heat of adsorption and so on (Pradhan and Sandle, 1999). The nitrogen adsorption isotherms obtained for different activated carbon samples are shown in Appendix B. It is noted that the specific surface areas of activated carbon evaluated by BET analysis decreased following the chemical oxidation and metal addition. In Figure 4.13 the nitrogen adsorption isotherms on the 6.0 M HNO₃, 6.0 M HNO₃ + Zn, and 10.0 M HNO₃ + Zn are compared in order to show the differences in their adsorption capacity and isotherm type. The treated activated carbons cause the downward shift of the isotherms. In the case of sample oxidized with 10.0 M HNO₃ and Zn addition, the shift is maximum. The similar N₂ adsorption isotherms on activated carbon treated with O₃ oxidation in a fluidized-bed at 210°C for 90 min and impregnated with Zn, and O₃ oxidation in a reflux column at about 100°C (for 60, 120, and 180 min) and impregnated with Zn are shown in Figure 4.14. Figure 4.15 shows the N₂ adsorption isotherms on the different treated samples. These isotherms obtained from the original (untreated), the original and impregnated with Zn, O₃ oxidation in a reflux column about 100°C for 60 min, and 6.0 M HNO₃ oxidation and impregnated with Zn samples. The sample that shows the maximum volume adsorbed (cm³/g) of N₂ is the original sample. All the isotherms can be classified as the type I isotherm which is typical of adsorption in microporous solids (Do, 1998). The lowering of N₂ adsorption of modified activated carbons suggests that some of the pores may be blocked by the presence of oxide functional groups introduced during

the chemical treatment (Jae-Woon, et al., 2001) so that N_2 molecules can not transport to the adsorptive sites.

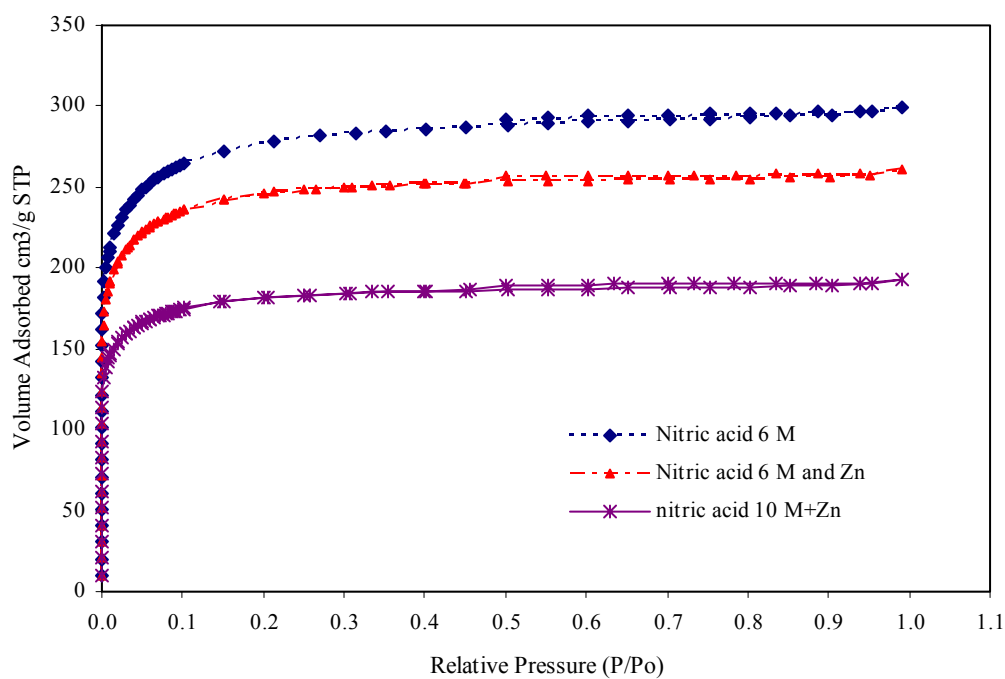


Figure 4.13 N_2 adsorption isotherms of activated carbons treated with HNO_3 oxidation and Zn addition at 77 K.

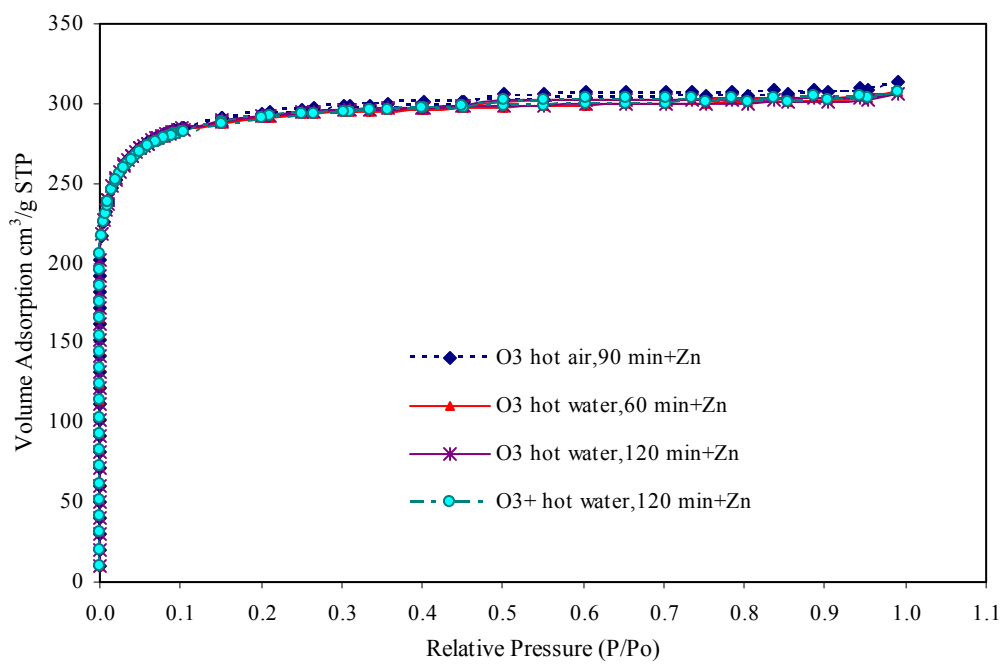


Figure 4.14 N₂ adsorption isotherms on activated carbons treated with O₃ oxidation and Zn addition at 77 K.

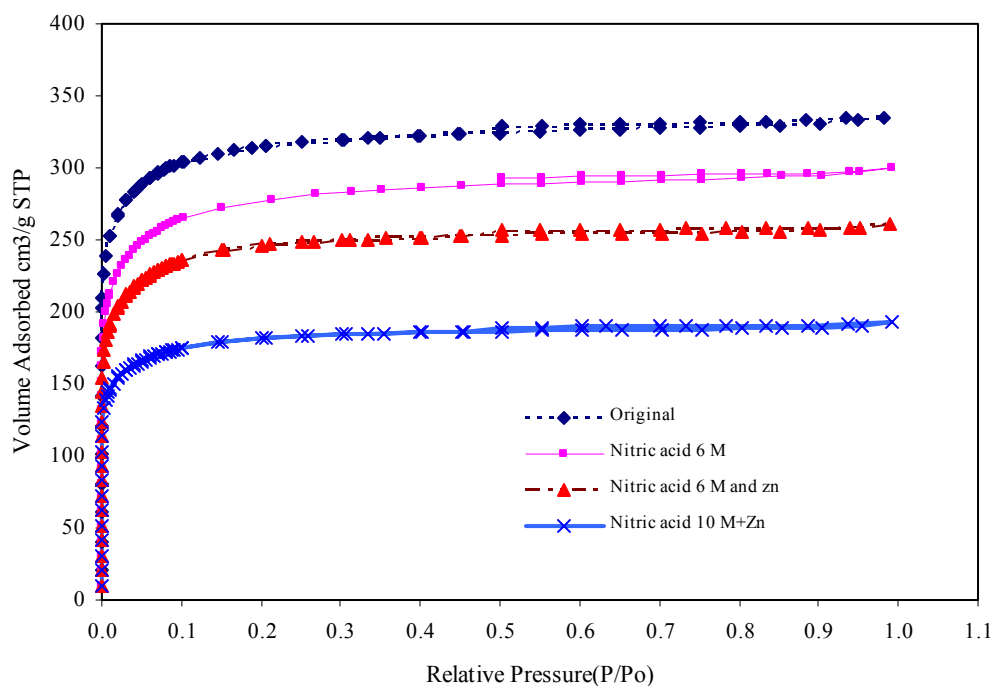


Figure 4.15 N₂ adsorption isotherms on the different treatments of activated carbons at 77 K.

4.7 Surface Area and Porosity Analysis

Table 4.10 shows the results of surface area and pore volume of the treated activated carbons. For HNO₃ oxidized samples, the decrease in surface area with different treatments is in the following order, 6.0 M HNO₃, 6.0 M HNO₃+Zn, 10.0 M HNO₃+Zn. The BET surface area considerably decreased possibly due to the blocking of the narrow pores by the surface complexes introduced during the treatment process so that N₂ molecules can not get access to the adsorption sites (Pradhan and Sandle, 1999). Oxygen surface groups are expected to locate at the edges of the basal planes which are relatively weak sites of carbon structure and oxidation progresses slowly into the basal planes (Jae-Woon, et al., 2001). The micropore volume also decreases with oxidation and metal addition of activated

carbon, and in the case of 10.0 M HNO₃ the decrease is maximum. In summary, the decreasing surface area and pore volume of the oxidized activated carbon samples is caused by the increase of some functional groups existing on the carbon surface (see Tables 4.3, 4.4 and 4.10 for comparison).

Table 4.10 Specific surface areas and porosities in activated carbon samples by N₂ adsorption.

Sample	Surface area analysis, m ² /g			Pore volume; cm ³ /g		Average pore size; nm
	Total	Micropore	External	Micropore	Total	
Original	1119	879	240	0.38	0.52	1.85
Original+ Zn	967	767	200	0.37	0.49	2.02
6M HNO ₃	909	640	269	0.31	0.46	2.04
6M HNO ₃ +Zn	808	593	215	0.28	0.40	1.20
10M HNO ₃ +Zn	597	454	143	0.22	0.30	2.00
O ₃ (fluidized-bed 210°C)+Zn	967	767	200	0.37	0.49	2.01
O ₃ (reflux 60 min) + Zn	959	791	168	0.38	0.47	1.98
O ₃ (reflux 120 min) + Zn	962	783	179	0.37	0.47	1.97
O ₃ (reflux 180 min) + Zn	957	766	191	0.36	0.47	1.99

4.8 H₂S Adsorption by Fixed Bed Activated Carbon

The term breakthrough used throughout this thesis is referred to as the condition at which a certain concentration of H₂S is first detected at the exit of the adsorber. In this experiment, the exit concentration of H₂S was continuously monitored by an electrochemical sensor instrument every 5 seconds and real-time experimental data were transferred to a personal computer. In this work, breakthrough in all H₂S adsorption experiments is based on three environmental standards, namely, NIOSH: ceiling 10, OSHA: ceiling 20, and OSHA: ceiling 50 corresponding to the ceiling limit of H₂S concentration of 10, 20, and 50 ppm, respectively, which are the exposure limit for H₂S gas (Chou, 2000). Accordingly, breakthrough time is defined as the time that the outlet gas H₂S concentrations reaches the 10, 20, and 50 ppm levels. The resulting breakthrough times of the original, HNO₃ oxidized, O₃ oxidized, and Zn impregnated samples for exposure limits of Time-Weighted Average (TWA value) are listed in Table 4.11 and 4.12. As a rough indication, the larger the value of the breakthrough time, the better the efficiency of H₂S removal by the carbon bed. The National Institute for Occupational Safety and Health (NIOSH) is a branch of the U.S. Department of Health and Human Services, Public Health Service, Centers for Disease Control and Prevention. It publishes recommended exposure limits for hazardous substances or concentrations in the work place. The Occupation Safety and Health Administration (OSHA) published the permissible exposure limits that are known as the General Industry Air Contaminants Standard for use in promulgating legal standards (Chou, 2000).

Table 4.11 Breakthrough times of HNO₃ oxidation and Zn addition for exposure limits (TWA value).

Sample description		NIOSH : ceiling = 10 ppm	OSHA : ceiling = 20 ppm	OSHA : ceiling = 50 ppm for 10- min
HNO ₃ oxidation and/or metal addition	Adsorption temp.(°C)	Breakthrough times(sec)	Breakthrough times (sec)	Breakthrough times (sec)
Original	30	620	645	680
2 M HNO ₃	30	235	260	295
6 M HNO ₃	30	285	310	350
6 M HNO ₃ +Zn	30	1315	1410	1530
10 M HNO ₃	30	115	200	320
10 M HNO ₃ +Zn	30	270	315	335
Original	10	1085	1095	1115
Original + Zn	10	1590	1600	1610
6 M HNO ₃	10	1040	1175	1385
6 M HNO ₃ +Zn	10	2015	2030	2065
Original	45	690	700	735
Original+ Zn	45	1530	1535	1540
6 M HNO ₃	45	135	170	210
6 M HNO ₃ + Zn	45	2345	2360	2365
10 M HNO ₃ + Zn	45	940	990	1055

Note NIOSH = The National Institute for Occupational Safety and Health

OSHA = The Occupational Safety and Health Administration

Table 4.12 Breakthrough times of O₃ oxidation and Zn addition for exposure limits
(TWA Value)

Sample description		NIOSH : ceiling = 10 ppm	OSHA : ceiling = 20 ppm	OSHA :ceiling = 50 ppm,for 10 -min
O3 oxidation and metal addition	Adsorption temp.(°C)	Breakthrough times(sec)	Breakthrough times(sec)	Breakthrough times(sec)
Fluidized-bed 210°C,90 min+Zn	30	1230	1275	1425
Hot water,90 °C 60 min+Zn	30	1710	1760	1925
Hot water,90°C 120 min+Zn	30	1575	1645	1745
Hot water,90 °C 180 min+Zn	30	1765	1840	1970
Fluidized-bed 210 °C,90 min+Zn	10	2050	2055	2060
Hot water,90 °C 60 min+Zn	10	2260	2265	2270
Hot water,90 °C 120 min+Zn	10	2125	2130	2140
Hot water,90 °C 180 min+Zn	10	1810	1830	1885
Fluidized-bed 210 °C,90 min+Zn	45	1540	1550	1595
Hot water,90 °C 60 min+Zn	45	1520	1525	1535
Hot water, 90 °C 120 min+Zn	45	1745	1750	1760
Hot water , 90 °C 180 min+Zn	45	1710	1715	1720

4.8.1 Adsorption capacity of untreated activated carbons

Figure 4.16, 4.17, and 4.18 show H₂S breakthrough curves for the original samples at three different temperatures (10, 30 and 45°), respectively. The corresponding breakthrough times for adsorption at 10, 30, and 45°C are 1095, 645, and 700 seconds, respectively (see Figure 4.19 for direct comparison). In the case of the original sample, adsorption of gas molecules on activated carbon is expected to be dominated by the van der Waals forces which is physical in nature. In addition, the small pore sizes and large surface area of activated carbon play the major role in gas adsorption (Yang, 2003). The maximum breakthrough time occurred at 10°C, because in physical adsorption the adsorption capacity generally increases with decreasing in adsorption temperature. However, the breakthrough time for adsorption at 45°C is higher than that at 30°C which should be otherwise. Figure 4.20 and 4.21 show H₂S breakthrough times for adsorption of the original activated carbon impregnated with Zn at 10 and 45°C respectively. Comparison of H₂S breakthrough times at 20 ppm between the untreated (original 10°C) and the original sample treated with Zn samples (original + Zn 10°C) is shown in Figure 4.22. The breakthrough times of the best untreated and the best treated with Zn samples for H₂S removal at the same adsorption temperature of 10°C were 1085 and 1590 seconds, respectively. In this figure, the original carbon impregnated with Zn had a longer breakthrough time for H₂S removal at 10°C than the breakthrough time of the original sample at 10°C. These results suggest that interaction between the H₂S gas and Zn metal on treated activated carbon sample surface enhances H₂S adsorption. In addition, the breakthrough time of the original impregnated with Zn sample for H₂S removal at 10°C is slightly greater than the original sample impregnated with Zn at 45°C. It is

probable that when the adsorption temperature is lowered (at 10°C) the effect of physical adsorption becomes more important than the chemical adsorption by Zn because the surface concentration of Zn is not high enough to dominate the adsorption mechanism.

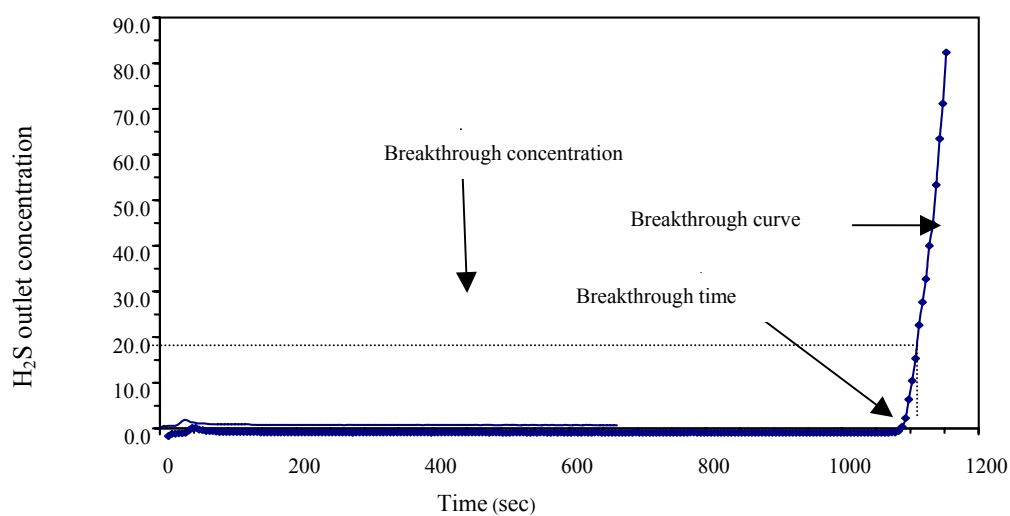


Figure 4.16 H₂S breakthrough curve for the original activated carbon sample. Gas composition: 1.01% H₂S, balance N₂. T = 10°C, P = 1.0 bar.

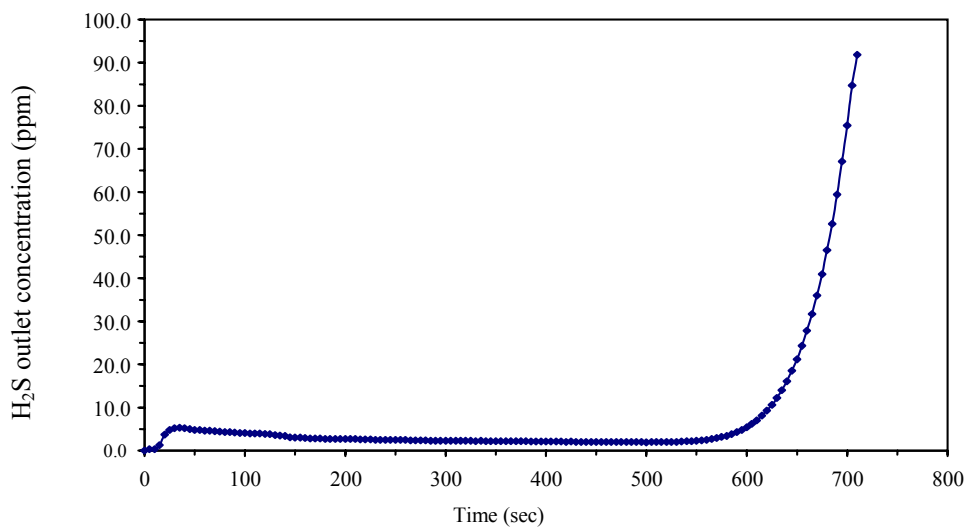


Figure 4.17 H₂S breakthrough curve for the original activated carbon sample. Gas composition: 1.01% H₂S, balance N₂. T = 30°C, P = 1.0 bar.

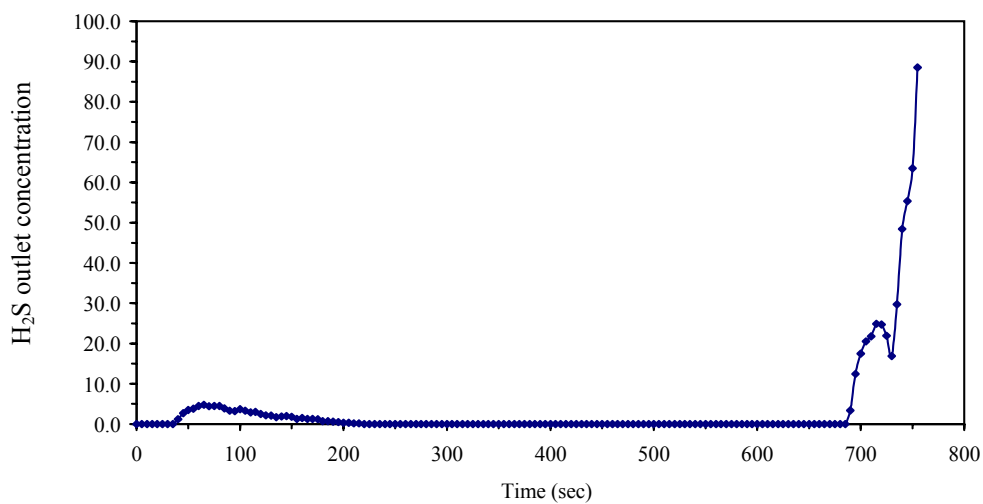


Figure 4.18 H₂S breakthrough curve for the original sample. Gas composition: 1.01% H₂S + balance N₂ (T = 45°C, P = 1.0 bar).

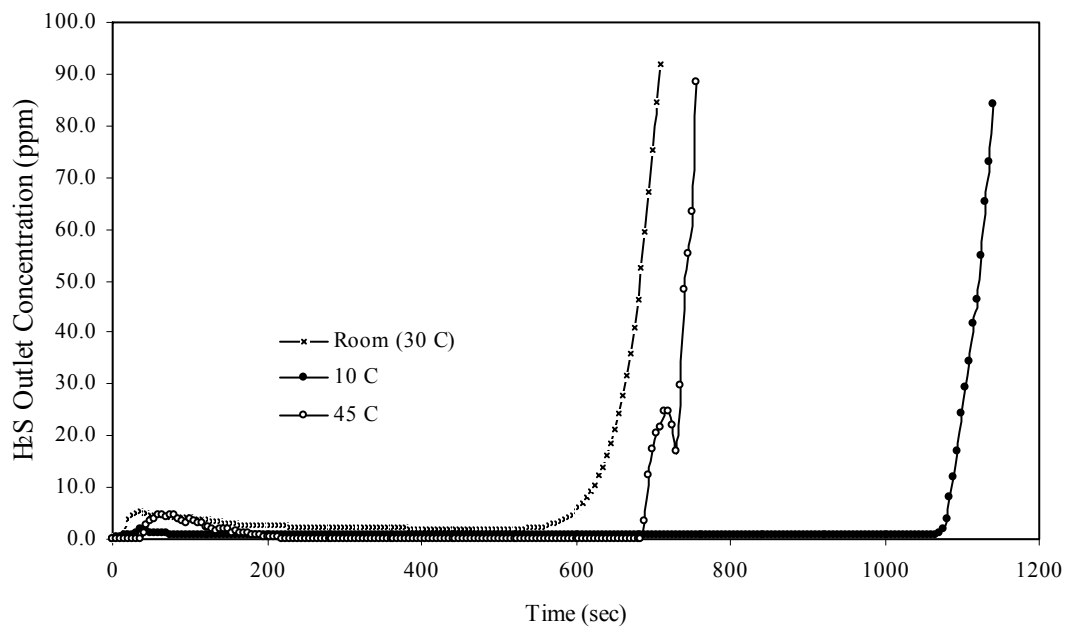


Figure 4.19 Comparison of H₂S breakthrough curves for the original activated carbon samples at various temperatures. Gas composition: 1.01% H₂S + balance N₂ and P=1.0 bar.

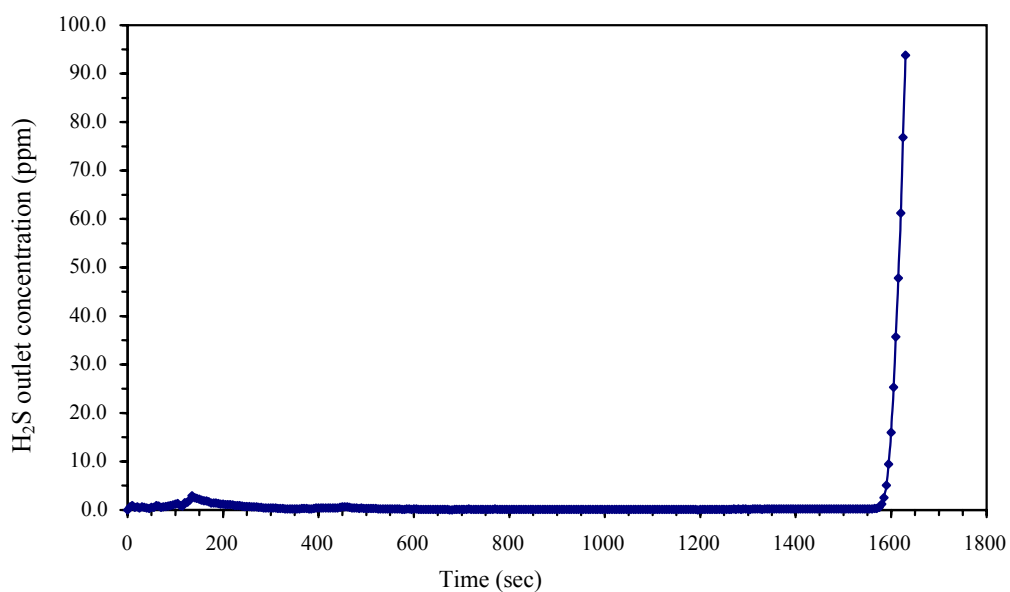


Figure 4.20 H₂S breakthrough curve for the original activated carbon sample after impregnated with Zn. Gas composition: 1.01% H₂S + balance N₂ (T = 10°C, P = 1.0 bar).

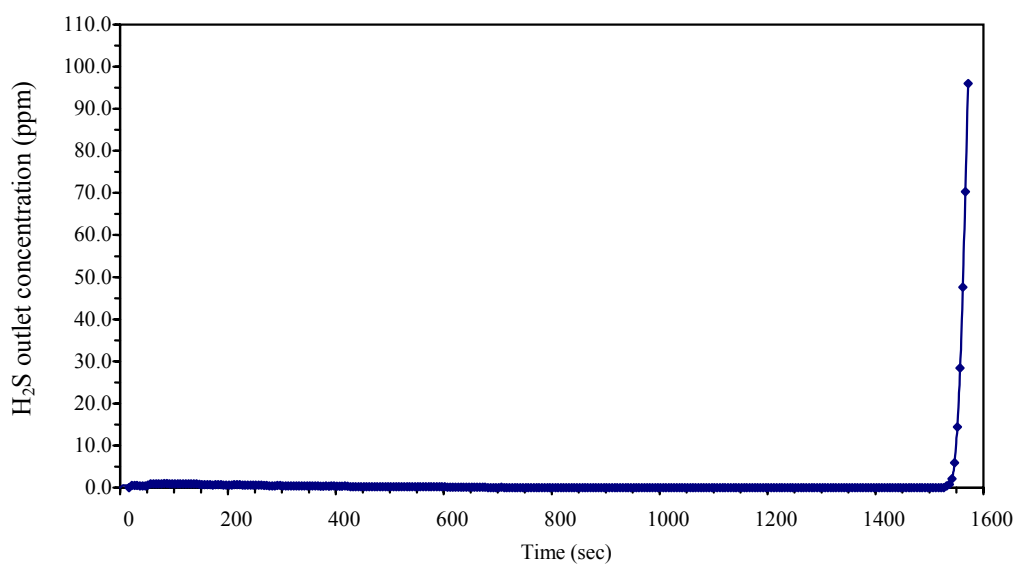


Figure 4.21 H₂S breakthrough curve for the original activated carbon sample after impregnated with Zn. Gas composition: 1.01% H₂S + balance N₂ (T = 45°C, P = 1.0 bar).

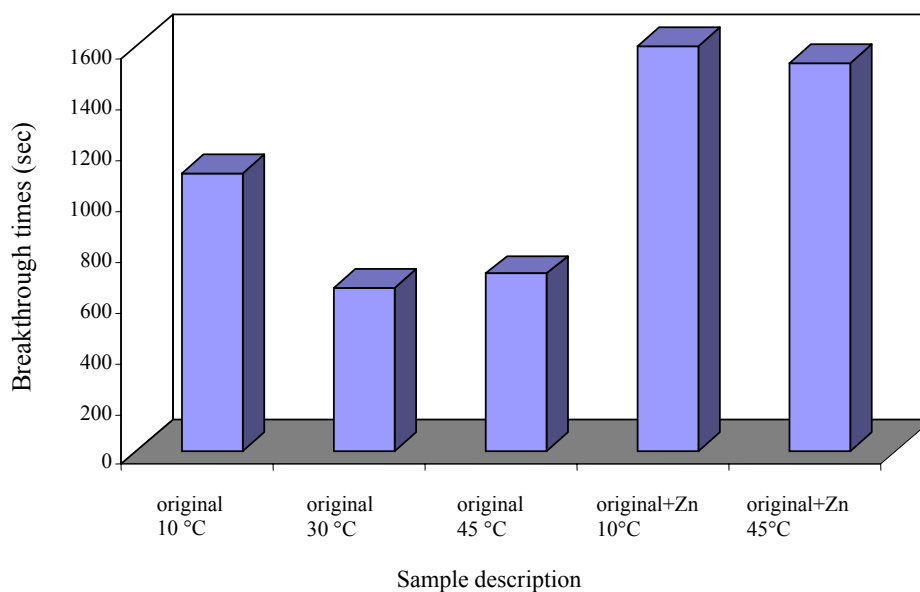


Figure 4.22 Comparison of H₂S breakthrough times for the original activated carbon and the original impregnated with Zn samples at various temperatures, P=1.0 bar. Gas composition: 1.01% H₂S in balance N₂.

4.8.2 Adsorption capacity of treated activated carbons (HNO₃ oxidation)

Figure 4.23, 4.24, 4.25, 4.26 and 4.27 show typical breakthrough curves for H₂S adsorption of HNO₃ oxidized samples at various temperatures and HNO₃ treated concentration. The shapes of these breakthrough curves were different from the results of untreated activated carbon samples. Their shapes were not closely parallel to the x axis before they reach the starting of the breakthrough time. These results indicate that certain amount of H₂S molecules can by-pass the adsorption bed without being adsorbed. Because carbon surface oxidation can either promote or inhibit adsorption depending on the nature of oxide, adsorbate and the solution chemistry (Chen et al., 2003). Adsorption can be influenced by surface charge, van der Waals forces, hydrogen bonding, π - π bonding, chemisorption and electron

transfer complexes (Radovic et al., 2001). The several possible causes that have been considered about the decreasing adsorption of gases by surface oxidation are

1. Micropore blocking effect; surface oxide formation decreases total access area for adsorption by blocking fine pores or pores mouths.
2. Steric hindrance effect, introducing surface functionality disrupts the close geometric accommodation between the adsorbate and the surface thus reducing the overall strength of attractive force (Chen, et al., 2003). This effect would be most important for large adsorbates and those capable of π - π bonding which relies on the atomic flatness of graphene basal plane segments.

Figure 4.28 shows the comparison of H₂S breakthrough curves for 6.0 M HNO₃ oxidized samples at 10, 30, and 45°C. The H₂S breakthrough times at 20 ppm for 6.0 M HNO₃ oxidized samples at 10, 30, and 45°C was approximately 1175, 310, and 170 sec respectively (see Table 4.10). Thus, the 6.0 M HNO₃ oxidized sample at 10°C gave the highest adsorption capacity for H₂S removal. These results support the role of physical adsorption for the adsorption of H₂S by surface oxidized carbons. Comparison of breakthrough curves for the original and oxidized samples at various concentrations of 2.0, 6.0, and 10.0 M HNO₃ at 30°C is shown in Figure 4.29. The H₂S breakthrough times at 20 ppm was approximately 645, 260, 310, and 200 sec, respectively (see Table 4.11). The best adsorbent in this condition for H₂S removal was the original sample. This again emphasizes the role of physical adsorption in the case of oxidized samples. The various HNO₃ concentrations used for sample oxidations in this study had an influence on the breakthrough curves for H₂S adsorption. For example, the breakthrough time of 6.0 M HNO₃ oxidized sample for H₂S removal at 30°C is longer than the breakthrough time of 10.0 M HNO₃ oxidized sample for H₂S removal at 30°C. The change of total peak areas or

concentrations of acidic groups on HNO_3 oxidized samples (see Tables 4.3 and 4.4 for comparison) can effect the interaction force between the polar H_2S molecules and the acidic functional groups on the oxidized sample surface. Thus, the probability of repulsion of H_2S molecules with similar partial charges of polar functional groups may increase with increasing the HNO_3 concentrations for sample oxidation.

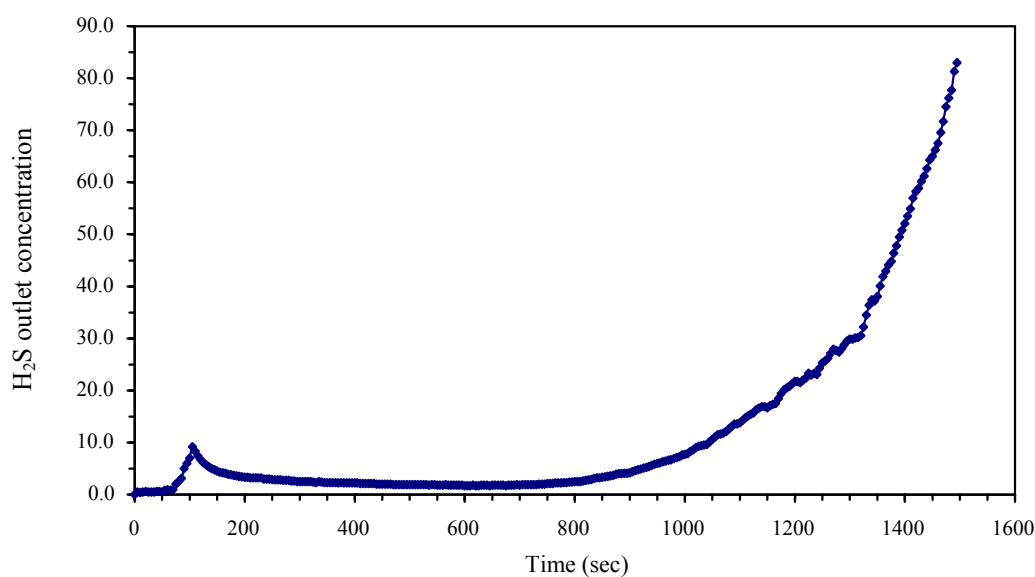


Figure 4.23 H_2S breakthrough curve for activated carbon sample after oxidized with 6.0 M HNO_3 . Gas composition: 1.01% H_2S , balance N_2 . $T = 10^\circ\text{C}$, $P = 1.0$ bar.

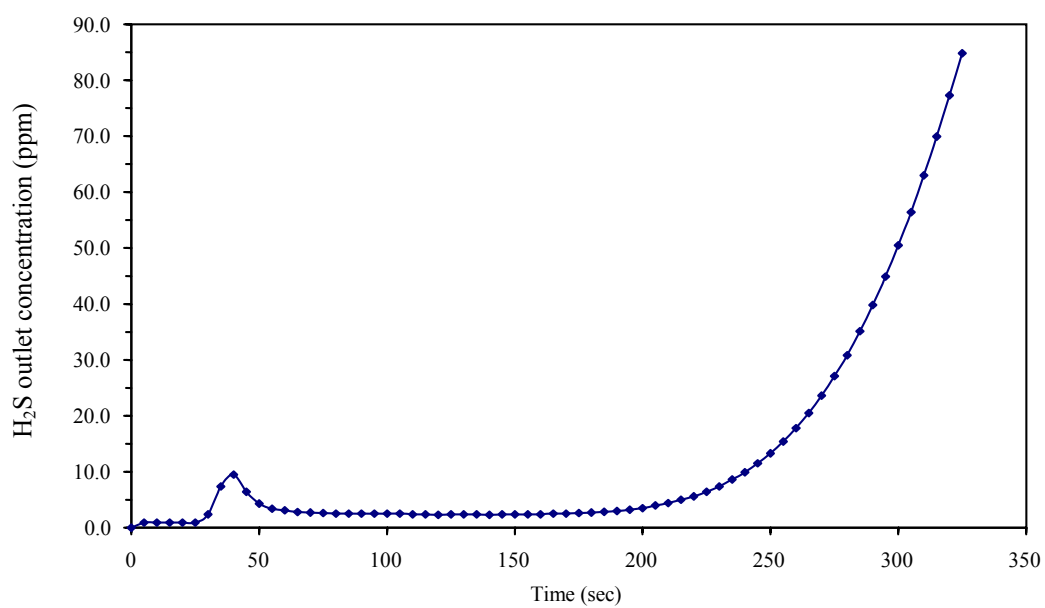


Figure 4.24 H₂S breakthrough curve for activated carbon sample after oxidized with 2.0 M HNO₃. Gas composition: 1.01% H₂S, balance N₂. T = 30°C, P = 1.0 bar.

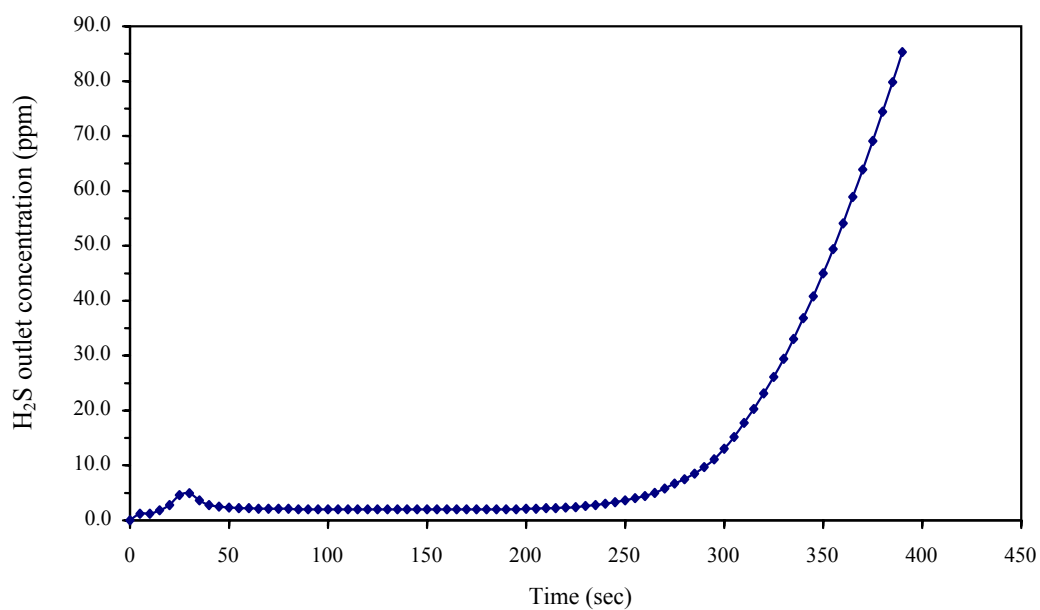


Figure 4.25 H₂S breakthrough curve for activated carbon sample after oxidized with 6.0 M HNO₃. Gas composition: 1.01% H₂S, balance N₂. T = 30°C, P = 1.0 bar.

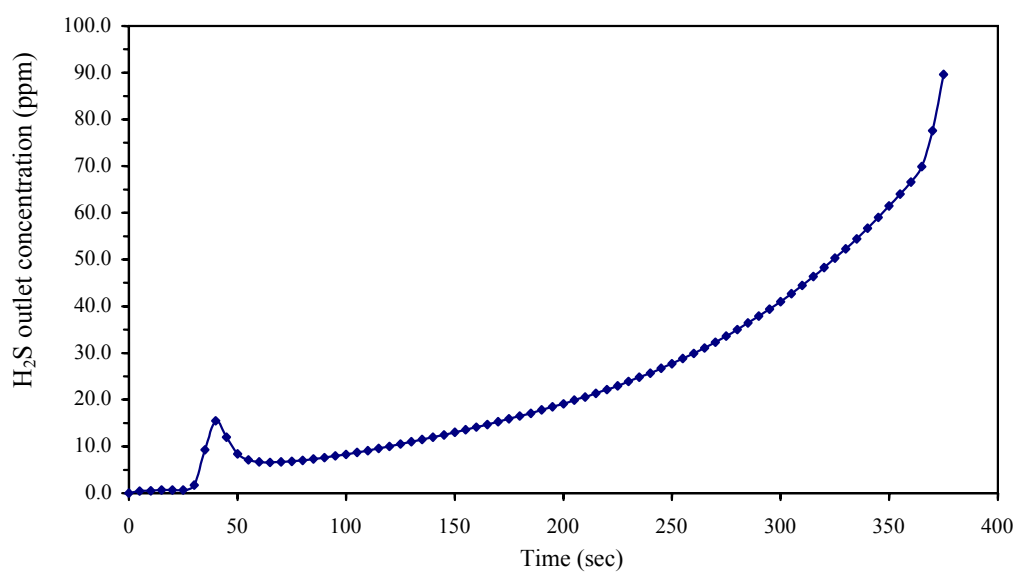


Figure 4.26 H₂S breakthrough curve for activated carbon sample after oxidized with 10.0 M HNO₃. Gas composition: 1.01% H₂S, balance N₂. T = 30°C, P = 1.0 bar.

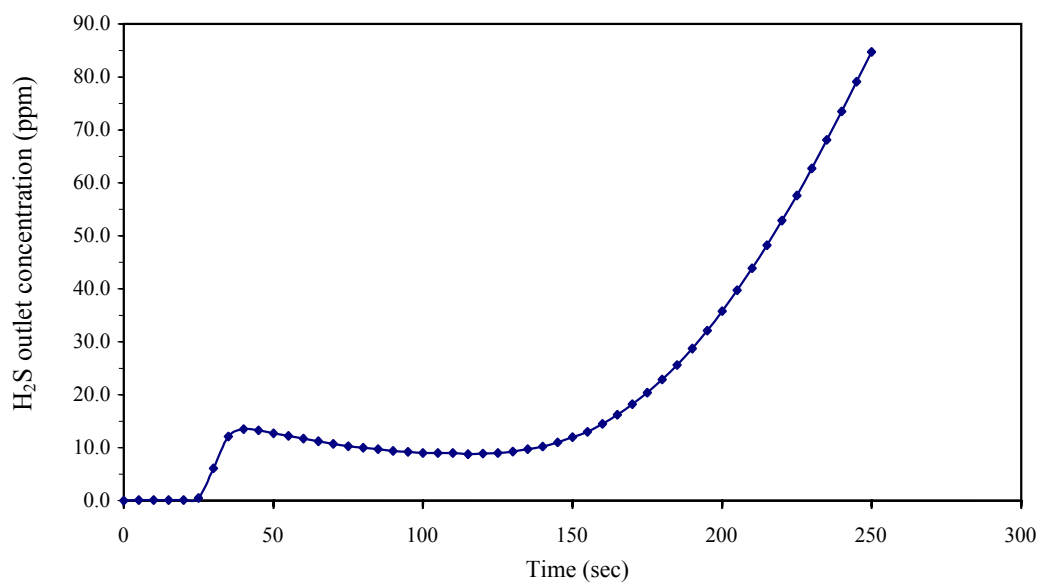


Figure 4.27 H₂S breakthrough curve for activated carbon sample after oxidized with 6.0 M HNO₃. Gas composition: 1.01% H₂S, balance N₂. T = 45°C, P = 1.0 bar.

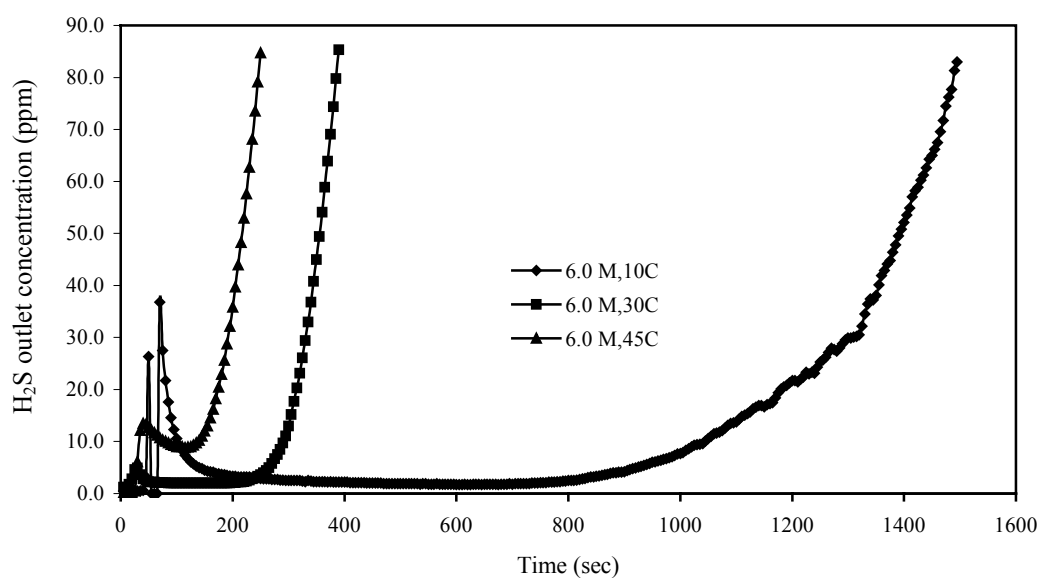


Figure 4.28 Comparison of H₂S breakthrough curves for 6.0 M HNO₃ oxidized samples with different treatment temperatures, P=1.0 bar. Gas composition: 1.01% H₂S, balance N₂.

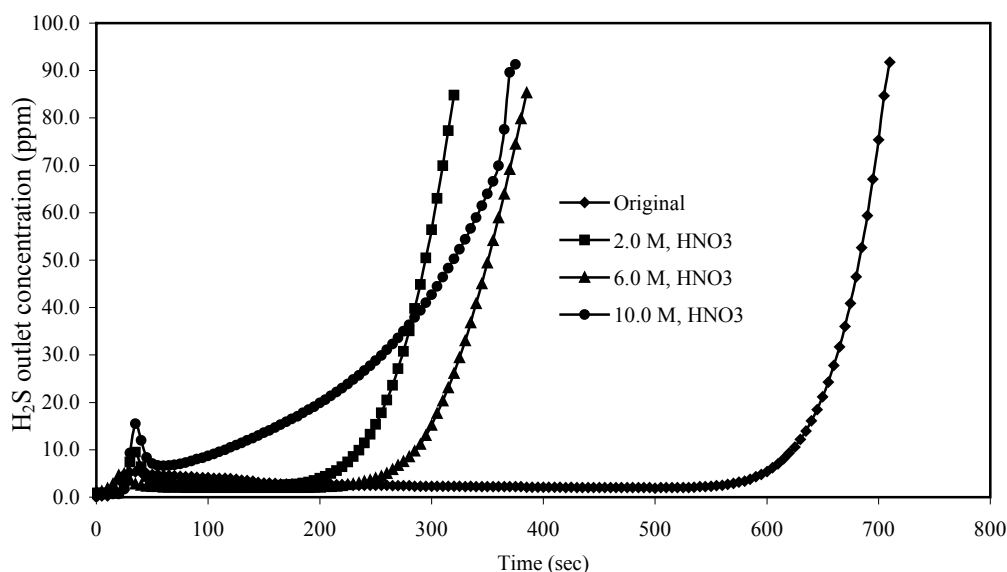


Figure 4.29 Comparison of H₂S breakthrough curves for HNO₃ oxidized samples at 30°C with different concentration, P=1.0 bar. Gas composition: 1.01% H₂S, balance N₂.

4.8.3 Further analysis of H₂S removal by oxidized samples

The mechanisms of H₂S removal by oxidized activated carbon samples can be explained in terms of intermolecular forces, the forces of interaction between molecules. The interaction forces are normally weakly attractive. Three types of attractive forces known to exist between neutral molecules are dipole-dipole forces, London forces, and hydrogen bonding forces (Birk, 1994). Intermolecular attractive forces, collectively called van der Waals forces are electrical in nature and result from the attraction of charge of opposite sign. One type of van der Waals force results from the electrostatic attraction of the positive end of one polar molecule for the negative end of another. Another component of the van der Waals forces, found with both nonpolar and polar molecules, is called the dispersion force or London

force. London forces are the weak attractive forces between molecules resulting from the small instantaneous dipoles that occur because of the varying positions of the electron during their motion about nuclei. London forces tend to increase with molecular weight because the forces increase in strength with the number of electrons. Polar molecules can attract one another through dipole-dipole forces. The dipole-dipole force is an attractive intermolecular force resulting from the tendency of polar molecules to align themselves such that the positive end of one molecule is near the negative end of another. A polar molecule has a dipole moment as a result of the electronic structure of the molecule. Hydrogen bonding is a special type of dipole-dipole attraction that results when hydrogen is found in compounds with very electronegative elements such as fluorine, oxygen, nitrogen, and chlorine, but is absent in sulfur atoms of H₂S compounds.

In this experiments, the polar H₂S molecules had the dipole-dipole forces but they could not form hydrogen bonding by themselves or with another molecules from the functional groups of oxidized activated carbon samples. While the hydrogen sulfide gas molecules in the adsorber collided with the other molecules from the functional groups of the oxidized activated carbon samples, some of H₂S molecules are attracted to each other but they are repulsed by similar partial negative charges (δ^-) of the polarity of C=O and/or C-O groups from the functional groups. Because of the polarity of C=O and/or C-O groups, such as carboxylic acids, esters, and ketones are polar compounds. Their molecules are attracted to each other, but not as strongly as they would be if they had OH groups instead and so could participate in hydrogen bonding. In addition, the other possible causes that are responsible for the decreasing adsorption by surface oxidation are micropore blockage and steric hindrance effects.

One of the outstanding results of kinetic theory was an explanation of gas temperature effect. The gas temperature is directly proportional to the average kinetic energy of the gas particles. In other words, when we heat a gas and raise its temperature, we increase the average molecular kinetic energy of its particles. When we cool a gas, we reduce the average molecular kinetic energy. The increased speed must result in more frequent collisions, so this helps us understand why temperature is a factor in H₂S removal rate.

4.8.4 Adsorption of treated activated carbons (HNO₃+Zn)

Figures 4.30, 4.31, 4.32, 4.33, and 4.34 show breakthrough curves for H₂S adsorption of the HNO₃ oxidized and impregnated with Zn samples at various the temperature of 10, 30, and 45°C also at various HNO₃ concentration. The effect of temperature on the breakthrough curves for H₂S adsorption experiments performed using the same fixed-bed for 6.0 M HNO₃ oxidation and Zn addition are shown in Figure 4.35. HNO₃ oxidation and Zn addition treated carbon exhibited longer breakthrough times than the untreated carbon samples (see Figure 4.19 for comparison). The best performing sample had the longest breakthrough time (2360 sec) for H₂S removal at 45°C (Figure 4.35) which can be ascribed to the role of chemisorption. The chemisorption involves chemical bonding, and chemisorbed molecules are fixed at specific sites (Noll, et al., 1992). A gas molecule must be capable of forming a chemical bond with the adsorbent surface for the chemisorption to occur and chemisorption forms only a monolayer of adsorbate molecules on the surface (Mycock, et al.,1995). Comparison of H₂S breakthrough times for 6.0 M HNO₃ oxidized only, and impregnated with Zn samples at various temperatures are shown in Figure 4.36. For the temperatures effect of 6.0 M HNO₃ oxidized samples

only, the breakthrough time obtained from adsorption temperature at 10°C gave the longest. The breakthrough time of 6.0 M HNO₃ oxidized and impregnated with Zinc sample show the longest breakthrough time for adsorption at 45°C. The results for the original activated carbon, and 6.0 M HNO₃ oxidized and impregnated with Zn samples are shown in Figure 4.37. This figure shows significant differences of adsorption temperature between 10°C and 30-45°C obtained from the original samples. On the other hand, 6.0 M HNO₃ oxidized and impregnated with Zn samples gave the longest breakthrough time of adsorption at temperature 45°C. Comparison of H₂S breakthrough times for 6.0 and 10.0 M HNO₃ oxidized and impregnated with Zn samples at various temperatures are shown in Figure 4.38. In this case, the same treated samples of 6.0 or 10.0 M HNO₃ oxidized and impregnated with Zinc sample, adsorption temperature at 45°C was found to give a higher breakthrough time than adsorption temperature at 30°C for H₂S removal. The chemisorption rate increases with increasing temperature, however, heat of adsorption is not usually a definite criterion. From these experiments, it can be concluded that the structure of the activated carbon samples is probably the most important factor affecting the primary adsorption process. However, the surface chemistry is another important factor affecting too.

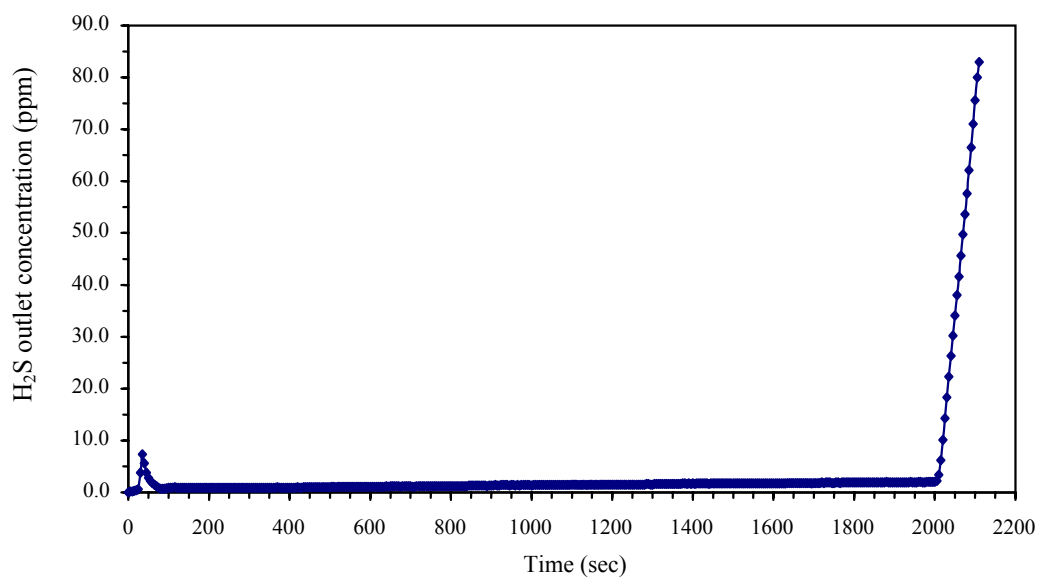


Figure 4.30 H₂S breakthrough curve for activated carbon sample after 6.0 M HNO₃ oxidized and impregnated with Zn. Gas composition: 1.01% H₂S, balance N₂ (T = 10°C, P = 1.0 bar).

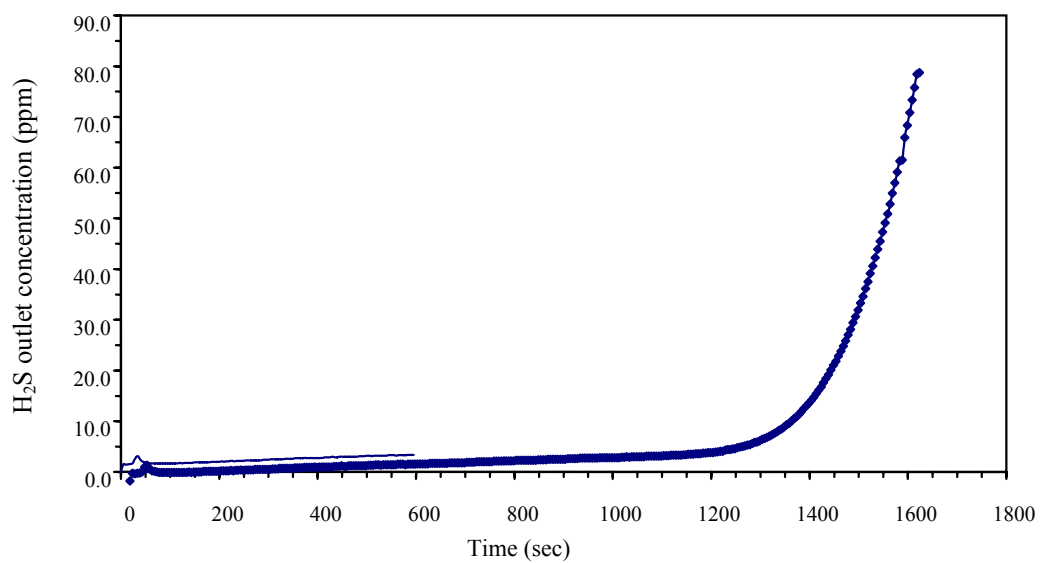


Figure 4.31 H₂S breakthrough curve for activated carbon sample after 6.0 M HNO₃ oxidized and impregnated with Zn. Gas composition: 1.01% H₂S, balance N₂. T = 30°C, P = 1.0 bar.

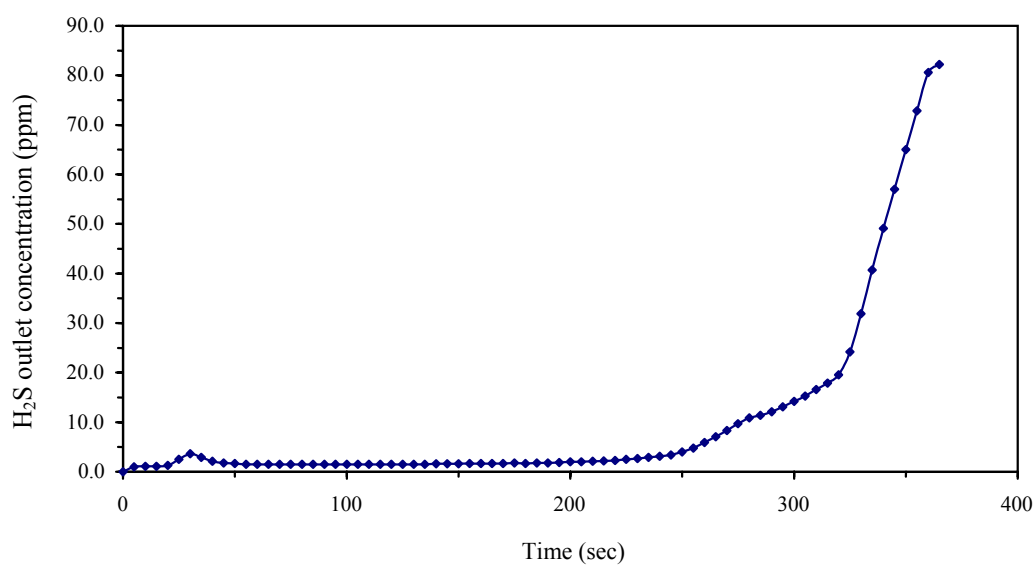


Figure 4.32 H₂S breakthrough curve for activated carbon sample after 10.0 M HNO₃ oxidized and impregnated with Zn. Gas composition: 1.01% H₂S, balance N₂. T = 30°C, P = 1.0 bar.

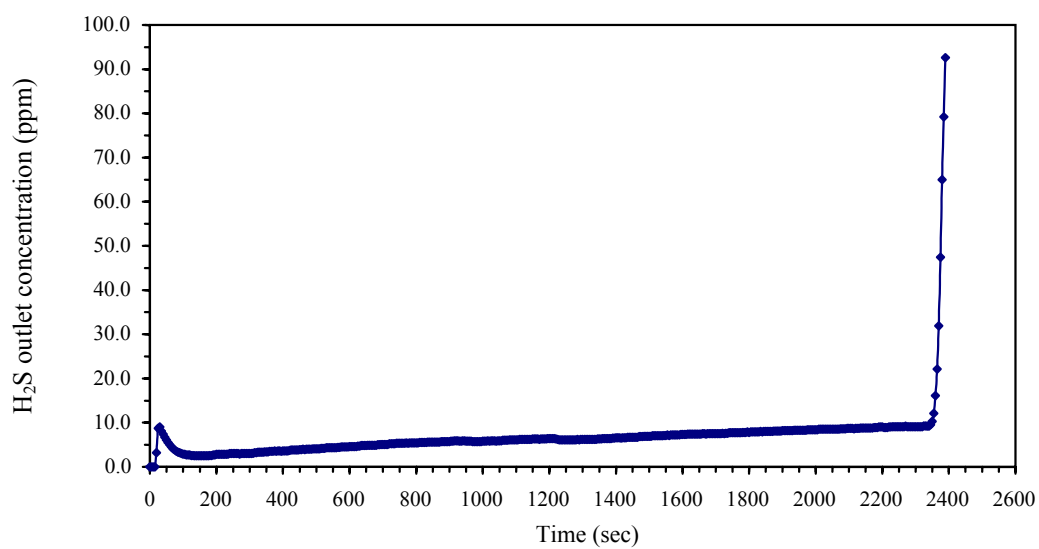


Figure 4.33 H₂S breakthrough curve for activated carbon sample after 6.0 M HNO₃ oxidized and impregnated with Zn. Gas composition: 1.01% H₂S, balance N₂. T = 45°C, P = 1.0 bar.

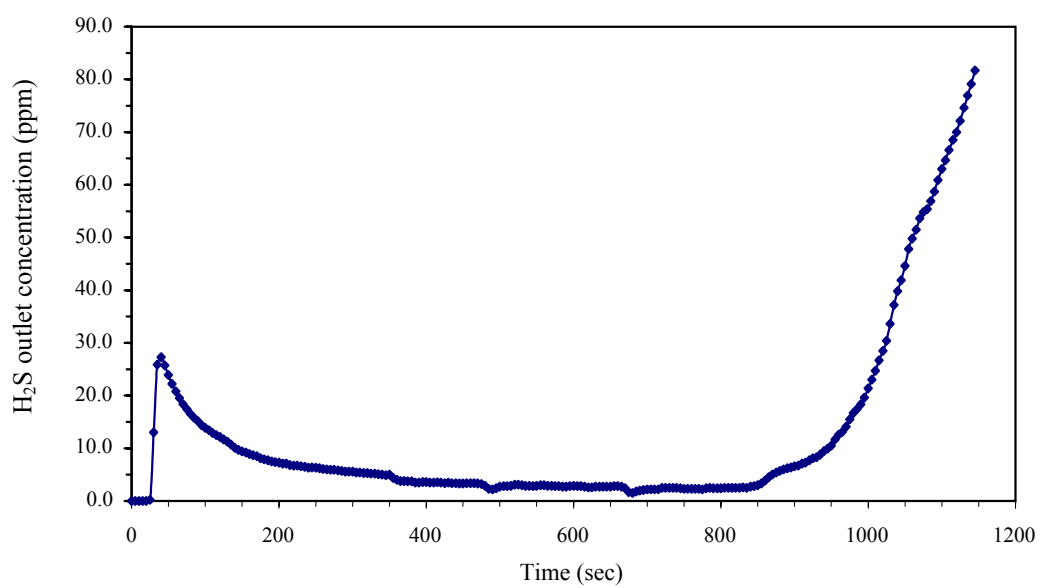


Figure 4.34 H₂S breakthrough curve for activated carbon sample after 10.0 M HNO₃ oxidized and impregnated with Zn. Gas composition: 1.01% H₂S, balance N₂. T = 45°C, P = 1.0 bar.

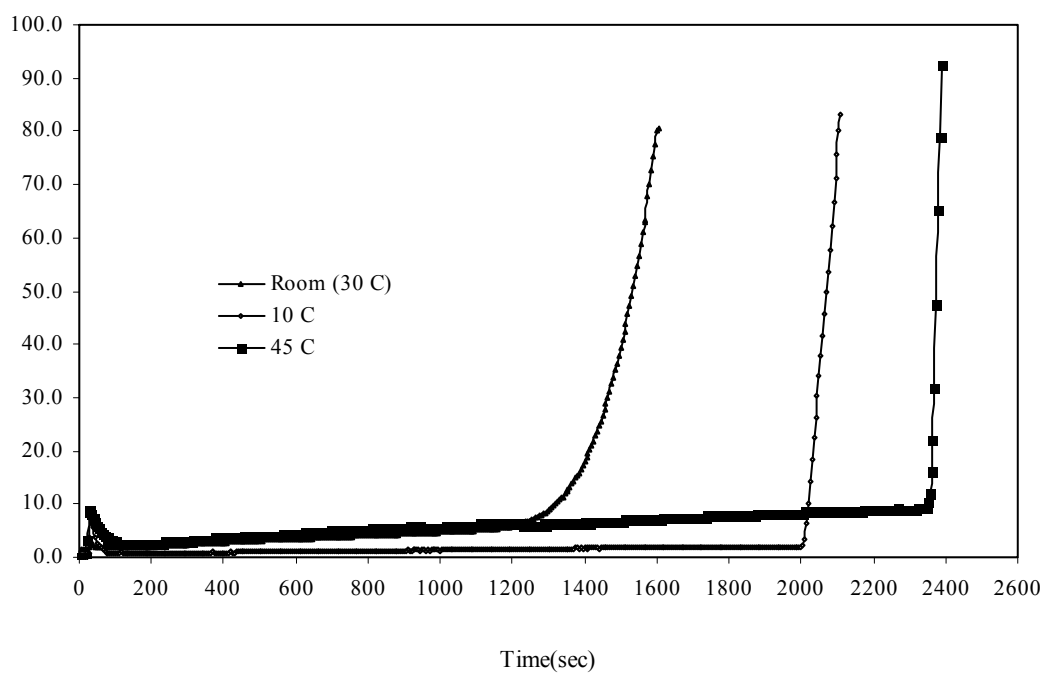


Figure 4.35 Comparison of H₂S breakthrough curves for 6.0 M HNO₃ oxidized and Zn impregnated samples at various temperatures. Gas composition: 1.01% H₂S, balance N₂. P=1.0 bar.

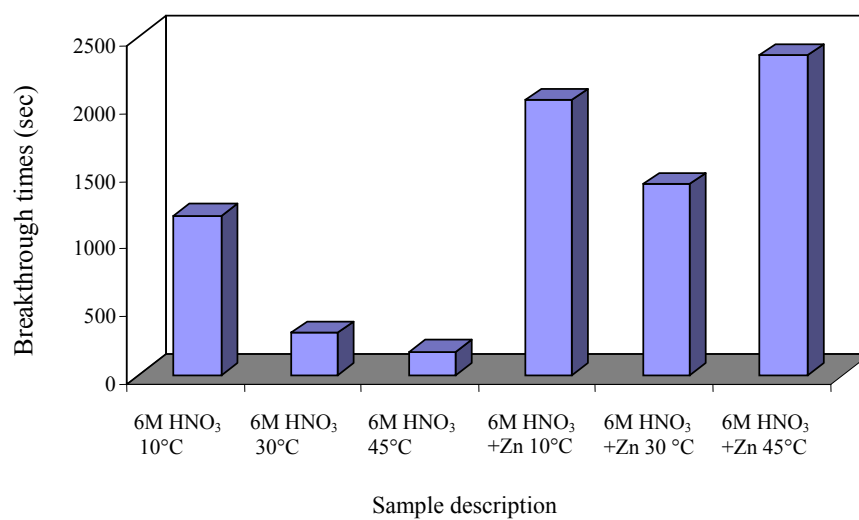


Figure 4.36 Comparison of H₂S breakthrough times for 6.0 M HNO₃ oxidized only and impregnated with Zn samples at various temperatures, P=1.0 bar. Gas composition: 1.01% H₂S in balance N₂.

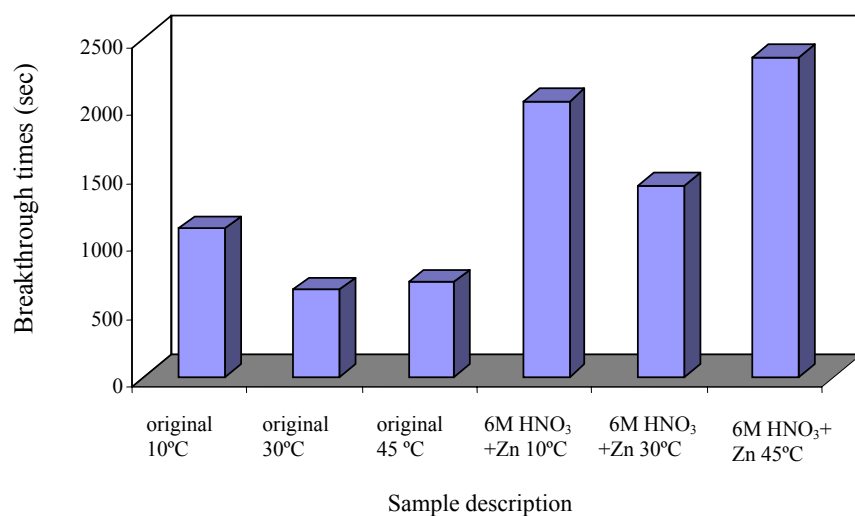


Figure 4.37 Comparison of H₂S breakthrough times for the original activated carbon and 6.0 M HNO₃ oxidized and impregnated with Zn samples at various temperatures, P=1.0 bar. Gas composition: 1.01% H₂S in balance N₂.

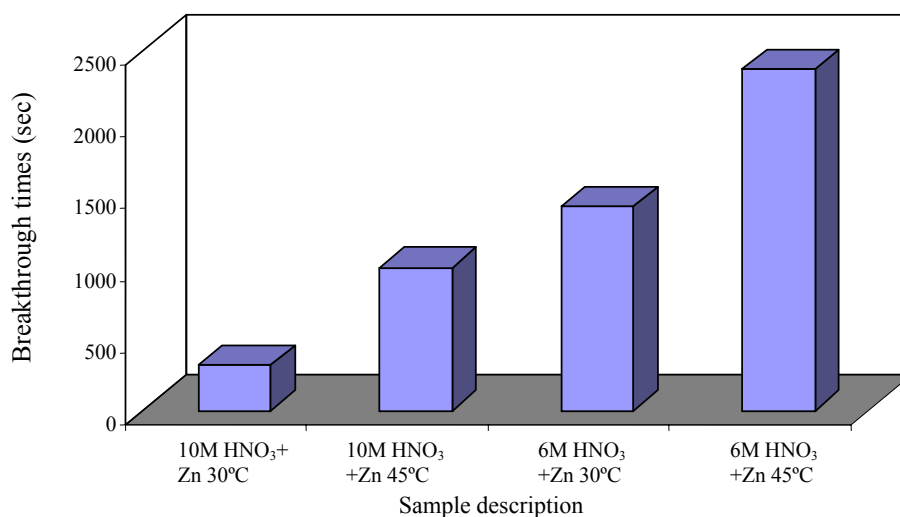


Figure 4.38 Comparison of H₂S breakthrough times for 6.0 and 10.0 M HNO₃ oxidized and impregnated with Zn samples at various temperatures,

P=1.0 bar. Gas composition: 1.01% H₂S in balance N₂.

4.8.5 Adsorption of treated activated carbons (O₃+Zn)

Figures 4.39-4.50 show H₂S breakthrough times for the O₃ oxidized and impregnated with Zn at various conditions. Comparison of H₂S breakthrough times for the O₃ oxidized and Zn impregnated samples at various temperatures 10, 30, and 45°C are shown in Figures 4.51, 4.52, and 4.53, respectively. Most of the breakthrough curves of adsorption temperature at 10°C gave a long breakthrough times because these samples had a great surface areas and pore volumes and adsorptions were done at low temperature, indicating the dominant role of physical adsorption for H₂S removal. Alternatively, the results at 45°C were better than the results at 30°C, largely due to the effect of chemical adsorption for H₂S removal at a higher temperature. Comparison of H₂S outlet concentration values of O₃ oxidized and impregnated with Zn samples at 10, 30, and 45°C are shown in Figures 4.54, 4.55, and 4.56 respectively.

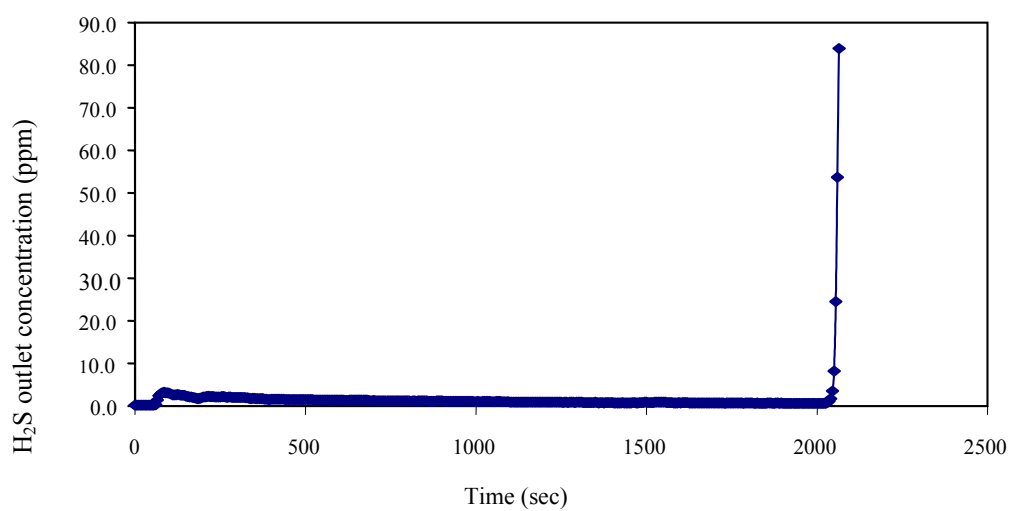


Figure 4.39 H₂S breakthrough curve for activated carbon sample after O₃ oxidized (in fluidized-bed, 210°C, 90 min) and impregnated with Zn Gas composition: 1.01% H₂S, balance N₂. T=10°C, P=1.0 bar.

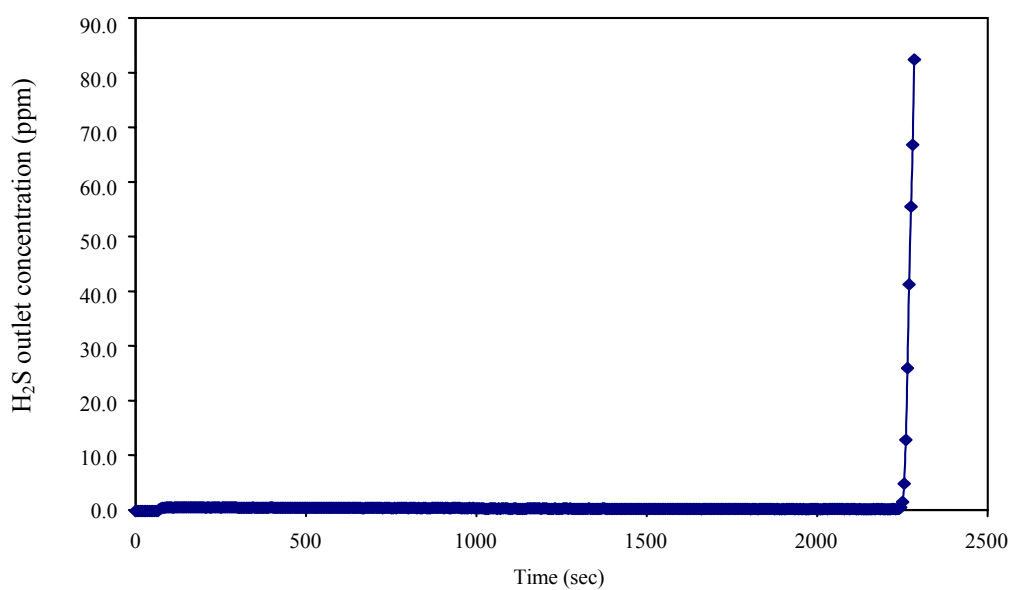


Figure 4.40 H₂S breakthrough curve for activated carbon sample after O₃ oxidized (in a reflux column, 90°C, 60 min) and impregnated with Zn. Gas composition: 1.01% H₂S, balance N₂. T=10°C, P=1.0 bar.

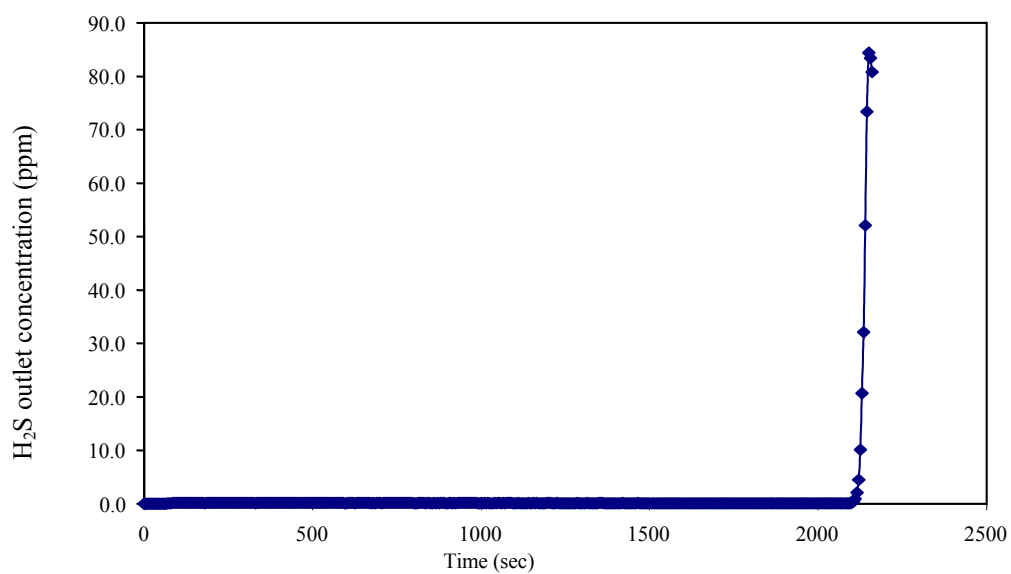


Figure 4.41 H₂S breakthrough curve for activated carbon sample after O₃ oxidized (in a reflux column, 90°C, 120 min) and impregnated with Zn. Gas composition: 1.01% H₂S, balance N₂. T=10°C, P=1.0 bar.

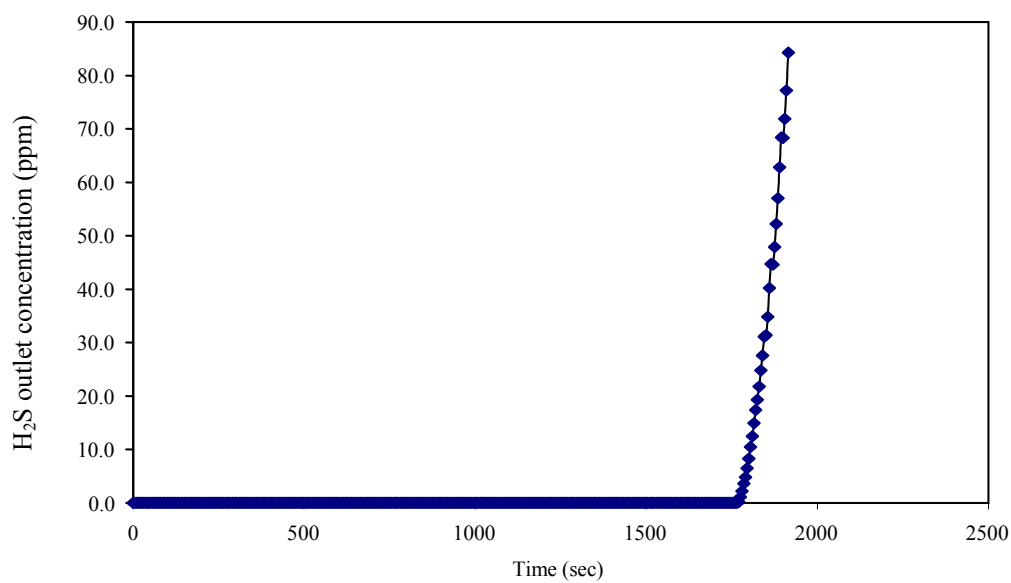


Figure 4.42 H₂S breakthrough curve for activated carbon sample after O₃ oxidized (in a reflux column, 90°C, 180 min) and impregnated with Zn. Gas composition: 1.01% H₂S, balance N₂. T=10°C, P=1.0 bar.

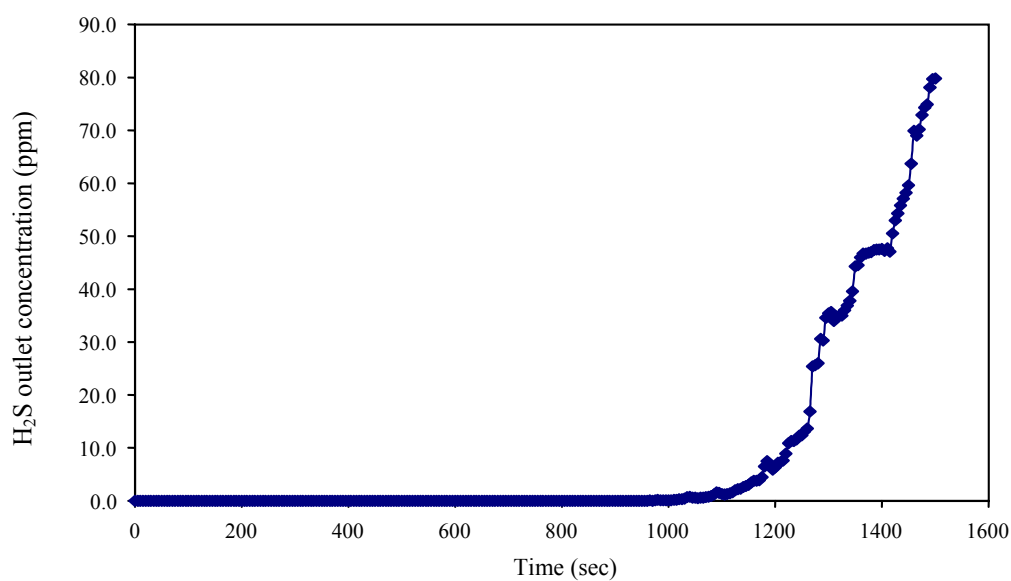


Figure 4.43 H₂S breakthrough curve for activated carbon sample after O₃ oxidized (in fluidized-bed, 210°C, 90 min) and impregnated with Zn. Gas composition: 1.01% H₂S, balance N₂. T= 30°C, P=1.0 bar.

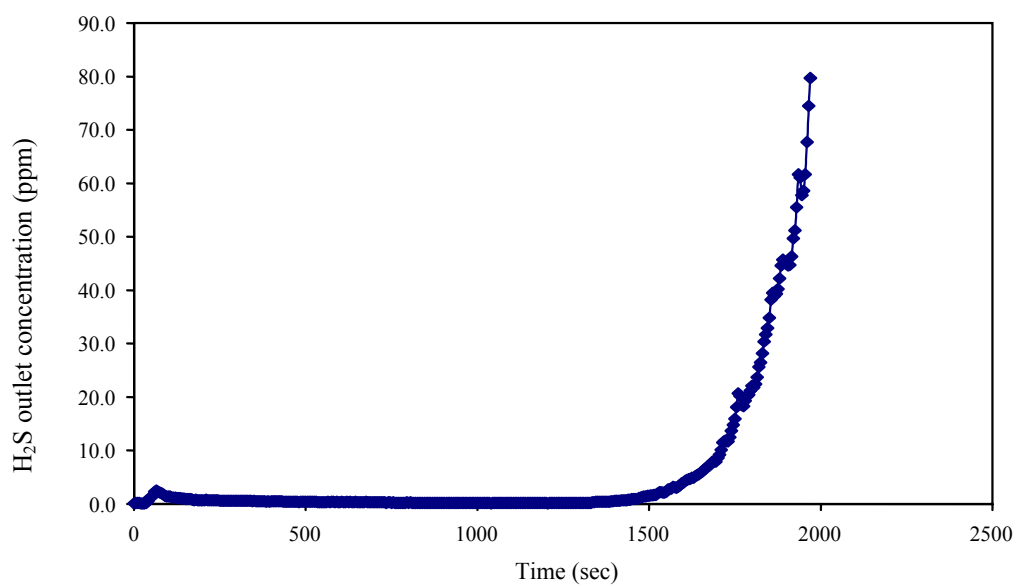


Figure 4.44 H₂S breakthrough curve for activated carbon sample after O₃ oxidized (in a reflux column, 90°C, 60 min) and impregnated with Zn. Gas composition: 1.01% H₂S, balance N₂. T= 30°C, P=1.0 bar.

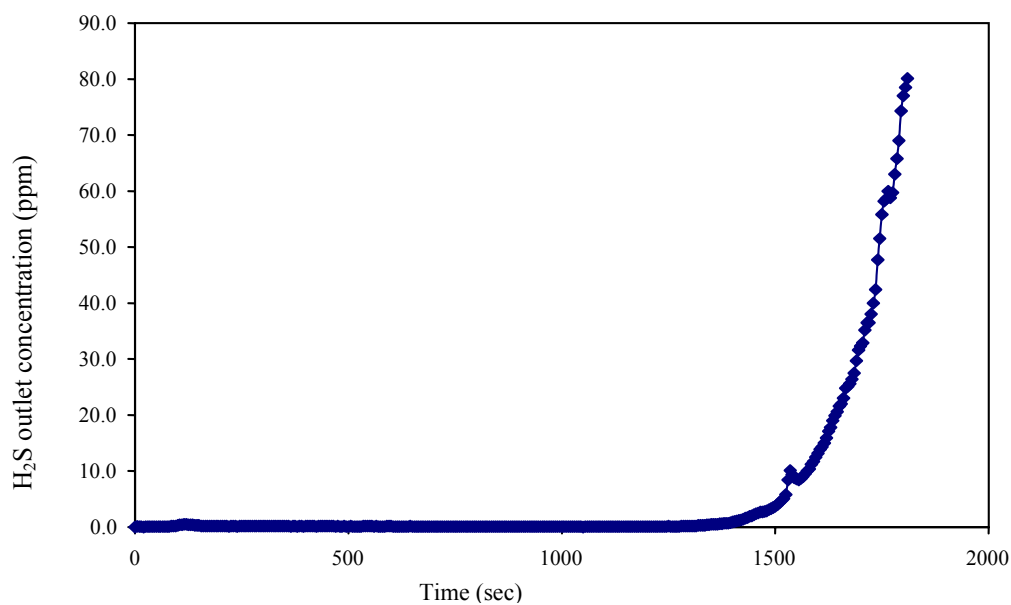


Figure 4.45 H₂S breakthrough curve for activated carbon sample after O₃ oxidized (in a reflux column, 90°C, 120 min) and impregnated with Zn. Gas composition: 1.01% H₂S, balance N₂. T= 30°C, P=1.0 bar.

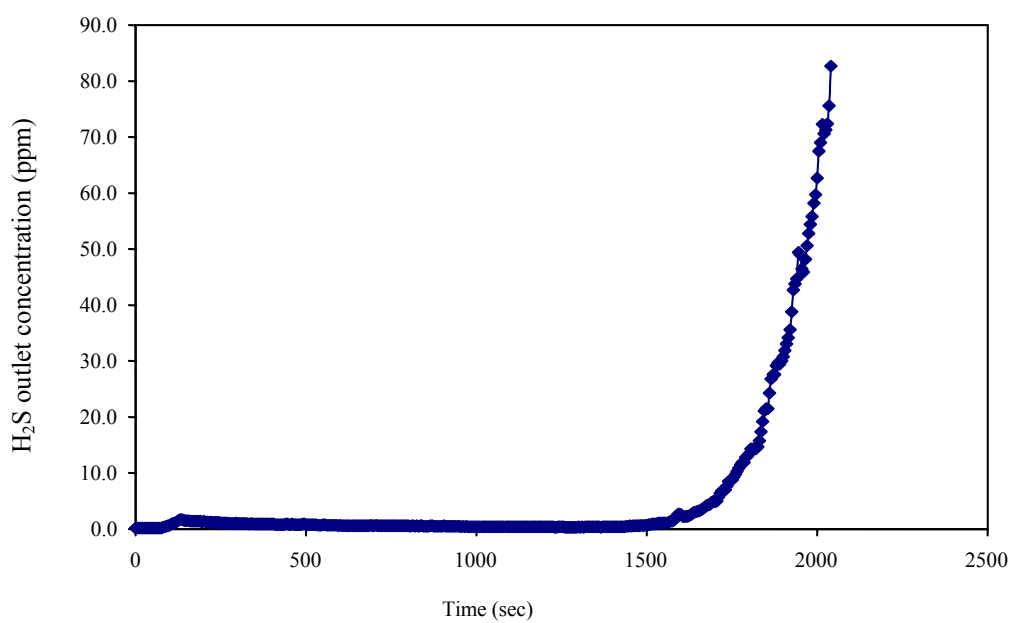


Figure 4.46 H₂S breakthrough curve for activated carbon sample after O₃ oxidized (in a reflux column, 90°C, 180 min) and impregnated with Zn. Gas composition: 1.01% H₂S, balance N₂. T= 30°C, P=1.0 bar.

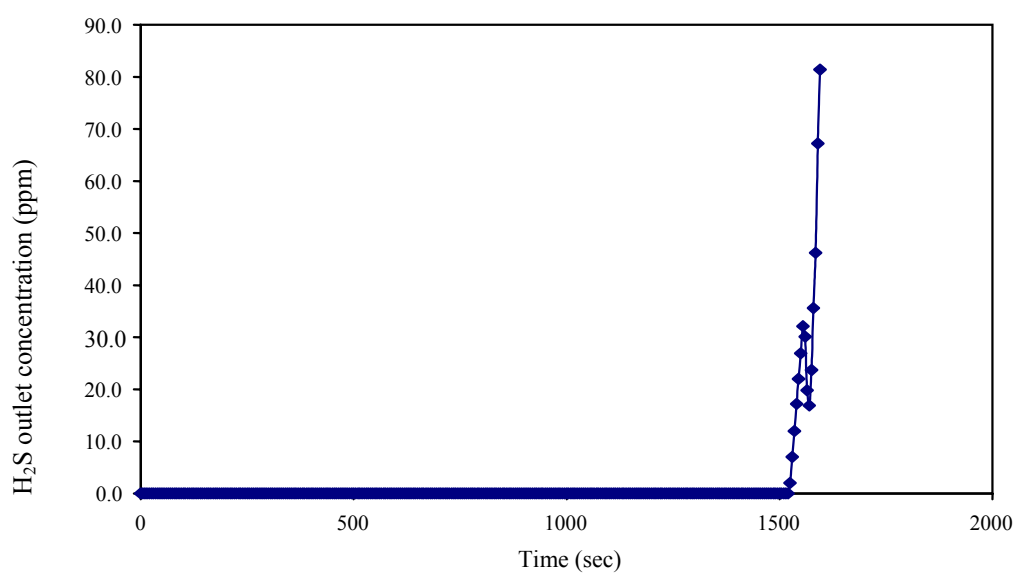


Figure 4.47 H₂S breakthrough curve for activated carbon sample after O₃ oxidized (in fluidized-bed, 210°C, 90 min) and impregnated with Zn. Gas composition: 1.01% H₂S, balance N₂. T= 45°C, P=1.0 bar.

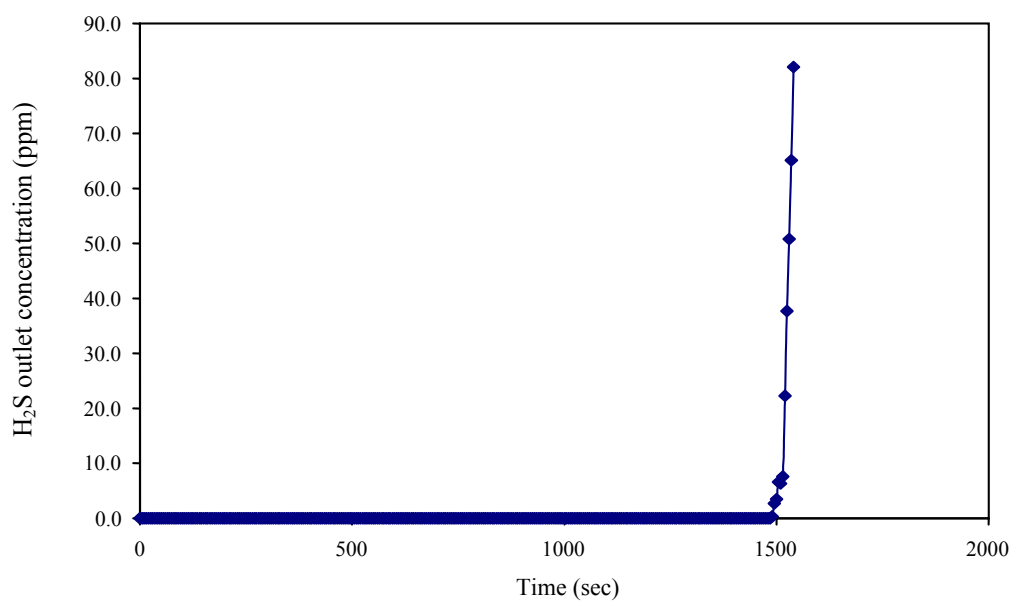


Figure 4.48 H₂S breakthrough curve for activated carbon sample after O₃ oxidized (in a reflux column, 90°C, 60 min) and impregnated with Zn. Gas composition: 1.01% H₂S, balance N₂. T= 45°C, P=1.0 bar.

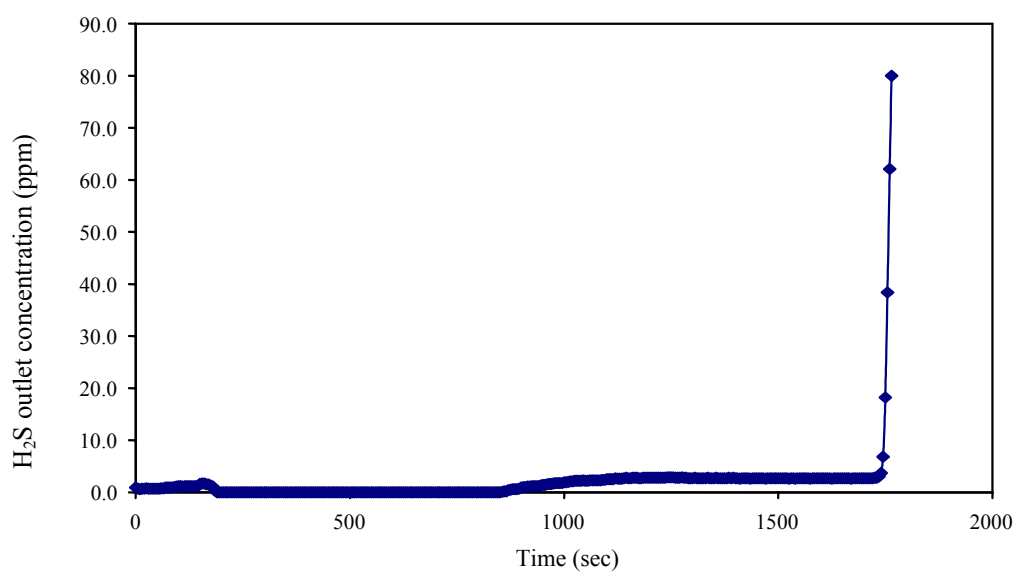


Figure 4.49 H₂S breakthrough curve for activated carbon mple after O₃ oxidized (in a reflux column, 90°C, 120 min) and impregnated with Zn. Gas composition: 1.01% H₂S, balance N₂. T= 45°C, P=1.0 bar.

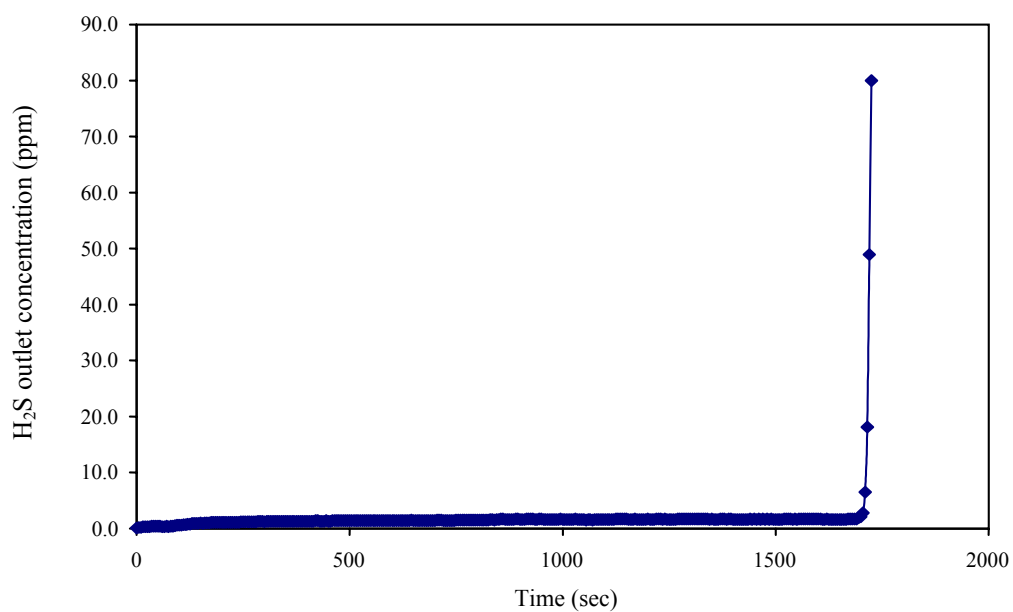


Figure 4.50 H₂S breakthrough curve for activated carbon sample after O₃ oxidized (in a reflux column, 90°C, 180 min) and impregnated with Zn. Gas composition: 1.01% H₂S, balance N₂. T= 45°C, P=1.0 bar.

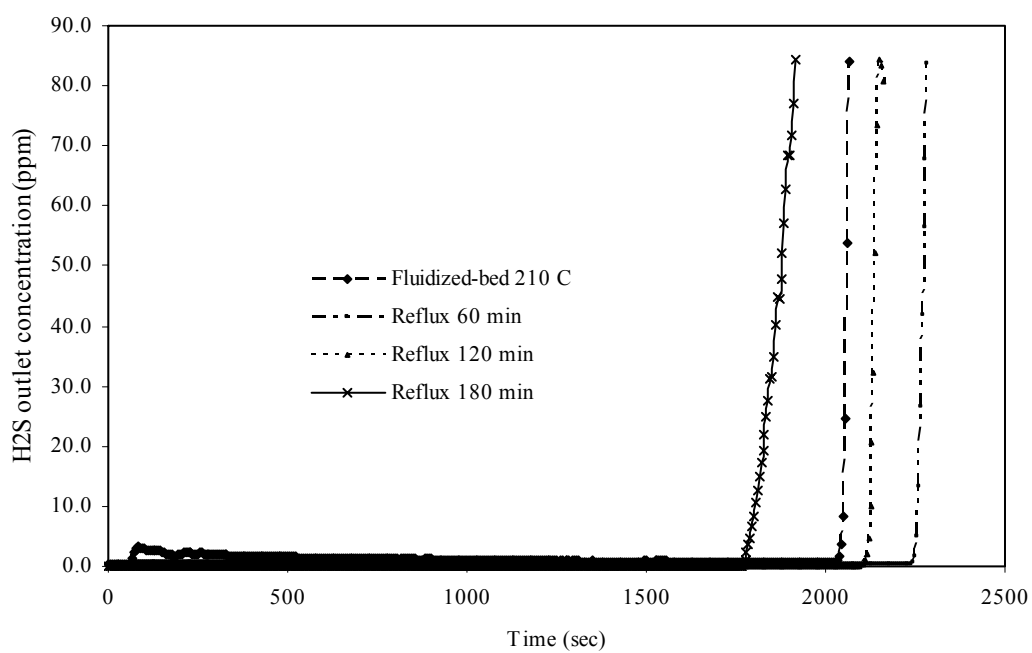


Figure 4.51 Comparison of H₂S breakthrough curves for O₃ oxidized and Zn impregnated samples at 10°C, P=1.0 bar, with different condition. Gas composition: 1.01% H₂S, balance N₂.

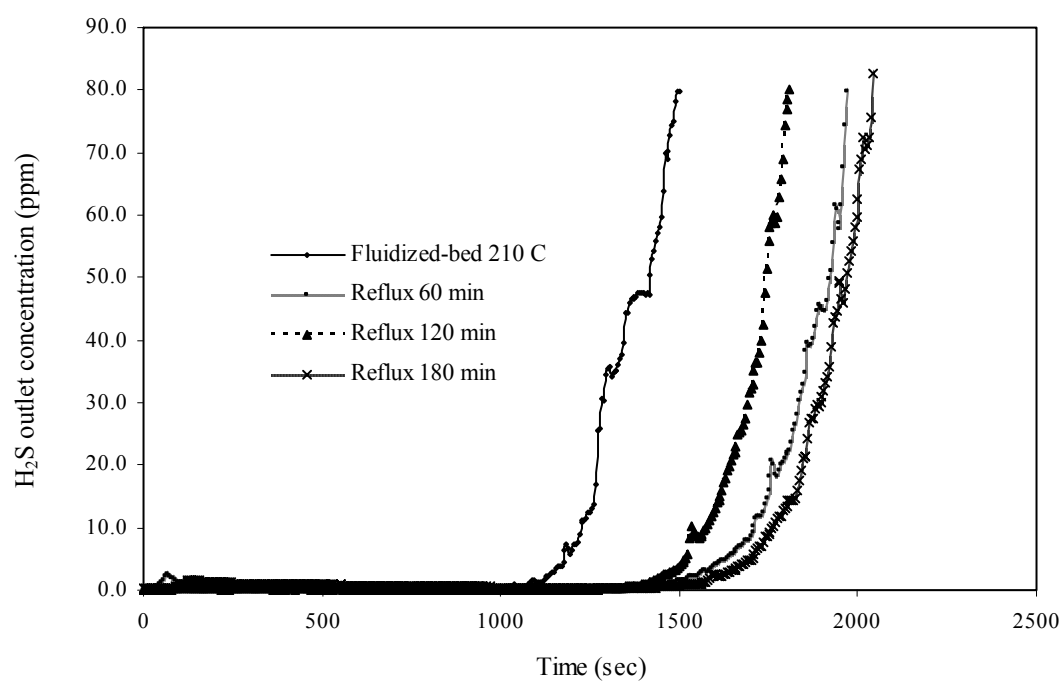


Figure 4.52 Comparison of H₂S breakthrough curves for O₃ oxidized and Zn impregnated samples at 30°C, P=1.0 bar, with different conditions. Gas composition: 1.01% H₂S, balance N₂.

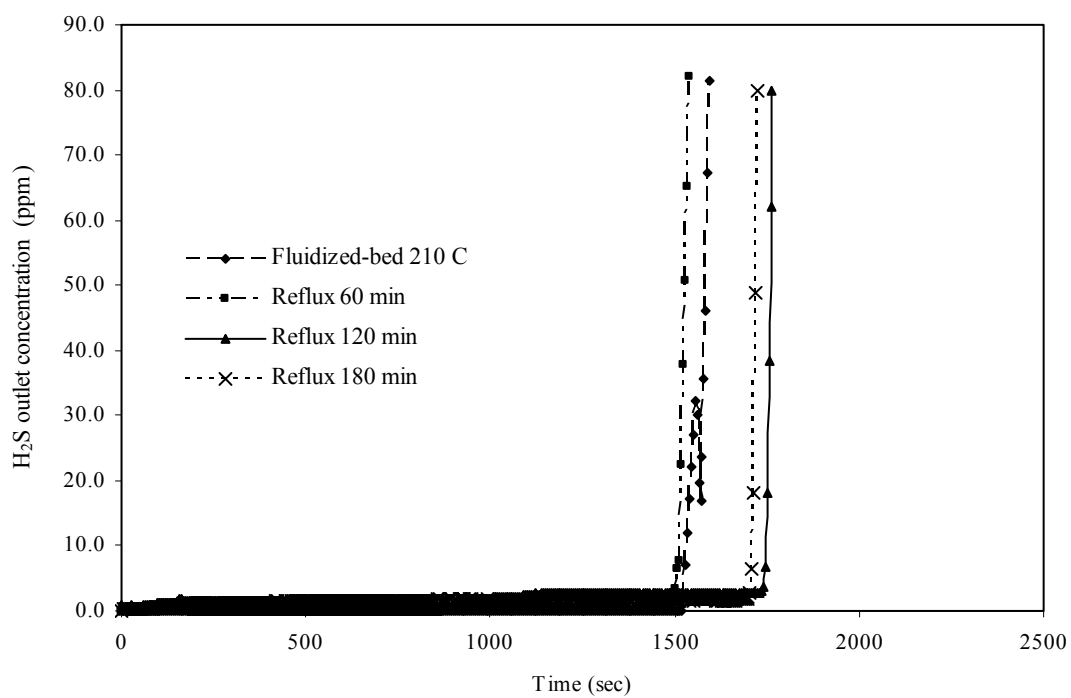


Figure 4.53 Comparison of H₂S breakthrough curves for O₃ oxidized and Zn Impregnated samples at 45°C, P=1.0 bar, with different conditions. Gas composition: 1.01% H₂S, balance N₂.

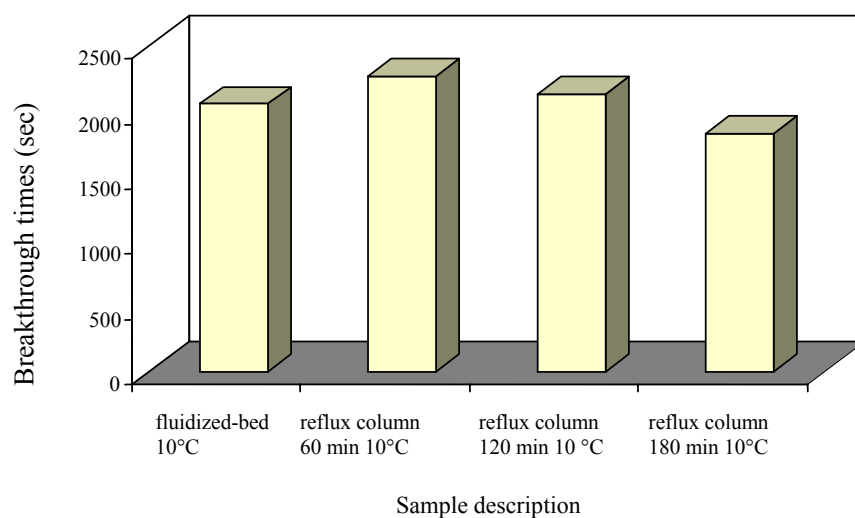


Figure 4.54 The H₂S outlet concentration values (ceiling limit = 20 ppm) of O₃ oxidized and impregnated with Zn samples at 10°C, P=1.0 bar with various conditions. Gas composition: 1.01% H₂S in balance N₂.

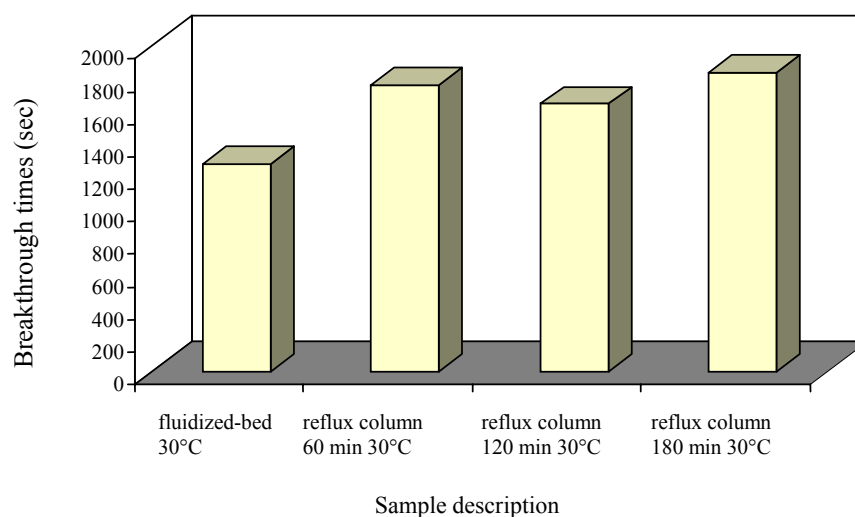


Figure 4.55 The H₂S outlet concentration values (ceiling limit = 20 ppm) of O₃ oxidized and impregnated with Zn samples at 30°C, P=1.0 bar with various conditions. Gas composition: 1.01% H₂S in balance N₂.

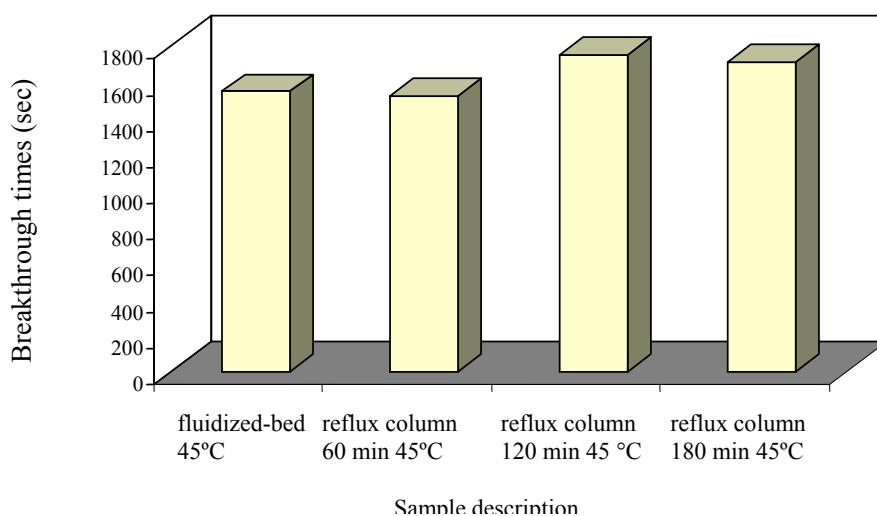


Figure 4.56 The H₂S outlet concentration values (ceiling limit = 20 ppm) of O₃ oxidized and impregnated with Zn samples at 45°C, P=1.0 bar with various conditions. Gas composition: 1.01% H₂S in balance N₂.

4.8.6 Mechanisms of H₂S removal by oxidized and impregnated with Zn samples

The chemisorption of oxidized and impregnated with Zn samples for H₂S removal can be explained in terms of coordination compounds or complexes. The metal ion or atom ion in a complex is called the central metal ion or atom, in this experiment is Zn²⁺. The groups attracted to it or Lewis bases are called ligands. The ligands may be either ions or neutral molecules in this experiment is H₂S. Metal ions can form coordination compounds in which central metal atoms or ions are bonded to two or more ligands by coordinate covalent bonds. The geometry of Zn²⁺ found in this complex is tetrahedral (a coordination number 4). Figure 4.57 shows the geometry of tetrahedral [Zn (H₂S)₄]²⁺.

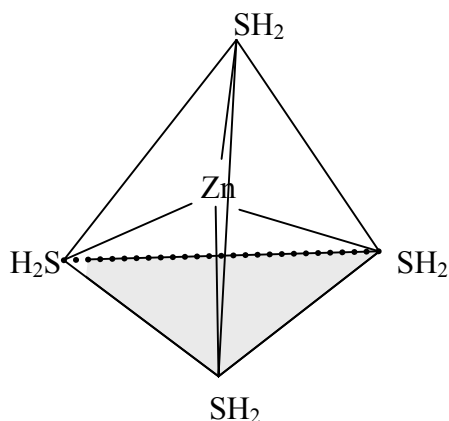


Figure 4.57 The geometry of $[\text{Zn}(\text{H}_2\text{S})_4]^{2+}$ complex ion.

The bonding in coordination compounds explain by the valence bond theory. This theory treats a metal-ligand bond as a coordinate covalent bond that forms when an orbital of donor atom overlaps a hybrid orbital of central metal atom. Electron pairs from ligands are shared with the metal, and each electron pair occupies both an atomic orbital of a ligand and one of several equivalent hybrid orbital of the metal (Henry et al., 1984). The ligand is a Lewis base but the metal is a Lewis acid. In the case of $[\text{Zn}(\text{H}_2\text{S})_4]^{2+}$, the electron configuration of Zn^{2+} is $1s^2 2s^2 2p^6 3s^2 3p^6 4d^{10}$. The 4s and 4p orbitals are empty (Figure 4.58).

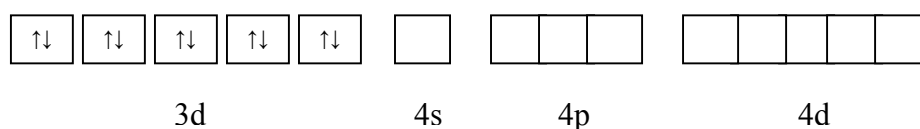


Figure 4.58 The orbitals of Zn^{2+} ion.

In order to get a tetrahedral geometry, we need a set of sp^3 hybrid orbitals, and in order to form Zn-S bond, these sp^3 orbitals must be empty since each sulfur contributes 2 electrons (Figure 4.59). The 4s and 4p orbitals are available for hybridization.

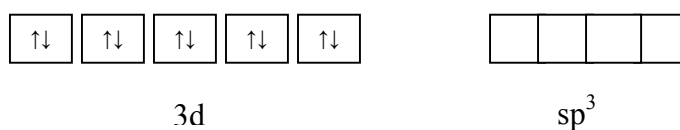


Figure 4.59 The orbitals of Zn^{2+} and sp^3 hybrid orbitals.

The use of the four sp^3 hybrid orbitals to bond with the 4 H_2S gives a tetrahedral complex. The 3d orbitals contain the 10 electrons from the Zn^{2+} and the hybrid orbitals contain the 4 electron pairs from the H_2S (Figure 4.60).

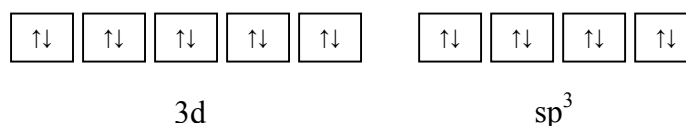


Figure 4.60 The orbitals of $[Zn(H_2S)_4]^{2+}$ complex ion.

4.8.7 Increasing the amounts of H_2S removal

The amounts of H_2S removal in mg- H_2S /g-sample from some samples in this study are summarized in Table 4.12. The H_2S ceiling limit from the Occupational Safety and Health Administration (OSHA) for use in promulgating legal standards is

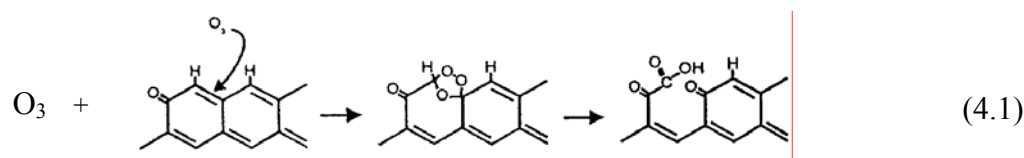
20 ppm (Chou, 2000). Thus, the concentration of H₂S (20 ppm) should not be exceeded at any time. Zn impregnation of the original samples removed 17.09 and 16.39 mg-H₂S/g-sample at 10 and 45°C, respectively. The increasing percentage for removal H₂S was approximately 118% (16.39 mg-H₂S/g-sample) over that of the original sample at 45°C. The carbon sample treated with 6.0 M HNO₃ and Zn impregnation gave the highest adsorption capacity for H₂S, giving increased adsorption efficiency of 230% over that of the untreated sample at 45°C. At the lowest temperature (10°C) the O₃ oxidized (reflux, 60 min) sample impregnated with Zn adsorbed 24.19 mg-H₂S/g-sample, giving the highest removal efficiency. The maximum increase of 180% (19.24 mg-H₂S/g-sample) adsorption efficiency at 30°C over that of the original sample was observed with the O₃ oxidized (reflux, 180min) sample impregnated with Zn. There was a tendency that the chemical adsorption of H₂S increased with the amount of Zn impregnated on the surface sample at temperatures of adsorption higher than 45°C, indicating the significant role of chemisorption for H₂S removal under this condition. A few H₂S adsorption experiments were oxidized with varied concentration of HNO₃ (2.0, 6.0, and 10.0 M) reduced adsorption efficiency for H₂S removal, except the adsorption of 6.0 M HNO₃ oxidized sample at 10°C (see Table 4.13). Because some of H₂S molecules were attracted to each other molecules on activated carbon sample surface but they are repulsed by similar partial negative charges (δ^-) of the polarity of C=O and/or C-O groups from the functional groups. Figures 4.61, 4.62, and 4.63 show the comparison of increasing % H₂S removal from the untreated activated carbon sample adsorption for different treated activated carbon samples at adsorption temperatures 10, 30, and 45°C respectively.

Table 4.13 Increasing H₂S removal efficiency of treated carbon samples over that of original untreated sample.

Sample description	Amount of H ₂ S removal, OSHA: ceiling=20 ppm (mg-H ₂ S/g-sample)			Increasing efficiency for H ₂ S removal		
	Adsorption (10°)	Adsorption (30°)	Adsorption (45°)	Temp. 10°C	Temp. 30°C	Temp. 45°C
Original	11.70	6.87	7.49	-	-	-
Original + Zn	17.09	-	16.39	46.1	-	118.8
6.0 M HNO ₃ + Zn	21.65	15.02	24.72	85.0	118.6	230.0
O ₃ fluidized-bed 210°C) +Zn	21.93	13.63	16.52	87.4	98.4	120.6
O ₃ (reflux 60 min) + Zn	24.19	18.83	16.28	106.8	174.2	117.3
O ₃ (reflux 120 min) + Zn	22.77	17.59	18.66	94.6	156.0	149.2
O ₃ (reflux 180 min) +Zn	19.58	19.24	18.31	67.4	180.0	144.4
2.0 M HNO ₃	-	2.77	-	-	-59.7	-
6.0 M HNO ₃	12.53	3.30	1.81	7.1	-52.0	-75.8
10.0 M HNO ₃	-	2.13	-	-	-69.0	-

In summary, there are several mechanisms involved in the adsorption of H₂S by activated carbon. Firstly, the adsorption of H₂S by the original activated carbon is expected to be dominated by the van der Waals forces which is physical in nature. Secondly, H₂S can be adsorbed by the oxidized activated carbon samples involve dipole-dipole forces, London forces, and chemisorption between H₂S and the polarity of C=O and/or C-O from the functional groups. Alternatively, H₂S is

repulsed by similar partial negative charges of the polarity of C=O and/or C-O from the functional groups, such as ketone structure on carbon surface by O_3 oxidation as shown in Equation 4.1.



Thirdly, H_2S can be adsorbed by the oxidized and impregnated with Zn samples which involves the two major mechanisms of physical adsorption (van der Waals forces) and chemisorption by coordinate covalent bonding due to coordination compound where H_2S ligands bond to metal (Zn) on the activated carbon samples (see Figure 4.57).

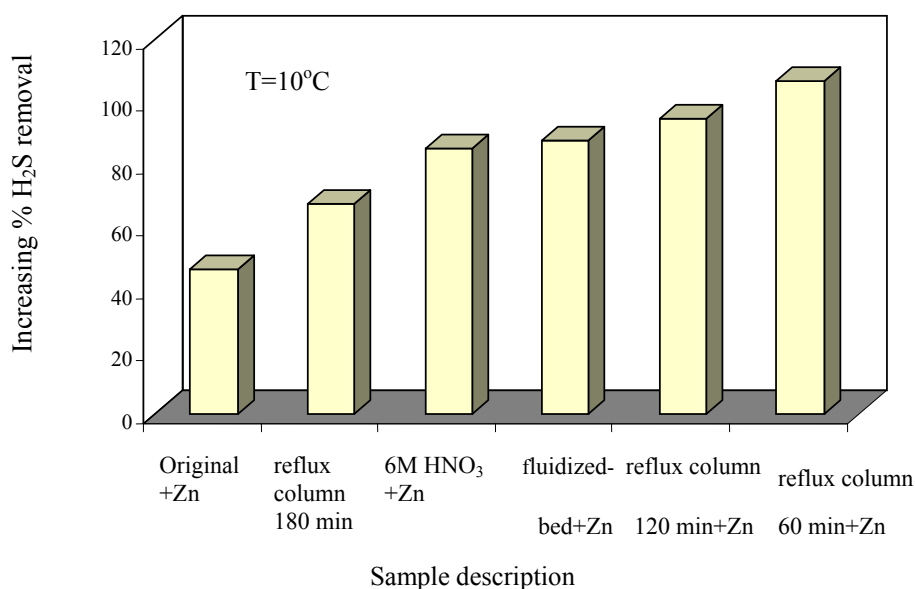


Figure 4.61 Comparison of increasing % H_2S removal at 20 ppm for different treated samples at $10^\circ C$ (adsorption temperature), $P=1.0$ bar. Gas composition: 1.01% H_2S in balance N_2 .

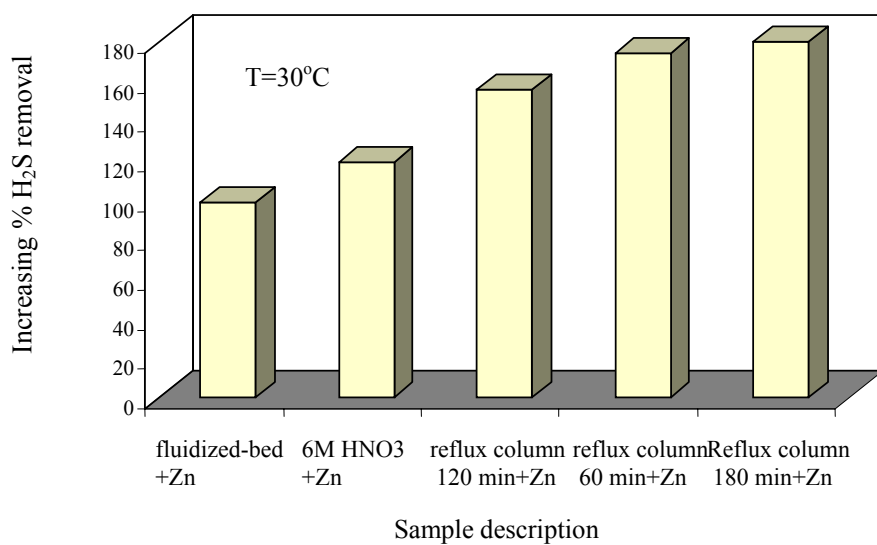


Figure 4.62 Comparison of increasing %H₂S removal at 20 ppm for different treated samples at 30°C (adsorption temperature), P=1.0 bar. Gas composition: 1.01% H₂S in balance N₂.

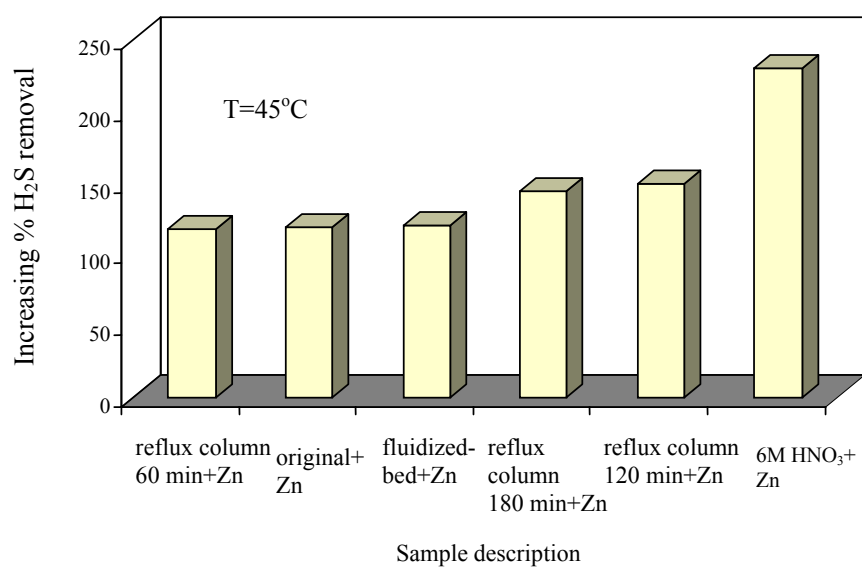


Figure 4.63 Comparison of increasing %H₂S removal at 20 ppm for different treated samples at 45°C (adsorption temperature), P=1.0 bar. Gas composition: 1.01% H₂S in balance N₂.

CHAPTER V

CONCLUSIONS AND RECOMMENDATIONS

5.1 Conclusions

1. FT-IR spectroscopy is a useful and rapid tool to determine the surface chemical structure of the original activated carbon and the oxidized samples. Typical oxygen functional groups identified were ester, alcohol, ether structures, ketone, and carboxylic acid groups. Boehm's titration is another technique that was used to determine the type and concentration of the surface groups in activated carbon and it was found that carbons oxidized by 10.0 M HNO₃ yielded maximum oxygen surface groups.

2. The oxidation of the original activated carbons, with different oxidizing agents like O₃ and HNO₃, gave the increased formation of surface oxygen functional groups.

3. The ozonation of activated carbons is a very effective method to form a variety of oxygen complexes, the concentration and types of which may be markedly influenced by the time and temperature of ozonation. It was found that oxidation condition at 90°C, 60 min in a reflux column gave the highest total peak area (498.91 A. cm⁻¹) of carboxylic acid or ketone groups.

4. In the case of the original activated carbon modified with HNO₃, this oxidation treatment gave rise to a large increase in the amount of total acidity and the intensity of the acidic groups, depending on the concentrations of HNO₃ used for the

treatment.

5. The elemental oxygen percentage of HNO₃ oxidized samples increased when the contact time and HNO₃ concentration in a reflux column were increased. The increasing temperature for the samples oxidized with O₃ obtained from the fluidized-bed reactor caused an increase of elemental oxygen value. The findings of increasing oxygen content confirms the effective enhancement of an acidic surface groups on the activated carbon by HNO₃ oxidation.

6. The amount of Zn metal in the Zn impregnated samples obtained by IE method depended on the concentration and type of oxidizing reagents used to modify the activated carbons. The maximum quantities of Zn metal introduced into the oxidized samples by O₃ in fluidized-bed reactor, O₃ in a reflux column, and HNO₃ in a reflux column were 36.04, 36.92, and 52.77 mg-Zn/g-sample respectively. It was also found that the lower surface area carbon samples contain a higher density of carbon surface functional groups such as C-O and C=O, resulting in more active polar ion-exchange sites.

7. The N₂ adsorption isotherms of all samples gave the type I isotherms (monolayer coverage) characterized by a plateau that is nearly horizontal to the P/P⁰ axis, typical of adsorption in microporous solids. The treated activated carbons caused the downward shift of the isotherms indicating lesser adsorption capacity for N₂ gas. This was probably due to porosities of the modified activated carbons being blocked by oxide functional groups introduced by the chemical treatment.

8. The BET surface area also decreased considerably due to the blocking of the narrow pores by the surface complexes introduced by oxidizing agents and/or Zn impregnated treatments. The micropore volume calculated from N₂ adsorption at 77

K revealed that about 70% of the adsorption capacity of the original activated carbon is due to micropores.

9. A synthetic gas mixture of 1.01wt % H₂S plus balance N₂ was used for the fixed-bed adsorption experiments. The outlet concentration of H₂S from the fixed-bed adsorber was followed as a function of time by electrochemical sensor. The breakthrough time and adsorption capacity (mg-H₂S adsorbate/g-adsorbent) up to the breakthrough time was used to assess the efficiency of H₂S removal.

10. The mechanism of H₂S removal by the original activated carbon sample is principally due to physical adsorption. Adsorption of gas molecules on activated carbon is expected to be dominated by the van der Waals forces which is physical in nature. In addition, the small pore sizes and large surface area of activated carbon play the major role in gas adsorption. The mechanism of H₂S removal by oxidized activated carbons still involves the mechanism of physical adsorption inside the pores. However, the existence of surface functional groups at the edges of graphitic layers of activated carbon could prevent the accessibility of adsorbate molecules from diffusing into the interval pore area. As a result of this hindrance effect, the oxidized carbon samples give less adsorptive capacity for H₂S in comparison with the original non-oxidized carbons.

11. The major mechanism of H₂S removal by oxidized and impregnated with Zn samples was chemisorption, which can be described in terms of coordination compounds. Zn ions can form coordination compounds in which central metal ions (Zn²⁺) are bonded to four ligands (H₂S) by coordinate covalent bonds. Both physical adsorption and chemisorption can occur in a fixed-bed adsorber by oxidized and impregnated with Zn samples adsorption.

12. The most important factor affecting the adsorption process is temperature. In the case of chemisorption the adsorption rate increases with increasing temperature but the physical adsorption rate increases with decreasing temperature.

13. Zn-impregnated samples gave higher adsorption capacity than O_3 or HNO_3 oxidized samples and the original samples at temperatures of 10, 30 and 45° C. The carbon sample treated with 6.0 M HNO_3 and impregnated with Zn gave the highest adsorption capacity for H_2S , giving increased adsorption efficiency of 230% (24.72 mg- H_2S /g-sample) over that of the original sample at 45°C. On the other hand, the O_3 oxidized sample and impregnated with Zn gave adsorption efficiency 180% (19.24 mg- H_2S /g-sample) over that of the original sample at 30°C. There was a tendency that the chemical adsorption of H_2S increased with the amount of Zn impregnated on the surface sample at temperatures of adsorption higher than 45°C, indicating the carbon surface chemistry by metal addition is significant factor influencing the performance of activated carbon for H_2S removal.

5.2 Recommendations

The results obtained in this study showed that adsorption of H_2S could be affected both by the physical adsorption and chemisorption. Both of these adsorption phenomena are complex and interrelated for H_2S removal in the fixed-bed adsorber. At low temperature, a smaller micropore size of activated carbon produced higher adsorption because the physical adsorption play the major role with adsorption increasing with decreasing temperature. Alternatively, the chemisorption of H_2S removal increased with increasing in temperature.

The following research topics are worth further investigations.

1. Study the underlying mechanisms of physical adsorption and chemisorption of low molecular weight gases adsorb at low and high temperatures.
2. Study functional groups on surface of activated carbon such as C-O and C=O effect to hydrogen bonding obtained from a high electronegativity atom of low molecular weight gases such as NH₃ (ammonia).
3. Study adsorption of activated carbon for low molecular weight gases removal at temperature adsorption higher than 45°C. Because adsorption by activated carbon can be effectively used for air purification at high temperature from some malodorous sources such as, the odor obtained from flue gases.
4. Study the role of the some functional groups such as ketone, ester, carboxylic and/or alkene on the surface activated carbon effect to metal addition in ion-exchange process for zinc, copper, iron and/or lead metals.

REFERENCES

- Adib, F., Bagreev, A. and Bandosz, T. J. (1999). Effect of surface characteristics of wood-based activated carbons on adsorption of hydrogen sulfide. **J. Colloid Interface Sci.** 15: 407-415.
- Bansal, R. C., Donnet, J.- B. and Stoeckli, F. (1988). **Activated Carbon.** New York: Marcel Dekker.
- Birk, J. P., (1994). **Chemistry.** Boston: Houghton Mifflin.
- Boudou, J. P., Martinez - Alonzo, A. and Tascon, J. M. D. (2000). Introduction of acidic groups at the surface of activated carbon by microwave-induced oxygen plasma at low pressure. **J. Carbon.** 38: 1021-1029.
- Burke, S. D. and Danheiser, R. L. (1999). **Handbook of Reagents for organic Synthesis Oxidation and Reducing Agents.** New York: John Wiley and Sons.
- Cal, M. P., Strickler, B. W. and Lizzio, A. A. (2000a). High temperature hydrogen sulfide adsorption on activated carbon I. Effect of gas composition and metal addition. **J. Carbon.** 38: 1757 –1765.
- Cal, M. P., Strickler, B. W., Lizzio, A. A. and Cangwal, S. K. (2000b). High temperature hydrogen sulfide adsorption on activated carbon II. Effects of gas temperature, gas pressure and sorbent regeneration. **J. Carbon.** 38: 1767–1774.

- Chaitiumwong, S. (1996). **Experiment of Chemical Quantitative Analysis**.(5th ed.). Bangkok: Chulalongkorn University.
- Chang, R. (2002).**Chemistry**. (7th ed.).New York: McGraw-Hill.
- Chen, x., Farber, M., Gao, Y., Kulaots, I., Suuberg, E. M. and Hurt, R. H. (2003). Mechanisms of surfactant adsorption on non-polar, air-oxidized and ozone-treated carbon surfaces. **J. Carbon**. 41: 1489-1500.
- Cheremisinoff, P. N. (1993). **Air Pollution Control and Design for Industry**. New York: M. Dekker.
- Chou, J. (2000). **Hazardous Gas Monitor: A Practical Guide to Selection, Operation and Application**. New York: McGraw – Hill.
- Chutima, K. (1996). **Principle of Chemistry** (Vol. 2). Bangkok: Chulalongkorn University.
- Cooper, C. D. and Alley, F. C. (2002). **Air Pollution Control a Design Approach**. (3rd ed.). Illinois: Waveland Press.
- Dean, J. A. (1999). **Lange's Hand Book of Chemistry**. (15th ed.). New York: McGraw-Hill.
- Do, D. D. (1998). **Adsorption Analysis: Equilibria and Kinetics** (vol.2). London: Imperial College Press.
- Fu, X., Lu, W. and Chung, D. D. L. (1998). Ozone treatment of carbon fiber for reinforcing cement. **J. Carbon**. 63: 1337 –1345.
- Geldart, D. (1986).**Gas Fluidization Technology**. New York: John Wiley and sons.
- Gomez-Serrano, V., Piriz-Almeida, F., Duran-Valle, C. J. and Pastor-Villegas, J. (1999). Formation of oxygen structures by air activation. A study by FT-IR spectroscopy. **J. Carbon**. 37:1517-1528.

- Gomez-Serrano, V., Alvarez, P. M., Jaramillo, J. and Beltran, F. J. (2002). Formation of oxygen complexes by ozonation of carbonaceous materials prepared from cherry stones. **J. Carbon.** 40: 513-522.
- Henry, F. H., Jr., William, R. R., and William, H. N. (1984). **General Chemistry.** (7th ed.). Toronto: D. C. health and company.
- Holum, J. R. (1994). **Fundamentals of General, organic and Biological Chemistry.** (5th ed.). New York
- Jae-Woon, S., Soon-Jin, P., and Seung-Kon, R.(2001). Effect of modification with HNO₃ and NaOH on metal adsorption by pitch-based activated carbon fibers. **J. Carbon** 39: 1635-1642.
- Lagowski, J. J. (1997). **Macmillan Encyclopedia of Chemistry.** New York: Simon and Schuster Macmillan.
- Langlais, B., Reckhow, D. A. and Brink, D. R. (1991). **Ozone in Water Treatment Application and Engineering.** Michigan: Lewis.
- Lee, W. H. and Reucroft, P. J. (1999a). Vapor adsorption on coal-and wood-based chemically activated carbons(I) Surface oxidation states and adsorption of H₂O. **J. Carbon.** 37: 7-14.
- Lee, W. H. and Reucroft, P. J. (1999b). Vapor adsorption on coal-and wood-based chemically activated carbons(II) adsorption of organic vapors. **J. Carbon.** 37: 15-20.
- Lee, W. H. and Reucroft, P. J. (1999c). Vapor adsorption on coal-and wood-based chemically activated carbons(III) NH₃ and H₂S adsorption in the low relative pressure range. **J. Carbon.** 37: 21-26.

- Manahan, S. E. (1993). **Fundamentals of Environmental Chemistry**. Boca Raton [Fla.]: Lewis.
- Masel, R. I. (1996). **Principle of Adsorption and Reaction on solid surfaces**. New York: John Wiley and Sons.
- Mawhinney, D. B. and Yates, J. T., Jr. (2001). FT-IR study of the oxidation of amorphous carbon by ozone at 300 K-Direct COOH formation. **J. Carbon**. 39: 1167-1173.
- Moreno-Castilla, C., Carrasco-Marin, F., Maldonado-Hodar, F.J. and Rivera-Utrilla, J. (1998). Effects of non-oxidant and oxidant acid treatments on the surface properties of an activated carbon with very low ash content. **J. Carbon**. 36:145-152.
- Mul, G., Neeft, J. P. A., Kapteijn, F. and Moulijn, J. A. (1997). The formation of carbon surface oxygen complexes by oxygen and ozone. The effect of transition metal oxides. **J. Carbon**. 36: 1269 - 1276.
- Mycock, J. C., McKenna, J. D., and Theodore, L.(1995). **Handbook of Air Pollution Control Engineering and Technology**. New York: Lewis.
- Noll, K. E., Gounaris, V. and Hou, W. S. (1992). **Adsorption Technology for Air and Water Pollution Control**. Michigan: Lewis.
- Parker, S. P. (1993). **McGraw-Hill Encyclopedia of Chemistry** (2nd ed.). New York: McGraw-Hill.
- Pradhan, B. K. and Sandle, N. K. (1999) Effect of different oxidizing agent treatments on the surface properties of activated carbons. **J. Carbon**. 37: 1323-1332.

- Radovic, L. R., Moreno-Castilla, C. and Rivera-Utrilla, J. (2001). **Carbon materials as adsorbents in aqueous solutions**. New York: Marcel Dekker.
- Rouquerol, F., Rouquerol, J. and Sing, K. (1999). **Adsorption by Powders and Porous Solids Principles, Methodology and Applications**. New York: Academic Press.
- Shibagaki, K. and Motojima, S. (2000). Surface properties of carbon micro-coils oxidized by a low concentration of oxygen gas. **J. Carbon**. 38: 2087-2093.
- Smith, B. C. (1999). **Infrared Spectral Interpretation a Systematic Approach**. New York: CRC Press.
- Snell, F. D. and Leslie, S. E. (1971). **Encyclopedia of Industrial Chemical Analysis**. Vol.13: USA.
- Spengler, J. D., Samet, Jonathan M. and McCathy, John F. (2000). **Indoo Air Quality Handbook**. New York: McGraw-Hill.
- Tchobanoglous, G., Burton, F. L. and Stensel, H. D. (2003). **Wastewater Engineering Treatment and Reuse** (4th ed.). New York: Metcalf & Eddy.
- Theodore, L., and Buonicore, A. (1994). **Air Pollution Control Equipment: Selection, Design, Operation, and maintenance**. New York: Springer-Verlag.
- Yan, R., Chin, T., Ng, Y. L., Duan, H., Liang, D. T. and Tay, J. H. (2004). Influence of surface properties on the mechanism of H₂S removal by alkaline activated carbons. **Environ Sci Technol**. 38: 316-323.
- Yang, R. T. (2003). **Adsorbents Fundamentals and Applications**. New Jersey: John Wiley and Sons.

APPENDIX A
FT-IR SPECTRA

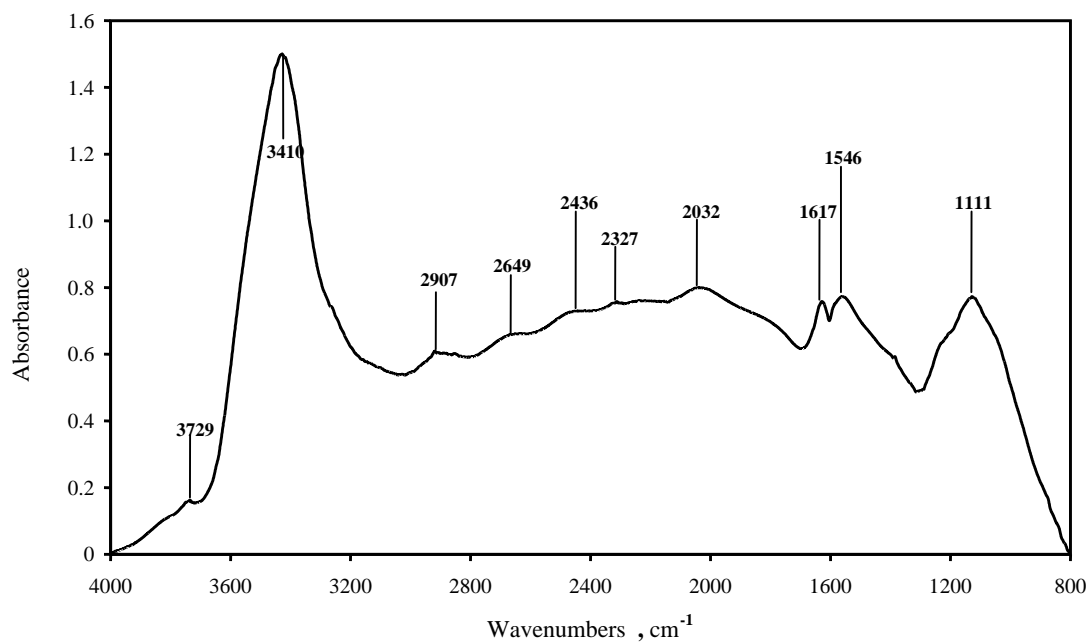


Figure A.1 The original sample from the company.

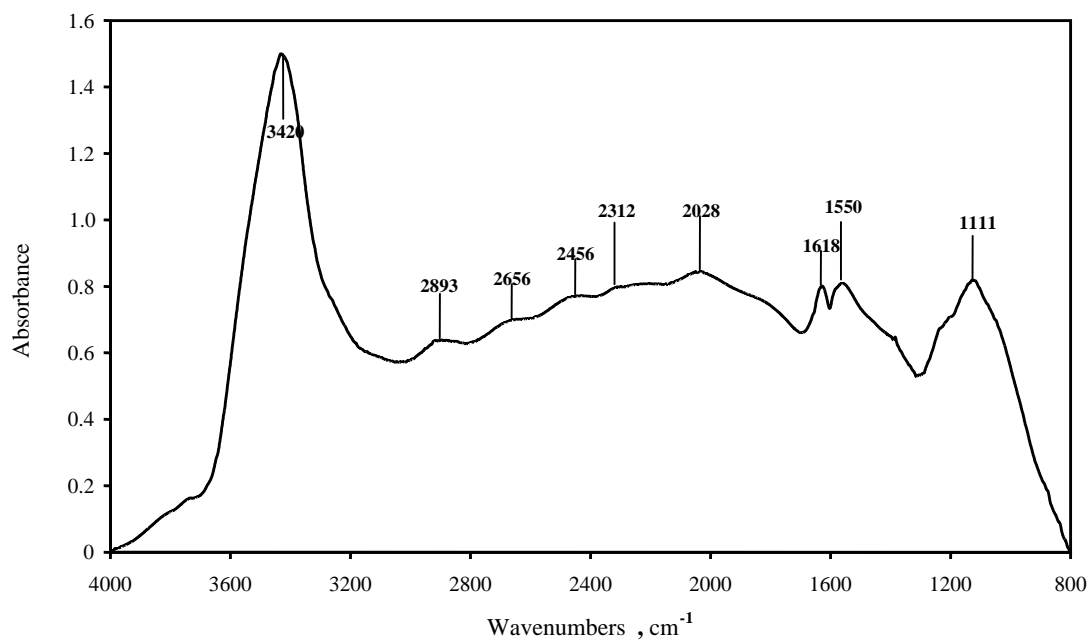


Figure A.2 An air oxidized sample in fluidized-bed at 150°C, flow rate 1.2 L/s, 90 min.

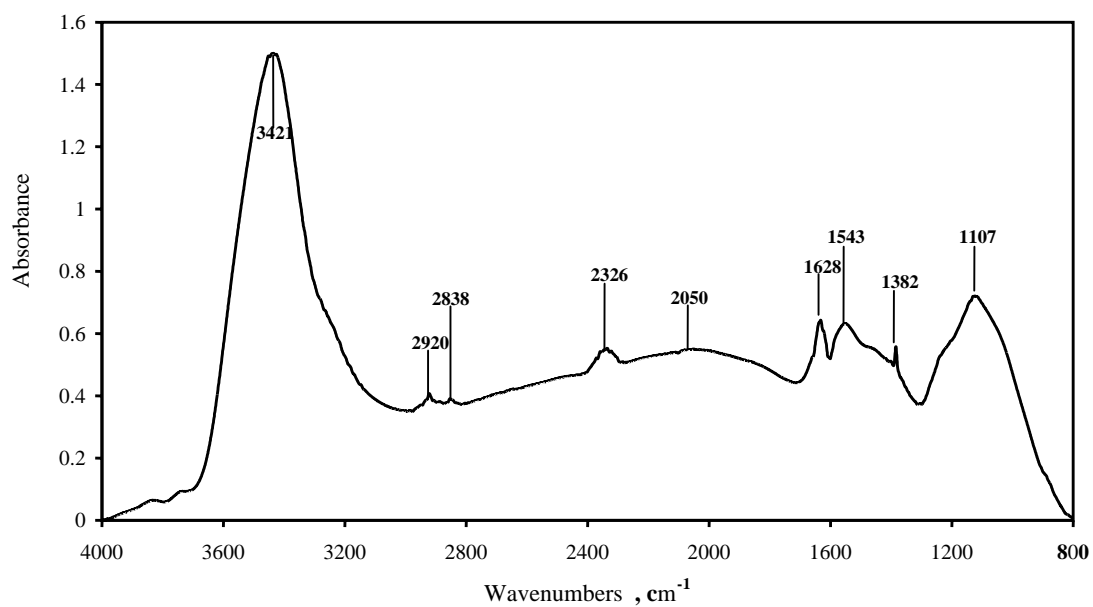


Figure A.3 An air oxidized sample in fluidized-bed at 205°C, flow rate 1.2 L/s, 100 min.

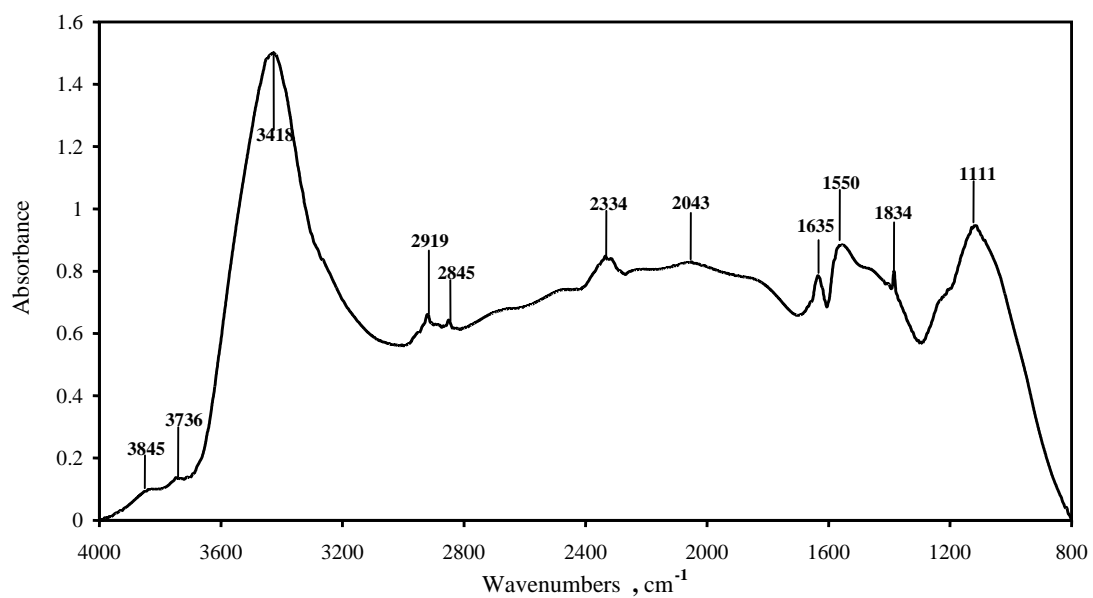


Figure A.4 An air oxidized sample in fluidized-bed at 225°C, flow rate 1.2 L/s, 90 min.

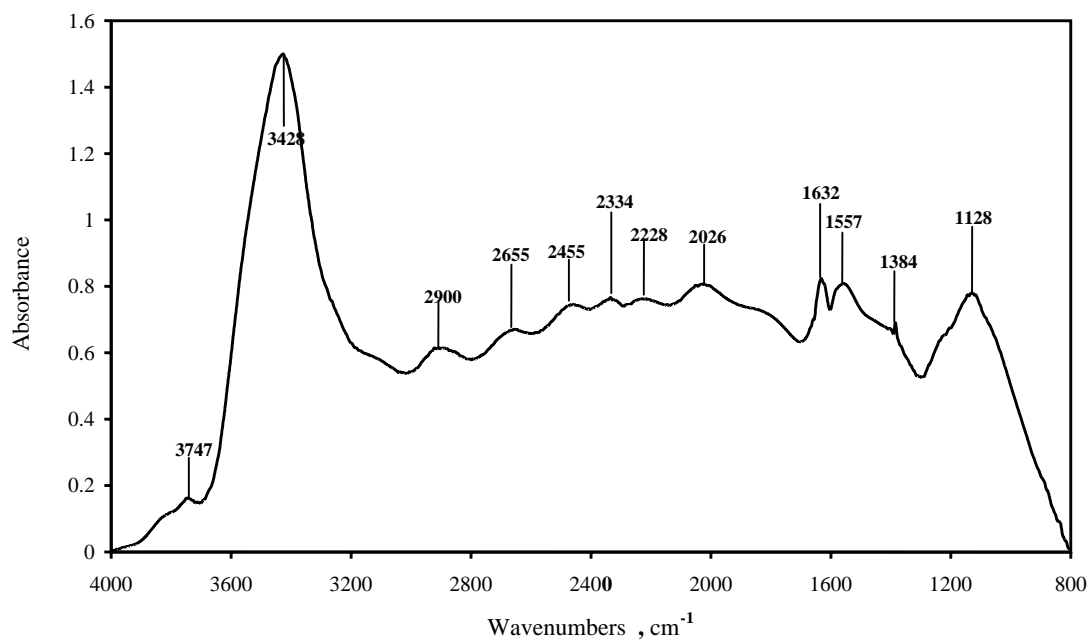


Figure A.5 An air oxidized sample in fluidized-bed at 275°C, flow rate 1.2 L/s, 90 min.

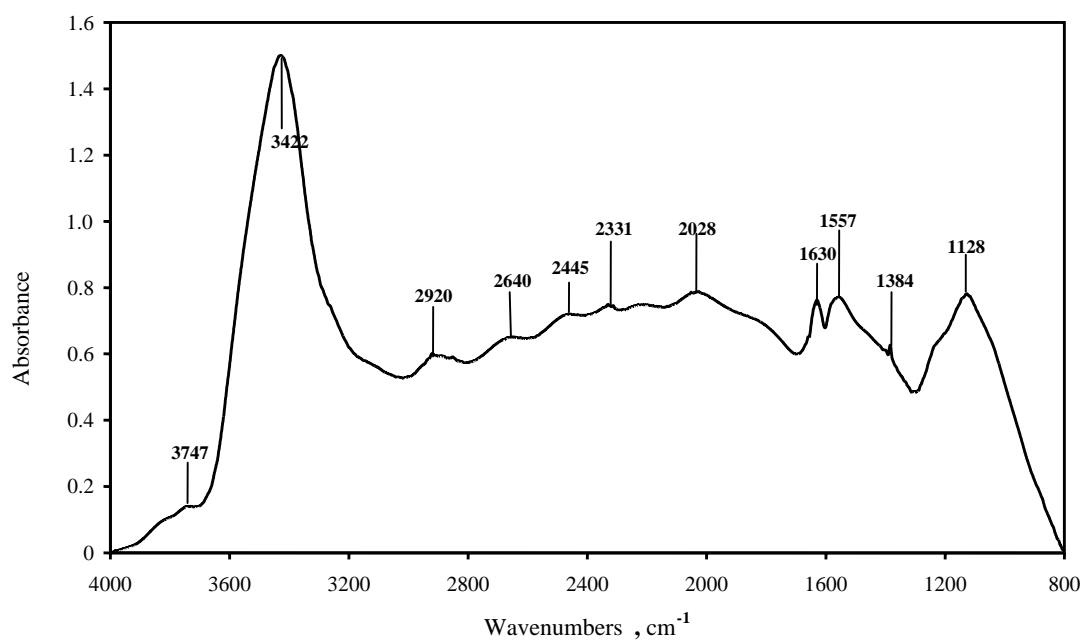


Figure A.6 An air oxidized sample in fluidized-bed at 275°C, flow rate 1.1 L/s, 90 min.

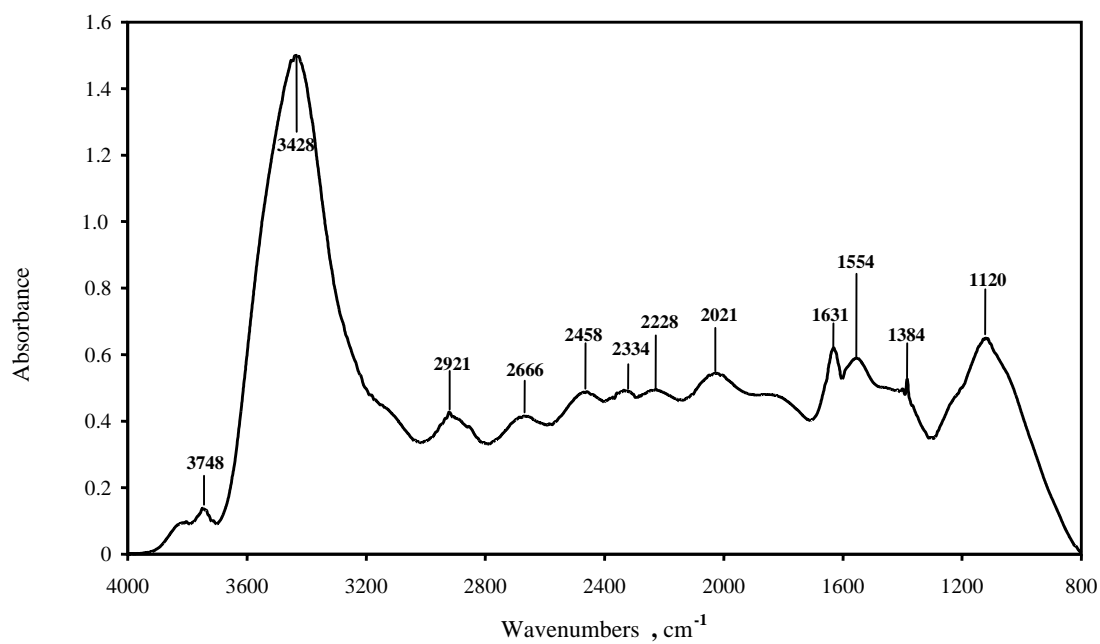


Figure A.7 An air oxidized sample in fluidized-bed at 275°C, flow rate 1.3 L/s, 90 min.

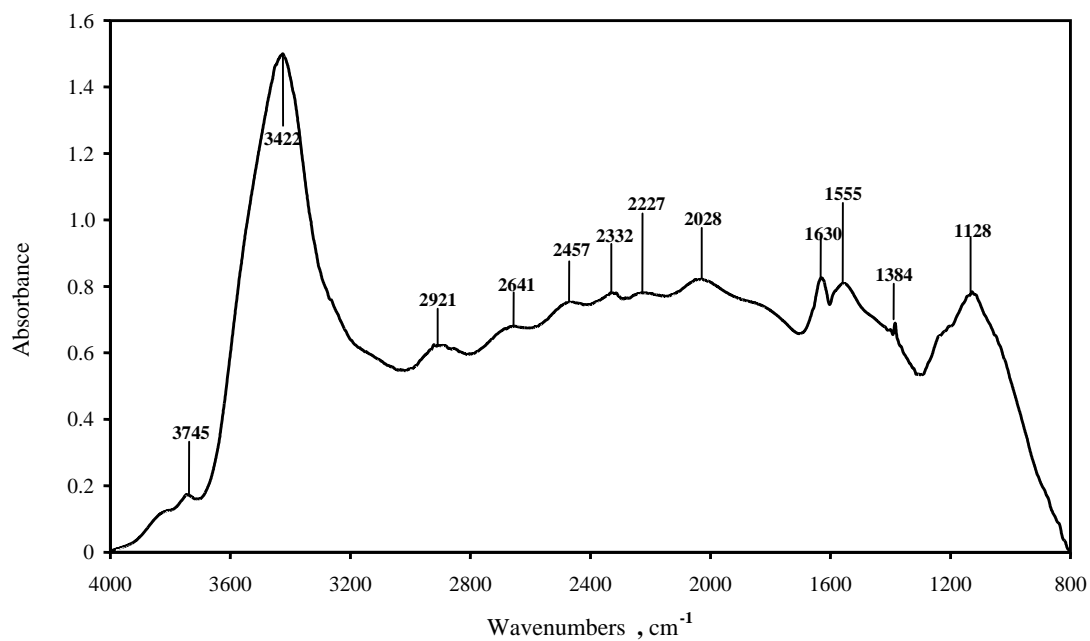


Figure A.8 An air oxidized sample in fluidized-bed at 245°C, flow rate 1.3 L/s, 90 min.

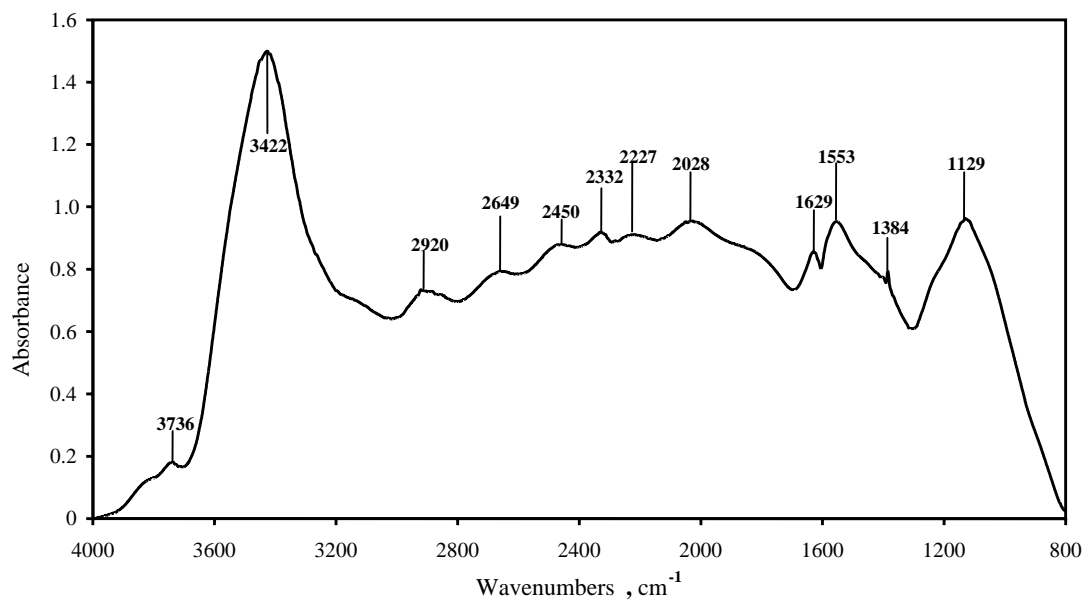


Figure A.9 An air oxidized sample in fluidized-bed at 265°C, flow rate 1.1 L/s, 90 min.

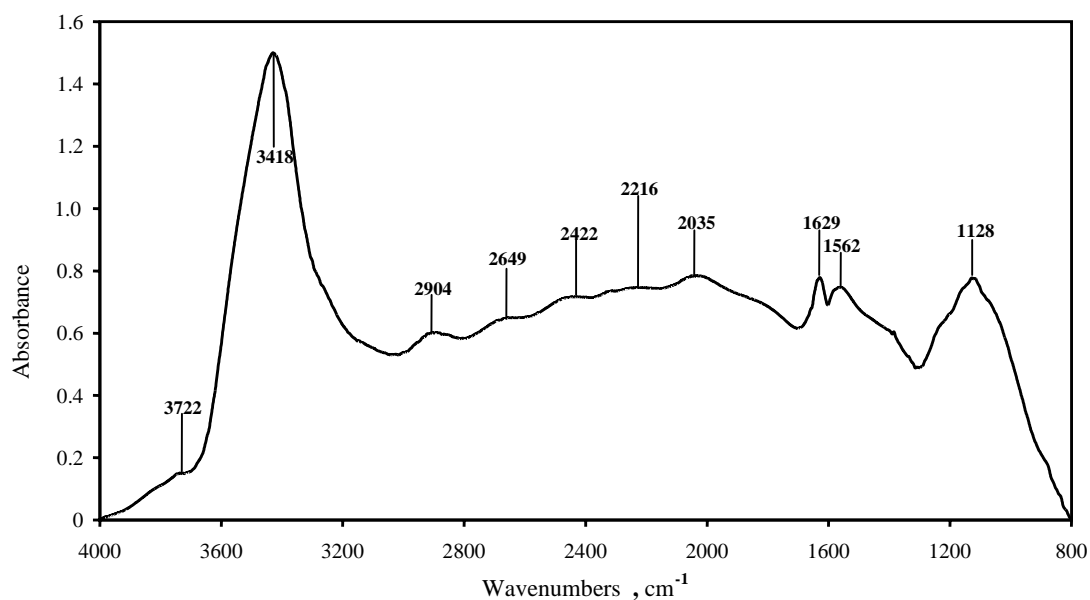


Figure A.10 An air oxidized sample in fluidized-bed at 225°C, flow rate 1.1 L/s, 90 min.

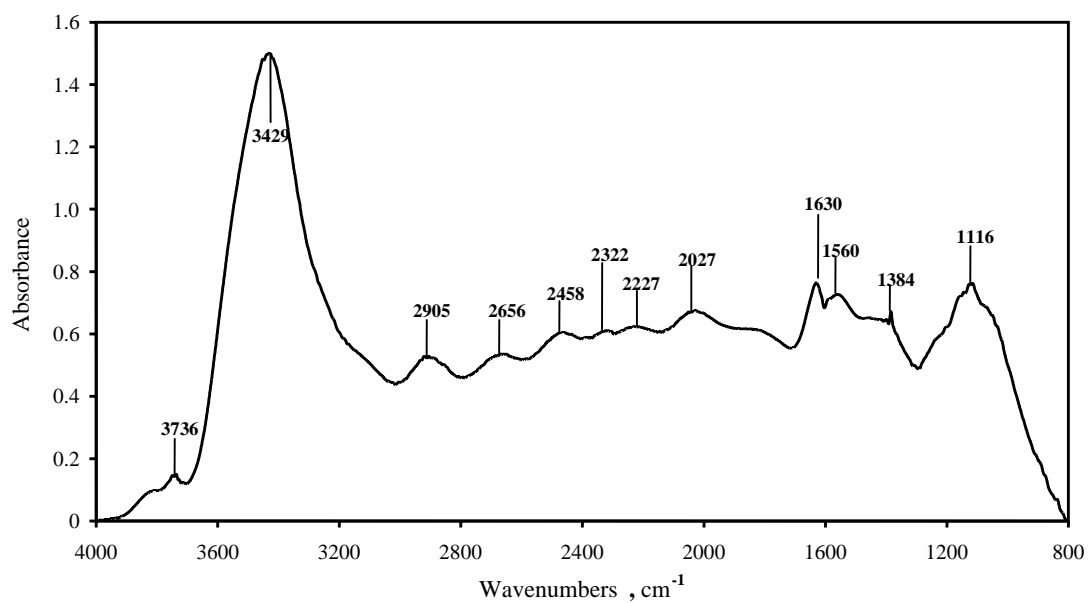


Figure A.11 An air oxidized sample in fluidized-bed at 225°C, flow rate 1.1 L/s, 30 min.

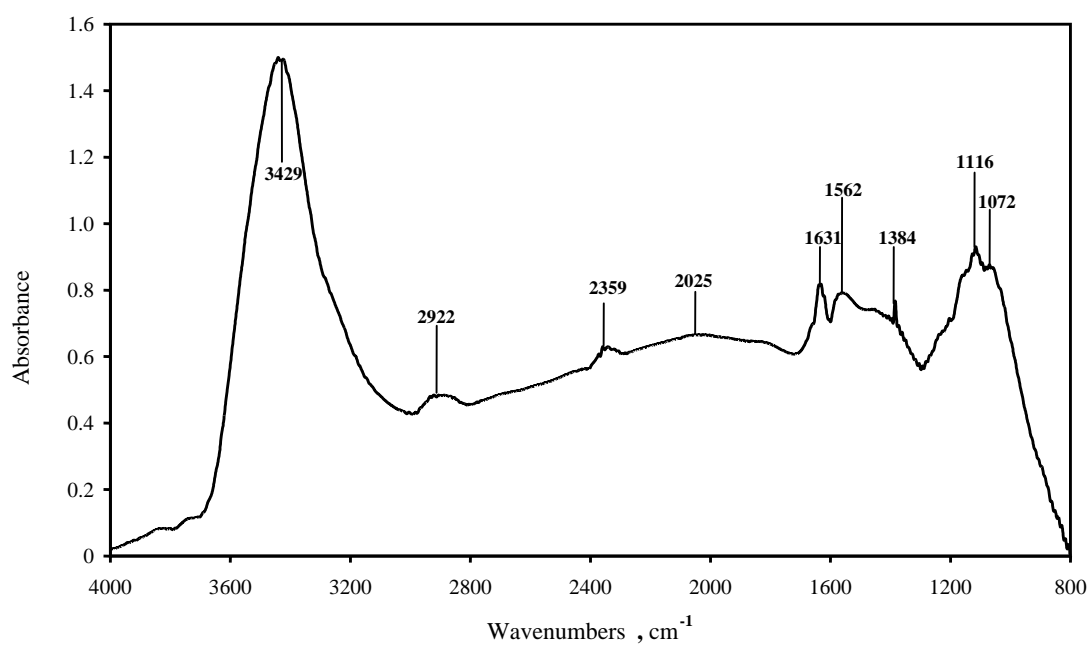


Figure A.12 An air oxidized sample in fluidized-bed at 180°C, flow rate 5.5 L/min, 90 min.

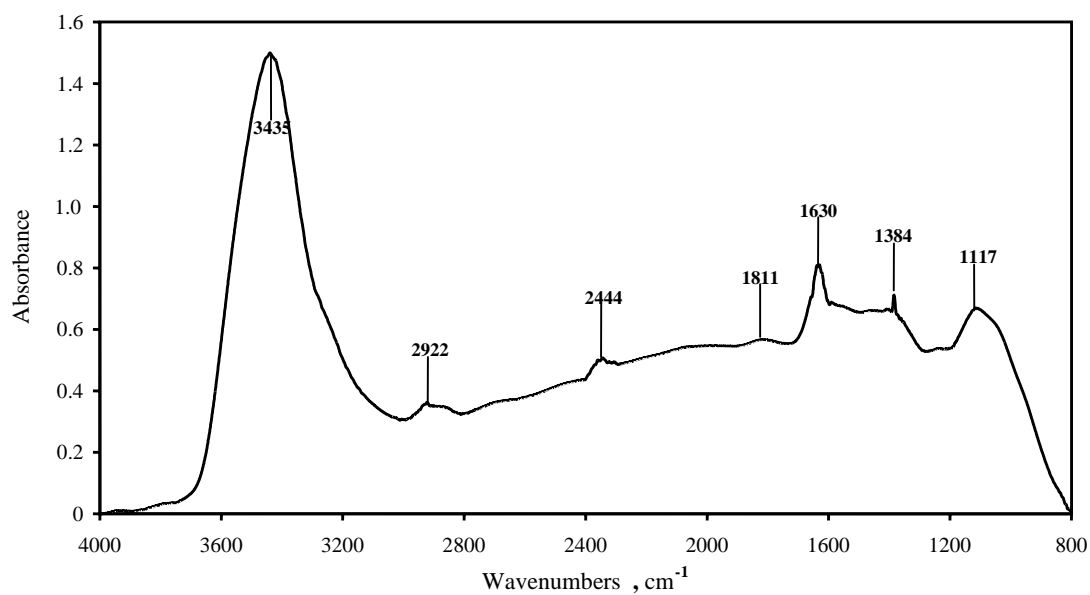


Figure A.13 An oxygen oxidized sample in fluidized-bed at 180°C, flow rate 5.5 L/min, 90min.

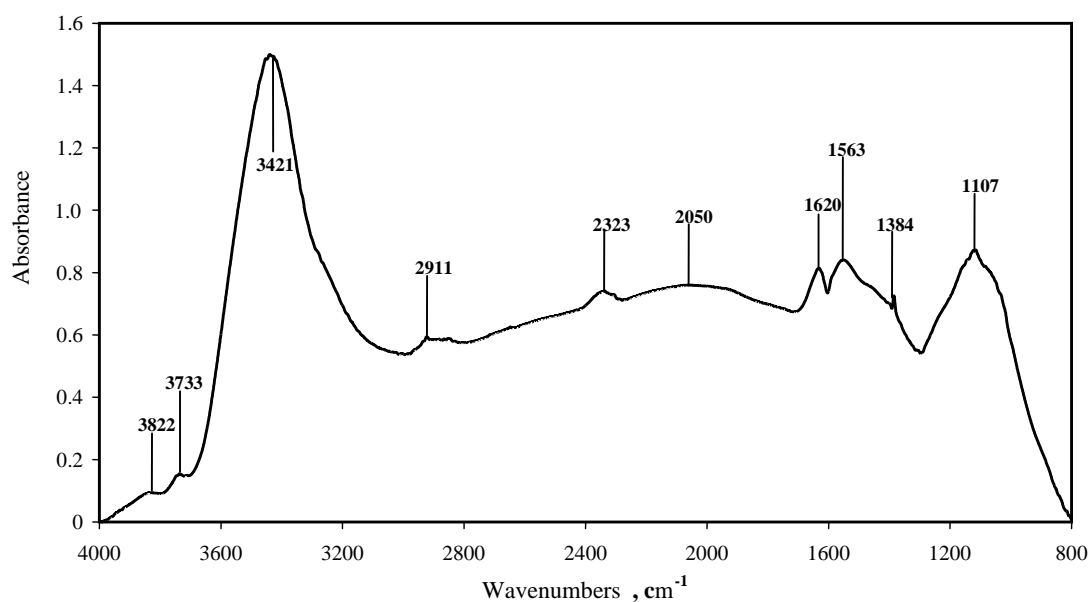


Figure A.14 An ozone oxidized sample in fluidized-bed at 150°C, flow rate 5.5 L/min, 30min.

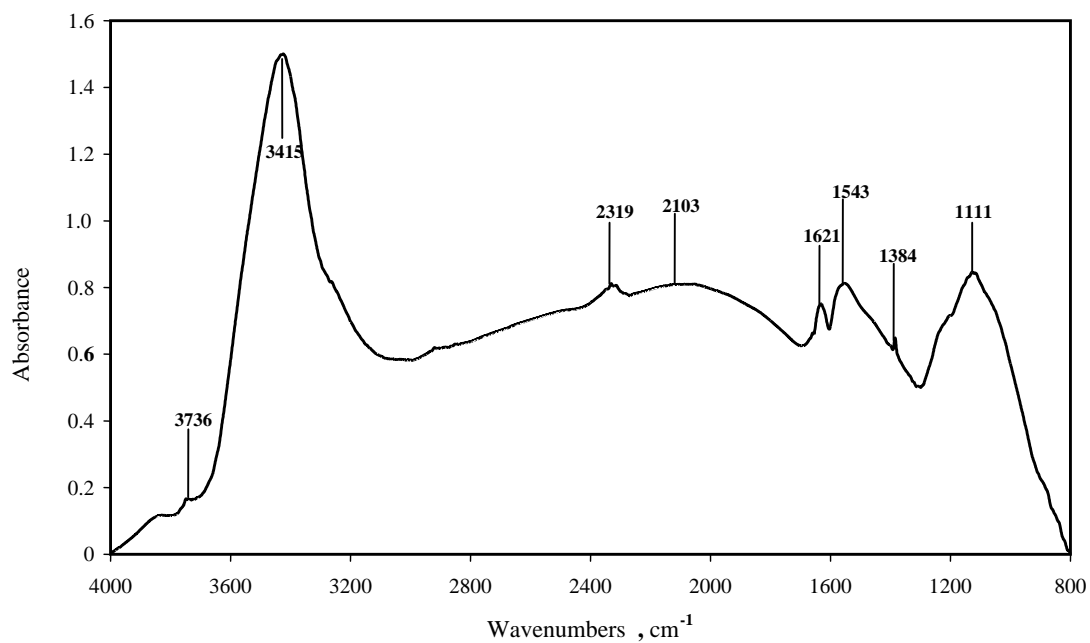


Figure A.15 An ozone oxidized sample in fluidized-bed at 150°C, flow rate 5.5 L/min, 60min.

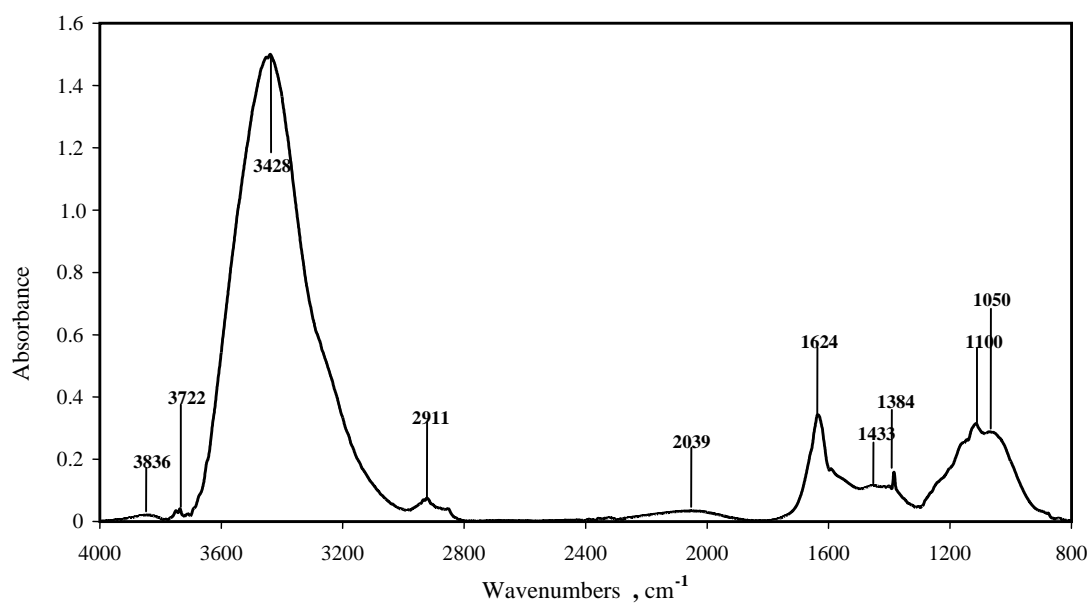


Figure A.16 An ozone oxidized sample in fluidized-bed at 90°C, flow rate 5.5 L/min, 30min.

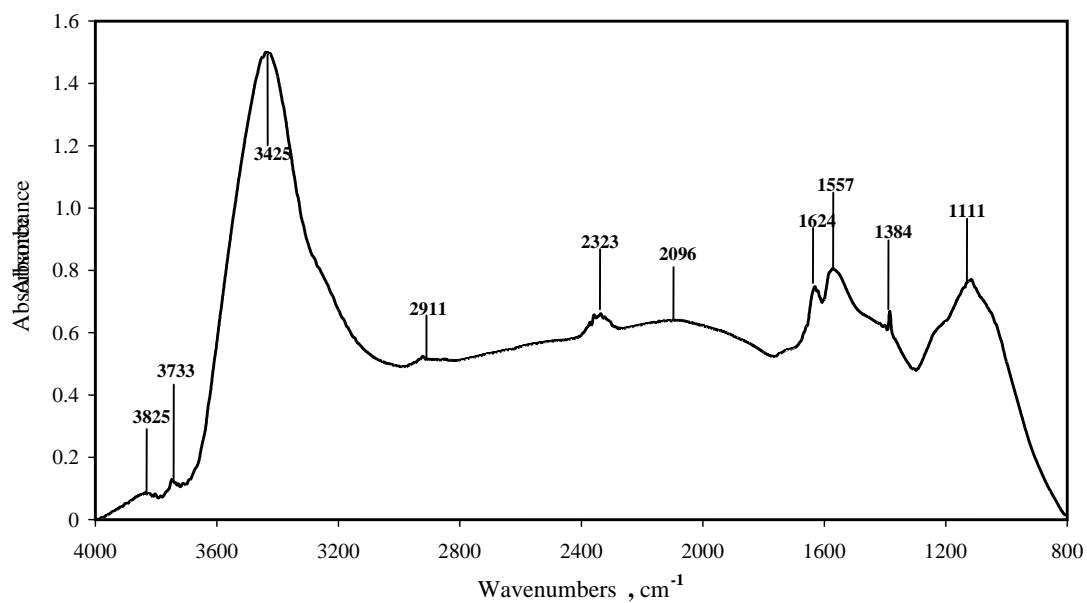


Figure A.17 An ozone oxidized sample in fluidized-bed at 180°C, flow rate 5.5 L/min, 30min.

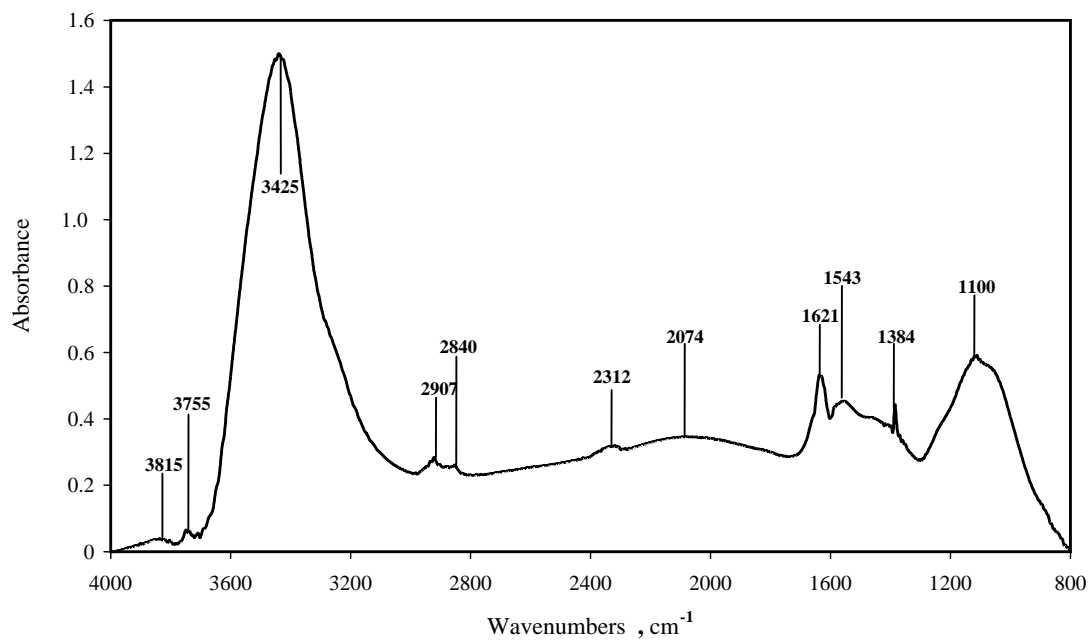


Figure A.18 An ozone oxidized sample in fluidized-bed at 240°C, flow rate 5.5 L/min, 30min.

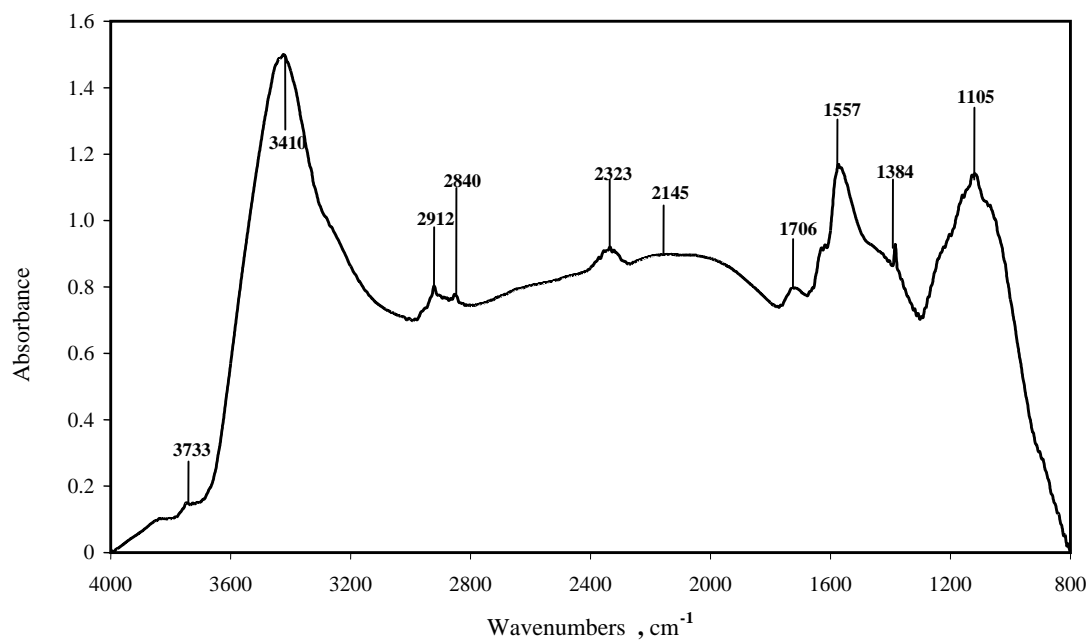


Figure A.19 An ozone oxidized sample in fluidized-bed at 190°C, flow rate 5.5 L/min, 60min.

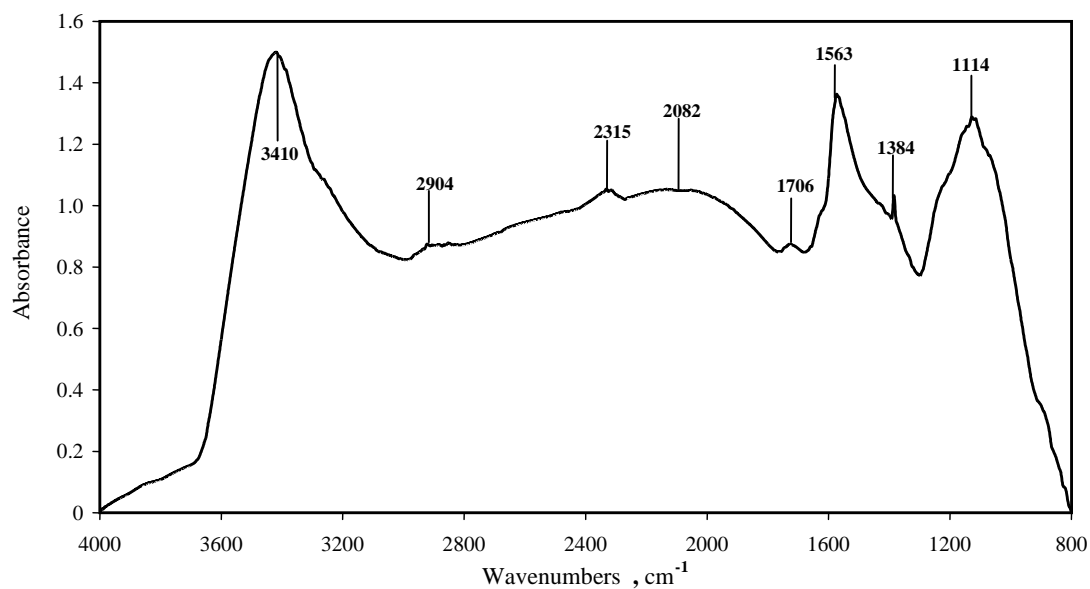


Figure A.20 An ozone oxidized sample in fluidized-bed at 180°C, flow rate 5.5 L/min, 90min.

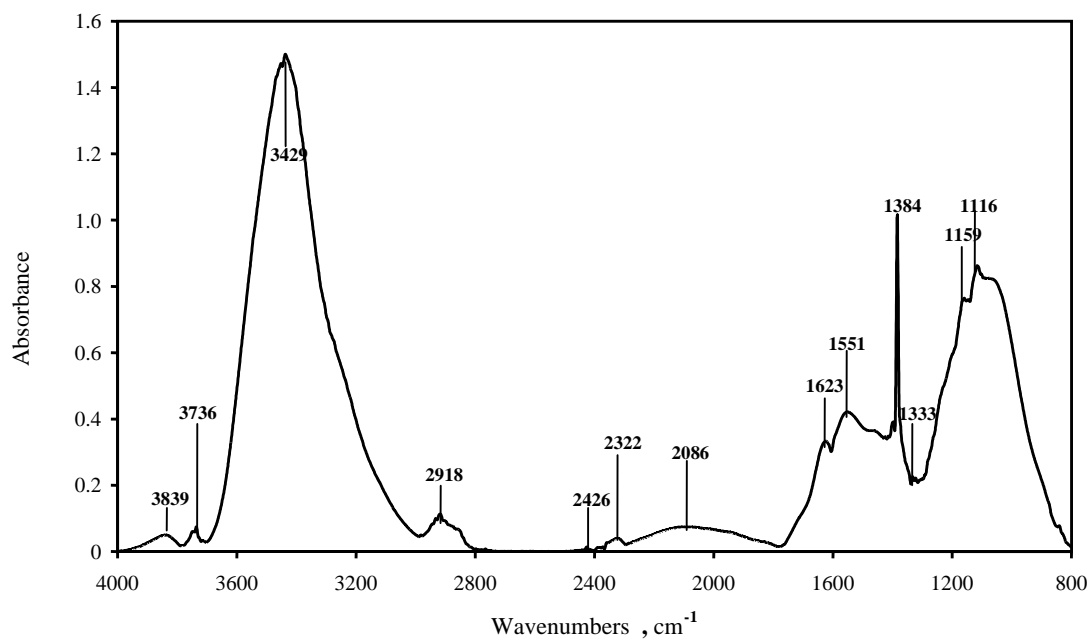


Figure A.21 A 2.0 M nitric acid oxidized sample in a reflux column at 100°C, 30min.

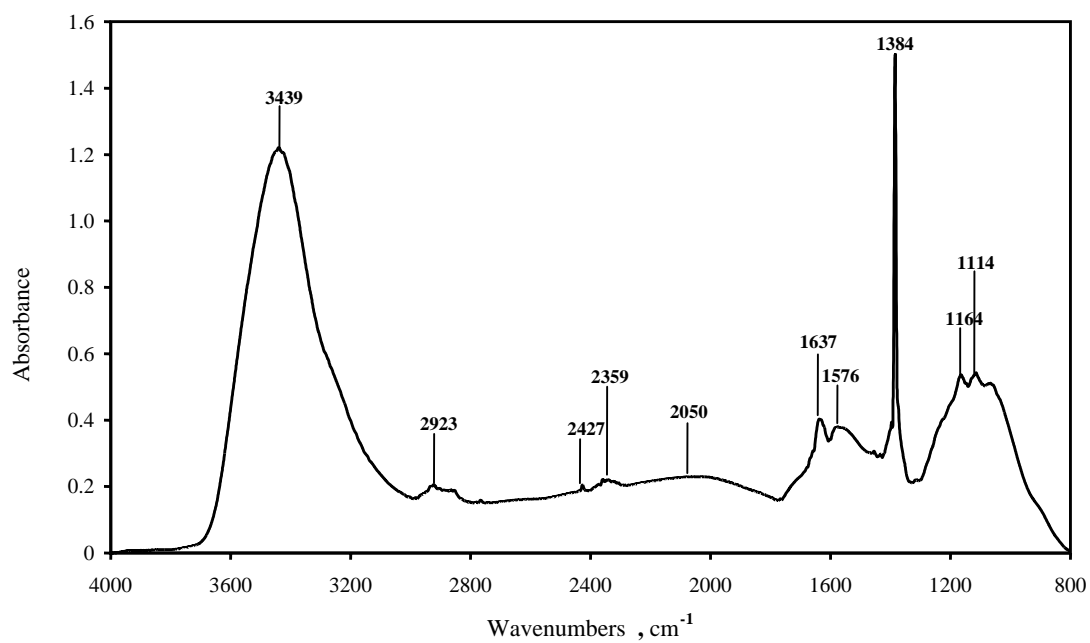


Figure A.22 A 2.0 M nitric acid oxidized sample in a reflux column at 100°C, 60min.

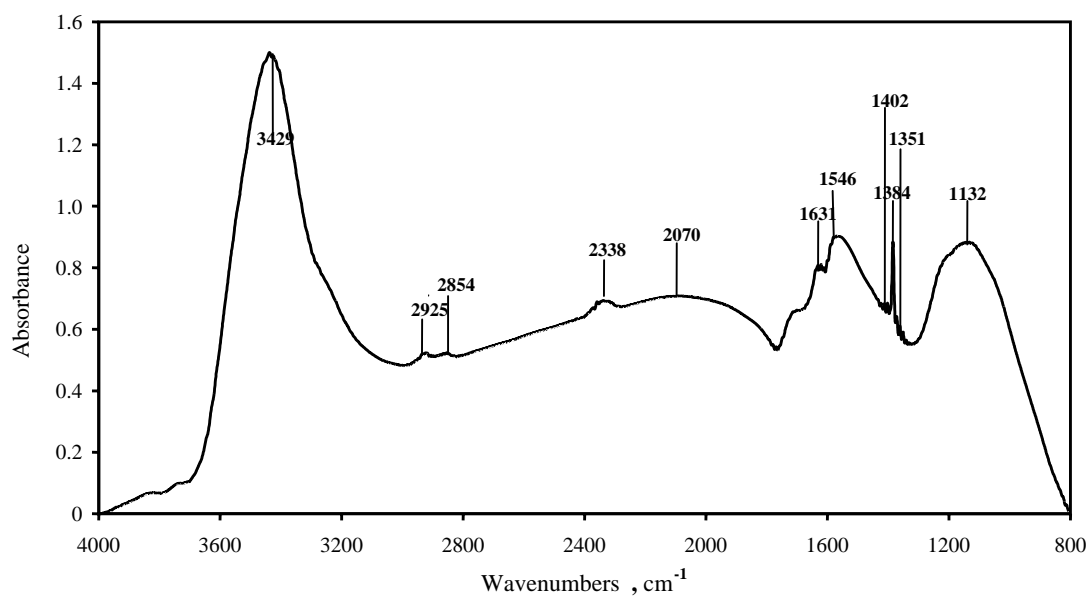


Figure A.23 A 2.0 M nitric acid oxidized sample in a reflux column at 100°C, 120 min.

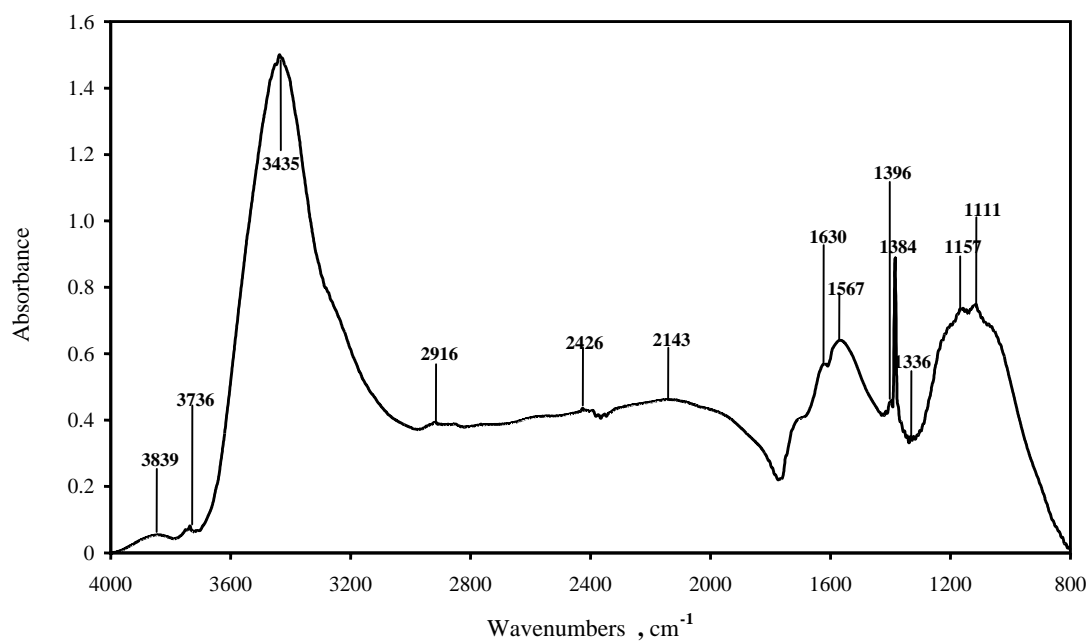


Figure A.24 A 4.0 M nitric acid oxidized sample in a reflux column at 105°C, 120 min.

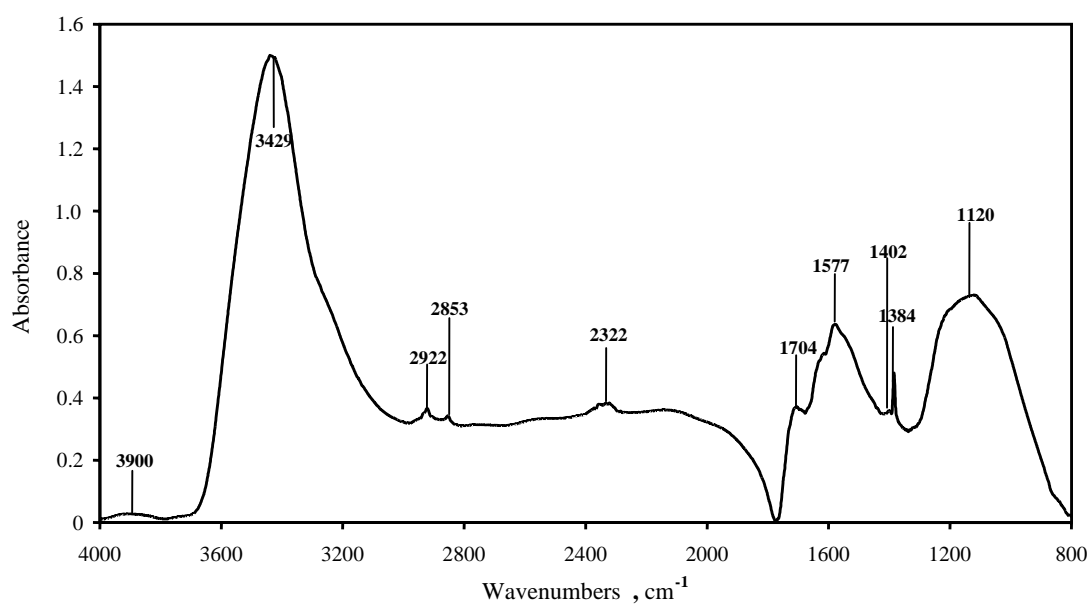


Figure A.25 A 6.0 M nitric acid oxidized sample in a reflux column at 105°C, 120 min.

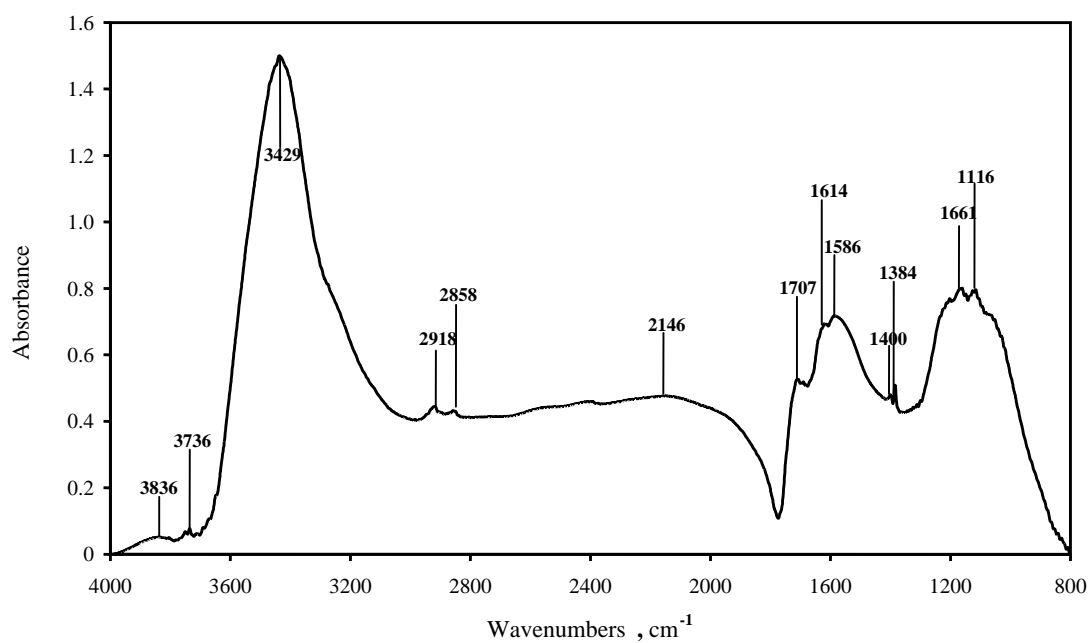


Figure A.26 A 8.0 M nitric acid oxidized sample in a reflux column at 105°C, 120 min.

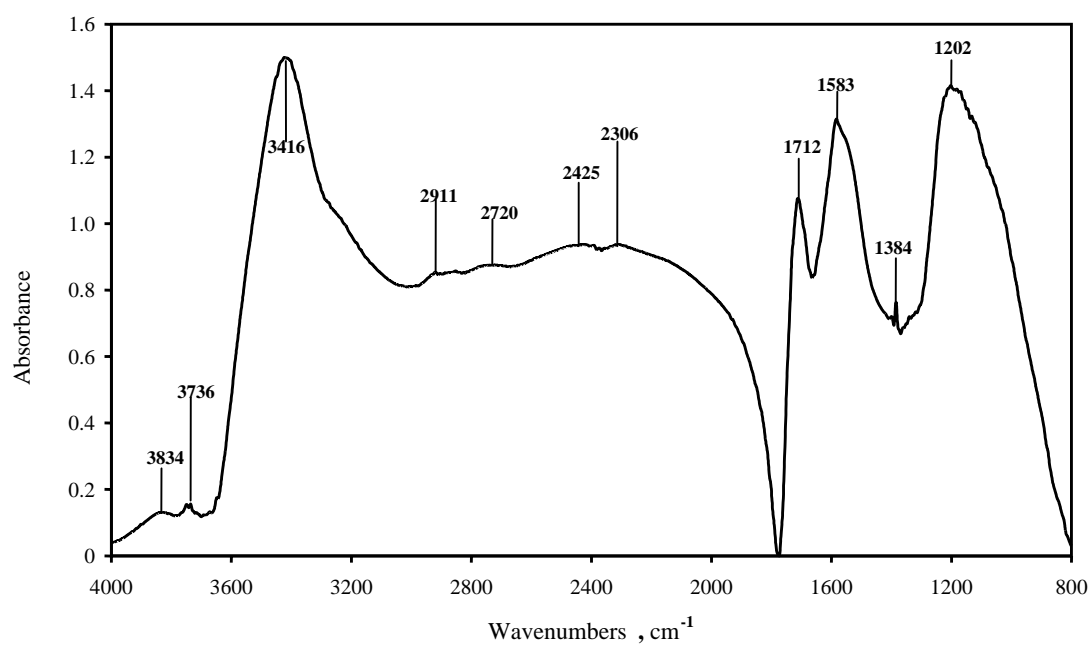


Figure A.27 A 10.0 M nitric acid oxidized sample in a reflux column at 105°C, 120 min.

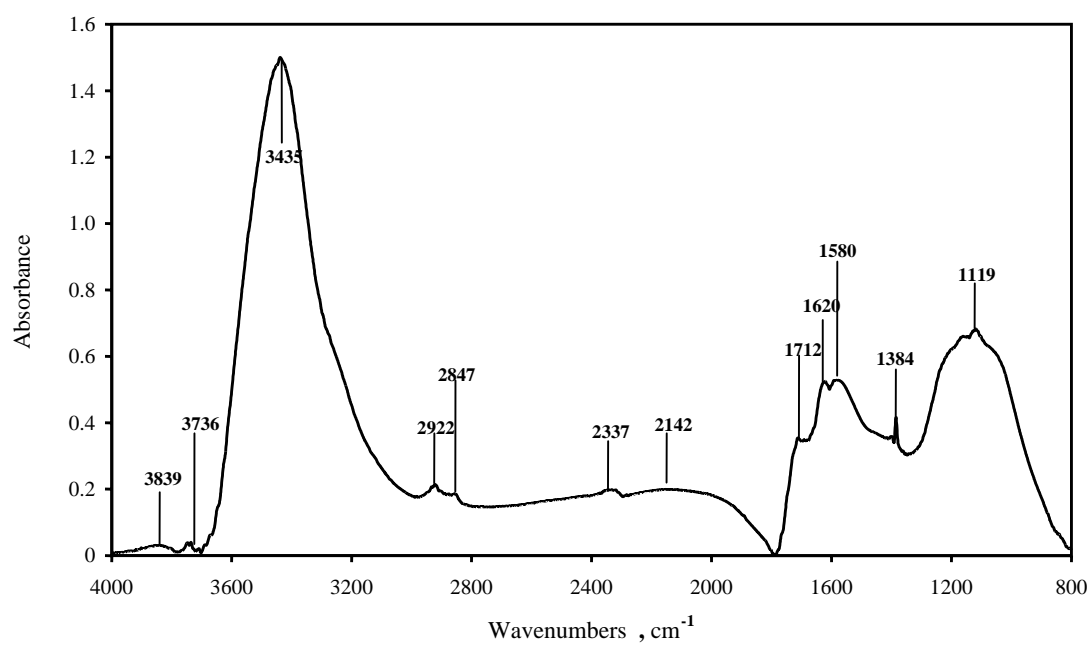


Figure A.28 A 2.0 M nitric acid oxidation sample in a reflux column at 100°C, 120 min, and repeated that with ozone oxidation for 30 min.

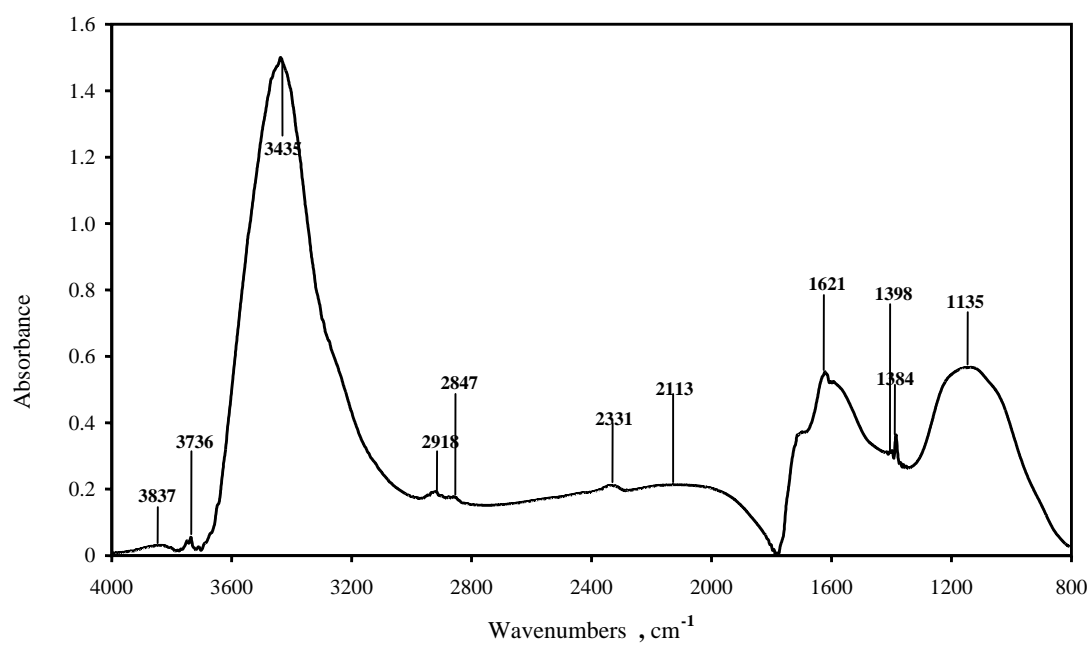


Figure A.29 A 6.0 M nitric acid oxidation sample in a reflux column at 105°C, 120 min, and repeated that with ozone oxidation for 30 min.

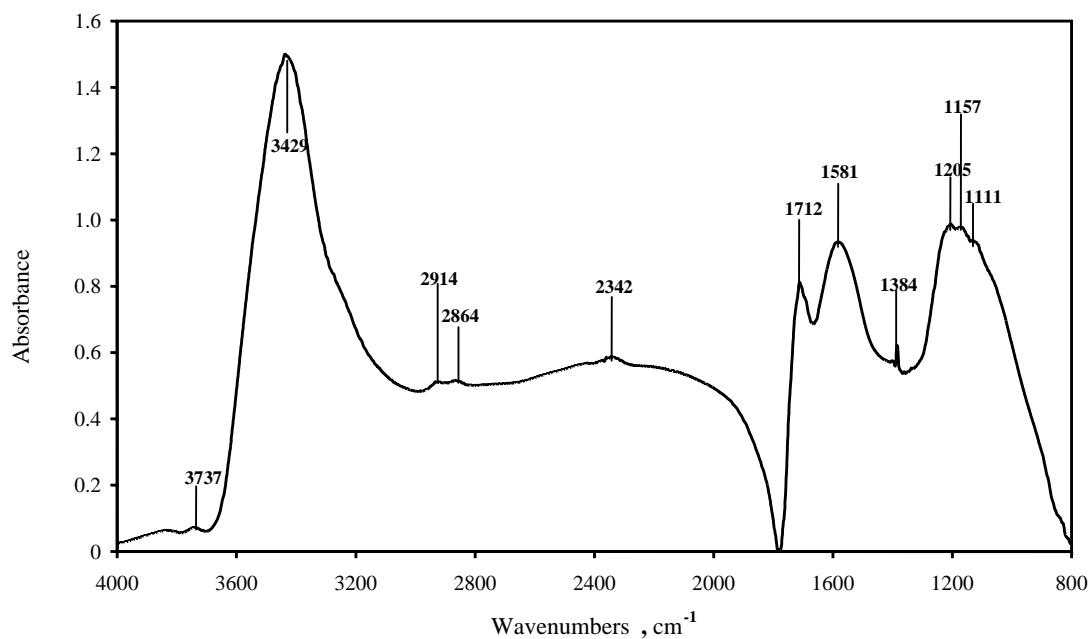


Figure A.30 A 10.0 M nitric acid oxidation sample in a reflux column at 105°C, 120 min, and repeated that with ozone oxidation for 30 min.

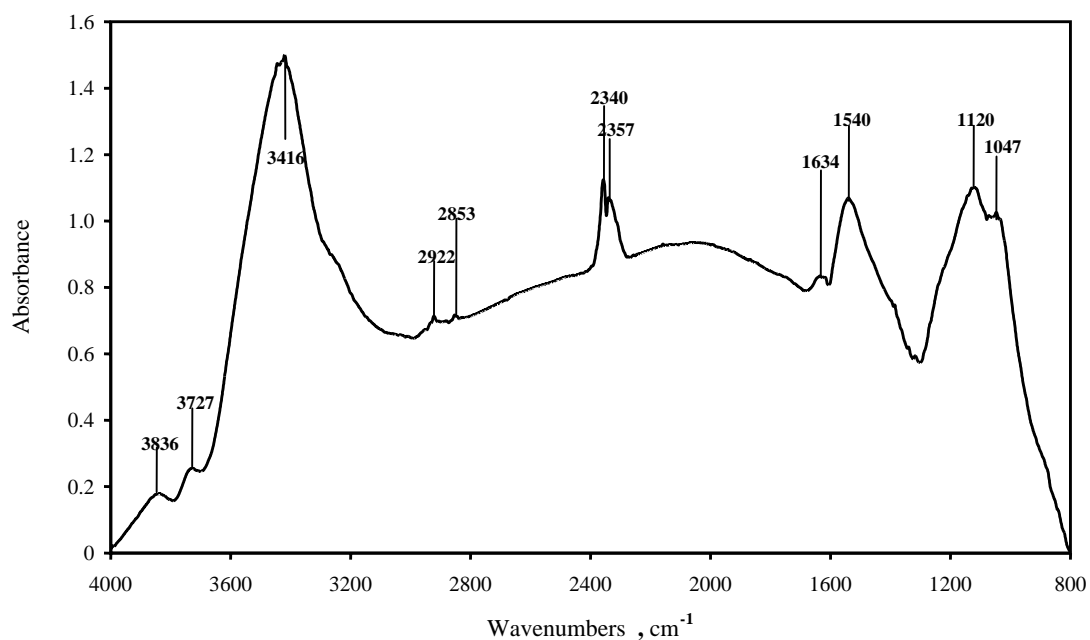


Figure A.31 An ozone oxidized sample in a reflux column (hot water 90°C), 60 min.

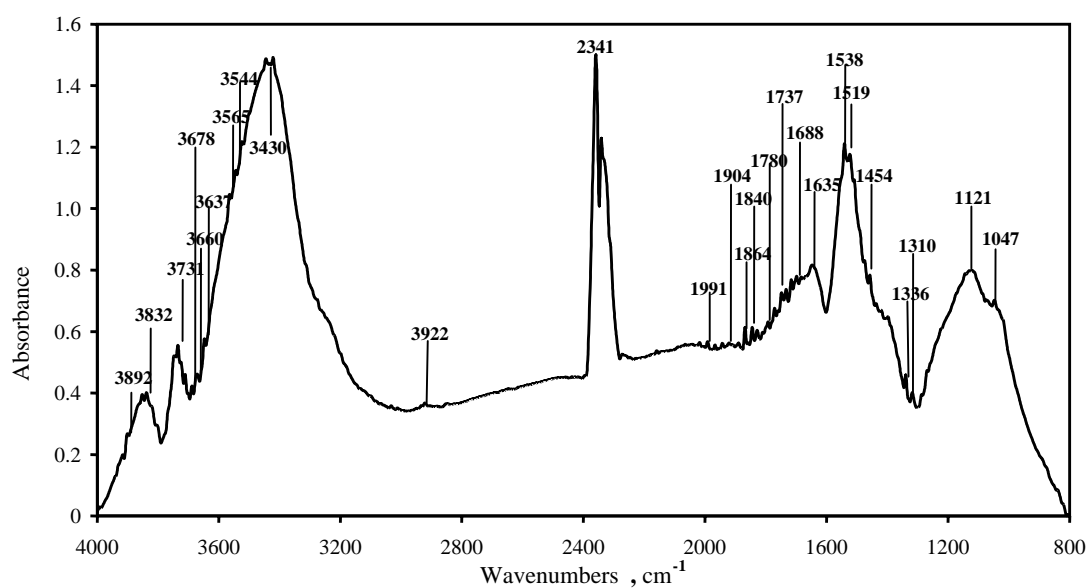


Figure A.32 An ozone oxidized sample in a reflux column (hot water 90°C), 60 min and Zn addition.

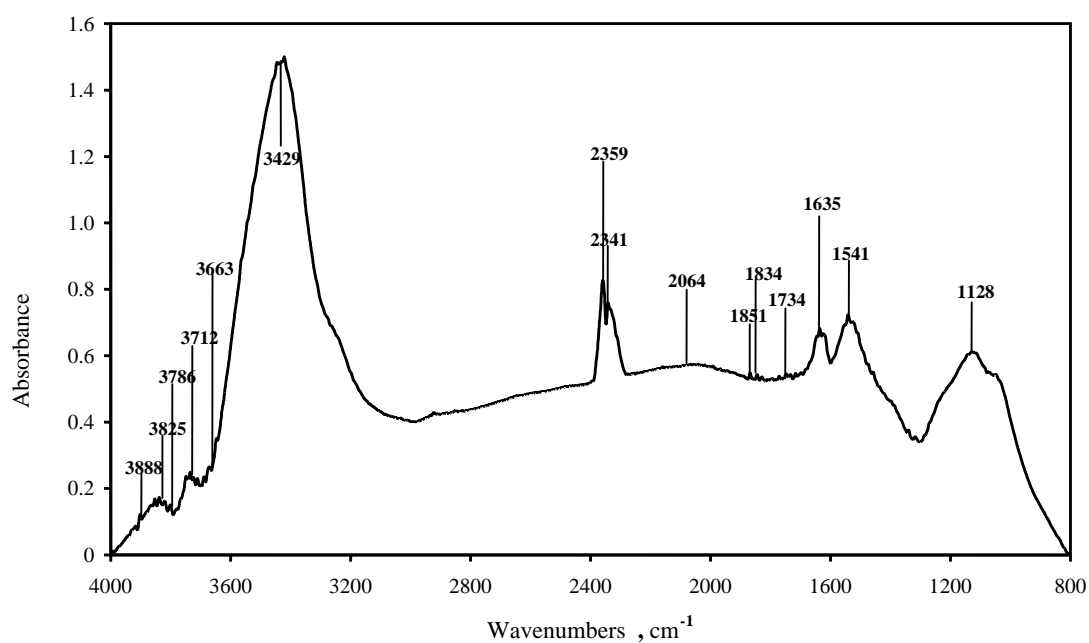


Figure A.33 An ozone oxidized sample in a reflux column (hot water 90°C), 120 min.

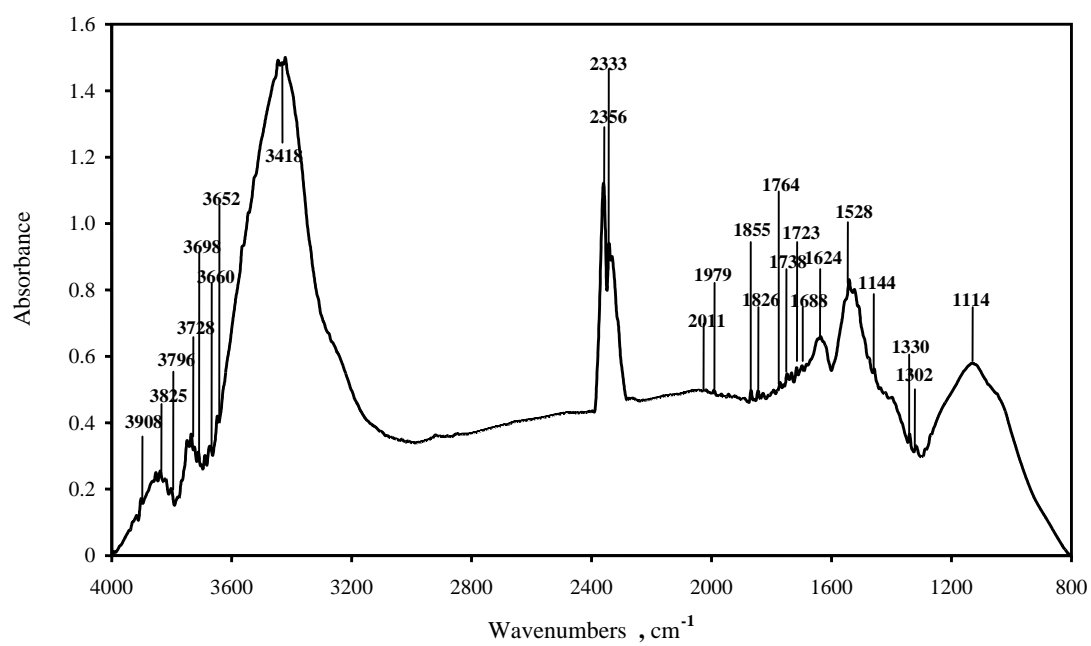


Figure A.34 An ozone oxidized sample in a reflux column (hot water 90°C), 120 min and Zn addition.

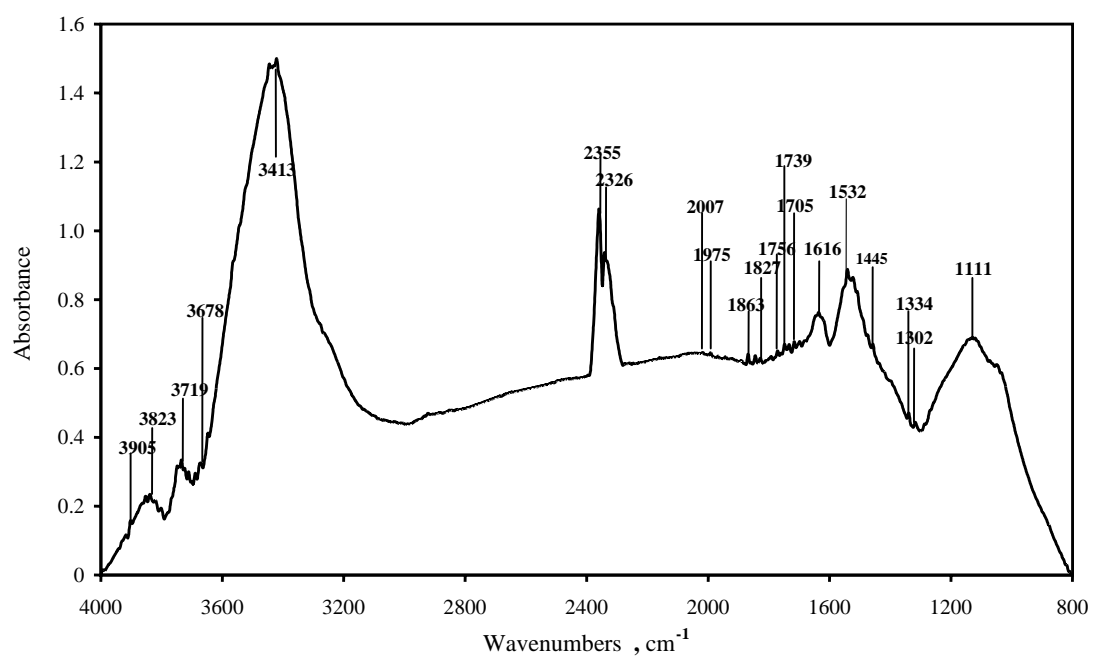


Figure A.35 An ozone oxidized sample in a reflux column (hot water 90°C),
180 min.

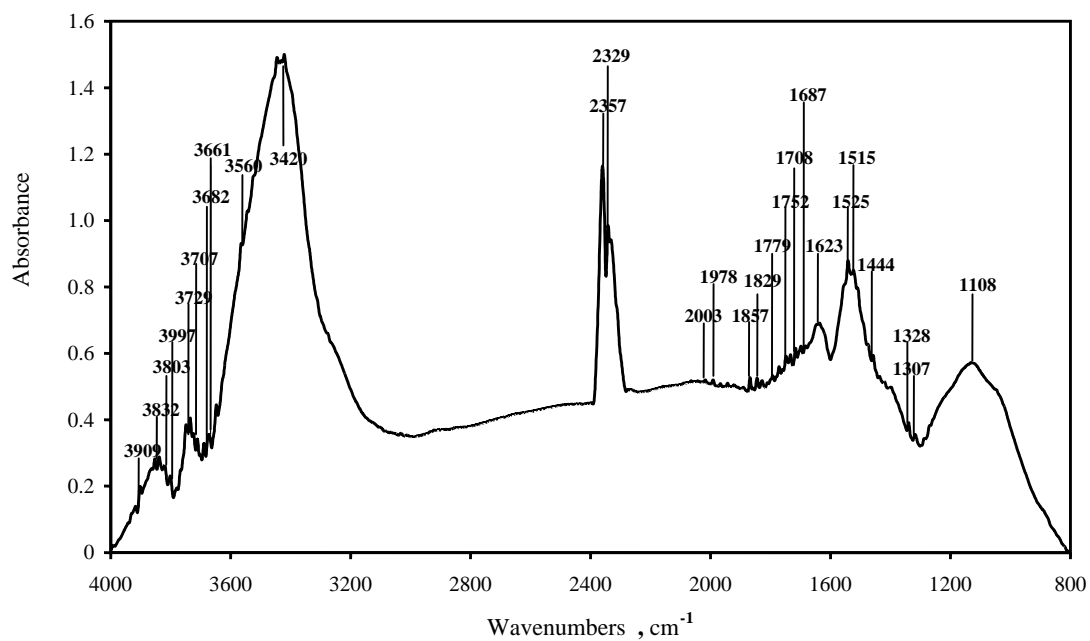


Figure A.36 An ozone oxidized sample in a reflux column (hot water 90°C), 180 min and Zn addition.

APPENDIX B
BET ISOTHERMS

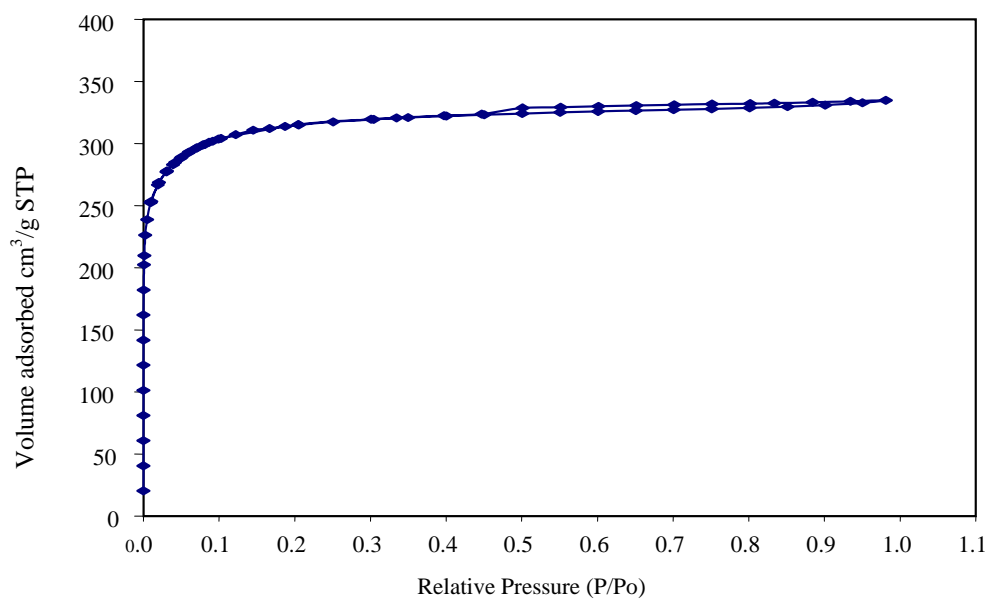


Figure B.1 Nitrogen adsorption isotherm at 77 K for the original activated carbon sample from the C-Gigantic company.

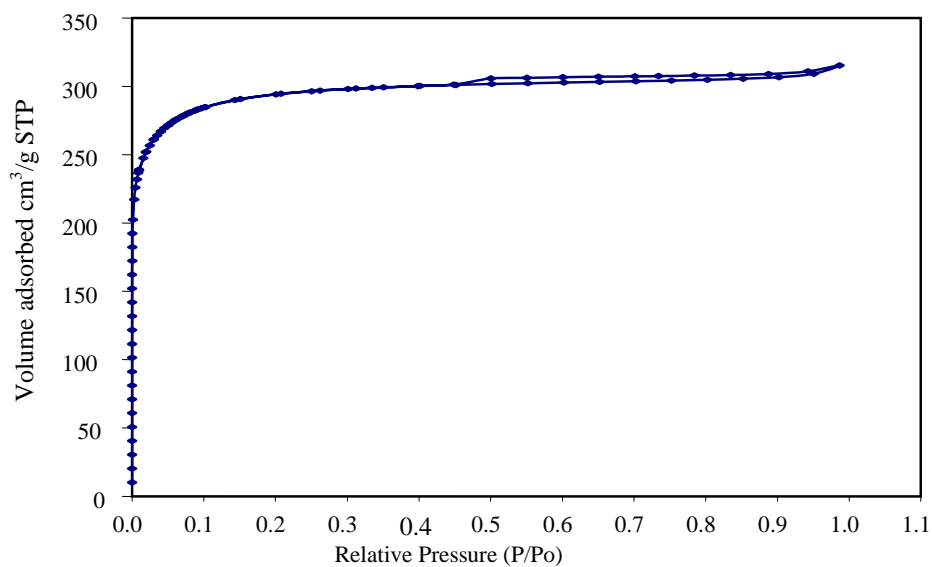


Figure B.2 Nitrogen adsorption isotherm at 77 K for the original activated carbon sample from the C-Gantic company after metal (Zn) addition.

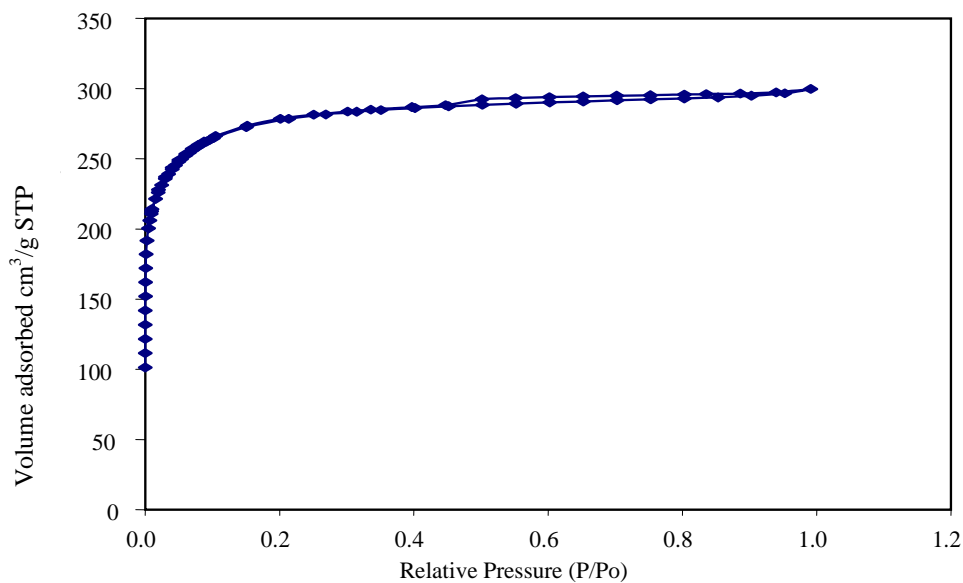


Figure B.3 Nitrogen adsorption isotherm at 77 K for activated carbon sample after nitric acid (6 M) oxidation.

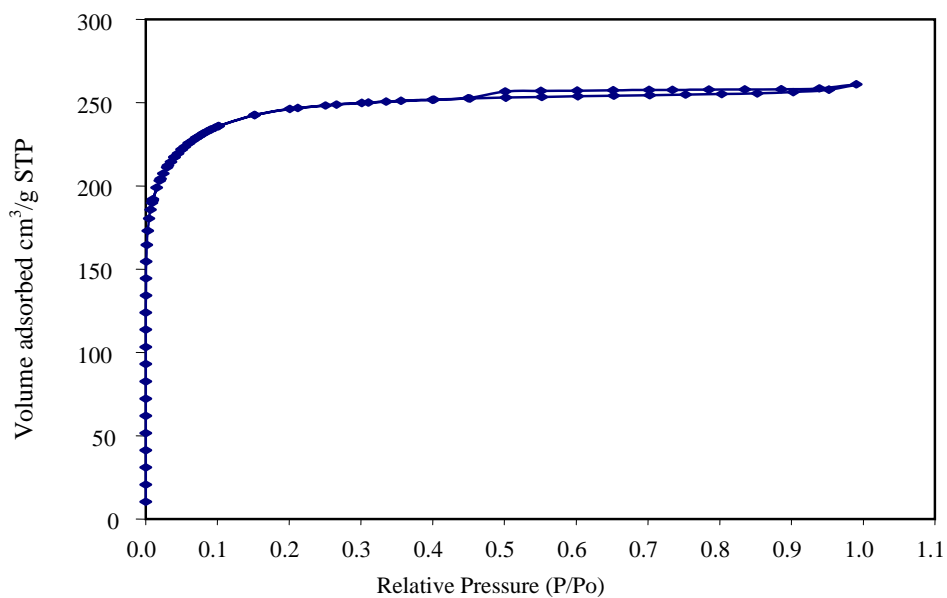


Figure B.4 Nitrogen adsorption isotherm at 77 K for activated carbon sample after nitric acid (6 M) oxidation and metal (Zn) addition.

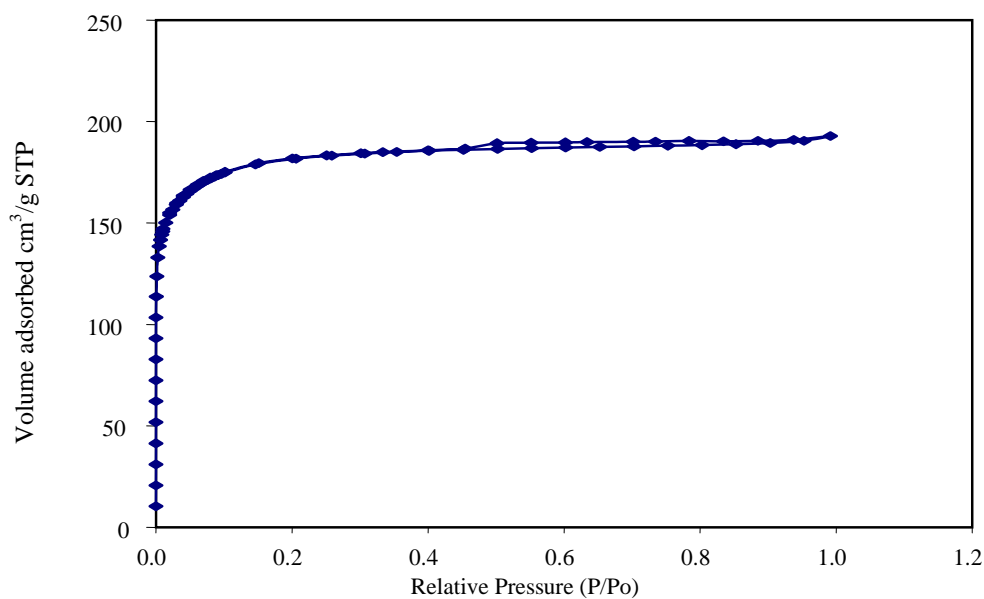


Figure B.5 Nitrogen adsorption isotherm at 77 K for activated carbon sample after nitric acid (10 M) oxidation and metal (Zn) addition.

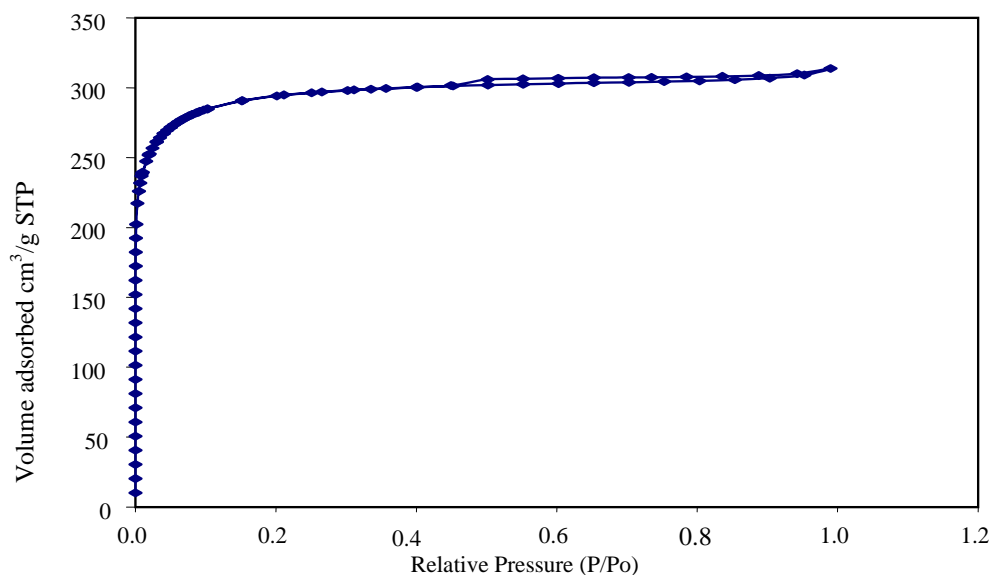


Figure B.6 Nitrogen adsorption isotherm at 77 K for activated carbon sample after ozone oxidation (in fluidized-bed, 90 min) and metal (Zn) addition.

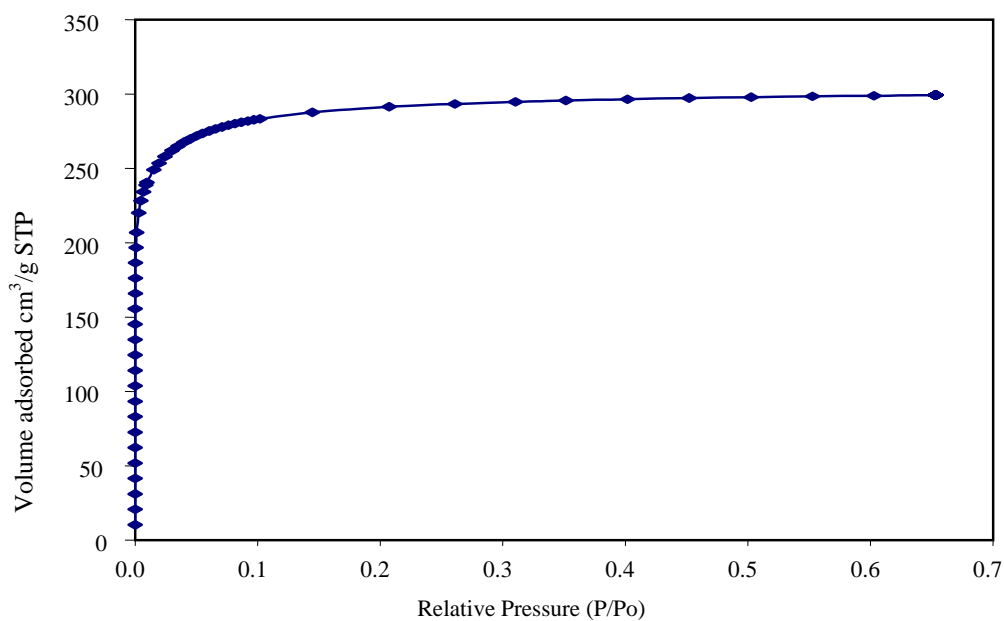


Figure B.7 Nitrogen adsorption isotherm at 77 K for activated carbon sample after ozone oxidation (in hot water, 60 min) and metal (Zn) addition.

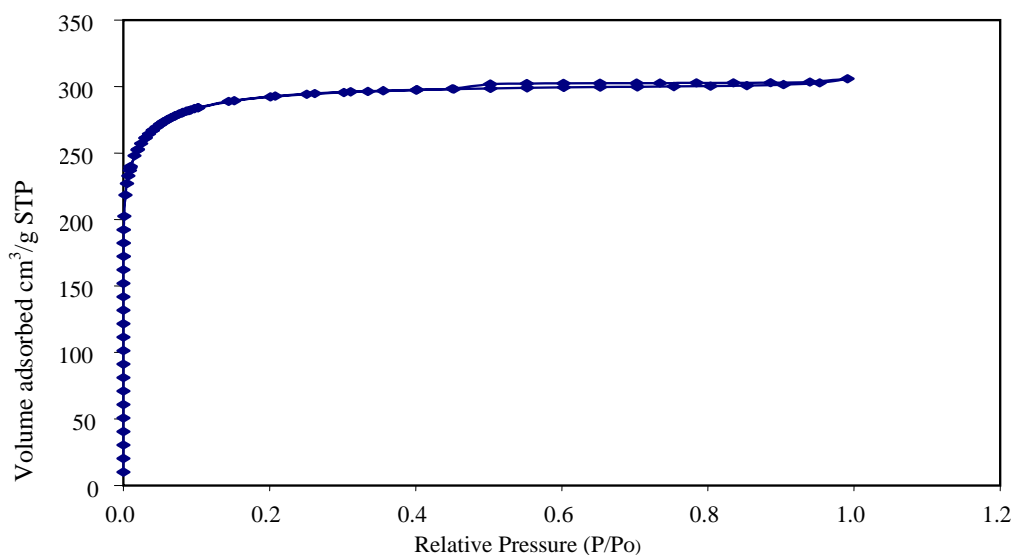


Figure B.8 Nitrogen adsorption isotherm at 77 K for activated carbon sample after ozone oxidation (in hot water, 120 min) and metal (Zn) addition.

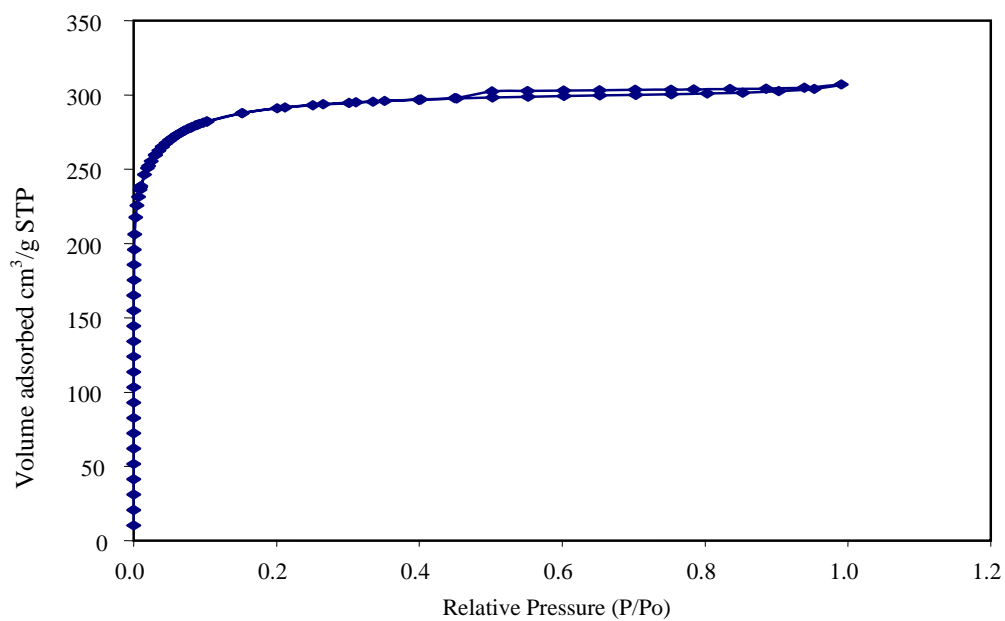


Figure B.9 Nitrogen adsorption isotherm at 77 K for activated carbon sample after ozone oxidation (in hot water, 180 min) and metal (Zn) addition.

APPENDIX C

ESTIMATION OF FLOW RATE FOR

GAS FLUIDIZATION

Estimation of Flow Rate for Gas Fluidization

Data:	d _p = sieve size for (8 x 16-mesh)	=	1.791x 10 ⁻³ m
	d _v = volume diameter	=	1.13 d _p
	ρ _p = particle density	=	1516.0 kg/m ³
	ρ _v = gas density at 30° C	=	1.17 kg/m ³
	μ _{air} = dynamic viscosity at 30° C	=	1.86 N.s/m ² or kg/m.s
	M = mass of activated carbon	=	53.0495 x 10 ⁻³ kg
	D = diameter of bed	=	5.0x10 ⁻² m
	A = cross-section area of bed[D ² .π/4]	=	0.0020 m ²
	H _{mf} = height of incipient fluidized bed	=	5.09 x 10 ⁻² m

Step 1: Calculate bed density (ρ_{Bmf}) at U_{mf}

$$\begin{aligned}\rho_{Bmf} &= (53.0495 \times 10^{-3} \text{ kg}) / \{ (\pi/4) \cdot (5.0 \times 10^{-2} \text{ m})^2 \cdot (5.09 \times 10^{-2} \text{ m}) \} \\ &= 530.495 \text{ kg/m}^3\end{aligned}$$

Step 2: Calculate voidages of packed incipiently (E_{mf})

$$\begin{aligned}E_{mf} &= 1 - \rho_{Bmf} / \rho_p \\ E_{mf} &= 1 - (530.495 \text{ kg/m}^3) / (1516.0 \text{ kg/m}^3) = 0.65\end{aligned}$$

Step 3: Calculate pressure drop across a fluidized bed Δp_F

$$\begin{aligned}\Delta p_F &= 0.1 M / A \\ \Delta p_F &= (0.1 \times 53.0495 \times 10^{-3} \text{ kg}) / \{ (\pi/4) \cdot (5.0 \times 10^{-2} \text{ m})^2 \} = 2.7007 \text{ kg/m}^2 \\ \Delta p_F &= 2.7007 \text{ cm w.g. (cm water gauge)}\end{aligned}$$

Step 4: Calculate volume diameter (d_v)

$$d_v = 1.13 d_p$$

$$d_v = 1.13 \times 1.791 \times 10^{-3} \text{ m} = 2.0238 \times 10^{-3} \text{ m}$$

Step 5: Calculate Archimedes number (Ar)

$$\text{Ar} = \rho_g \cdot \rho_p \cdot g \cdot (d_v)^3 / (\mu_{\text{air}})^2$$

$$\text{Ar} = 1.17 \text{ kg/m}^3 \cdot 1516 \text{ kg/m}^3 \times 9.81 \text{ m/s}^2 \cdot (2.0238 \text{ m})^3 / (1.86 \times 10^{-5} \text{ kg/m.s})^2$$

$$\text{Ar} = 416899.0992$$

Step 6: Calculate Reynolds number at incipient fluidization velocity (Re_{mf})

$$\text{Re}_{\text{mf}} = \{1135.7 + (0.0408 \times \text{Ar})\}^{1/2} - 33.7$$

$$\text{Re}_{\text{mf}} = \{1135.7 + (0.0408 \times 416899.0992)\}^{1/2} - 33.7 = 101.0041$$

Step 7: Velocity (U_{mf})

$$U_{\text{mf}} = \text{Re}_{\text{mf}} \cdot \mu_{\text{air}} / \rho_g \cdot d_v$$

$$U_{\text{mf}} = (101.0041 \times 1.86 \times 10^{-5} \text{ kg/m.s}) / (1.17 \times 2.0238 \times 10^{-3} \text{ kg/m}^3 \cdot \text{m})$$

$$U_{\text{mf}} = 0.793411 \approx 0.79 \text{ m/s}$$

Step 8: Calculate flow rate of gas for fluidization

$$\text{Flow rate} = A \times U_{\text{mf}} \quad \text{m}^2 \cdot \text{m/s} = \text{m}^3/\text{s}$$

Reference: Geldart, D. (1986). Gas Fluidization Technology New York: John Wiley and sons.

APPENDIX D

INCREASING EFFICIENCY FOR

H₂S REMOVAL CALCULATION

Increasing efficiency for H₂S removal calculation

For example, the mixed gases of 1.01% H₂S balance in N₂ used for adsorption experiment. The original activated carbon impregnated with Zn sample was put into the adsorber used for adsorption at 10°C having a weight of 3.3086 g. The corresponding time for adsorption in this case is 1600 sec. The following data can be used:

$$\begin{aligned}
 1.40 \text{ mg-H}_2\text{S/m}^3(\text{mixed gases}) &= 1 \text{ ppm} \\
 1.01\% \text{ H}_2\text{S} &= 10,100 \text{ ppm} \\
 \text{mixed gases flow rate} &= 150 \text{ cm}^3/\text{min} \\
 &= 2.5 \times 10^{-6} \text{ m}^3/\text{s}
 \end{aligned}$$

step 1: calculate mg-H₂S/m³(mixed gases)

$$\begin{aligned}
 &= 1.40 \text{ mg-H}_2\text{S/m}^3 \times 1/\text{ppm} \times 10,100 \text{ ppm} \\
 &= 1.414 \times 10^4 \text{ mg-H}_2\text{S/m}^3
 \end{aligned}$$

step 2: calculate volume of mixed gases used for adsorption

$$\begin{aligned}
 &= \text{mixed gases flow rate, (m}^3/\text{s)} \times \text{corresponding time for} \\
 &\quad \text{adsorption, (s)} \\
 &= 2.5 \times 10^{-6} \text{ m}^3/\text{s} \times 1600 \text{ s} = 4.0 \times 10^{-3} \text{ m}^3
 \end{aligned}$$

step 3: calculate mg-H₂S/g-sample for H₂S removal

$$\begin{aligned}
 &= \text{volume of mixed gases, (m}^3) \times \text{mg-H}_2\text{S/m}^3 \times \text{amount of} \\
 &\quad \text{sample, (g)} \\
 &= 4.0 \times 10^{-3} \text{ m}^3 \times 1.414 \times 10^4 \text{ mg-H}_2\text{S/m}^3 \times 1/3.3086 \text{ g-sample} \\
 &= 17.09 \text{ mg-H}_2\text{S/g-sample}
 \end{aligned}$$

In this case, untreated sample having a mg-H₂S/g-sample for H₂S removal of 11.17 mg.

step 4: calculate increasing efficiency of treated sample for H₂S removal compared with the untreated sample

$$\begin{aligned} &= \frac{\text{mg H}_2\text{S/g treated sample} - \text{mg H}_2\text{S/g untreated sample}}{\text{mg H}_2\text{S/g untreated sample}} \times 100 \\ &= \frac{(17.09 - 11.70) \times 100}{11.70} \\ &= 46.1 \% \end{aligned}$$

APPENDIX E

SPECIFIC SURFACE AREAS AND POROSITY

Table E.1 Specific surface areas in activated carbon samples by nitrogen adsorption

Sample	Surface Area Analysis :m ² /g						
	Single Point	BET	Lang.	Micropore	BJH Ads..	BJH Des.	External
Original	1089.9657	1119.3458	1380.5135	878.5813	116.5906	163.5856	240.7645
Original + Zn	893.1454	967.2251	1286.0204	766.6663	143.8717	177.7115	200.5588
6M HNO ₃	845.1697	908.8211	1217.5707	639.5146	198.8899	244.1644	269.3065
6M HNO ₃ +Zn	750.7339	807.5625	1078.4270	592.9543	151.4582	188.4464	241.6082
10M HNO ₃ +Zn	555.6662	579.1033	795.8797	453.7476	100.7849	123.3949	143.3560
O ₃ (fluidized-bed 210°C) + Zn	894.8551	967.2793	1286.6103	767.3399	144.4635	177.7251	199.9394
O ₃ (reflux 60 min)+ Zn	885.0738	959.4744	1272.5969	791.4411	121.2609	148.7324	168.0333
O ₃ (reflux 120 min)+ Zn	887.9624	962.4440	1277.6106	783.4696	125.5175	156.0683	178.9745
O ₃ (reflux 180 min) + Zn	884.9885	957.1686	1273.2000	765.6285	137.5618	169.3941	191.5401

Table E.2 Porosity in activated carbon samples by nitrogen adsorption

Sample	Pore Volume Analysis:cm ³ /g				Pore Size Analysis: nm		
	Total	Micropore	BJH Ads.	BJH Des.	BET	BJH Ads.	BJH Des.
Original	0.5180	0.3810	0.0798	0.0976	1.8510	2.7364	2.3873
Original+Zn	0.4877	0.3657	0.0993	0.0976	2.0171	2.7601	2.5633
6M HNO ₃	0.4635	0.3089	0.1262	0.1139	2.0401	2.5371	2.3635
6M HNO ₃ +Zn	0.4037	0.2848	0.0931	0.1443	1.9996	2.4581	2.3131
10M HNO ₃ +Zn	0.2983	0.2170	0.0642	0.1090	1.9986	2.5477	2.3791
O ₃ (fluidized-bed 210°C)+ Zn	0.4853	0.3660	0.0970	0.0734	2.0068	2.6857	2.5110
O ₃ (reflux 60 min)+ Zn	0.4745	0.3756	0.0801	0.1116	1.9781	2.6423	2.4780
O ₃ (reflux 120 min)+ Zn	0.4731	0.3726	0.0788	0.0921	1.9662	2.5103	2.3624
O ₃ (reflux 180 min)+ Zn	0.4750	0.3649	0.0883	0.0922	1.9852	2.5665	2.4153

APPENDIX F
SELECTED FUNCTIONAL GROUPS

Selected Functional Groups			
Group Name	Structure	IUPAC Suffix	Example
Alkene	$\begin{array}{c} \diagup \\ \text{C}=\text{C} \\ \diagdown \end{array}$	-ene	$\text{CH}_3\text{CH}_2\text{CH}=\text{CH}_2$ 1-Butene
Alkyne	$-\text{C}\equiv\text{C}-$	-yne	$\text{CH}_3\text{C}\equiv\text{CCH}_3$ 2-Butyne
Alcohol	$-\text{OH}$	-ol	$\text{CH}_3\text{CH}(\text{OH})\text{CH}_3$ 2-Propanol
Amine	$-\text{NH}_2$	-amine	$\text{CH}_3\text{CH}_2\text{CH}_2\text{NH}_2$ 1-Propanamine
Aldehyde	$\begin{array}{c} \text{O} \\ \\ -\text{C}-\text{H} \end{array}$	-al	$\text{CH}_3\text{CH}_2\text{CHO}$ Propanal
Ketone	$\begin{array}{c} \text{O} \\ \\ -\text{C}- \end{array}$	-one	$\text{CH}_3\text{CH}_2\text{COCH}_3$ 2-Butanone
Carboxylic acid	$\begin{array}{c} \text{O} \\ \\ -\text{C}-\text{OH} \end{array}$	-oic acid	$\text{CH}_3\text{CH}_2\text{COOH}$ Propanoic acid

Fig.F1 Select functional group. (Holum, 1994)

APPENDIX G

GROUP ASSIGNMENTS IN INFRARED SPECTRA

Type of Bond	Group	Family of Compounds	Range (cm ⁻¹)
Single Bonds	C—H	Alkanes	2850–3300
	=C—H	Alkenes, aromatics	3000–3100
	≡C—H	Alkynes	3300–3320
	O—H	Alcohols	3200–3600
	N—H	Amines	3300–3500
Double Bonds	C=C	Alkenes, aromatics	1600–1680
	C=O	Carbonyls	1680–1750
		Aldehydes, ketones	1710–1750
		Carboxylic acids	1700–1725
		Esters, amides	1680–1750
C=N	Imines	1500–1650	
Triple Bonds	C≡C	Alkynes	2100–2200
	C≡N	Nitriles	2200–2300

The figure shows a horizontal axis for Wavenumber (cm⁻¹) ranging from 3800 to 1400. Vertical lines indicate characteristic absorption bands for various functional groups. The assignments are as follows:

- O—H: ~3400 cm⁻¹
- N—H: ~3300 cm⁻¹
- C—H: 2850–3000 cm⁻¹
- C≡C: ~2200 cm⁻¹
- C≡N: ~2100 cm⁻¹
- C=O: 1680–1750 cm⁻¹
- C=C: 1600–1680 cm⁻¹
- C=N: 1500–1650 cm⁻¹

Fig .G1 Group Assignments in Infrared Spectra. (Dean, 1999)

BIOGRAPHY

Mr. Somkiat Kruaysawat was born on April 7, 1959, in Nakhon Ratchasima Province, North Eastern of Thailand. After the secondary school at Buayai school, Nakhon Ratchasima, secondary teacher certificate in general science at Nakhon Ratchasima Teacher College and continued the Bachelor degree at Srinakharinvirot University (Mahasarakham campus) in Chemistry. With the Bachelor degree, he work as a lecturer at Department of Chemistry, Ubon Ratchathani Agricultural College and continued the Master program in Teaching Chemistry from Chiang Mai University. Subsequently, he worked as Board committee to direct the specification of the “Science Analysis Instrument”, Laboratorial Chemistry Curriculum, and Petro-Chemistry Curriculum of the Vocational Department, Ministry of Education. Afterwards, he had got a scholarship from Sripatum University to study the Ph.D. program in Environmental Engineering at Suranaree University of Technology, in the first trimester of 2001. Up to the present time, he has been working as a lecturer (Assistant Professor in chemistry) at Department of Applied Science, Institute of General Education, Sripatum University since 1997.